

2
m 1 X

REPORT NO. GDCA-DDE72-004
CONTRACT NAS8-26916

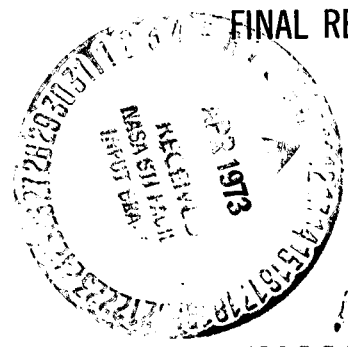
(NASA-CR-124113) COMBINED LOADING
CRITERIAL INFLUENCE ON STRUCTURAL
PERFORMANCE Final Report (General
Dynamics/Convair) 187 p HC \$11.50

N73-20874

Unclas
CSSL 22B G3/31 16179

COMBINED LOADING CRITERIA INFLUENCE ON STRUCTURAL PERFORMANCE

FINAL REPORT



GENERAL DYNAMICS
Convair Aerospace Division

178

REPORT NO. GDCA-DDE72-004

**COMBINED LOADING CRITERIA INFLUENCE
ON STRUCTURAL PERFORMANCE**

FINAL REPORT

30 June 1972

Prepared Under
Contract NAS8-26916

Submitted to
National Aeronautics and Space Administration
GEORGE C. MARSHALL SPACE FLIGHT CENTER
Huntsville, Alabama

Prepared by
CONVAIR AEROSPACE DIVISION OF GENERAL DYNAMICS
San Diego, California

1

Preceding page blank

FOREWORD

This investigation was performed under Contract NAS8-26916 for the NASA George C. Marshall Space Flight Center under the technical direction of the Astronautics Laboratory, Materials Division. The technical monitor was Mr. Robert L. McComas. The study was performed by B. J. Kuchta, D. M. Sealey, and L. J. Howell of Convair Aerospace Division of General Dynamics, San Diego, California.

Preceding page blank

TABLE OF CONTENTS

PART I

PHASE I, RELATIVE WEIGHT SENSITIVITY TO LOADING

<u>Section</u>		<u>Page</u>
1	INTRODUCTION	I-9
2	BASELINE CRITERIA	I-15
3	STRUCTURAL CONFIGURATION	I-27
4	BOOSTER WEIGHT SUMMARY	I-41
5	STRUCTURAL ANALYSIS	I-47
6	DESIGN CONDITION IDENTIFICATION	I-53
7	BOOSTER SERVICE LOAD SPECTRA	I-63
8	FATIGUE ANALYSIS	I-73

PART II

PHASE II, SENSITIVITY TO LOADING PARAMETERS

1	INTRODUCTION	II-7
2	STRUCTURAL WEIGHT/LOAD SENSITIVITY	II-9
3	SENSITIVITIES OF LOADS TO VARIOUS CONFIGURATION AND FLIGHT PARAMETER CHANGES	II-49
4	REFERENCES	II-55

PART III

**PHASE III, LOADING PARAMETER VARIABILITY, INADEQUACY,
AND PROBABILITY AS A FUNCTION OF SYSTEM DESIGN**

1	INTRODUCTION	III-5
2	DISCIPLINE INVOLVEMENT IN DESIGN DEFINITION	III-7
3	CRITICALITY OF LOAD PARAMETERS AND LOADING PROBABILITY AND VARIABILITY	III-13
4	VARIABILITY OF LOAD PARAMETERS WITH PROGRAM SCHEDULE	III-21
5	INADEQUATE LOAD DATA -- POSSIBLE IMPROVEMENTS	III-25

TABLE OF CONTENTS, Contd

PART IV

PHASE IV, METHODS FOR DETERMINING STATISTICS
OF TOTAL LOAD EXCEEDANCES

<u>Section</u>		<u>Page</u>
1	INTRODUCTION	IV- 5
2	DESIGN PHILOSOPHY	IV- 7
3	PROBABILITY OF SURVIVAL	IV- 9
4	LOAD LEVEL EXCEEDANCES FOR COMBINED LOADING	IV- 19
5	APPLICATION TO SIGNIFICANT SPACE SHUTTLE LOADING SITUATIONS	IV- 23
6	CONCLUSIONS AND RECOMMENDATIONS FOR FURTHER STUDY	IV- 27
7	REFERENCES	IV- 29
<u>Appendix</u>		
A	BASIC STATISTICAL CONCEPTS	IV- 31

SUMMARY

An investigation was conducted to determine the influence of combined loading criteria on the space shuttle structural performance. The study consisted of four primary phases:

Phase I. The determination of the sensitivity of structural weight to the various loading parameters associated with the space shuttle.

Phase II. The determination of the sensitivity of structural weight to various levels of loading parameter variability and probability.

Phase III. The determination of shuttle mission loading parameter variability and probability as a function of design evolution and the identification of those loading parameters where inadequate data exists.

Phase IV. The determination of rational methods of combining both deterministic time varying and probabilistic loading parameters to provide realistic design criteria.

This final report contains the study results. These results are presented in four parts, each of which describes an individual phase. Each of the four parts contains a summary and an introduction as well as the significant results obtained during that phase of the study.

PART I

PHASE I, RELATIVE WEIGHT SENSITIVITY TO LOADING



TABLE OF CONTENTS

<u>Section</u>		<u>Page</u>
1	INTRODUCTION	I-9
2	BASELINE CRITERIA	I-15
	2.1 DESIGN CRITERIA	I-15
	2.2 DESIGN CONDITIONS	I-16
	2.3 PROPELLANT TANK PRESSURE	I-21
	2.4 DESIGN TEMPERATURES	I-22
3	STRUCTURAL CONFIGURATION	I-27
	3.1 FUSELAGE STRUCTURE	I-29
	3.2 WING STRUCTURE	I-29
	3.3 VERTICAL TAIL STRUCTURE	I-35
	3.4 BOOSTER STRUCTURAL MATERIALS	I-35
4	BOOSTER WEIGHT SUMMARY	I-41
5	STRUCTURAL ANALYSIS	I-47
	5.1 WING STRUCTURAL ANALYSIS	I-47
	5.2 VERTICAL TAIL STRUCTURAL ANALYSIS	I-49
	5.3 FUSELAGE STRUCTURAL ANALYSIS	I-50
6	DESIGN CONDITION IDENTIFICATION	I-53
	6.1 WING STRUCTURAL WEIGHT SENSITIVITIES	I-53
	6.2 VERTICAL TAIL WEIGHT SENSITIVITIES	I-55
	6.3 FUSELAGE STRUCTURAL SENSITIVITIES	I-56
7	BOOSTER SERVICE LOAD SPECTRA	I-63
	7.1 WING LOAD SPECTRA	I-63
	7.2 VERTICAL TAIL SPECTRA	I-63
	7.3 FUSELAGE LOAD SPECTRA	I-63
	7.4 ORBITER-TO-BOOSTER ATTACHMENT LOAD SPECTRA	I-63
	7.5 THRUST LOAD SPECTRA	I-69
	7.6 PROPELLANT TANKS PRESSURE LOAD SPECTRA	I-69
8	FATIGUE ANALYSIS	I-73
	8.1 WING ANALYSIS	I-75
	8.2 VERTICAL TAIL ANALYSIS	I-75
	8.3 FUSELAGE ANALYSIS	I-75
	8.4 AFT ORBITER SUPPORT FRAME ANALYSIS	I-76
	8.5 THRUST STRUCTURE ANALYSIS	I-76
	8.6 PROPELLANT TANK ANALYSIS	I-76

Preceding page blank

LIST OF FIGURES

<u>Figure</u>		<u>Page</u>
1-1	Elements of Space Shuttle Operations	I-10
1-2	Booster Flight Profile	I-11
1-3	Ascent Trajectory Parameters	I-12
1-4	Nominal Booster Return Trajectory	I-13
2-1	Booster B-9U Peak Limit Load Intensities	I-20
2-2	LH ₂ Tank Gage Pressures Versus Tank Length	I-23
2-3	LO ₂ Tank Gage Pressures Versus Tank Length	I-23
2-4	Wing Loads (Limit)	I-25
2-5	Canard Loads (Limit)	I-25
2-6	Vertical Stabilizer Loads (Limit)	I-26
3-1	B-9U Delta Wing Booster Vehicle Configuration	I-28
3-2	B-9U Delta-Wing Booster, Three View	I-28
3-3	Inboard Profile B-9U Booster	I-31
3-4	B-9U Booster Body Structure	I-33
3-5	B-9U Wing General Description	I-34
3-6	B-9U Vertical Stabilizer Configuration	I-36
5-1	B-9U Wing Box Structural Simulation Model	I-47
5-2	Wing Upper Surface Radiation Equilibrium Temperatures	I-48
5-3	TPS Wing Lower Surface Temperature, Inner Skin	I-48
5-4	Wing Upper Surface Rib Cap Temperature Distribution	I-49
5-5	B-9U Vertical Stabilizer Structural Simulation Model	I-49
5-6	B-9U Vertical Stabilizer Airfoil Sections	I-50
5-7	B-9U Fuselage Structural Model	I-51
6-1	Booster Wing Structure Weight for the Critical Design Conditions (Weight for One Side of the Vehicle)	I-53
6-2	Booster Wing Structure Weight for Various Resizings	I-55

LIST OF FIGURES, Contd

<u>Figure</u>		<u>Page</u>
6-3	Location of Load Intensity Output from NETLD2	I-57
6-4	Critical Design Conditions for Axial Bar Members	I-60
6-5	Critical Design Conditions for Shear Panels	I-60
6-6	Critical Design Conditions for Frame Beam Element Members	I-61
6-7	B-9U Critical Loading Conditions	I-62
7-1	Wing Load Spectra	I-64
7-2	B-9U Vertical Tail Load Spectra	I-65
7-3	B-9U Fuselage Station 2600 Load Spectra	I-66
7-4	B-9U/Orbiter Forward Attach Load Spectra	I-67
7-5	B-9U/Orbiter Aft Attachment Load Spectra	I-68
7-6	Total Mean Booster Main Engine Thrust	I-69
7-7	Thrust Spectra (One Flight)	I-70
7-8	Booster Main LH ₂ Tank Pressure Schedule	I-70
7-9	Booster Main LO ₂ Tank Pressure Schedule	I-71
8-1	Estimated Fatigue Curves for 2219-T87 at Room Temperature with $K_t = 3.0$	I-73
8-2	Fatigue Curves for Annealed 6Al-4V Ti at Room Temperature with $K_t = 3.0$	I-74
8-3	Fatigue Curves for Annealed 6Al-4V Ti at 650° F with $K_t = 3.0$	I-74

LIST OF TABLES

<u>Table</u>		<u>Page</u>
2-1	Design Criteria	I-15
2-2	Limit Airloads	I-17
2-3	Booster B-9U Wing, Canard and Vertical Tail Design Conditions	I-18
2-4	Summary of Design Conditions	I-19
2-5	Booster/Orbiter Interconnection Loads	I-22
2-6	Summary of Design Conditions	I-24
3-1	Booster Materials	I-37
4-1	Delta Booster Weight Summary	I-42
4-2	Wing Group Weight Breakdown	I-43
4-3	Vertical Tail Group Weight Breakdown	I-44
4-4	Body Group Weight Breakdown	I-45
6-1	Weight Sensitivity of B-9U Wing to Loads	I-54
6-2	B-9U Vertical Tail - Weight Sensitivity to Loads	I-56
6-3	B-9U/161-C Ultimate Internal Loads (Baseline)	I-57
6-4	B-9U/161-C Ultimate Tension Internal Loads (Baseline)	I-58
6-5	B-9U/161-C Ultimate Compression Internal Loads (Baseline)	I-59
8-1	B-9U Tankage Pressure Cycles	I-76
8-2	Results of Safe Fatigue Life Analysis	I-77

Preceding page blank

SUMMARY

This part documents the work performed under Phase I of the study.

The summary table presents for each major load condition or flight phase: 1) the major structural components designed by the load condition; 2) the major parameters that affect the loading condition, 3) the effect of temperature, and 4) the potential fatigue damage due to this loading condition or flight phase. The study was conducted on the Convair Aerospace/North American Phase B B-9U delta wing booster. The structural aerodynamic and trajectory data used was generated by the Phase B study.

The design of the vehicle is not sensitive to any single condition, but it is sensitive to a group of conditions: liftoff plus one hour ground winds, ascent wind, maximum ascent thrust, and entry. For the wing, the ascent headwinds and maximum entry g conditions are equally critical. The magnitude of the load for the ascent headwind condition is greater than for the entry condition; however, for the entry condition, temperature effects reduce material properties. When considering the vertical tail, the major design condition is the ascent wind. If load relief or β -feedback control laws are used, however, the subsonic gust condition becomes critical. The fuselage is basically designed by ascent winds, liftoff with ground winds, and maximum thrust. The LO₂ tank is designed by proof pressure loads. These fuselage load conditions are relatively equal in criticality. The structural weights of these major vehicle components are:

Wing	71,000 pounds
Tail	13,000 pounds
Fuselage	178,000 pounds

These weights indicate that load variation and sensitivities that primarily affect the fuselage will provide the most variation in system performance.

The structural design conditions identified include both probabilistic and deterministic loads. In the design of both the wing and fuselage, statistically defined wind loads are combined directly with deterministic thrust or g loads. In this phase of the study, these loads were combined on a one-to-one basis; i. e., deterministic loads and the mean plus three sigma values of random loads were combined according to standard superposition techniques. Assessment of methods for combining random and deterministic loads was the subject of Phase IV study.

PRECEDING PAGE BLANK NOT FILMED

Summary of Booster Design Load and Weight Sensitivity

Load Condition	Type of Load	Designs	Cond. Rank	Major Parameters	Thermal Effects	Fatigue Effects
Servicing	Deterministic	None	-	Erection procedure Hoist loads	None	None
Pressurization	Deterministic	Fuselage	3	Pressure level	None	Major damage fuselage
Towing	Deterministic	None	-	Towing load	None	None
Pad Winds + Liftoff	Probabilistic	Fuselage sides & forward lower	5	Exposure time Wind probability	None None	Minor fuselage and wing
Ascent Tail Wind	Probabilistic	Orbit aft attach	7	Dynamic pressure Guidance and control Wind probability	Interference impingement	Major on wing and fuselage
Head Wind	Probabilistic	Wing, Fuselage, aft lower	2	Wind probability	Interference impingement	Major on wing and fuselage
Side Wind	Probabilistic	Vertical Tail	6	Wind probability	Interference impingement	Major on wing and fuselage vertical tail
Max Thrust	Deterministic	Upper fuselage Thrust structure	1	g limit mission	Interference impingement	Thrust structure Fuselage
Staging	Deterministic	None	-	Method of staging	Plume impingement	None
Entry Max g	Deterministic	Wing	4	Control system max g limit	Fuselage and wing temperatures	Wing and fuse- lage
Max Temp	Deterministic	Wing leading edge	9	Entry angle	Fuselage and wing temperatures	Wing and fuse- lage
Flyback Subsonic Gust	Probabilistic	None	-	Cruise altitude Wind probability	None	Minor wing and fuselage
Rudder Kick	Deterministic	Vertical tail	8	Amount of rudder	None	Minor vertical tail
Maneuver	Deterministic	Canard	-	Limit g	None	Minor wing
Landing	Probabilistic	Landing gear	-	Sink speed, Gear characteristics	None	Minor on fuselage
Taxi	Probabilistic	Landing gear	-	Runway roughness	None	Local gear structure

SECTION 1

INTRODUCTION

The primary objective of this phase of the study was to establish the relative importance of the various probabilistic and deterministic loading conditions in all operational phases of flight of a space shuttle vehicle.

The operational phases considered are:

- a. Launch Pad
- b. Ascent
- c. Entry
- d. Subsonic Flight
- e. Landing and Taxi

Another objective is to show the relative sensitivities of structural weight to all loading parameters and to identify regions of critical design loads and maximum fatigue damage.

The objective of the space shuttle program is to provide a space transportation system capable of placing and/or retrieving payloads in earth orbit. The specific mission considered in this study consists of launching an orbiter vehicle into a 100-n.mi. south polar orbit from WTR with a 40,000-pound payload. These objectives are achieved using a two-stage (booster and orbiter) vehicle capable of boost and earth entry with cruise-back to a designated landing site. This cycle is accomplished with reasonable acceleration levels and shirt-sleeve cabin environment. The significant elements of this mission are ground operations, mating of booster and orbiter, launch followed by staging of the two vehicles, and return of the booster to the launch area with the orbiter continuing to its prescribed orbit. A complete mission cycle is shown in Figure 1-1. A typical mission flight profile for the booster is shown in Figure 1-2.

The baseline delta wing/canard booster selected is the latest configuration available from Phase B studies. This booster (Convair Aerospace Model B-9U) is designed to perform the mission outlined in Figure 1-2 100 times.

Figure 1-3 shows a variety of ascent trajectory parameters. The booster weight decreases from 4,188,000 pounds at launch to about 808,000 pounds at separation, while achieving a velocity of 10,824 fps at an altitude of 244,784 feet. After separation, the orbiter continues on its mission and the booster is positioned for entry.

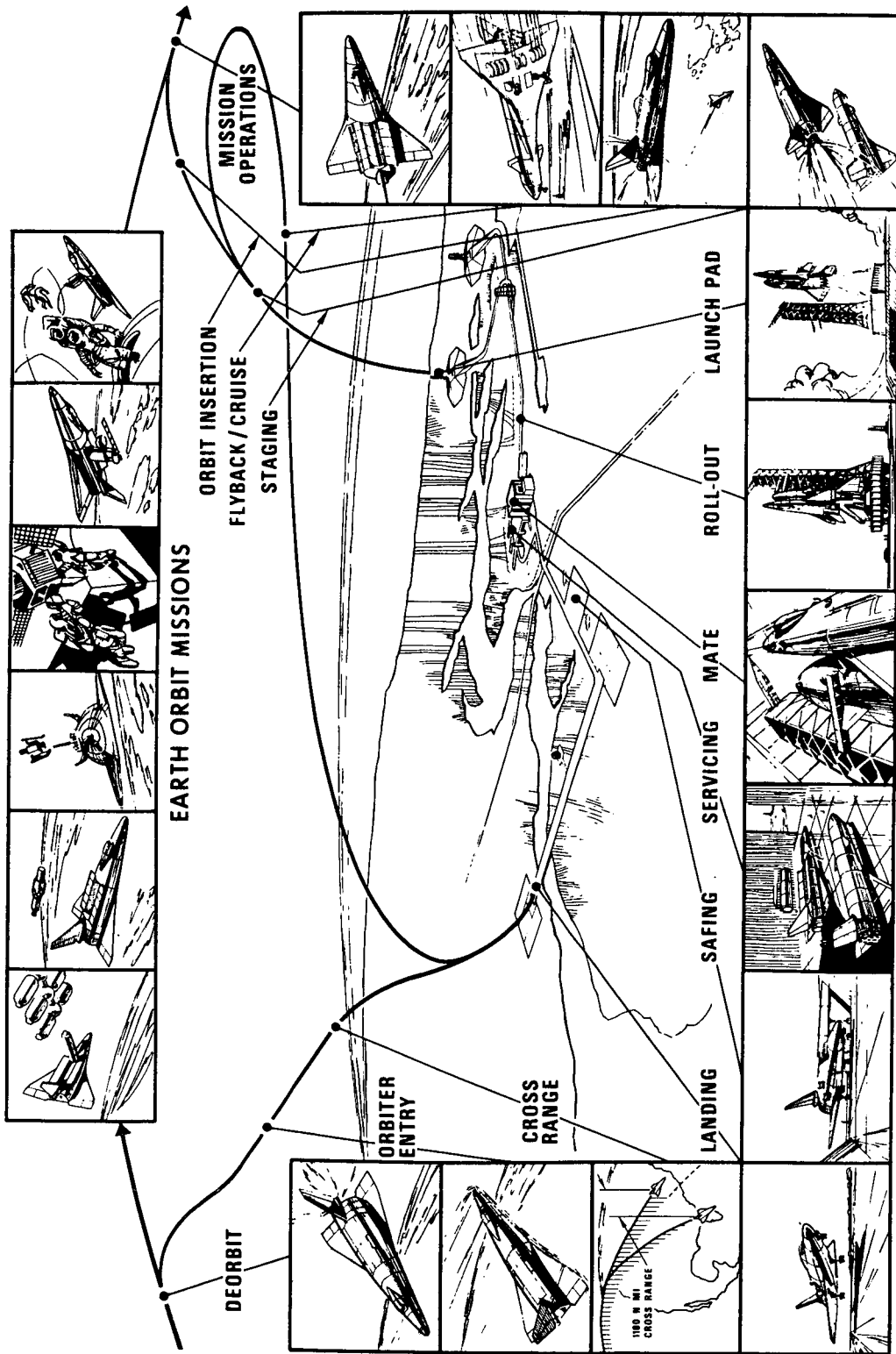


Figure 1-1. Elements of Space Shuttle Operations

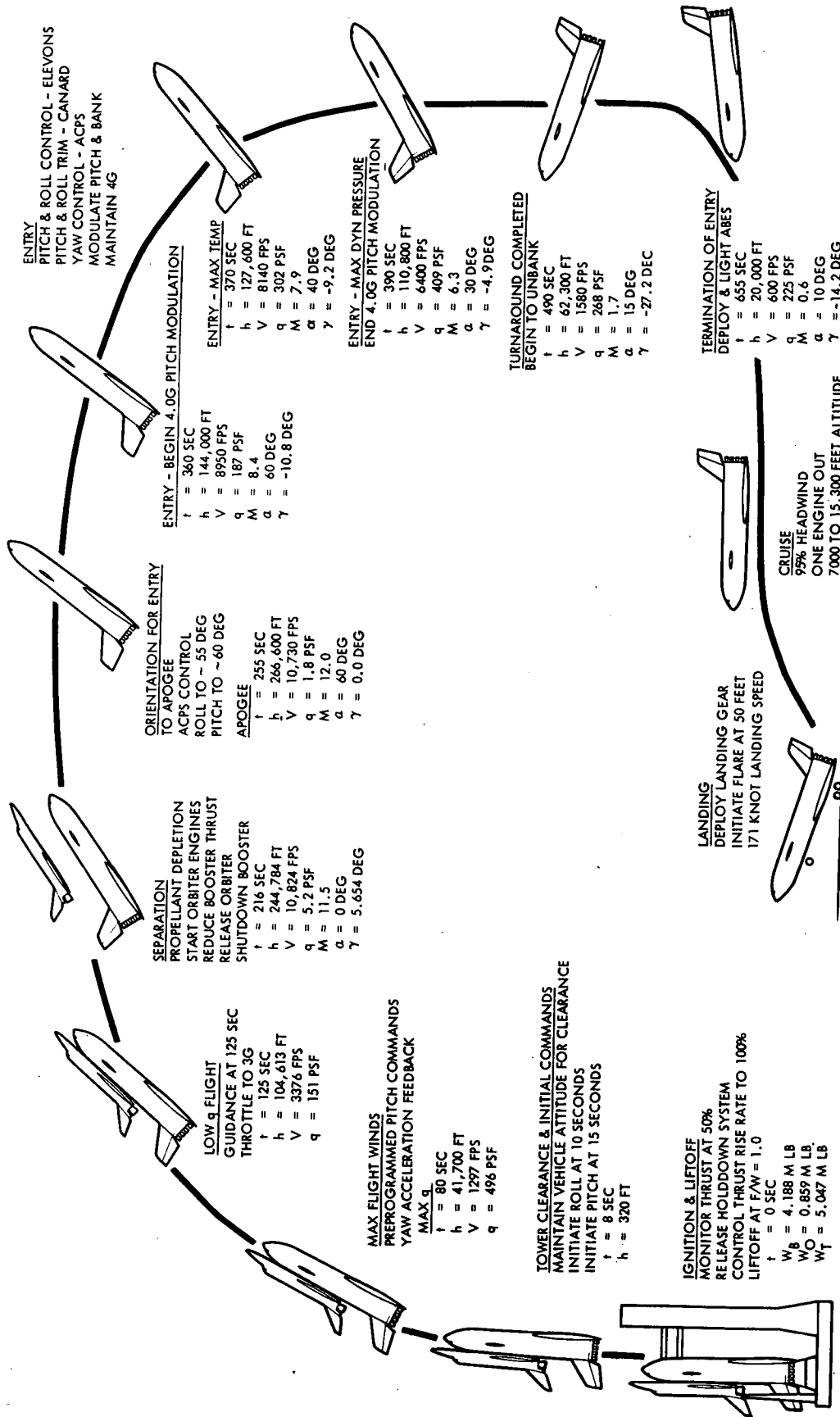


Figure 1-2. Booster Flight Profile

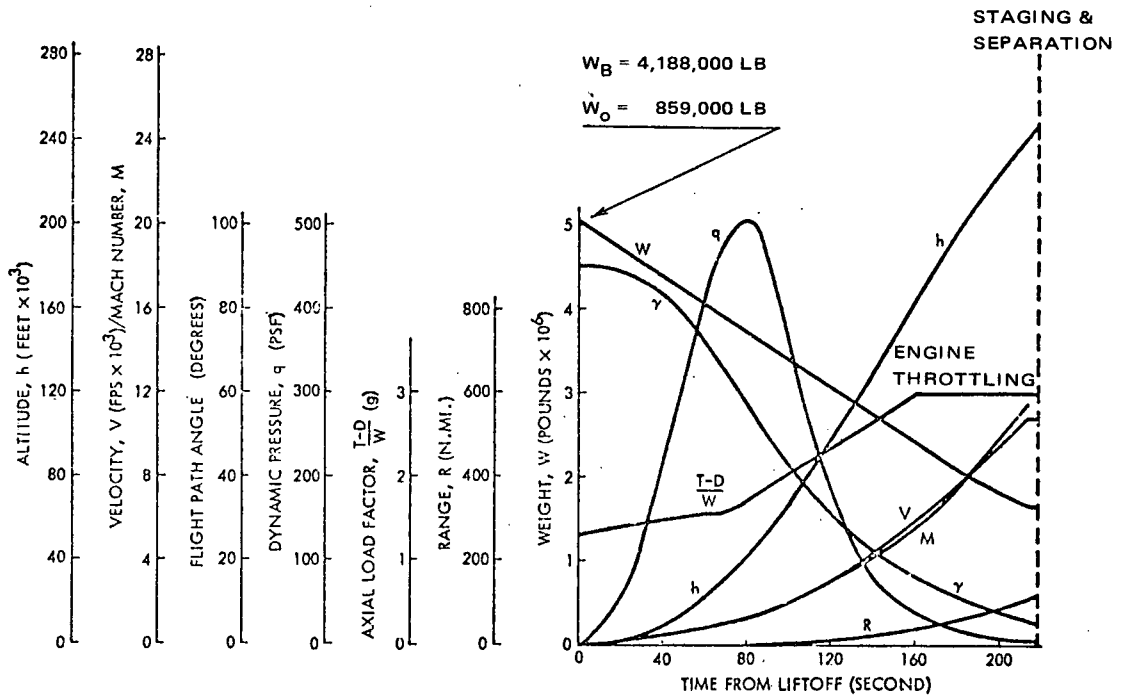


Figure 1-3. Ascent Trajectory Parameters

The entry mode for the booster is a supersonic gradual transition. During the first 40 seconds after staging, the booster pitches to 60 degrees angle of attack and banks to 48 degrees. That attitude is maintained until the resultant load factor reaches 4.0g, occurring at Mach 8.6 and 142,700 feet altitude. Pitch modulation starts at this time to keep from exceeding 4.0g. The lower stability limit constrains the angle of attack from going below 30 degrees during this maneuver. Upon reaching 30 degrees, the bank angle is raised to 75 degrees, which is held until the vehicle has completed its turn. A maximum q of 415 psf is reached at Mach 6.75 and 113,800 feet altitude. By Mach 3.25, the angle of attack has returned to 56 degrees. Beginning there, the angle of attack is constrained by the upper stability limit, reducing to 5 degrees at Mach 1.1. When the booster reaches 20,000 feet, the flyback range is 404 n.mi. At the completion of the entry phase, the gross weight of the booster has decreased slightly to about 787,000 pounds.

Some results from a six-degree-of-freedom program, limiting the resultant load factor to 4.0g, are given in Figure 1-4.

At approximately 20,000 feet, the air-breathing engines are deployed and the return cruise is initiated. The vehicle descends to approximately 13,000 feet and is flown at the altitude that is for best cruise specific range (maximum nautical miles per pound of fuel) for the required flyback range of 404 n.mi. Landing is based on a

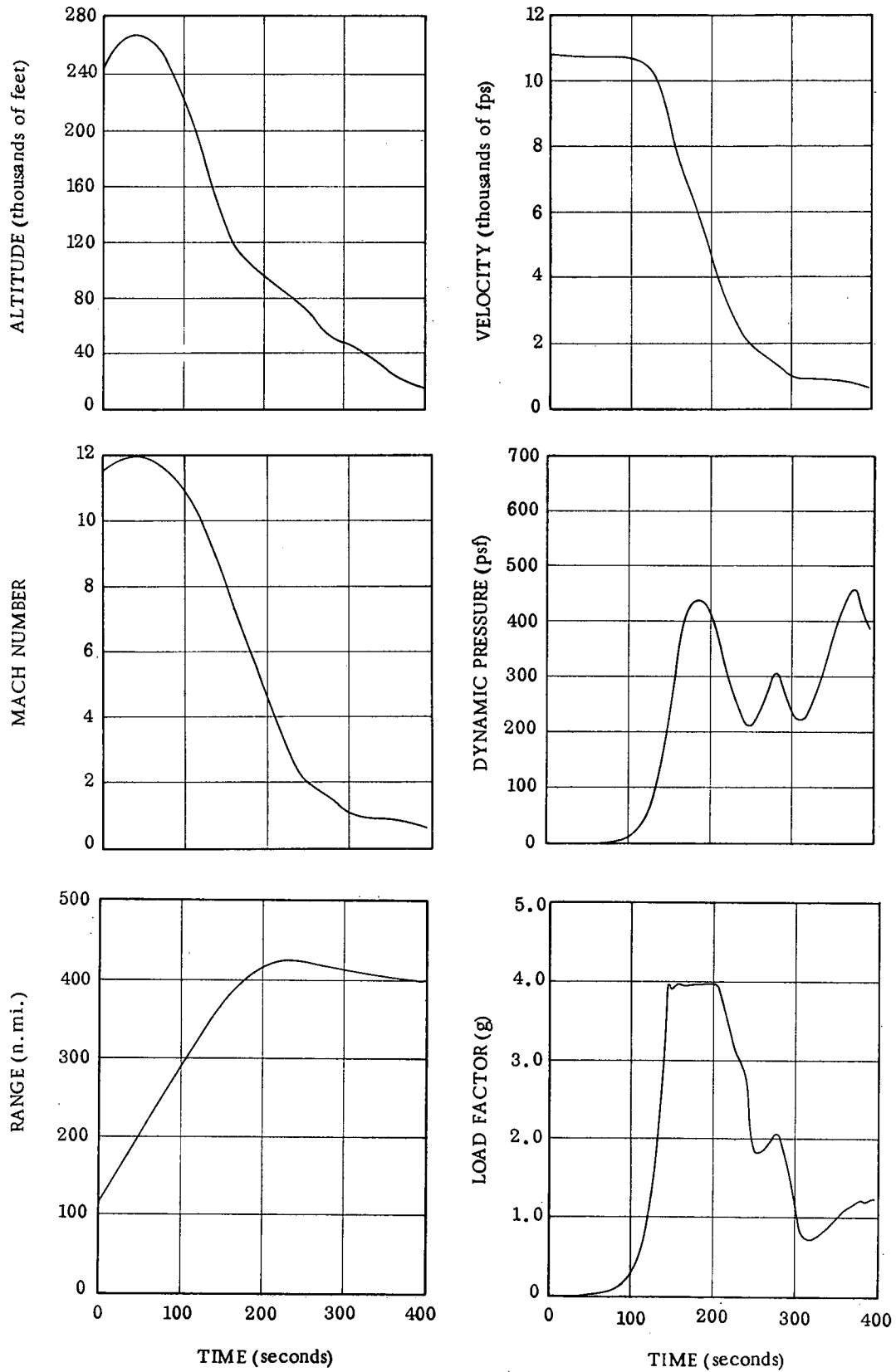


Figure 1-4. Nominal Booster Return Trajectory

touchdown speed at the trimmed power-off C_L for an angle of attack of 14 degrees. The landing distance varies with the vehicle gross weight, but with a touchdown weight of 640,000 pounds, about 5625 feet is required for landing over a 50-foot obstacle. This distance is for a standard-day condition at sea level using braking on a dry concrete runway.

SECTION 2

BASELINE CRITERIA

The booster vehicle is designed to provide adequate structural strength for a safe life of 100 missions, or for a ten year life, without the need for major repairs. This design is capable of withstanding the service life of flight and pressure loads combined with the thermal and acoustic environment. Booster structure is designed for minimum weight commensurate with overall costs and the vehicle is designed to minimize post-flight inspection requirements for rapid turnaround. Design technology will represent that prevalent in 1972.

2.1 DESIGN CRITERIA

Structural components are designed to provide the yield and ultimate factors of safety, proof, and other factors used in the booster design, as shown in Table 2-1. Static and fatigue factors are both summarized in Table 2-1.

Table 2-1. Design Criteria

Component	Yield	Ultimate	Proof	Applied On
Main Propellant Tanks	1.10	1.40	*	Maximum relief valve pressure only
	1.10	1.40	—	Loads (+ limit pressure)
	1.00	—	—	Proof pressures
Personnel Compartments, Windows, Doors, Hatches	1.10	1.50	—	Loads (+ limit pressure)
	1.50	2.00	1.50	Maximum operating pressure only
	1.00	—	—	Proof pressure
Airframe Structure	1.10	1.40	—	Boost + entry loads
	1.10	1.50	—	Aircraft mode loads
Pressure Vessels	—	2.00	1.50	Maximum operating pressure
Pressurized Lines Fittings	—	2.50	1.50	Maximum operating pressure
Fatigue	4.00	—	—	Number of cycles
Flow Growth to Leak or Failure	1.50	—	—	Number of cycles
Thermal Stresses	1.00	—	—	Temperature gradients
*Based on Fracture Mechanics Analysis		Assumed service life = 100 missions		

The LO₂ tank is designed to be proof-tested in segments because of weight savings, using a three-phase proof test. The entire LH₂ tank is designed to be pneumatically proof-tested at room temperature. The thermal protection system (TPS) structure is also designed for the load factors in Table 2-1, as applicable. In addition, an allowable creep strain of 0.2 percent per 10 hours exposure at maximum temperature will be used, and for corrugated panels in the transverse direction, 1.0 percent creep strain per 10 hours exposure at maximum temperature. A minimum clearance of 1.0 inch between the inner tank structure and the outer TPS structure will be maintained at limit load.

The booster is designed to withstand the repeated loads incurred in 400 flights without failure, including acoustic fatigue loads. It will withstand the mission thermal environments with a minimum of post-flight inspection and subsequent structural refurbishment and/or replacement.

The primary structural components will be designed fail-safe insofar as practical, considering weight, cost, and manufacturing. When primary structure fail-safe design is not practical, a safe-life design concept will be applied. The primary structure includes the wing box, tanks, fin box, thrust structure, major bulkheads, inter-tank adapter, and similar major load-carrying structural components or elements such as spar caps and wing/body attach links.

Safe-life designs will be compatible with latest NDI (nondestructive inspection) techniques and limitations, and residual strength and crack propagation analyses will be used to ensure that adequate safe-life has been provided.

Conventional strength, fail-safe, and fatigue analyses will be supplemented by fracture mechanics analysis to determine critical flaw sizes and residual life assuming pre-existing flaws.

2.2 DESIGN CONDITIONS

Booster design conditions were generated from ground handling procedures and from mission flight characteristics. The flight conditions investigated include: launch, ascent, entry, subsonic cruise, and horizontal takeoff and landing. Effects of Mach number, angle of attack, and control surface deflections on longitudinal and lateral directional characteristics were also included. The ground conditions investigated were taxi, towing, mating, and launch preparation and erection.

In most instances, the aerodynamic data was based on available experimental data adjusted for differences between tested and current configuration.

Tables 2-2 and 2-3 summarize limit flight loads for a number of the critical mission conditions. Maximum loads on the body, wing, and canard occur during maximum g

Table 2-2. Limit Airloads

Booster Component	Flight Conditions				
	Max α q Ascent Headwind (Tailwind) (pounds)	Max β q Ascent (pounds)	Max g Recovery (pounds)	Subsonic Gust (pounds)	Landing (pounds)
Body Normal Loads	+537,000 (-220,000)	+130,000	+1,507,000	+488,000	+208,000
Wing (Total Exposed)	+1,446,000 (+173,000)	+665,000	+1,690,000	+1,091,000	+376,000
Canard (Total Exposed)	+80,000 (-80,000)	-41,000	-193,000	+150,000	+47,000
Vertical Stabilizer	—	$\pm 340,000$	—	$\pm 272,000$	—

recovery (i. e., entry), while maximum βq during ascent yields the greatest load on the vertical stabilizer. Design load factors, ground wind conditions, and maximum αq and βq are summarized in Table 2-4.

Internal loads consisting of axial and shear loads and bending and torsion moments were determined at 48 stations along the body length for 16 load conditions. The conditions investigated are:

1. One-hour ground head winds, fueled, unpressurized.
2. One-hour ground tail winds, fueled, unpressurized.
3. One-hour ground side winds, fueled, unpressurized.
4. Liftoff + 1-hour ground head winds.
5. Liftoff + 1-hour ground tail winds.
6. Liftoff + 1-hour ground side winds.
7. Maximum α q head winds.
8. Maximum α q tail winds.
9. Maximum β q.
10. Three-g maximum thrust.
11. Booster burn-out.
12. Maximum g entry.
13. Subsonic gust.
14. Two-point landing.
15. Three-point landing.
16. Two-g taxi.

Table 2-3. Booster B-9U Wing, Canard and Vertical Tail Design Conditions

Condition Description	Component	Cond. No.	Mach No.	Alt. (ft)	α Body (deg)	β (deg)	q (psf)	n_X (g)	n_Y (g)	n_Z (g)	Airload Normal Forces (lb/panel)
Max α q (Headwind)	Wing	W1	1.2	35,000	5	-	500	1.61	0	0.432	723,000
	Canard	C1	1.2	35,000	5	-	500	1.61	0	0.432	40,000
Max α q (Tailwind)	Wing	1	1.2	35,000	-5	-	500	1.67	0	-0.190	56,500
	Canard	1	1.2	35,000	-5	-	500	1.67	0	-0.190	-40,000
Max β q (Launch)	Wing	1	1.2	31,200	-2	4	600	1.60	± 0.213	0.016	333,500
	Canard	1	1.2	31,200	-2	4	600	1.60	± 0.213	0.016	-20,500
	Vertical Tail	T1	1.2	31,200	-2	4	600	1.60	± 0.213	0.016	$\pm 340,000$
Max g Recovery	Wing	W2	6.6	109,550	27.5	-	465	-0.45	0	4.2	845,000
	Canard	C2	6.6	109,550	27.5	-	465	-0.45	0	4.2	-96,500
Entry	Vertical Tail	2	-	-	-	-	-	-	-	-	$\pm 4,270$
	Wing	W3	0.5	SL	5	-	370	0	0	2.2	545,500
	Canard	C3	0.5	SL	5	-	370	0	0	2.2	75,000
Rudder Kick	Vertical Tail	T2	0.5	SL	5	-	370	0	0.50	1.0	$\pm 272,000$
	Vertical Tail	T3	0.5	SL	-	-	370	-	-	-	$\pm 255,000$
3.0g Max Thrust	Wing	3	-	-	-	-	-	3.3	0	0.242	-
	Wing	3	-	-	-	-	-	3.3	0	0.343	-
Landing	Wing	1	0.27	SL	15	-	110	0	± 0.35	2.35	138,000
	Canard	1	0.27	SL	15	-	110	0	± 0.35	2.35	23,500

Notes:

- Covered by other conditions.
- Load-temperature combination not critical.
- Inertia loads for wing-to-body attachment design.
- $\alpha_{wing} = \alpha_{body} + 2 \text{ deg}$
- $\delta_{canard} = -60 \text{ deg (trailing edge up)}$

Table 2-4. Summary of Design Conditions

Condition	Axial Load Factor	Lateral Load Factor	Wind Speed at 60 Feet or αq (βq)	Remarks
Two-Week Standby	1.0		72.1 knots	Unfueled, unpressurized
One-Day Hold	1.0		48 knots	Fueled, pressurized
One Hour to Launch	1.0		34.4 knots	Fueled, unpressurized
Liftoff				
LO ₂ mass	1.31 ± 0.15			
LH ₂ mass	1.31 ± 0.25			
Orbiter & Other	1.31 ± 0.21			
Maximum Dynamic Pressure				
αq	1.71	+0.62, -0.20	±2800 deg-psf	
βq	1.71	±0.15	±2400 deg-psf	
Maximum Thrust	3.0 ± 0.30		±480 deg-psf	
Booster Burnout	3.0 ± 0.30		±100 deg-psf	
Booster Recovery		4.0		
Subsonic Gust		2.05		
Landing		2.0 ± 0.35		

An envelope of the resulting peak load intensities (N_x) for the most critical conditions is shown in Figure 2-1, where N_x is the longitudinal axial load in the tank wall. The major loading conditions on the forward skirt are due to axial loads occurring during boost phase and shear loads during landing and taxiing conditions.

Proof pressures on the LO₂ tank determine the skin gages of domes and the cylinder. Stiffening on the cylindrical body is required for flight and ground loads. The aft dome is grid-stiffened close to the equator because of compressive hoop loads occurring in the partially filled condition. External stiffening, consisting of tee stringers and trussed frames, was optimized for the low load intensities typical of the LO₂ tank, and the results are incorporated in the present design.

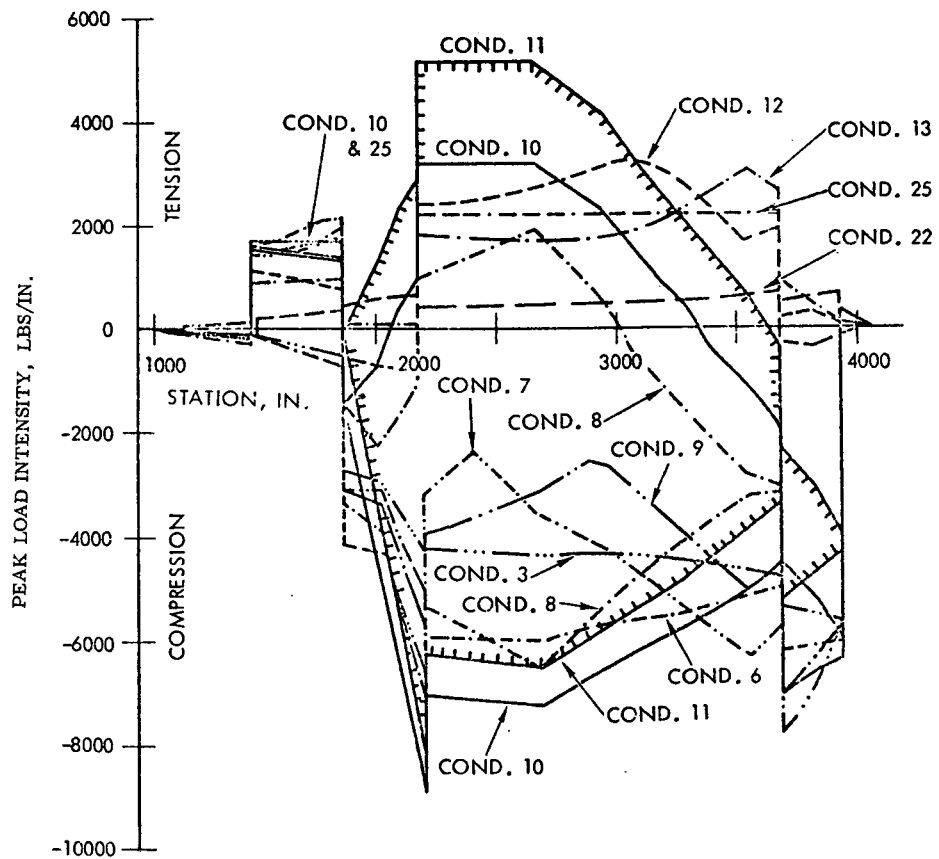
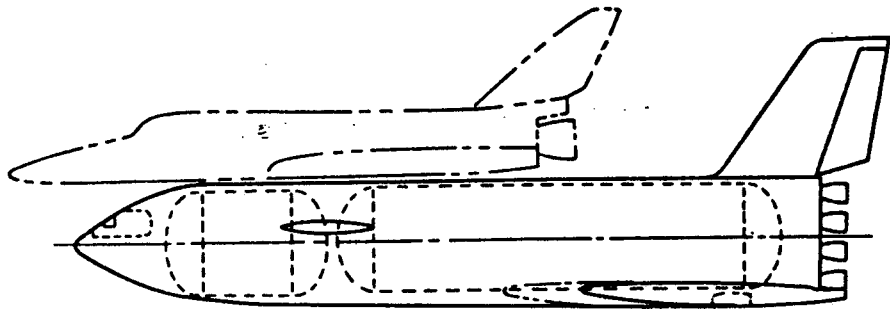


Figure 2-1. Booster B-9U Peak Limit Load Intensities

LH₂ tank skin gages of domes and cylinders are determined by proof-test requirements. Tank stiffening is in the form of external frames and tee stringers sized from axial and bending loads occurring during ground-wind and boost phase loads. An optimization study was performed on stiffening requirements and the results are incorporated in the present design.

Critical design conditions for the intertank adapter are derived from axial loads due to the LO₂ weight forward and the bending and axial load introduced at the forward attachment by the eccentric orbiter weight.

A total of 27 loading conditions on the thrust structure were investigated, including ground-wind, launch, and boost phase loads with and without engine-out conditions. Ground-wind conditions are critical for hold-down fittings, back-up longerons, and adjacent skin on the skirt. Thrust beams, posts, frames, and skin away from hold-down longerons are critical for maximum αq and 3g maximum thrust conditions with one engine out.

Table 2-5 summarizes the orbiter/booster interconnection loads, including loads for a number of critical conditions.

2.3 PROPELLANT TANK PRESSURE

Total gage pressure (including dynamic head) versus tank station at various times during boost is shown in Figure 2-2 for the LH₂ tank. These pressures correspond to the upper bound of a 3 psi regulating band. Also shown is the pressure line for a pneumatic proof test, which requires a proof factor equal to 1.13 based on 150 missions.

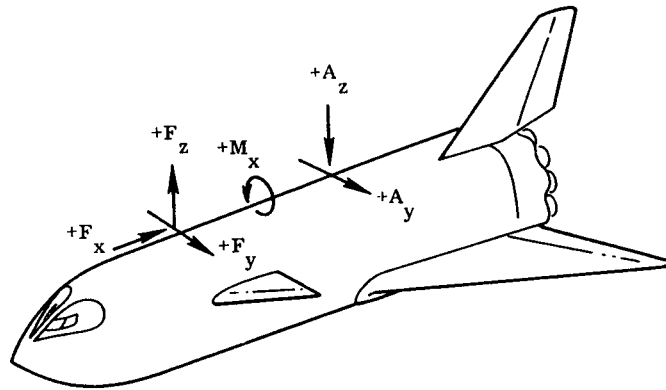
Total gage pressure for the LO₂ tank (including dynamic head) versus tank station at various times during boost is shown in Figure 2-3. These pressures pertain to the upper bound of the relief valve tolerance band. Also shown are the pressure lines for a three-phase proof test program using a 1g LN₂ head on a vertical tank position for the first two phases and a room-temperature pneumatic phase as shown in Figure 2-3. A proof factor of 1.23 is required based on 150 missions.

The tank proof test factors of 1.13 and 1.23 are based on fracture mechanics analysis, assuming the given service life spectrum, material, and flaw growth characteristics.

Critical design conditions for the wing, canard, and vertical tail structure components are summarized in Table 2-6.

Figures 2-4, 2-5, and 2-6 present critical shear moment and torque values, together with bending moment curves, for the wing, canard, and vertical tail respectively.

Table 2-5. Booster/Orbiter Interconnection Loads



Condition	Wind	F_x ($\times 10^3$ lb)	F_y ($\times 10^3$ lb)	F_z ($\times 10^3$ lb)	A_y ($\times 10^3$ lb)	A_z ($\times 10^3$ lb)	M_x (10^6 in-lb)
Two-Week	Head	268		65		-46	
Ground Winds	Tail	268		-151		179	
Unfueled	Side	268	± 121	31	± 37	38	∓ 22.2
1-Hr Ground	Head	859		84		76	
Winds Fueled	Tail	859		25		137	
Unpressurized	Side	859	± 33	75	± 10	99	∓ 6.10
Dynamic Liftoff	Head	1296		112		133	
+ 1-Hr Ground	Tail	1296		74		180	
Winds	Side	1296	± 21	113	± 2	149	∓ 4.52
Max α -q	Head	1628		66		-367	
	Tail	1674		162		846	
Max β -q	Side	1659	∓ 37	134	± 341	488	∓ 50.33
3g Max Thrust	—	2822		168		376	
Booster Burnout	—	2816		115		410	

2.4 DESIGN TEMPERATURES

The major critical thermal environment for the booster occurs during the entry portion of the mission. Local critical heating of the base heat shield and rudder occurs during ascent, and the top of the body and the vertical tail leading edge receive critical heating during orbiter separation.

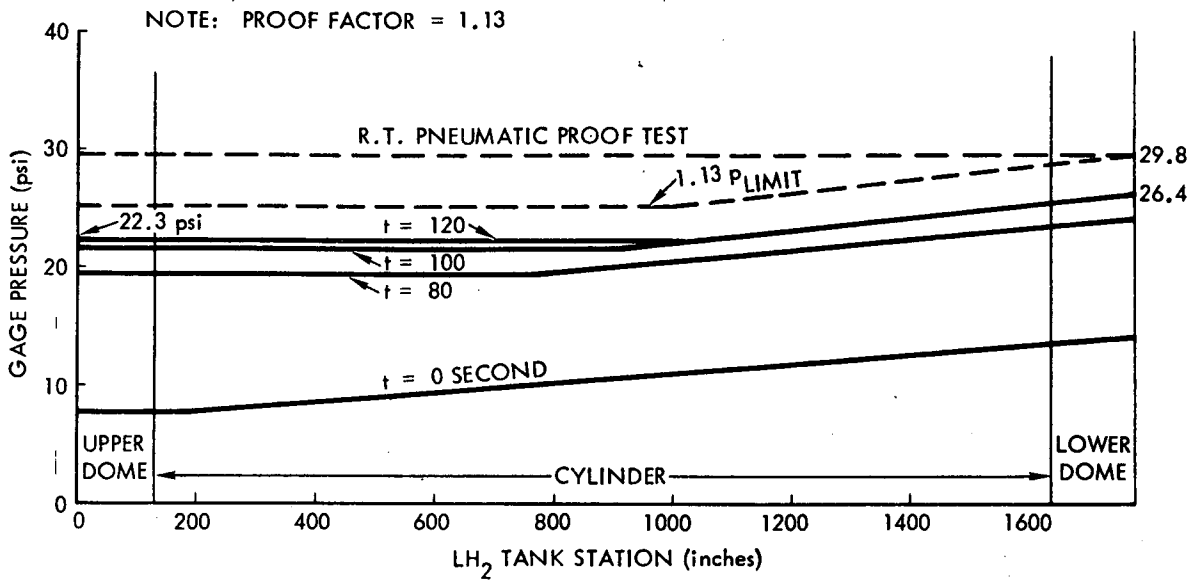


Figure 2-2. LH₂ Tank Gage Pressures Versus Tank Length

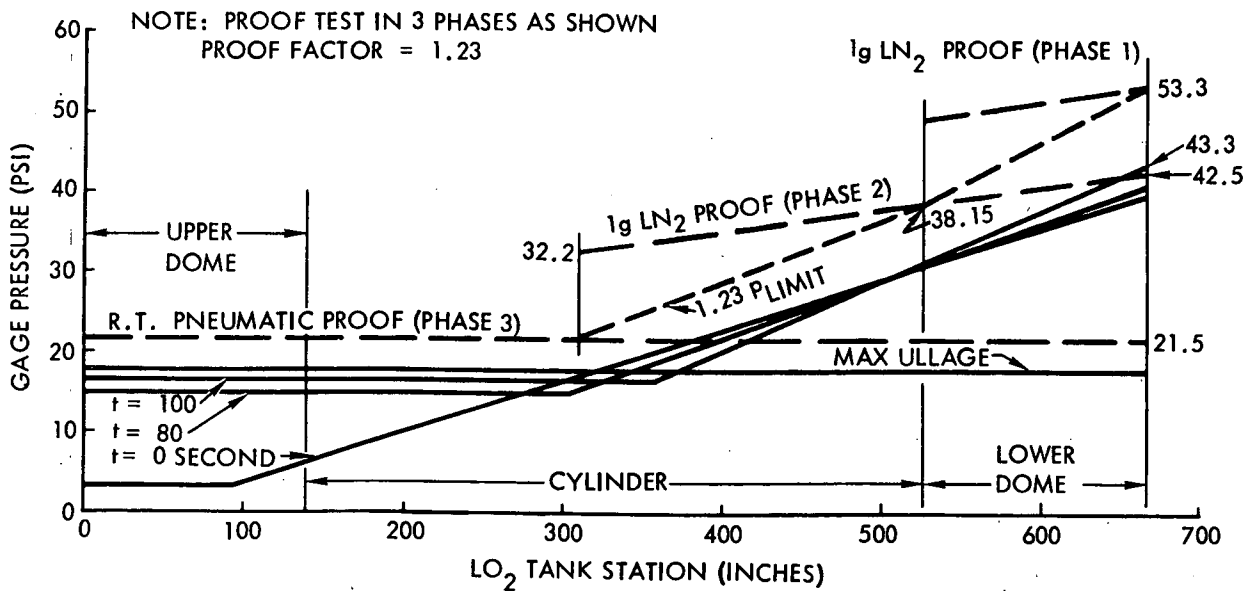


Figure 2-3. LO₂ Tank Gage Pressures Versus Tank Length

Table 2-6. Summary of Design Conditions

Structural Design Summary Chart		
Structural Component	Critical Condition	Design Considerations
Wing: Primary Sub-Structure Upper Skin Panels Lower Skin Panels TPS Heat Shield Elevon Sub-Structure Leading Edge	Max αq ~ Boost Liftoff Sound Pressure Max g ~ Recovery Liftoff Sound Pressure Max g ~ Recovery Max Heating ~ Recovery	Wing Shear & Bending Sonic Fatigue Pressure & Temp Differential Sonic Fatigue Air Pressure Pressure & Temperature
Wing/Body Attachment: Fwd Vertical Attach Center Vertical Attach Aft Vertical Attach Drag Attach Fwd Side Load Attach Aft Side Load Attach Center Side Load Attach	Subsonic Gust ~ Flyback Max αq ~ Boost Max αq ~ Boost Max Thrust ~ Boost Max Thrust ~ Boost Max Thrust ~ Boost Taxi	Safe-Life Safe-Life Safe-Life Fail-Safe Fail-Safe Fail-Safe Fail-Safe
Canard Primary Substructure Torque Tube	Max g ~ Recovery	Canard Structure & Torque Tube Shear, Bending, Torsion
Vert. Tail Primary Structure	Max βq ~ Launch	Box Shear, Bending

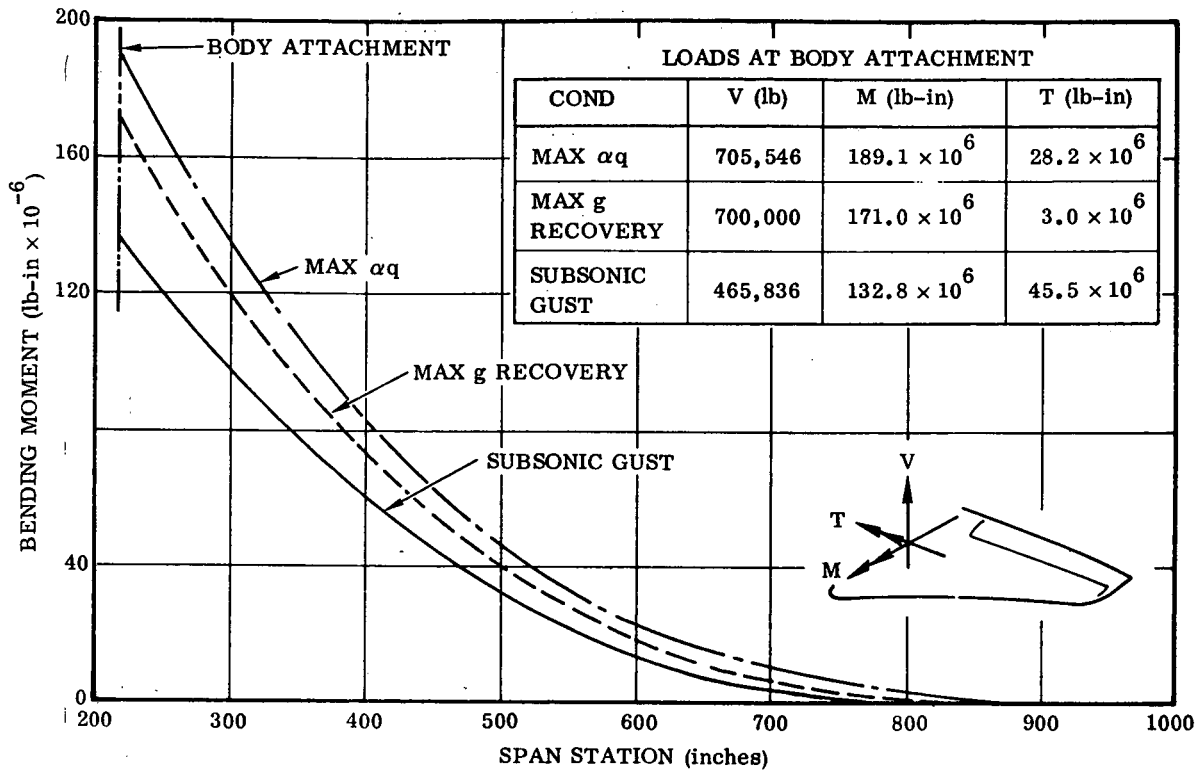


Figure 2-4. Wing Loads (Limit)

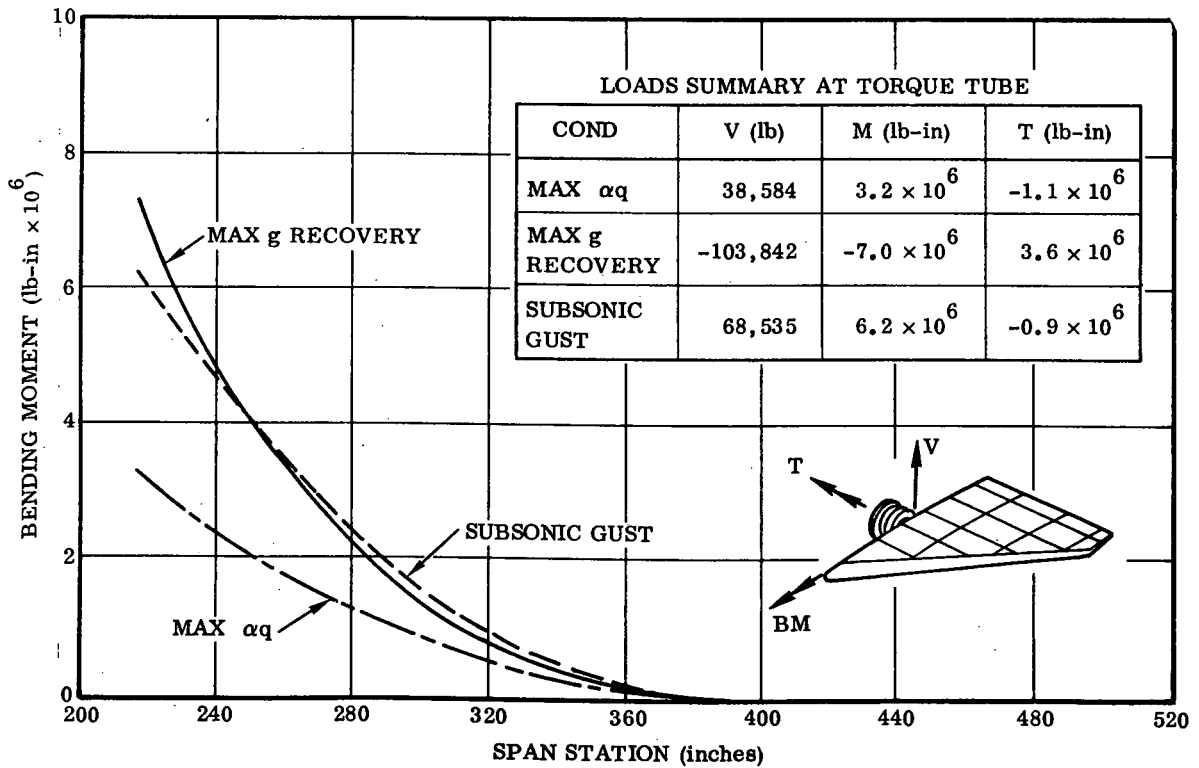


Figure 2-5. Canard Loads (Limit)

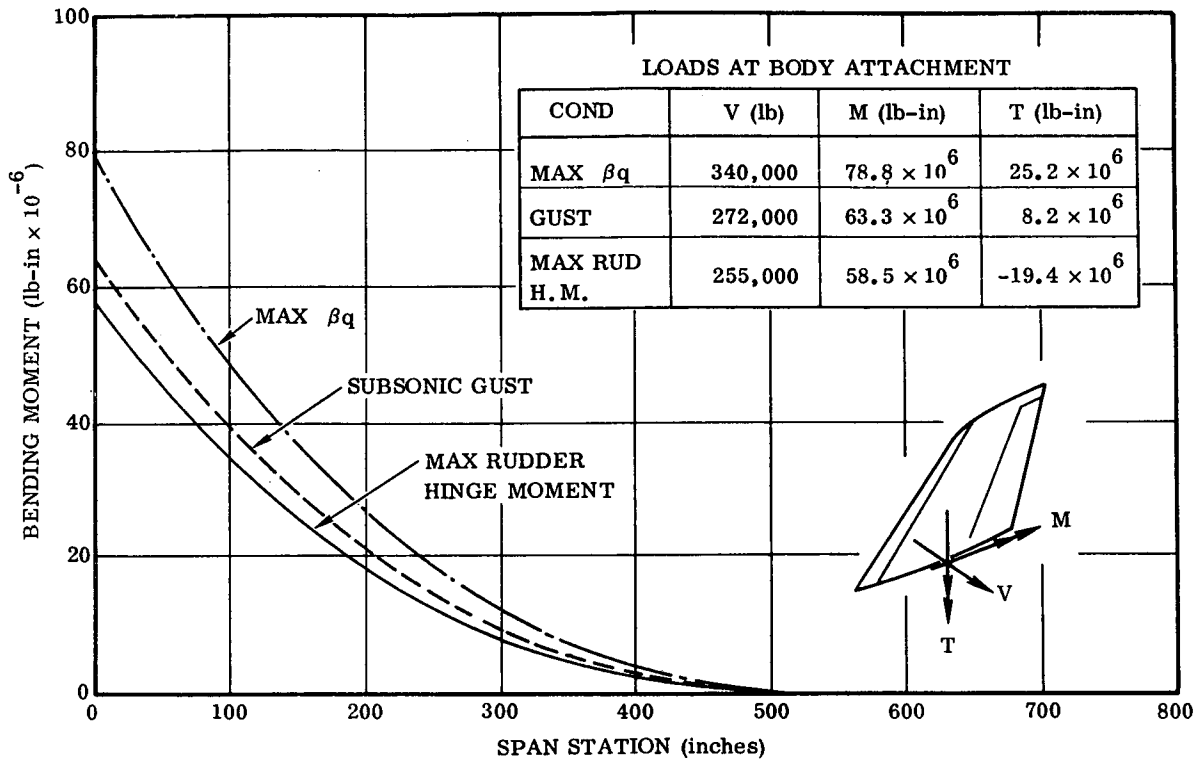


Figure 2-6. Vertical Stabilizer Loads (Limit)

SECTION 3

STRUCTURAL CONFIGURATION

The typical space shuttle vehicle configurations and structural arrangements used throughout the study are for the Convair Phase B B9U delta-wing booster. It has a low wing with a single vertical tail and a small canard surface mounted forward above the body centerline. The body is basically a cylinder with fairings added to streamline the intersections with aerodynamic surfaces. Figure 3-1 is a general view and Figure 3-2 a three-view drawing of the delta-wing booster.

The baseline booster configuration consists of cylindrical tanks to contain the launch propellants and to serve as the structural backbone. Surrounding the basic body structure is an outer heat shield assembly that provides the protective layer against aerodynamic heating and serves as an aerodynamic surface for the body. The aerodynamic surface is a round body-section from the nose to the delta wing, which is attached to the underside of the body structure. The delta wing (with its elevons), canards, and the vertical tail provide the aerodynamic surfaces required for stability and control for both supersonic and subsonic flight.

For the vertical launch mated with the orbiter, booster thrust is provided by 12 main propulsion engines, with a nominal thrust of 550,000 pounds per engine. The engines burn LH_2 and LO_2 and are arranged in the aft end of the vehicle.

Control of the vehicle during powered ascent is provided by gimbaling the main engines for thrust vector control and by using elevons for additional roll control. Subsonic cruise thrust for flyback after a space mission or for ferry flight is provided by 12 airbreathing engines mounted in nacelles. These engines are normally stowed within the wing and body structure envelope during vertical flight and entry.

Attitude control outside the earth's atmosphere is provided by the attitude control propulsion system (ACPS) engines installed on the fuselage and wings. The ACPS engines use LO_2/LH_2 propellants and provide 2100 pounds thrust each.

Landing is accomplished using a conventional tricycle landing gear, including two 4-wheel-bogie main landing gear assemblies and a dual-wheel steerable nose gear assembly.

The booster incorporates a mating and separation system on its top surface to support the orbiter during vertical flight and to separate the two vehicles.

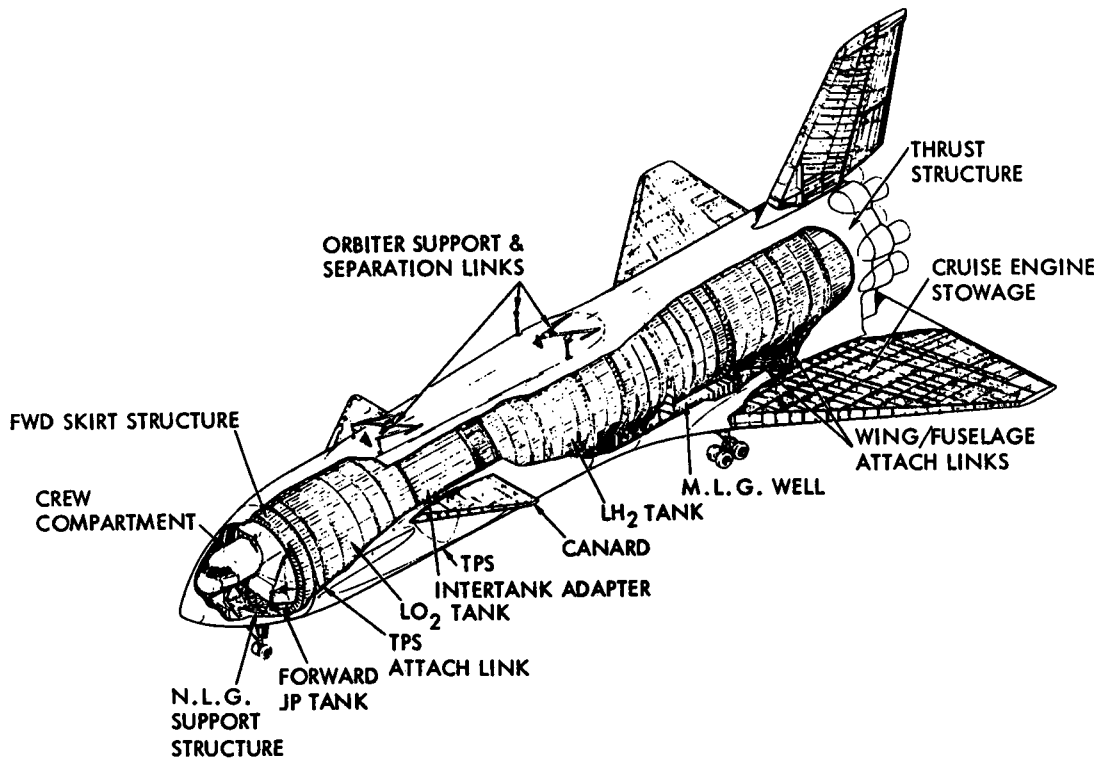


Figure 3-1. B-9U Delta Wing Booster Vehicle Configuration

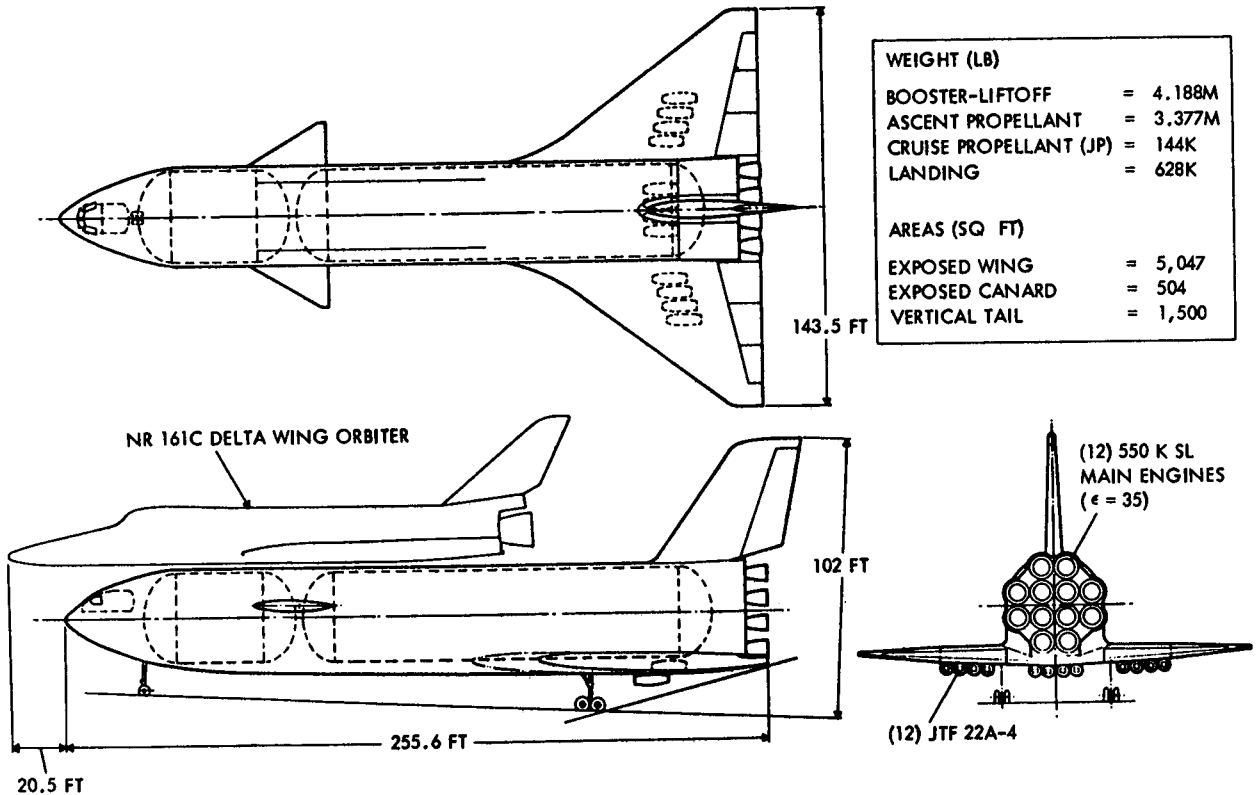


Figure 3-2. B-9U Delta-Wing Booster, Three View

3.1 FUSELAGE STRUCTURE

Internally, the booster is arranged with the LO₂ tank forward and the LH₂ tank aft, as shown in Figures 3-3 and 3-4. The selection of cylindrical tanks with separate, state-of-the-art bulkheads, and of cylindrical intertank section and thrust barrel all combined into a primary load-carrying structure was made to maintain simplicity of the design and manufacture, to increase confidence, and to reduce development risk.

3.2 WING STRUCTURE

The delta wing of the B-9U booster (Figure 3-5) has a continuous carrythrough structure extending underneath the body. Wing geometry reflects an aspect ratio of 2.289 and a maximum thickness ratio that varies from 10.5 percent at Span Station 507 to 8 percent at Span Station 207. The B-9U wing structural concept comprises:

- a. A reusable TPS, which covers the lower surface of the wing and limits wing structure temperatures to moderate levels.
- b. Utilization of highly efficient titanium structure.
- c. Multi-spar, multi-rib substructure sized to ensure that the wing is fail-safe. The wing substructure arrangement is shown in the detail in Figure 3-5.
- d. A wing-to-body attach link system designed to minimize thermal stresses and provide fail-safe capability.

The wing structural arrangement uses open corrugation cover panels on the upper and lower surface. The TPS on the lower surface reduces the temperature sufficiently to allow the use of titanium in the primary structural assemblies. The cover corrugations are positioned in a chordwise direction to minimize thermal stress by accommodating skin expansion relative to the spar caps. The covers transmit air loads to the spars and react wing torsional loads. The wing has a hot leading edge, two primary structural boxes, an under-body carry-through structure, and trailing-edge elevons. The elevons consist of three segments on each side, each segment having two hinge points with actuator attach fittings. Boost-phase venting is accommodated through the gap between the elevon and the fixed trailing edge upper surface.

The wing inboard closing bulkhead redistributes spar shear loads to wing-to-body support fittings, with the wing loads reacted to the body through wing-to-body attach links. The corrugated bulkhead shear web allows for differential chordwise thermal expansion and the attach links accommodate wing deflection and relative thermal expansion between wing and body. Twelve flyback airbreathing engines are submerged in the wing structure during boost and recovery and are deployed for subsonic cruise and landing.

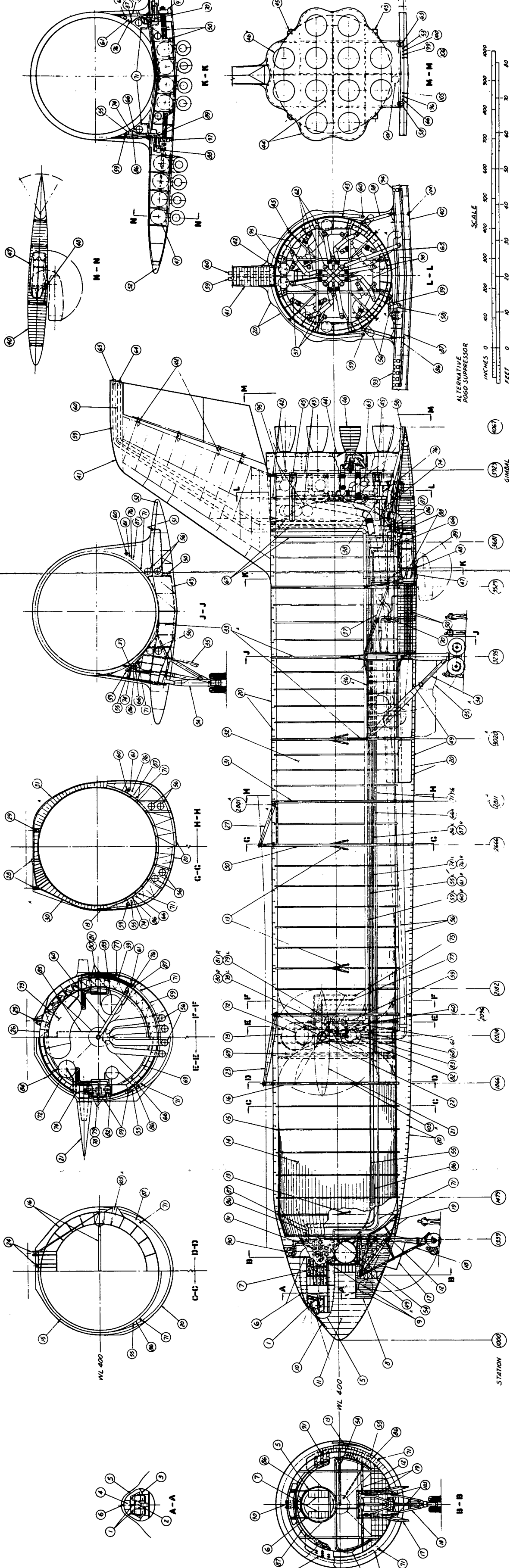
The leading edge, consisting of thin-coated columbium shells, extends forward of the six percent chordline. Extensive segmentation is used to accommodate thermal expansion. A truss linkage system is incorporated to provide support without inducing thermal stresses in the chordwise planes.

The wing TPS is a layer of fibrous insulation covered by a thin corrugated metallic heat shield supported by multiple standoff clips. The heat shield beams the airloads between support clips and protects the insulation from aerodynamic and rain erosion. Although heating rates on the B-9U are substantial, the recovery flight path generates only a modest total heat load because the time at peak heating is relatively low. It is therefore feasible to limit structural temperatures to moderate levels. Sufficient insulation is provided to limit structural temperatures to 650° F. Standoff support clips are distributed at the rate of 1 for every 25 square inches of surface area. Thus, the weight penalties associated with sonic fatigue and creep strain are minimized.

Wing primary structural components are constructed of 6Al-4V annealed titanium, combining high structural efficiency with good fracture toughness characteristics. The reduced working stress levels associated with the fail-safe approach allow longer critical crack lengths and add to the basic integrity of the wing structure. The 650° F structural temperature limit coupled with the short thermal exposure times ensures that problems associated with salt stress corrosion and thermal instability will not arise.

The B-9U wing couples a relatively low aspect ratio with a relatively high thickness ratio. Consequently, the effective cover load intensity due to bending is low, and structural stability requirements penalize distributed cap-type structural concepts in favor of concentrated cap arrangements. The structural concept is based on a concentrated cap approach using square-tube truss construction for spar caps, spar uprights, and spar diagonals. Structural weight comparison studies performed on wing spar components showed the truss-type construction to be substantially more efficient than corrugated webs for carrying spar shear loads. Therefore, corrugated spar webs are used only in the engine bays.

In general, the wing ribs are relatively lightly loaded so that minimum-gage construction can be used in many areas. However, substantial rib stiffness is desirable to ensure effective load redistribution. Minimum-gage corrugated webs are expected to provide a higher stiffness-to-weight ratio than minimum-gage trusses and were thus selected for the wing ribs. The corrugated webs also tend to minimize thermal stress effects. Wing vertical and chordwise shear loads as well as wing torsion loads are redistributed to the wing/body attach fittings by the root closure rib at Span Station 207. In addition, redistribution ribs are provided for all elevon and engine support loads.



LEGEND

1. Pilot Seats
2. Instrument Panel
3. Consoles
4. Overhead Panel
5. Crew Module
6. Crew Module Support
7. Avionics Equipment Racks
8. Nose Gear Wheel Well
9. Crew Access Hatches
10. Retractable Heat Shield
11. Nose Structure
12. Nose Gear Support Bulkhead
13. TPS Support Lines
14. Main LO₂ Tank Structure
15. LO₂ Tank Frame
16. Orbiter Mechanism Support Bulkhead
17. Nose Landing Gear Doors
18. Nose Landing Gear Assembly
19. Nose Gear Support Structure
20. TPS Support Structure
21. Canard Structure Assembly
22. Canard Actuators
23. Forward Orbiter Attachment Mechanism
24. Orbiter Mechanism Attachment Fittings
25. Orbiter Mechanism Attachment Fitting
26. Orbiter Mechanism Support Bulkhead
27. Aft Orbiter Attachment Mechanism
28. Orbiter Mechanism Attachment Fittings
29. Orbiter Mechanism Attachment Fitting
30. Orbiter Mechanism Support Bulkhead
31. Orbiter Mechanism Support Bulkhead
32. Main Hydrogen Tank Structure
33. Main Landing Gear Support Bulkheads
34. Main Landing Gear Assembly
35. Main Landing Gear Doors
36. Landing Gear Drag Load Structural Link
37. Wing Drag Load Structural Link
38. Wing Body Vertical Attach Links
39. Wing Body Side Load Attach Link
40. Wing Structure Assembly
41. Vertical Tail Structure Assembly
42. Vertical Tail Attach Fittings
43. Thrust Structure Assembly
44. Base Heat Shield Assembly
45. Pad Hold-Down & Support Fittings
46. Main Rocket Engines
47. Air Breathing Engine Pods
48. Engine Deployment Power Hinge
49. JP Fuel Tanks
50. JP Fuel Distribution System
51. JP Fuel Refuel Fitting (Level Attitude)
52. JP Fuel Vent Line to Wing Tip
53. JP Fuel Rise-Off Disconnect
54. Main LO₂ Tank Vent Line
55. LO₂ Tank Pressurization Line
56. Main LO₂ Feed Lines
57. Main LO₂ Distribution System
58. Main LO₂ Fill/Drain Line
59. Gas Exhaust Line
60. Main Hydrogen Tank Vent Line
61. Hydrogen Tank Pressurization Line
62. Main LH₂ Distribution System
63. Main LH₂ Fill/Drain Line
64. Main LH₂ Vent
65. Gas Exhaust Vent
66. Purge Nitrogen On-Pad Disconnect
67. Aft Nitrogen Purge Rings
68. Purge Nitrogen To Hydrogen Tank
69. Forward Nitrogen Purge Ring
70. Air Cycle Refrigeration System (2)
71. Refrigeration Lines to Crew Module
72. APS LO₂ Storage Tank Vent Line
73. APS LH₂ Storage Supply
74. APS LO₂ Fill/Drain Line (On-Pad)
75. APS LO₂ Fill/Drain Fitting (Level Attitude)
76. APS LH₂ Fill/Drain Line (On-Pad)
77. APS LH₂ Fill/Drain Line (Level Attitude)
78. APS LO₂ Heat Exchanger (3)
79. APS LO₂ Turbopumps (3)
80. APS LH₂ Heat Exchanger (3)
81. APS LH₂ Turbopumps (3)
82. APS GO Accumulator
83. APS GH₂ Accumulator
84. APS LO₂ Storage Tank Vent Line
85. APS LH₂ Storage Tank Vent Line
86. APS GO₂ Distribution Line
87. APS GH₂ Distribution Line
88. Auxiliary Power Unit (4)
89. APU Exhaust Lines
90. APS Thrusters - (4) Fwd. Pitch
91. APS Thrusters - (8) LH Fwd. Yaw
92. APS Thrusters - (8) RH Fwd. Yaw
93. APS Thrusters - (5) LH Aft Pitch-Roll
94. APS Thrusters - (5) RH Aft Pitch-Roll
95. GHe Storage Supply
96. Helium Fill/Drain Disconnect
97. APU Avionics Racks
98. Aft Avionics Racks
99. Vehicle On-Pad Power Connection
100. ECS On-Pad Connection
101. Maintenance Access Door
102. Rudder Actuators (4)
103. On-Pad Sway Brace Attachment
104. Jack Points
105. APS GO Ground Charge
106. APS GH₂ Ground Charge

Figure 3-3. Inboard Profile B-9U Booster

I-31/32

FOLDOUT FRAME

FOLDOUT FRAME

FOLDOUT FRAME

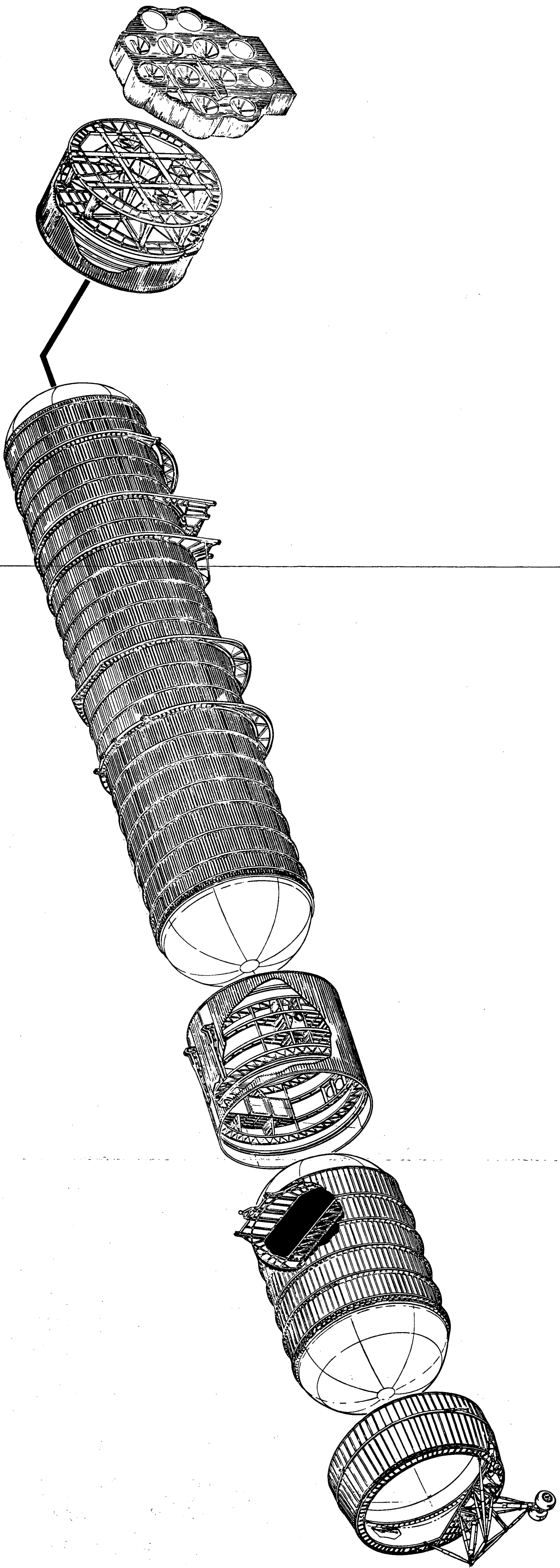


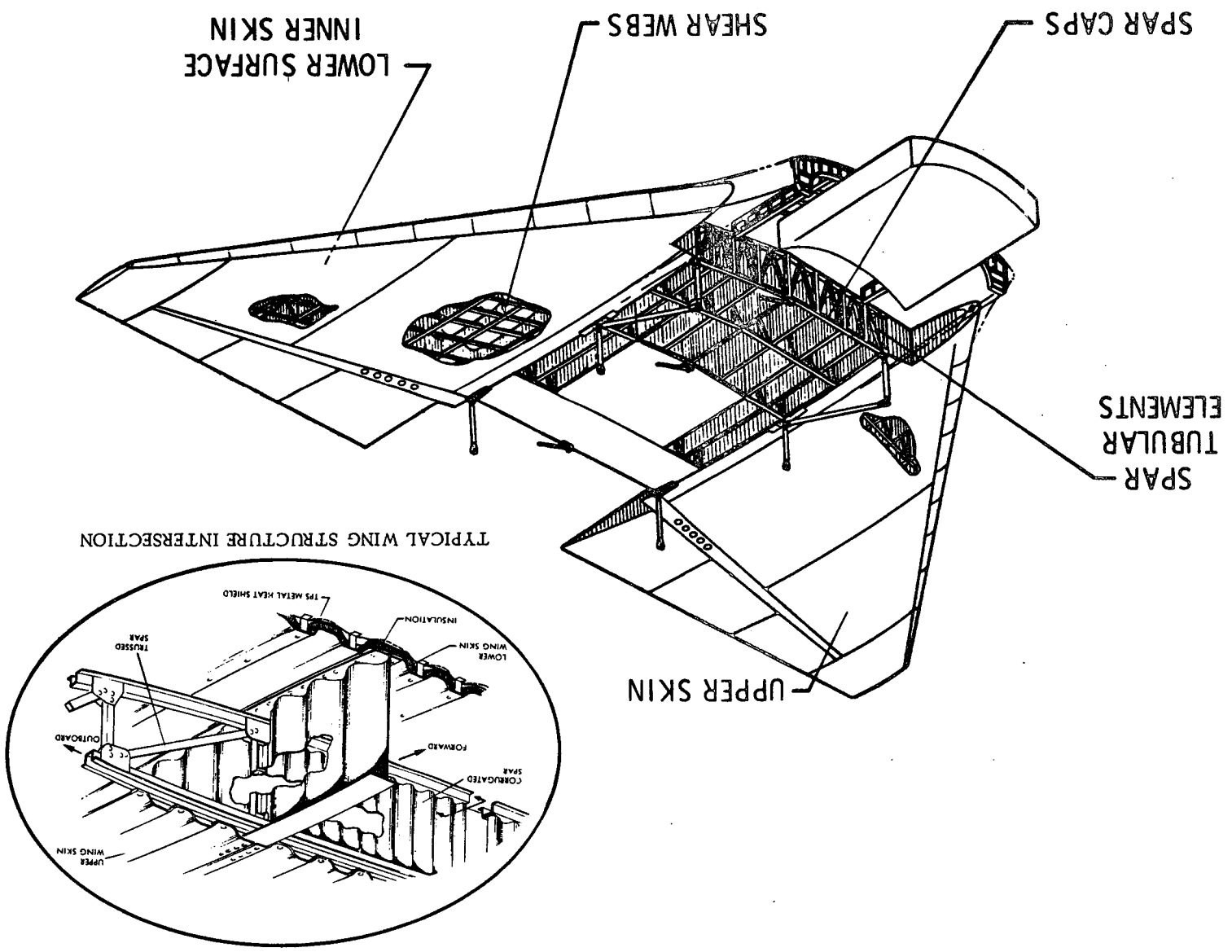
Figure 3-4. B-9U Booster Body Structure
I-33

FOLDOUT FRAME 2

FOLDOUT FRAME 1

FOLDOUT FRAME 3

Figure 3-5. B-9U Wing General Description



Open skin corrugations oriented parallel to the ribs were selected to relieve thermal stresses and provide high resistance to sonic fatigue. The primary structural functions of the skins are to provide torsional shear continuity and to beam air pressure loads chordwise to spanwise support formers. In addition, the lower-surface skin panels provide support for the TPS.

Six wing-to-body vertical attach links and three side load attach links are provided. However, only two drag links are provided in order to eliminate chordwise interaction loads induced by differential thermal expansion between the wing and body. Fail-safe is ensured in all three directions by sizing the side load fittings to react the moments generated by failure of a single drag link. All wing/body attach links are two-force members with spherical bearings at each end. The attach link configuration is designed to minimize wing/body interaction loads due to wing flexure and differential thermal expansion.

3.3 VERTICAL TAIL STRUCTURE

The vertical stabilizer structural arrangement is shown in Figure 3-6. Since the vertical stabilizer and rudder are relatively protected upon reentry by the booster body, 6Al-4V titanium was considered for the skins and substructure of the structural box and rudder. The 6Al-4V titanium material was selected primarily for environmental (650° F) and weight considerations. The selected structural configuration with the bending moments carried in the skins requires a low density material for structural efficiency. Thermal expansion compatibility and environmental considerations led to the selection of the same material for the understructure. In the vertical stabilizer box and the rudder, the spar caps are in contact with the outer skin. Since they are of the same material and nearly the same thickness as the outer skin, differential thermal expansion between the skin and spar caps is minimized. The corrugated webs permit differential thermal expansion between the skin and web.

The vertical tail has an exposed planform area of 1500 square feet, an aspect ratio of 1.28, leading edge sweep angle of 35 degrees, and NACA 0113-64 root chord and NACA 0011-64 tip chord airfoil sections. The rudder hinge line is at 65 percent chord. There are three vertical stabilizer spars: at 10, 37, and 60 percent chord. All three spars carry shear, but only the aft two spars transfer the vertical tail bending moments to the fuselage.

3.4 BOOSTER STRUCTURAL MATERIALS

Materials for the space shuttle booster structure fall into several general categories: 1) aluminum alloys, 2) beryllium alloys, 3) titanium alloys, 4) nickel-base alloys, 5) cobalt-base alloys, 6) columbium alloys, and 7) composite materials. Primary candidate materials have been selected on existing properties data or data generated under space shuttle studies. To provide an efficient final design, the properties of

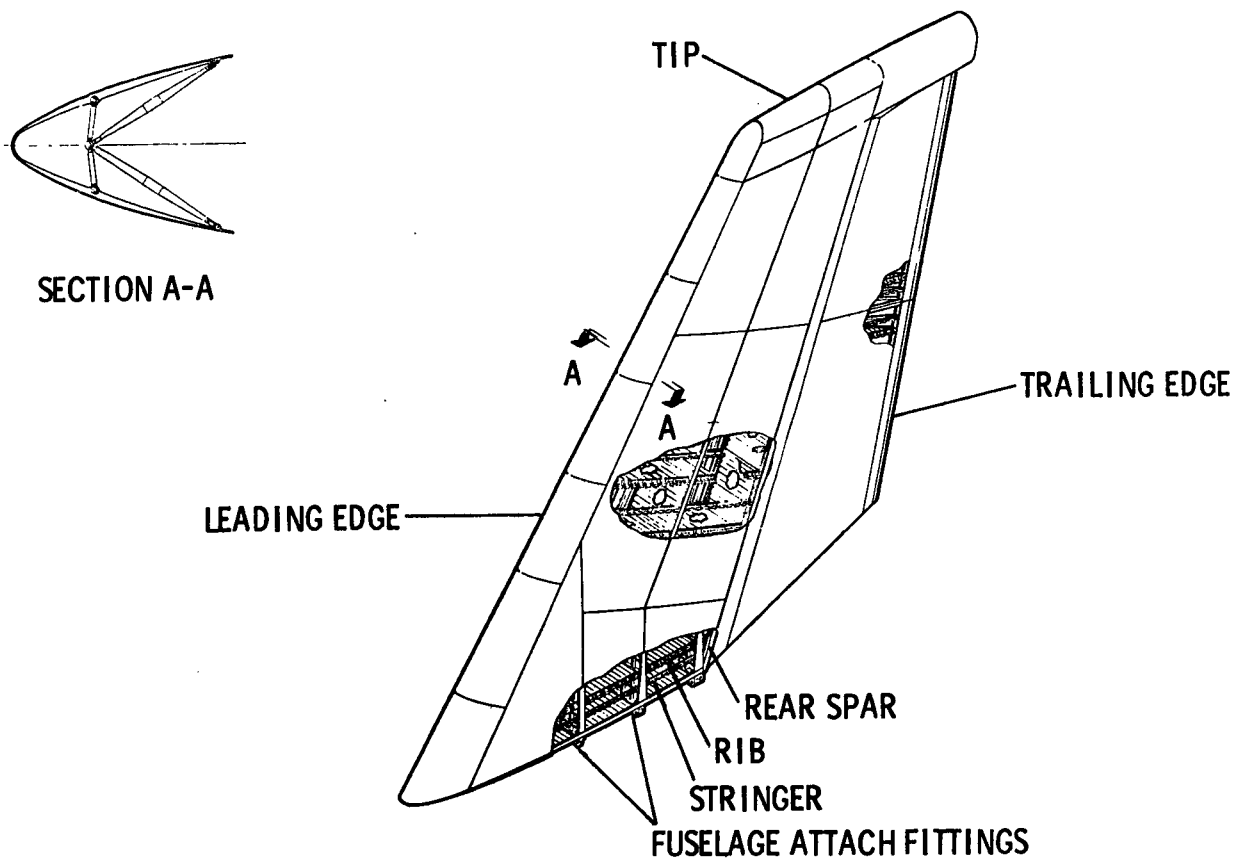


Figure 3-6. B-9U Vertical Stabilizer Configuration

some of these materials must be further investigated to determine their allowable properties after exposure to the expected environments. Table 3-1 lists the primary structural materials for each booster system under detailed study.

The wing box is primarily fabricated from titanium, with a thermal limit of 800° F. Titanium was selected due to its high specific modulus and strength and low thermal stress index at 650° F. It has well defined mechanical and physical properties and the fabrication, machining, and welding techniques are well known.

The basic structural concept of the wing is based on the use of a metallic standoff heat shield combined with insulation between the shield and the wing lower surface structure to provide thermal protection for the entire wing structure (except the hot leading edge). This allows efficient use of titanium for all of the primary and secondary structure above the TPS while allowing the TPS shield itself to be made of HS188 and coated columbium. Haynes 188 material is thermally limited to about 1900° F and coated columbium to 2500° F. Both materials were selected for their thermal strength properties.

The vertical stabilizer structural arrangement is a three-spar, multi-rib configuration with integrally stiffened skin/stringer panels. Spar and rib webs are of corrugated or trussed construction to allow for differential thermal expansion. The rudder is of

Table 3-1. Booster Materials

Booster Components	Sub-Components	Materials
Wing Box	Spar Caps	Annealed Titanium (6Al-4V)
	Spar Webs	Annealed Titanium (6Al-4V)
	Rib Caps	Annealed Titanium (6Al-4V)
	Rib Webs	Annealed Titanium (6Al-4V)
	Intercostals	Annealed Titanium (6Al-4V)
	Lower Surface Thermal Skins	Haynes HS-188/Coated Columbium
	Upper & Lower Structural Skins	Annealed Titanium
	Trusses	Annealed Titanium
Vertical Tail Box	Fasteners	Conventional Except for Lower Thermal Skin
	Spar Caps	Annealed Titanium (6Al-4V)
	Spar Webs	Annealed Titanium (6Al-4V)
	Ribs and Bulkhead Caps	Annealed Titanium (6Al-4V)
	Ribs and Bulkhead Webs	Annealed Titanium (6Al-4V)
	Integrally Stiffened Skins	Annealed Titanium (6Al-4V)
	Stiffeners	Annealed Titanium (6Al-4V)
	Fasteners	Conventional
LO ₂ Tank	Integrally Stiffened Skins	Aluminum Alloy 2219-T87
	Frame Caps	Aluminum Alloy 2219-T8511
	Frame Webs	Aluminum Alloy 2219-T81
	Bulkheads (Dome)	Aluminum Alloy 2219-T81
	Fasteners	Conventional
LH ₂ Tank	Note LO ₂ Tank	Same as LO ₂ Tank Except for Polyphenylene Oxide Insulation
Orbiter Support Bulkhead	Beam Caps	Aluminum Alloy 2219-T81/T851
	Beam Web	Aluminum Alloy 2219-T81/T851
	Bulkhead Caps	Aluminum Alloy 2219-T81/T851
	Bulkhead Webs	Aluminum Alloy 2219-T81/T851
	Fasteners	Conventional
Thrust Structure	Skins	Annealed Titanium (6Al-4V)
	Thrust Beams	Annealed Titanium (6Al-4V)
	Thrust Posts	Annealed Titanium (6Al-4V)
	Bulkheads	Annealed Titanium (6Al-4V)
	Vertical Stabilizer Attach Fittings	Annealed Titanium (6Al-4V)
	Intermediate Frames	Annealed Titanium (6Al-4V)
	Attachment Flange	Annealed Titanium (6Al-4V)
	Fasteners	Conventional
	Base Heat Shield	René 41 & coated Columbium

similar construction. The entire structure is titanium except for the leading edge, which is Inconel 718. The segment of leading edge subjected to orbiter engine exhaust impingement is heat-sink designed to withstand the increased temperature.

The main LO₂ and LH₂ fuel tanks are fabricated almost entirely of 2219 aluminum. Both 2219 and 2014 aluminum alloys were considered for the main tanks and other body structures. Both alloys possess excellent strength-toughness properties in the base metal at all temperatures down to -423° F, with the 2014 alloy somewhat stronger than 2219. However, welded joints in the 2014 alloy exhibit a tendency towards brittle, premature fracture and greater sensitivity to minor weld flaws at LO₂ to LH₂ temperatures. The significantly greater resistance to stress-corrosion possessed by the 2219 alloy has been thoroughly demonstrated, as has its superior weldability and weld repairability. The combination of better fracture toughness in welded joints at reduced temperatures and superior resistance to stress and corrosion result in a significantly higher reliability for the 2219 alloy.

Both 2219 and 2014 exhibit a decrease in strength properties as plate thickness increases, although the ultimate and yield tensile strengths of 2014 decrease at a greater rate than those of 2219. Consequently, if the tank walls must be machined from 3- to 4-inch plate to accommodate integral stiffeners or weld lands, the strength advantage of 2014 is minimized.

Although 2014 shows an advantage in strength of the base metal, Convair Aerospace's choice of the 2219 aluminum alloy for the space shuttle propellant tankage is based on superior weldability, much better resistance to stress/corrosion cracking, better overall toughness, and better reliability for the reusable manned space launch vehicle.

The LO₂ tank is a welded assembly of 2219 aluminum alloy with forward and aft circumferential bolt patterns for joining it to the forward skirt and to the intertank adapter structures. Tank wall segments, with integral stringers, are milled from aluminum alloy plates, age-formed to radius and butt-welded together to make the cylindrical tank section.

Stabilizing frames, external to the LO₂ tank are spaced at 77-inch intervals. The frames are built up of a series of V forgings riveted between an outboard T flange and the longitudinal stringers of the tank. The Vs, in conjunction with the outboard flange and the tank wall, form a truss-webbed stabilizing frame.

Since the temperature of LO₂ will not liquify air on the tank's exterior, no cryogenic insulation is installed.

The LH₂ tank is similar in construction to the LO₂ tank, although the integral T-section stringers are more closely spaced to develop higher compression allowables. Polyphenylene oxide (PPO) foam attached to the inside of the tank wall provides cryogenic insulation and prevents condensation of liquid air on the exterior surface.

With all stringers, frames, and bulkheads external to the LH₂ tank, the inside of the tank wall presents a smooth surface for a reliable bonded attachment of the PPO foam insulation. A silane modified polyurethane adhesive (7343) is currently being considered.

The forward orbiter attachment station is at the tangency of the ellipsoidal dome with the cylindrical section of the LO₂ tank. A machined aluminum alloy internal/external bulkhead is integrated with the tank wall at this station. To achieve maximum bulkhead depth, part of the bulkhead extends beyond the tank skin to support the forward orbiter attachment links. A short segment of tank wall integrally machined with stiffeners and a circumferential bulkhead flange provides bulkhead cap structure and allows installation of the inner and outer bulkhead structure. Tank skin forward and aft of the bulkhead is butt-welded to the short integral section. The orbiter bulkhead is stiffened using a removable beam running internally across the tank.

The thrust structure is a stiffened titanium shell bolted to the aft end of the LH₂ tank. It contains two transverse trussed-type bulkheads spaced 81 inches apart. These bulkheads distribute loads from the vertical stabilizer, the aft wing attachment struts, and the gimballed rocket engines into the shell structure. Trusses in longitudinal planes between the bulkheads comprise four thrust beams to which the rocket engines are attached.

Spherical segments are installed on each rocket engine to provide a sealing surface for deflected engine positions. A mating ring and seal for each engine is supported from the aft structural bulkhead of the thrust structure.

A heat shield fabricated from coated columbium and René 41 corrugated panels and backed by insulation material is installed between and supported from the seal rings. The circumference of the base heat shield is defined by the rocket engine fairings. The skin extending forward of the base heat shield is part of the body TPS.

SECTION 4

BOOSTER WEIGHT SUMMARY

Table 4-1 is a summary weight statement for the delta wing booster in the launch condition. This launch condition is for the mission described earlier, and assumes that the orbiter launch weight will be about 859,000 pounds. The weights are broken down to show individual major system weights.

Table 4-2 shows the wing group weight breakdown. Weights are detailed to show both exposed wing and carry-through structure. The wing structural weights are separated into major components such as spars, ribs, skins, etc.

Table 4-3 details the weight breakdown for the entire vertical tail. Individual weights are shown for the spars, ribs, skins, etc.

Table 4-4 shows the body group weights, which are broken down to show individual details for the thrust structure and the main LO_2 and LH_2 tanks. The body outer heat shield is not included as part of the body weight, but is covered under induced environmental protection in Table 4-1.

Table 4-1. Delta Booster Weight Summary

	Weight (pounds)
Wing Group (See Table 4-2 for breakdown.)	70,875
Tail Group	20,634
Vertical Tail (See Table 4-3 for breakdown.)	13,121
Canard	7,513
Body Group	177,612
LH ₂ Tank (See Table 4-4 for breakdown.)	67,109
LO ₂ Tank (See Table 4-4 for breakdown.)	18,405
Thrust Structure (See Table 4-4 for breakdown.)	30,000
Other Body Structure	62,098
Induced Environmental Protection	72,031
Landing, Docking	27,361
Propulsion, Ascent	130,038
Propulsion, Cruise	46,404
Propulsion, Auxiliary	9,864
Prime Power	3,011
Electrical Conversion and Distribution	1,438
Hydraulic Conversion and Distribution	1,862
Surface Controls	7,889
Avionics	5,468
Environmental Control	1,475
Personnel Provision	985
Contingency	49,593
Subtotal (dry weight)	626,540
Personnel	476
Residual Fluids	11,534
Subtotal (inert weight)	638,550
Inflight Losses	22,080
Propellant - Ascent	3,382,307
Propellant - Cruise	143,786
Propellant - Maneuver and ACS	1,500
Total Booster Weight at Liftoff	4,188,223

Table 4-2. Wing Group Weight Breakdown

	Weight (pounds)
EXPOSED WING	54,203
Structural Box	29,469
Spars	14,550
Webs	4,176
Caps	6,868
Splices	3,506
Ribs	5,156
Webs	3,512
Caps	1,644
Upper Covers	5,360
Covers	4,378
Formers	982
Lower Covers	4,403
Covers	2,558
Formers	764
Engine Bay Formers	1,081
Leading Edge	3,996
Trailing Edge	681
Secondary Structure	11,678
Thermal Protections Skins, Insulation, and Standoffs	8,122
Fairings - Wing to Fuselage	1,000
Engine Bay Doors	2,108
Door Actuation	448
Elevons	8,379
WING CARRY-THROUGH STRUCTURE	16,672
Structural Box	15,450
Spars	9,073
Webs	1,669
Caps	7,404
Ribs	4,333
Webs	2,498
Caps	1,835
Lower Covers	1,650
Covers	818
Formers	292
Engine Bay Formers	540
Wing-to-Fuselage Attach Fittings	394
Leading Edge	622
Secondary Structure	600
Wing-to-Fuselage Attach Links	600
Total Wing Group Weight	70,875
NOTE: The wing carry-through lower surface coverings and doors blanked out by the fuselage act as body heat shield structure; therefore, their weights have been included under Induced Environmental Protection. The items allocated to Induced Environmental Protection include:	
Belly Skins, Insulation, and Standoffs	3,765
Engine Bay Doors	1,054
Main Landing Gear Doors	2,108
Total	6,927

Table 4-3. Vertical Tail Group Weight Breakdown

	Weight (pounds)
STRUCTURAL BOX	9,301
Spar Caps	779
Front	49
Intermediate	351
Rear	338
Auxiliary	41
Spar Webs	1,249
Front	146
Intermediate	443
Rear	464
Auxiliary	196
Ribs and Bulkheads	1,485
Root Rib	271
Interspar Ribs	379
Bulkheads	835
Chordwise Stiffeners	567
Covers	4,517
Hinge Fittings (Integral with Spars)	168
Tail to Fuselage Attach Fittings and Fasteners	536
LEADING EDGE	866
Covers	292
Trusses and Supports	574
TRAILING EDGE	316
Covers	235
Stiffeners	30
Ribs	51
TIP	509
RUDDER	2,129
Total Vertical Tail Group Weight	13,121

Table 4-4. Body Group Weight Breakdown

	Weight (pounds)
MAIN LH ₂ TANK	67,109
Forward Dome	1,947
Aft Dome	1,947
Barrel Section	57,290
Skin/Stiffeners	52,658
Frames	4,632
Baffles	575
Orbiter Attach Structure	5,350
Forward Bulkhead	1,650
Aft Bulkhead	800
Load Distribution (weight required for)	2,900
LH ₂ TANK INTERNAL INSULATION (PPO FOAM)	7,168
MAIN LO ₂ TANK	18,405
Forward Dome	1,405
Aft Dome	2,902
Barrel Section	9,583
Skin/Stiffeners	9,138
Frames	445
Baffles	1,200
Orbiter Attach Structure	3,315
Forward Bulkhead	2,690
Load Distribution (weight required for)	625
NOSE SECTION	10,135
FORWARD ADAPTER SECTION	3,652
INTERTANK BASIC STRUCTURE	14,141
ORBITER BULKHEADS — INTERTANK SECTION	5,482
THRUST STRUCTURE	30,000
Skin Panels	9,579
Frames	2,470
Thrust Beams	6,284
Thrust Posts	3,060
Ground Fittings	1,332
Bulkheads	5,509
LO ₂ Line Backup	200
Tank Attach Bolts	250
Joints,Splices, and Fasteners	1,316
OTHER MISCELLANEOUS AND SECONDARY STRUCTURE	21,520
Crew and Avionics Compartment	1,800
Engine Heat Protection	5,235
Orbiter Attach and Separation Mechanism	3,655
Main Landing Gear and Wing Bulkheads	10,830
Total Body Group Weight	177,612

- b. Condition W2. Recovery at maximum g. Maximum g occurs 150 seconds into the flight return (reference Figure 1-4), which is 335 seconds from liftoff. Temperatures vary throughout the structure at this time, as shown in Figures 5-2 through 5-4, and an average temperature of 300° F is assumed constant for the complete box. Limit loads are factored by 1.4 to arrive at ultimate design loads.
- c. Condition W3. 50 foot per second gust in the subsonic flight regime. The structure is at room temperature and an inertia relief (2.2 g) is included in the loads. Since the vehicle is flying in the airplane mode, the loads are factored by 1.5 to determine ultimate design loads.
- d. Condition W4. Recovery at maximum temperature. From Figures 5-2 through 5-4, maximum temperatures occur between 385 and 460 seconds after liftoff, approximately 220 seconds into the return flight. At this time (reference Figure 1-4), the vertical inertia factor $n_z = 3.5$. This relief is accounted for in the wing loads and an ultimate load factor of 1.4 is used. An average temperature of 700° F is applied to the complete box structure.

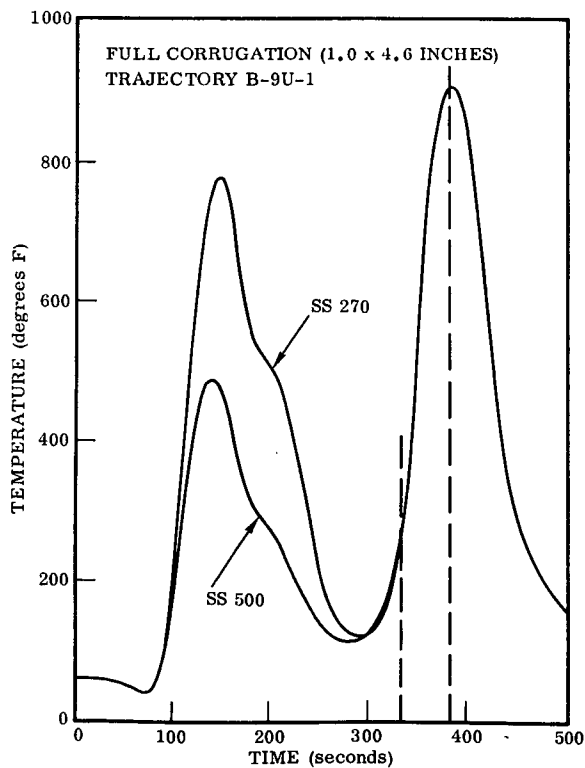


Figure 5-2. Wing Upper Surface Radiation Equilibrium Temperatures

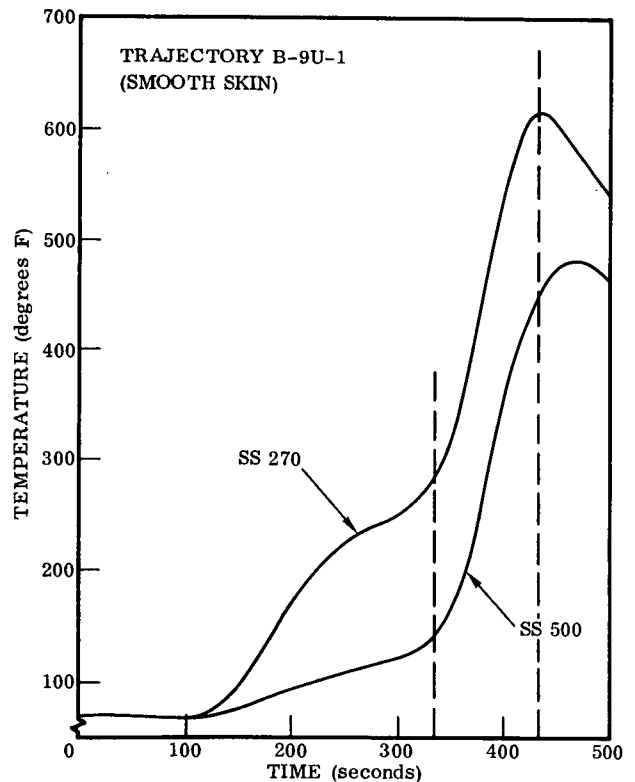


Figure 5-3. TPS Wing Lower Surface Temperature, Inner Skin

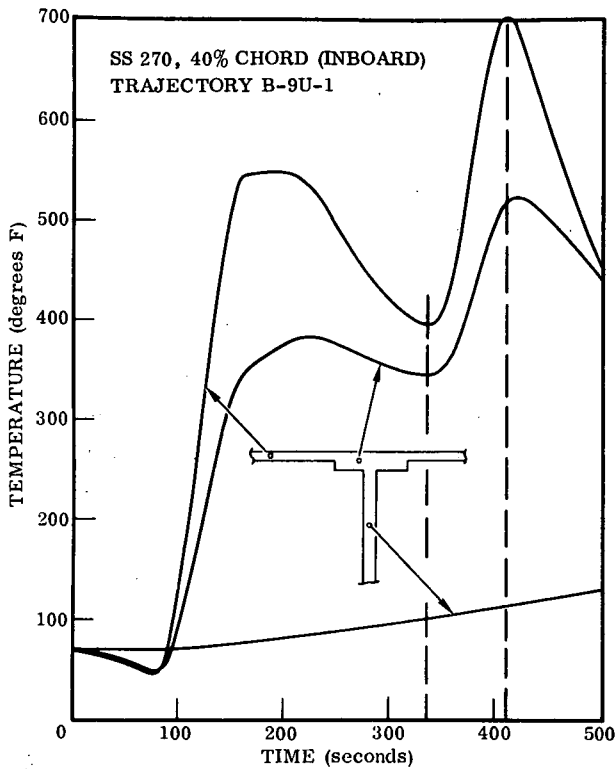


Figure 5-4. Wing Upper Surface Rib Cap Temperature Distribution

5.2 VERTICAL TAIL STRUCTURAL ANALYSIS

Because the vertical stabilizer structural box is swept and because of the very localized pickup at the fuselage, the structure does not lend itself to a simple box beam analysis. To account for this, a finite-element solution has been prepared using the program developed for analyzing the wing structure. The structural simulation model, which consists of 80 nodes and 383 constant stress elements, is shown in Figure 5-5. The X and Y coordinates for the various nodes are shown in the figure; the Z coordinates were obtained from the two airfoil sections plotted in Figure 5-6. Quadrilateral plate elements simulate the skin in shear; orthotropic triangles with negligible shear stiffness are superimposed to simulate the unidirectional extensional stiffness of the skin.

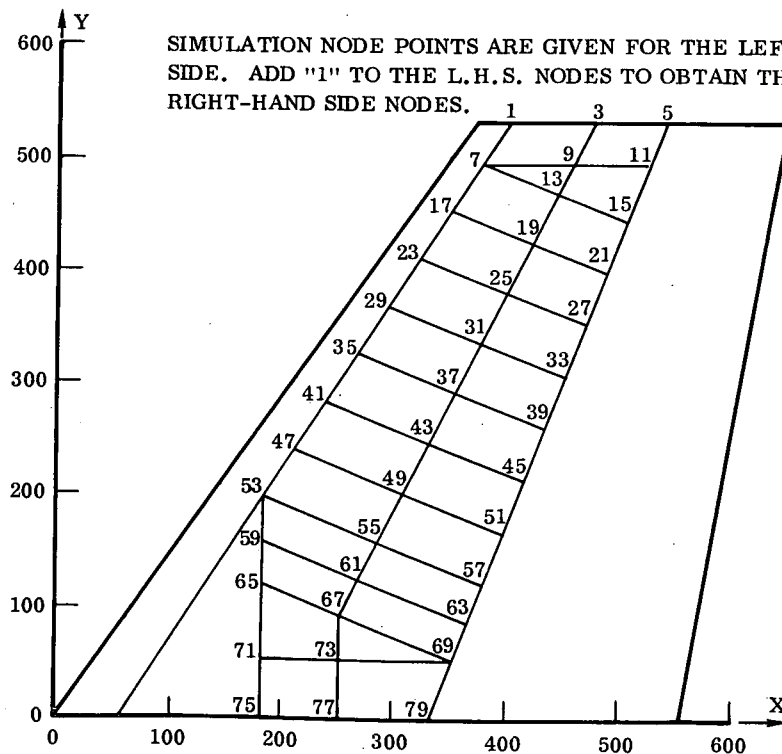


Figure 5-5. B-9U Vertical Stabilizer Structural Simulation Model

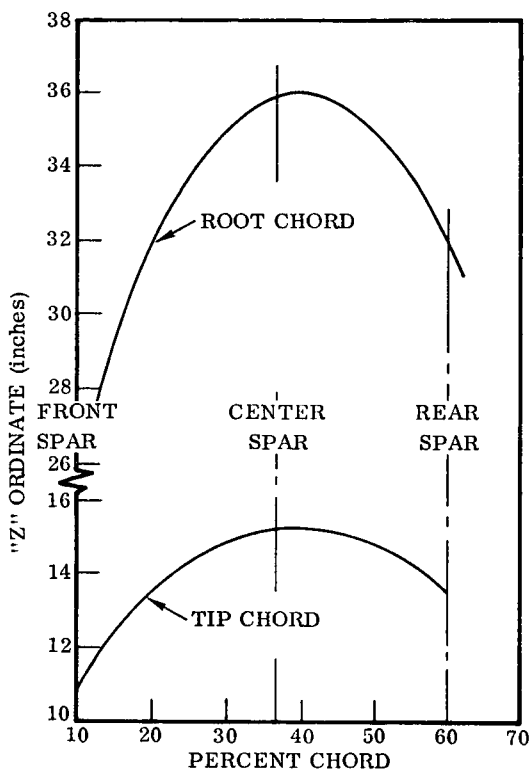


Figure 5-6. B-9U Vertical Stabilizer Airfoil Sections

NETLD 2 computer program. This program determines net station loads due to a specified loading system for each of two interconnected vehicles at specified stations along the vehicle longitudinal reference axis. The loading system consists of the external and internal loading systems.

The external loading system includes aerodynamic loads, point loads, engine thrust loads, and trim loads due to engine gimbaling. Aerodynamic loads for each vehicle are input in the form of running load distributions along the longitudinal reference axis of each vehicle. These loads consist of a distribution for vertical lift loads, lateral lift loads, and axial drag loads. Point loads for each vehicle are input in the form of load and moment components at any specified coordinate location in the directions of the vehicle local axis system. Total engine thrust for each vehicle is also a required input.

The internal loading system includes longitudinal and spanwise weight distributions from which loads due to vehicle acceleration in the three coordinate directions (as well as pitch, roll, and yaw accelerations) are calculated. Fuel weight distributions are obtained for each flight condition.

Three vertical tail conditions are investigated:

- Condition T1 — Maximum βq , during launch.
- Condition T2 — Subsonic gust.
- Condition T3 — Rudder kick.*

All three conditions are considered at room temperature. Condition T1 has an ultimate load factor of 1.4, while the other conditions, being in the airplane mode, have a 1.5 ultimate load factor over the design limit loads.

* Rudder kick is a condition whereby the rudder is abruptly moved from zero deflection to maximum deflection.

5.3 FUSELAGE STRUCTURAL ANALYSIS

Net external loads along the length of the fuselage are calculated with the aid of the

Mated vehicle interconnect loads are determined by isolating each vehicle and calculating the loads required to put each vehicle in balance with the individual external and internal loading system. The interconnect loads are then included in the external loading system of the individual vehicle and net loads determined at the specified stations. Critical axial load intensities in the fuselage shell are then derived using the loads from NETLD 2.

To analyze the fuselage structure, the computer program described in AFFDL-TR-70-118, An Automated Procedure for the Optimization of Practical Aerospace Structures, was used. This automated structural optimization program (ASOP) is used to aid in the near-minimum weight design of large-scale aerospace structures subjected to statically applied loads with both stress and deflection limitation. The program incorporates a newly developed synthesis algorithm with the well known finite-element methods of analysis. A detailed discussion of the synthesis algorithm and its implementation is presented in the AFFDL report. This program makes it possible to investigate detailed structural weight sensitivities to various loading parameters.

With modification to the NETLD 2 program, point loads are derived in the format required by ASOP. These loads are applied to the structural model shown in Figure 5-7, with the model constrained at the thrust structure. Output includes member loads, areas, stresses, and weights plus a total weight for the complete structure.

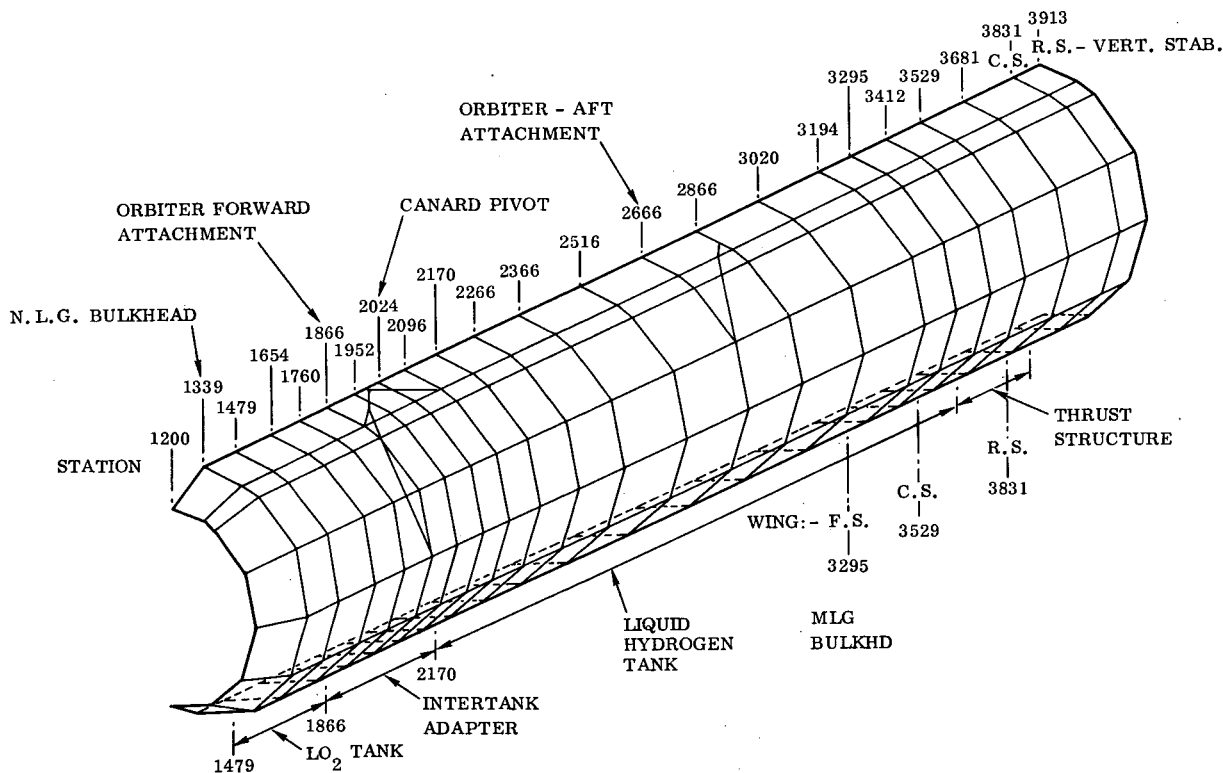


Figure 5-7. B-9U Fuselage Structural Model

SECTION 6

DESIGN CONDITION IDENTIFICATION

6.1 WING STRUCTURAL WEIGHT SENSITIVITIES

The finite-element program calculates weights for the basic box structure excluding the leading edge, elevons, and trailing edge. Weights are presented for the wing on one side of the vehicle only.

Figure 6-1 shows Condition W2, recovery with maximum g, to be the most critical condition. Condition W1, maximum ascent αq , has a greater wing load, but this is offset by the combination of wing load with elevated temperature for Condition W2. The maximum temperature condition, W4, does not prove to be critical and the subsonic gust condition, W3, is the least critical of the four conditions considered.

Table 6-1 indicates that wing weight is not particularly sensitive to any loading parameter. (There is only 17 percent difference in weight between the lightest and heaviest structures.) Conditions W1 and W2 have almost identical structural weights. Total weights for each material type show Condition W2 to be the critical design condition;

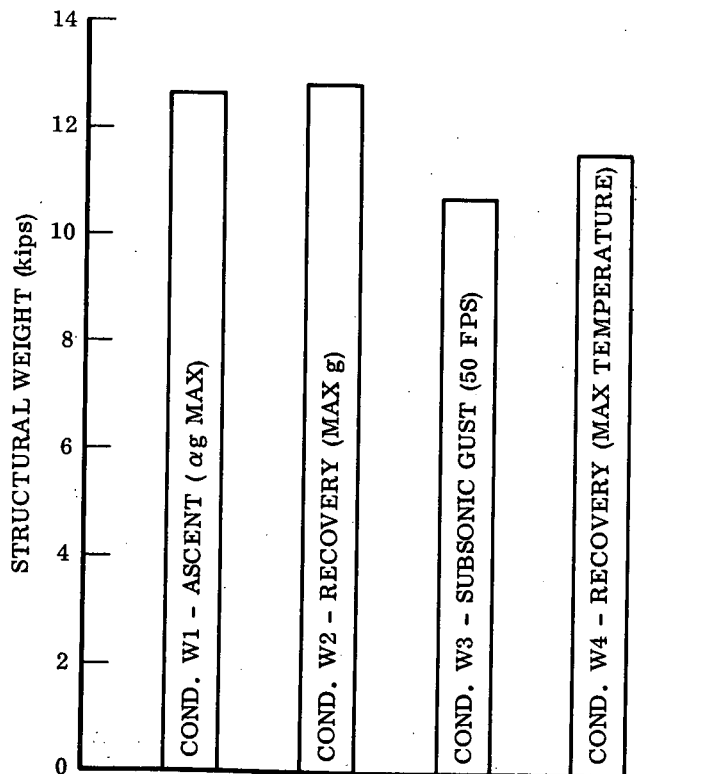


Figure 6-1. Booster Wing Structure Weight for the Critical Design Conditions (Weight for One Side of the Vehicle)

Table 6-1. Weight Sensitivity of B-9U Wing to Loads

Material Type		Baseline Design:												
		Resized Structure				First Iteration								
		W3	W4	W1	W2	Input	W3	W4	W1	W2	W3	W4	W1	W2
		Structural Weight (pounds)												
		(2500 psf-deg)												
		(4.2 g)												
		(50 fps)												
		(700° F)												
Ribs		121	153	179	192	195	108	109	112	113	108	109	112	113
Upper Caps		113	170	197	222	222	105	123	131	142	105	123	131	142
Lower Caps		1,186	1,267	1,323	1,336	1,336	1,171	1,228	1,268	1,277	1,171	1,228	1,268	1,277
Webs		190	237	241	252	276	185	233	238	250	185	233	238	250
Stiffeners														
Spars														
Upper Caps		2,244	2,676	3,018	3,030	3,111	2,257	2,686	3,047	3,063	2,257	2,686	3,047	3,063
Lower Caps		2,051	2,422	2,708	2,710	2,765	2,075	2,423	2,765	2,768	2,075	2,423	2,765	2,768
Webs		255	306	339	339	344	256	295	325	324	256	295	325	324
Diagonals		357	461	492	507	553	348	458	499	519	348	458	499	519
Skins														
Upper (Quadrilateral)		1,779	1,779	1,779	1,779	1,779	1,779	1,779	1,779	1,779	1,779	1,779	1,779	1,779
Lower (Quadrilateral)		1,874	1,874	1,874	1,874	1,874	1,874	1,874	1,874	1,874	1,874	1,874	1,874	1,874
Upper (Triangular)		91	91	91	91	91	91	91	91	91	91	91	91	91
Lower (Triangular)		91	91	91	91	91	91	91	91	91	91	91	91	91
Total Structural Weight		10,353	11,525	12,332	12,423	12,637	10,339	11,391	12,219	12,292	10,339	11,391	12,219	12,292

however, some individual elements are more critical for other conditions in local areas. After the first sizing, the structural weight input, based on a fully-stressed design, is 12,637 pounds. This is slightly higher than Conditions W1 and W2 and is further indication that some of the structure is designed by the other conditions.

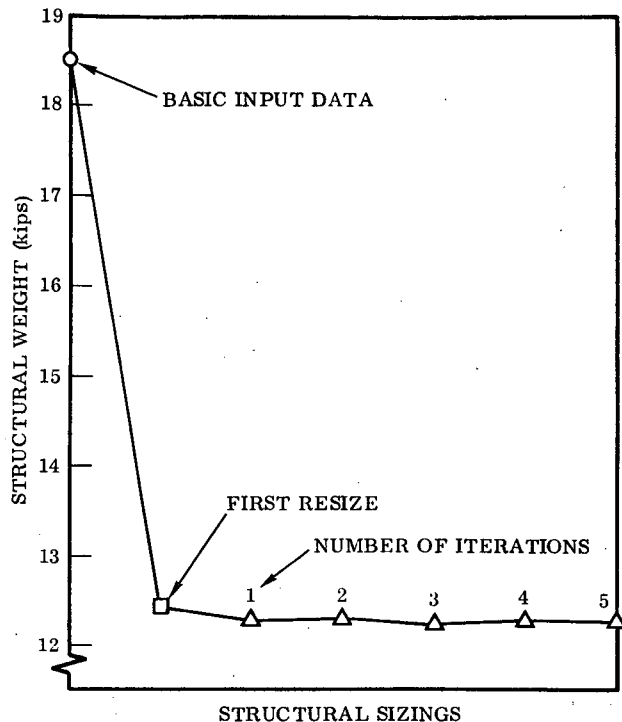


Figure 6-2. Booster Wing Structure Weight for Various Resizings

Structural weight changes are negligible after one iteration, and Conditions W1 and W2 are still almost identical. It is not hard to see why Conditions W1 and W2 weigh much the same, since the loads and load distributions are similar. Although Condition W1 has slightly higher loads, these are offset by the thermal effects of the entry condition of W2. As can be seen, the skin panels are always at minimum gage (0.04), and there is no change in weight across the complete table.

Initial studies showed that the structural weight of the wing finite-element model varied very slightly after two iterations of the program. To ensure that the weight did stabilize this early, the most critical wing condition, recovery at maximum g (W2), has been cycled through five iterations. The data is plotted in Figure 6-2, and it can be seen that the weight settles down after the first resizing.

6.2 VERTICAL TAIL WEIGHT SENSITIVITIES

The vertical tail has been analyzed using the same program as that used for the wing analysis. Only the main structural box between the spars that attach to the fuselage are included in the mathematical model. It does not include anything outside of these spars, nor does it include the chordwise stiffeners between the ribs.

Table 6-2 shows that T1, maximum βq , is the most critical condition. The rib webs and stiffeners are at minimum gages. Condition T3, rudder kick, designs the rudder hinge support rib caps, but otherwise the vertical tail is designed by the maximum βq condition. The subsonic gust condition is not critical in any way, and the βq condition would have to be relieved by 25 percent before the subsonic condition became critical.

Table 6-2. B-9U Vertical Tail - Weight Sensitivity to Loads

Baseline Design:							
T1 - Maximum βq (2400 psf-deg)							
T2 - Subsonic Gust							
T3 - Rudder Kick							
Material Type	Structural Weight (pounds)						
	Resized Structure			First Iteration			
	T1	T2	T3	Input	T1	T2	T3
Ribs							
Caps	122	117	148	157	124	119	160
Webs	342	342	342	342	342	342	342
Stiffeners	23	23	23	23	23	23	23
Spars							
Caps	434	307	272	436	440	301	245
Webs	290	254	268	302	288	253	272
Skins							
Quadrilateral	2,293	1,806	1,723	2,295	2,306	1,801	1,727
Triangular	128	96	119	128	150	107	141
Total Structural Weight	3,632	2,945	2,895	3,684	3,674	2,945	2,910

6.3 FUSELAGE STRUCTURAL SENSITIVITIES

Load intensities are given at eight points around the booster at each of 48 stations. Figure 6-3 shows the numbering system used for the node points at which load intensities are listed. Table 6-3 lists the design conditions used for sizing the fuselage, and Tables 6-4 and 6-5 present the peak ultimate axial tension and compression load intensities, respectively. The number in parentheses after each entry indicates the critical condition for that point. Conditions 4 through 11 (Table 6-3) have been further analyzed with the ASOP program.

Figures 6-4 through 6-6 show the critical design conditions for the axial bar members, the shear panels, and the frame beam element members, respectively. Four conditions predominate in the design of the booster fuselage: 1) the 3g maximum thrust for a large portion of the upper fuselage structure, 2) liftoff + 1-hour ground side winds at the sides, 3) liftoff + 1-hour ground headwinds for the forward lower fuselage, and 4) maximum αq headwinds for the aft lower fuselage. The orbiter forward attachment bulkhead is designed by the liftoff + 1-hour ground side wind condition and the aft attachment by the maximum αq tail wind condition.

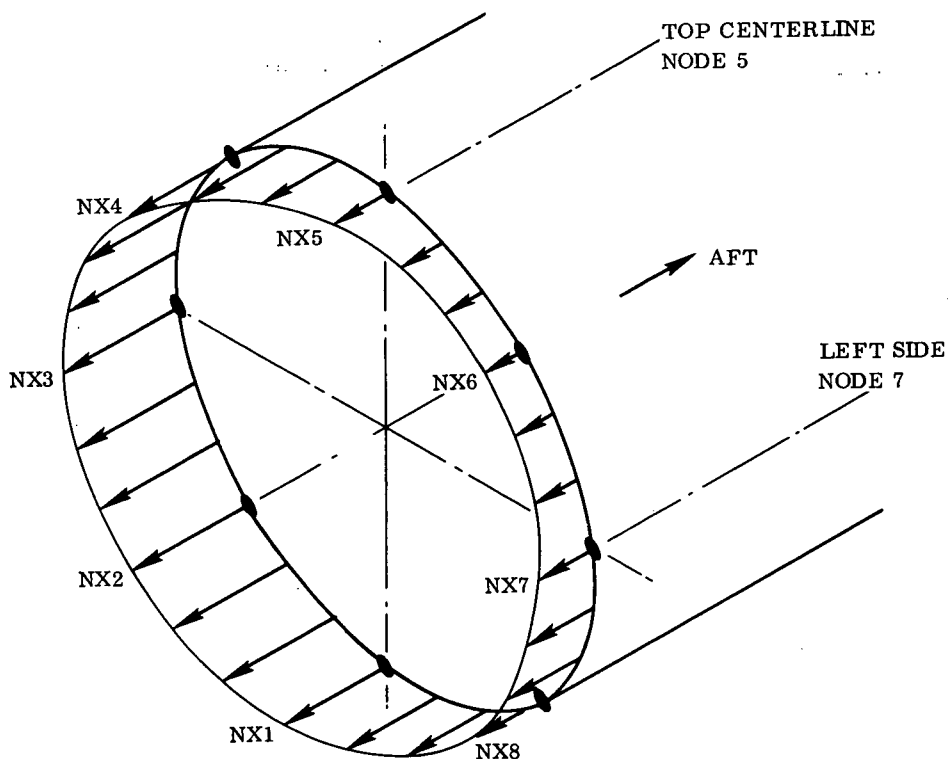


Figure 6-3. Location of Load Intensity Output from NETLD2

Table 6-3. B-9U/161-C Ultimate Internal Loads (Baseline)

Condition	
1	Booster B-9U/Orbiter NR 161-C 1 hr Ground Headwinds Tanked Unpress
2	Booster B-9U/Orbiter NR 161-C 1 hr Ground Tailwinds Tanked Unpress
3	Booster B-9U/Orbiter NR 161-C 1 hr Ground Sidewinds Tanked Unpress
4	Booster B-9U/Orbiter NR 161-C Lift Off + 1 hr Ground Headwinds
5	Booster B-9U/Orbiter NR 161-C Lift Off + 1 hr Ground Tailwinds
6	Booster B-9U/Orbiter NR 161-C Lift Off + 1 hr Ground Sidewinds
7	Booster B-9U/Orbiter NR 161-C Max Alpha-q Headwinds $\alpha q = 2800$
8	Booster B-9U/Orbiter NR 161-C Max Alpha-q Tailwinds $\alpha q = -2800$
9	Booster B-9U/Orbiter NR 161-C Max Beta-q (2400)
10	Booster B-9U/Orbiter NR 161-C 3g Max Thrust
11	Booster B-9U Booster Burnout
12	Booster B-9U Booster Recovery
13	Booster B-9U Booster Subsonic Gust
14	Booster B-9U Booster 2 Point Landing
15	Booster B-9U Booster 3 Point Landing
16	Booster B-9U Booster 2g Taxi

Table 6-4. B-9U/161-C Ultimate Tension Internal Loads (Baseline)

PEAK ULTIMATE AXIAL TENSION LOAD INTENSITIES

STATION (IN)	NX1 (LB/IN)	NX2 (LR/IN)	NX3 (LB/IN)	NX4 (LB/IN)	NX5 (LB/IN)	NX6 (LB/IN)	NX7 (LB/IN)	NX8 (LB/IN)
1000	0(16)	0(16)	0(16)	0(16)	0(16)	0(16)	0(16)	0(16)
1036	5(12)	4(12)	0(15)	0(16)	1(11)	0(16)	0(15)	4(12)
1072	45(12)	32(12)	1(15)	3(11)	8(11)	3(11)	1(15)	32(12)
1131	73(12)	51(12)	3(15)	7(16)	13(8)	7(16)	3(15)	51(12)
1278	141(12)	98(12)	7(15)	28(16)	58(8)	28(16)	7(15)	98(12)
1337	173(12)	121(12)	9(15)	42(9)	89(8)	42(8)	9(15)	121(12)
1341	177(12)	124(12)	8(14)	121(15)	192(15)	121(15)	8(14)	124(12)
1477	288(12)	203(12)	14(14)	99(8)	191(8)	99(8)	14(14)	203(12)
1481	1411(12)	1322(12)	1229(10)	1280(8)	1374(8)	1280(8)	1229(10)	1322(12)
1500	1569(12)	1430(12)	1194(10)	1377(8)	1531(8)	1377(8)	1194(10)	1430(12)
1750	1820(12)	1601(12)	1149(10)	1539(8)	1791(8)	1539(8)	1153(9)	1601(12)
1854	2042(12)	1753(12)	1102(10)	1510(8)	1780(8)	1510(8)	1102(10)	1753(12)
1858	931(12)	640(12)	35(14)	86(13)	140(13)	85(13)	35(14)	640(12)
2006	1932(11)	852(11)	47(14)	155(13)	242(13)	153(13)	47(14)	853(11)
2022	2207(11)	996(11)	40(14)	166(13)	258(13)	164(13)	43(14)	996(11)
2026	2274(11)	1031(11)	45(14)	160(13)	251(13)	158(13)	45(14)	1031(11)
2042	2544(11)	1169(11)	47(14)	152(13)	242(13)	150(13)	47(14)	1169(11)
2094	3431(11)	1631(11)	52(14)	141(14)	219(13)	141(14)	52(14)	1631(11)
2098	3476(11)	1650(11)	52(14)	142(14)	217(13)	142(14)	52(14)	1650(11)
2180	3878(11)	1678(11)	60(14)	168(14)	213(14)	168(14)	60(14)	1678(11)
2184	5758(11)	3588(11)	1454(13)	1653(13)	1734(13)	1650(13)	1450(13)	3588(11)
2300	5803(11)	3577(11)	1444(13)	1656(13)	1743(13)	1653(13)	1439(13)	3577(11)
2400	5813(11)	3574(11)	1437(13)	1675(13)	1772(13)	1671(13)	1431(13)	3574(11)
2500	5820(11)	3568(11)	1433(13)	1709(13)	1821(13)	1704(13)	1426(13)	3568(11)
2600	5822(11)	3559(11)	1432(13)	1756(13)	1888(13)	1751(13)	1424(13)	3559(11)
2664	5822(11)	3552(11)	1431(13)	1793(13)	1940(13)	1787(13)	1422(13)	3552(11)
2668	5813(11)	3545(11)	1431(13)	1795(13)	1944(13)	1789(13)	1422(13)	3545(11)
2800	5193(11)	3092(11)	1429(13)	1806(13)	2072(13)	1879(13)	1419(13)	3092(11)
2864	4889(11)	2871(11)	1429(13)	1937(13)	2144(13)	1930(13)	1418(13)	2871(11)
2868	4870(11)	2855(11)	1429(13)	1940(13)	2149(13)	1933(13)	1418(13)	2855(11)
2950	4450(11)	2977(12)	1428(13)	2015(13)	2254(13)	2007(13)	1417(13)	2977(12)
3050	3796(12)	3103(12)	1428(12)	2172(13)	2477(13)	2164(13)	1428(12)	3102(12)
3161	3683(12)	3033(12)	1464(12)	2487(13)	2921(13)	2477(13)	1464(12)	3033(12)
3165	3615(12)	2980(12)	1448(12)	2497(13)	2938(13)	2487(13)	1448(12)	2980(12)
3293	2979(12)	2538(12)	1473(12)	2631(16)	3721(16)	2631(16)	1473(12)	2538(12)
3295	2968(12)	2530(12)	1473(12)	2643(16)	3737(16)	2643(16)	1473(12)	2530(12)
3373	2475(12)	2185(12)	1486(12)	2737(13)	3272(13)	2726(13)	1486(12)	2185(12)
3377	2394(12)	2123(12)	1469(12)	2742(13)	3281(13)	2730(13)	1469(12)	2123(12)
3538	1465(12)	1471(12)	1486(12)	2654(13)	3156(13)	2642(13)	1486(12)	1471(12)
3542	1391(12)	1414(12)	1469(12)	2651(13)	3155(13)	2639(13)	1469(12)	1414(12)
3679	943(12)	1105(12)	1559(13)	2228(13)	2506(13)	2229(13)	1561(13)	1105(12)
3683	-609(12)	-442(12)	25(13)	770(16)	1088(16)	770(16)	26(13)	-442(12)
3820	-447(16)	-316(16)	16(13)	516(12)	743(12)	516(12)	16(13)	-316(16)
3921	-119(16)	-84(16)	15(13)	132(12)	196(12)	132(12)	15(13)	-84(16)
3925	538(11)	478(11)	333(10)	290(10)	272(10)	290(10)	333(10)	478(11)
4065	0(7)	1(6)	2(6)	1(6)	0(7)	0(7)	0(7)	0(7)
4069	0(16)	1(6)	2(6)	1(6)	0(6)	0(16)	0(16)	0(16)
4300	0(16)	0(16)	0(16)	0(16)	0(16)	0(16)	0(16)	0(16)

Table 6-5. B-9U/161-C Ultimate Compression Internal Loads (Baseline)

PEAK ULTIMATE AXIAL COMPRESSION LOAD INTENSITIES

STATION (IN)	NX1 (LB/IN)	NX2 (LB/IN)	NX3 (LB/IN)	NX4 (LB/IN)	NX5 (LB/IN)	NX6 (LB/IN)	NX7 (LB/IN)	NX8 (LB/IN)
1000	0(16)	0(16)	0(16)	0(16)	0(16)	0(16)	0(16)	0(16)
1936	-5(11)	-4(11)	-4(9)	-4(12)	-5(12)	-4(12)	-3(9)	-4(11)
1972	-23(11)	-21(9)	-25(9)	-34(12)	-47(12)	-34(12)	-8(9)	-18(11)
1131	-57(11)	-50(9)	-59(9)	-55(9)	-75(12)	-53(12)	-24(10)	-48(11)
1278	-171(8)	-136(8)	-122(9)	-105(12)	-147(12)	-105(12)	-65(10)	-138(8)
1337	-231(8)	-184(8)	-142(9)	-132(12)	-185(12)	-132(12)	-77(10)	-184(8)
1341	-295(15)	-224(15)	-144(9)	-136(12)	-189(12)	-136(12)	-79(10)	-224(15)
1477	-435(8)	-343(8)	-205(9)	-225(12)	-313(12)	-225(12)	-131(7)	-343(8)
1481	-135(15)	-107(15)	-39(15)	-50(16)	-82(16)	-58(16)	-62(3)	-107(15)
1500	-232(6)	-167(6)	-50(2)	-111(16)	-158(16)	-111(16)	-90(3)	-176(6)
1750	-446(4)	-337(6)	-65(6)	-154(16)	-218(16)	-154(16)	-135(3)	-329(4)
1864	-665(4)	-503(6)	-117(6)	-166(16)	-234(16)	-166(16)	-178(3)	-490(4)
1868	-5396(4)	-5238(6)	-4868(6)	-4514(5)	-4388(5)	-4514(5)	-4819(4)	-5227(4)
2006	-4429(4)	-4742(4)	-5564(6)	-6397(5)	-7050(10)	-6397(5)	-5498(4)	-4742(4)
2022	-4315(4)	-4685(4)	-5640(6)	-6671(5)	-7670(10)	-6621(5)	-5579(4)	-4685(4)
2026	-4286(4)	-4671(4)	-5669(6)	-6678(5)	-7825(10)	-6678(5)	-5599(4)	-4671(4)
2042	-4171(4)	-4613(4)	-5753(6)	-7144(10)	-8447(10)	-7144(10)	-5681(4)	-4613(4)
2094	-3791(4)	-4421(4)	-6023(6)	-8733(10)	-10458(10)	-8733(10)	-5942(4)	-4421(4)
2098	-3773(4)	-4414(4)	-6043(6)	-8337(10)	-10507(10)	-8837(10)	-5962(4)	-4414(4)
2180	-3651(7)	-4437(4)	-6458(6)	-10594(10)	-12710(10)	-10594(10)	-6364(4)	-4437(4)
2184	-3166(4)	-3968(4)	-5999(6)	-8728(10)	-10852(10)	-8728(10)	-5905(4)	-3968(4)
2300	-3238(4)	-4026(4)	-6036(6)	-8773(10)	-10895(10)	-8773(10)	-5928(4)	-4026(4)
2400	-3343(7)	-4072(4)	-6052(6)	-8803(10)	-10923(10)	-8803(10)	-5944(4)	-4072(4)
2500	-4011(7)	-4118(4)	-6086(6)	-8830(10)	-10945(10)	-8830(10)	-5961(4)	-4118(4)
2503	-4675(7)	-4452(7)	-6187(6)	-8853(10)	-10963(10)	-8853(10)	-5978(4)	-4452(7)
2664	-5091(7)	-4751(7)	-6119(6)	-8886(10)	-10972(10)	-8866(10)	-5989(4)	-4751(7)
2668	-5111(7)	-4766(7)	-6120(6)	-8861(10)	-10964(10)	-8861(10)	-5990(4)	-4766(7)
2800	-5563(7)	-5096(7)	-6138(6)	-8485(10)	-10412(10)	-8485(10)	-6012(4)	-5096(7)
2864	-5773(7)	-5250(7)	-6146(6)	-8301(10)	-10141(10)	-8301(10)	-6023(4)	-5250(7)
2868	-5787(7)	-5260(7)	-6146(6)	-8289(10)	-10125(10)	-8289(10)	-6023(4)	-5260(7)
2950	-6060(7)	-5463(7)	-6162(6)	-8065(10)	-9788(10)	-8065(10)	-6045(4)	-5463(7)
3050	-6519(7)	-5828(7)	-6276(6)	-7956(10)	-9525(10)	-7956(10)	-6167(4)	-5828(7)
3161	-7061(7)	-6256(7)	-6401(6)	-7817(10)	-9206(10)	-7817(10)	-6301(4)	-6256(7)
3165	-7174(7)	-6346(7)	-6405(6)	-7812(10)	-9194(10)	-7812(10)	-6306(4)	-6346(7)
3293	-7480(7)	-6597(7)	-6491(6)	-7566(5)	-8701(10)	-7566(5)	-6404(4)	-6597(7)
3295	-7485(7)	-6601(7)	-6492(6)	-7564(5)	-8693(10)	-7564(5)	-6406(4)	-6601(7)
3373	-7671(7)	-6751(7)	-6536(6)	-7484(5)	-8368(10)	-7484(5)	-6458(4)	-6751(7)
3377	-7770(7)	-6831(7)	-6536(6)	-7479(5)	-8349(10)	-7479(5)	-6459(4)	-6831(7)
3538	-7646(7)	-6771(7)	-6593(6)	-7277(5)	-7584(5)	-7277(5)	-6536(4)	-6771(7)
3542	-7732(7)	-6841(7)	-6594(6)	-7271(5)	-7576(5)	-7271(5)	-6538(4)	-6841(7)
3679	-7196(7)	-6499(7)	-6681(6)	-7125(5)	-7325(5)	-7125(5)	-6743(3)	-6499(7)
3683	-9708(7)	-9017(7)	-8198(6)	-9135(10)	-9682(10)	-9195(10)	-8162(4)	-9017(7)
3920	-8869(7)	-8464(7)	-8263(6)	-8763(10)	-8991(10)	-8763(10)	-8251(4)	-8464(7)
3921	-8474(10)	-8497(10)	-8551(10)	-8605(10)	-8627(10)	-8605(10)	-8551(10)	-8497(10)
3925	-243(12)	-184(12)	-113(9)	-124(9)	-116(9)	-94(9)	-71(9)	-184(12)
4065	-0(15)	-0(15)	-0(15)	-0(15)	-0(15)	-1(6)	-2(6)	-1(6)
4069	0(16)	0(16)	0(16)	0(16)	0(16)	-1(6)	-2(6)	-1(6)
4300	0(16)	0(16)	0(16)	0(16)	0(16)	0(16)	0(16)	0(16)

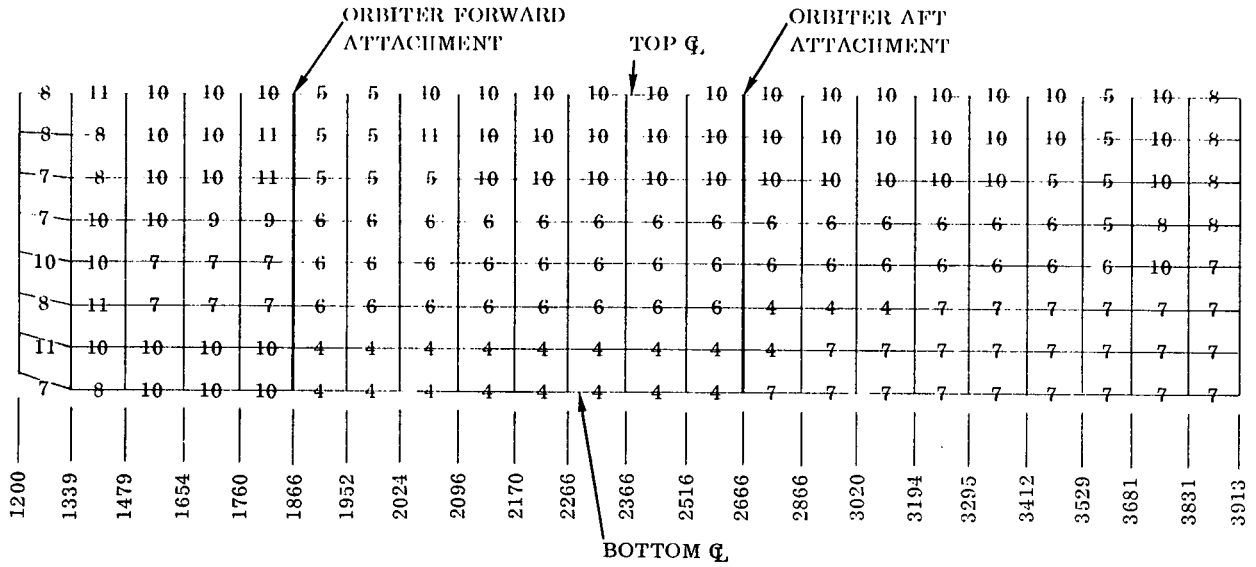


Figure 6-4. Critical Design Conditions for Axial Bar Members

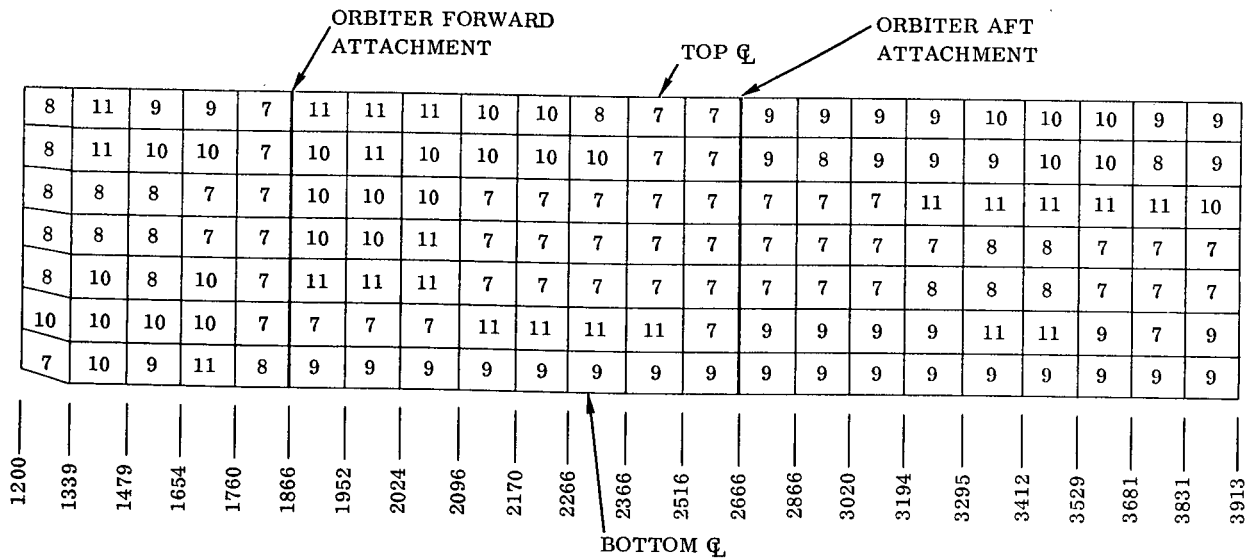


Figure 6-5. Critical Design Conditions for Shear Panels

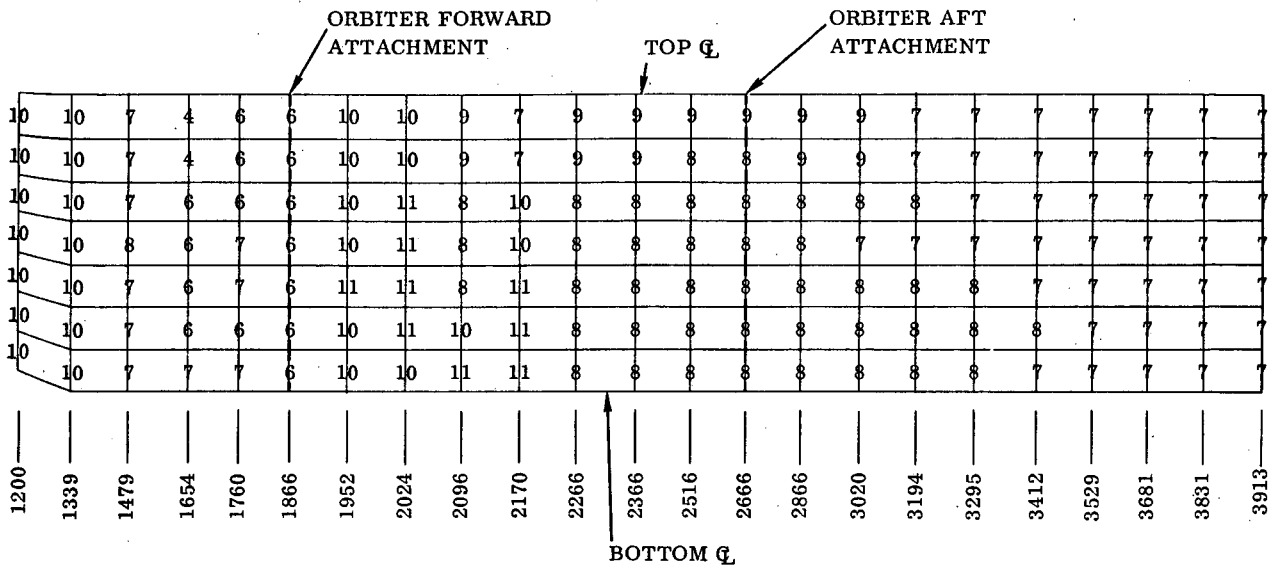


Figure 6-6. Critical Design Conditions for Frame Beam Element Members

A summary of the B-9U booster critical loading conditions is shown in Figure 6-7. Here the complete booster structure is divided into areas designed by particular loading conditions:

a. Fuselage

1. LO₂ tank - proof pressure.
2. Upper fuselage - 3g maximum thrust.
3. Side and forward lower fuselage - liftoff and ground winds.
4. Aft lower fuselage - maximum αq headwinds.

b. Wing

Maximum αq headwinds and maximum g recovery.

c. Vertical Tail

Maximum βq .

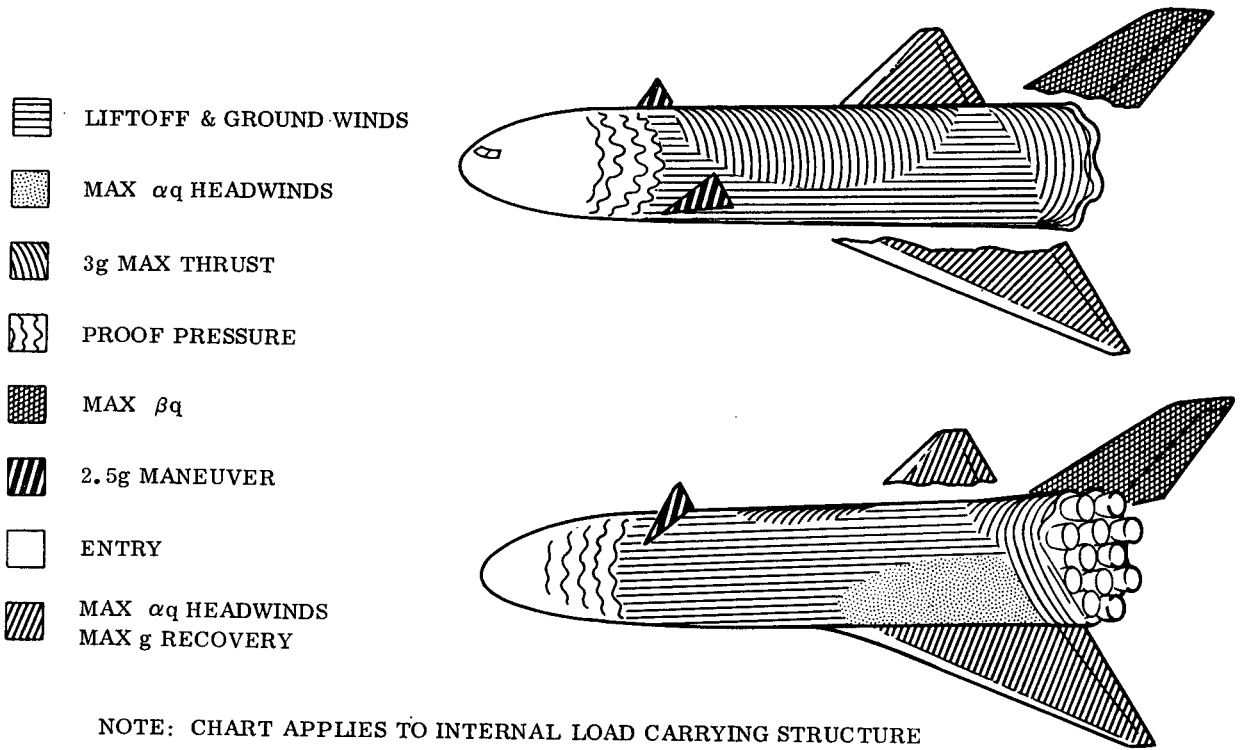


Figure 6-7. B-9U Critical Loading Conditions

SECTION 7

BOOSTER SERVICE LOAD SPECTRA

This section presents the flight load and pressure load spectra expected during the 100-mission service life of the space shuttle booster. Load spectra for the components selected for detail study (i.e., tanks, wing, vertical tail, thrust structure, and orbiter support) are presented. These spectra are obtained from the work accomplished under MDAC Contract L.S. 2590-A3 (Determination of Load Spectra).

7.1 WING LOAD SPECTRA

Figure 7-1 presents the wing flight load spectra for a 100-mission vehicle life under ascent, entry, cruise/landing, and taxi conditions. The spectra are expressed in terms of number of exceedences versus alternating and mean bending moment, which are shown in percent of the critical value for the condition considered. These values are converted to number of cycles of mean and alternating stress, with the ascent condition represented by various segments of the total ascent flight to orbiter separation.

7.2 VERTICAL TAIL SPECTRA

The vertical tail flight load spectra is presented in Figure 7-2. As with the wing, the numbered lines represent various segments of the ascent flight.

7.3 FUSELAGE LOAD SPECTRA

The spectra of booster fuselage axial load intensity (i.e., net longitudinal load in the tank shell due to axial and bending loads, in lb/in.) is presented in Figure 7-3 for the top and bottom centerline locations at Fuselage Station 2600. Station 2600 is located at the aft orbiter-to-booster attachment and is the most highly loaded fuselage section. For the top centerline location, the design load intensity and cyclic load are compression. For the bottom centerline location, the design load intensity and cyclic load are tension.

7.4 ORBITER-TO-BOOSTER ATTACHMENT LOAD SPECTRA

The forward orbiter-to-booster attachment flight load spectra is presented in Figure 7-4. Only vertical (F_Z) and lateral (F_Y) loads are shown, as the drag load (i.e., F_X) is taken through the aft attachment.

The aft orbiter-to-booster attachment flight load spectra is given in Figure 7-5.

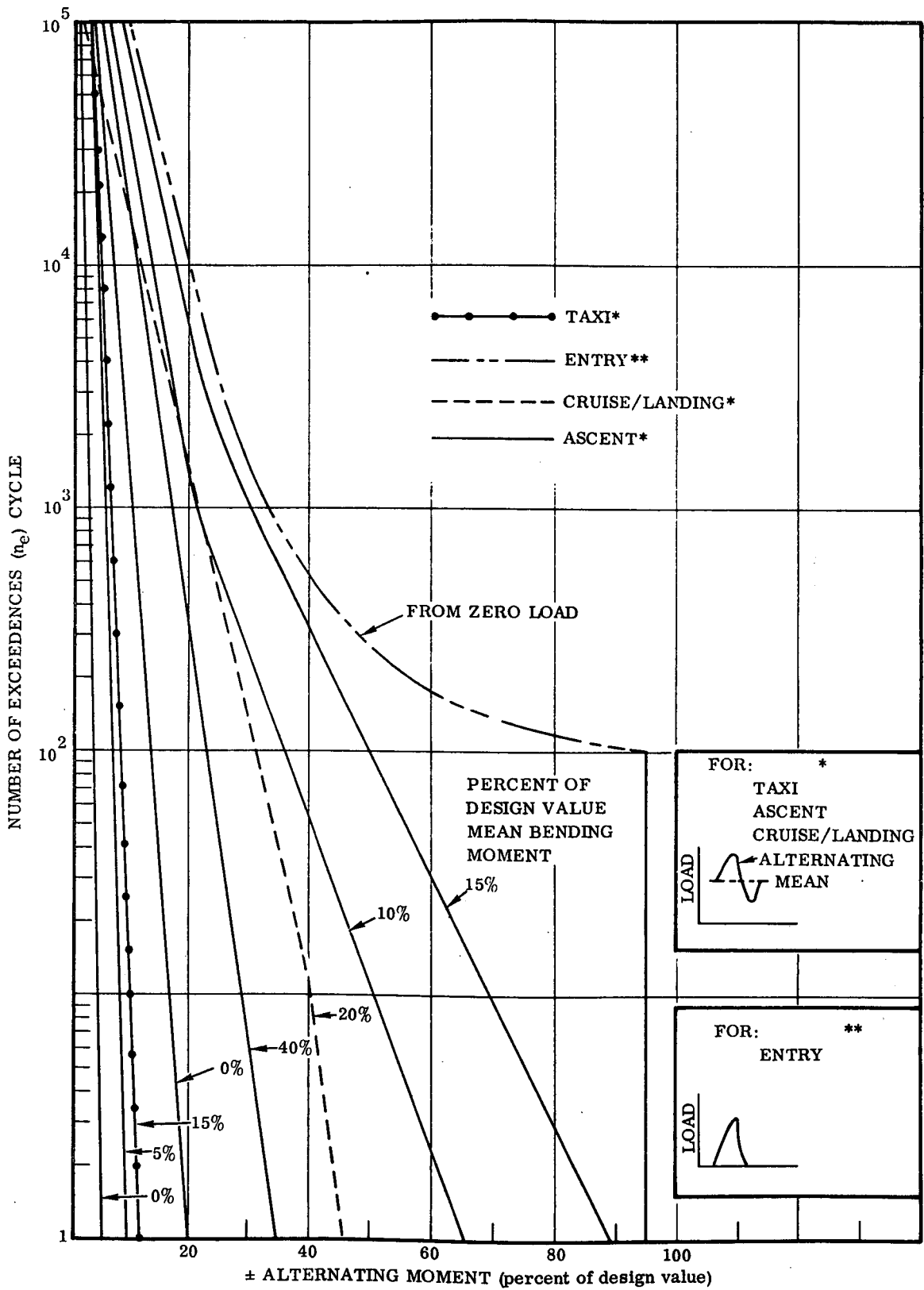


Figure 7-1. Wing Load Spectra

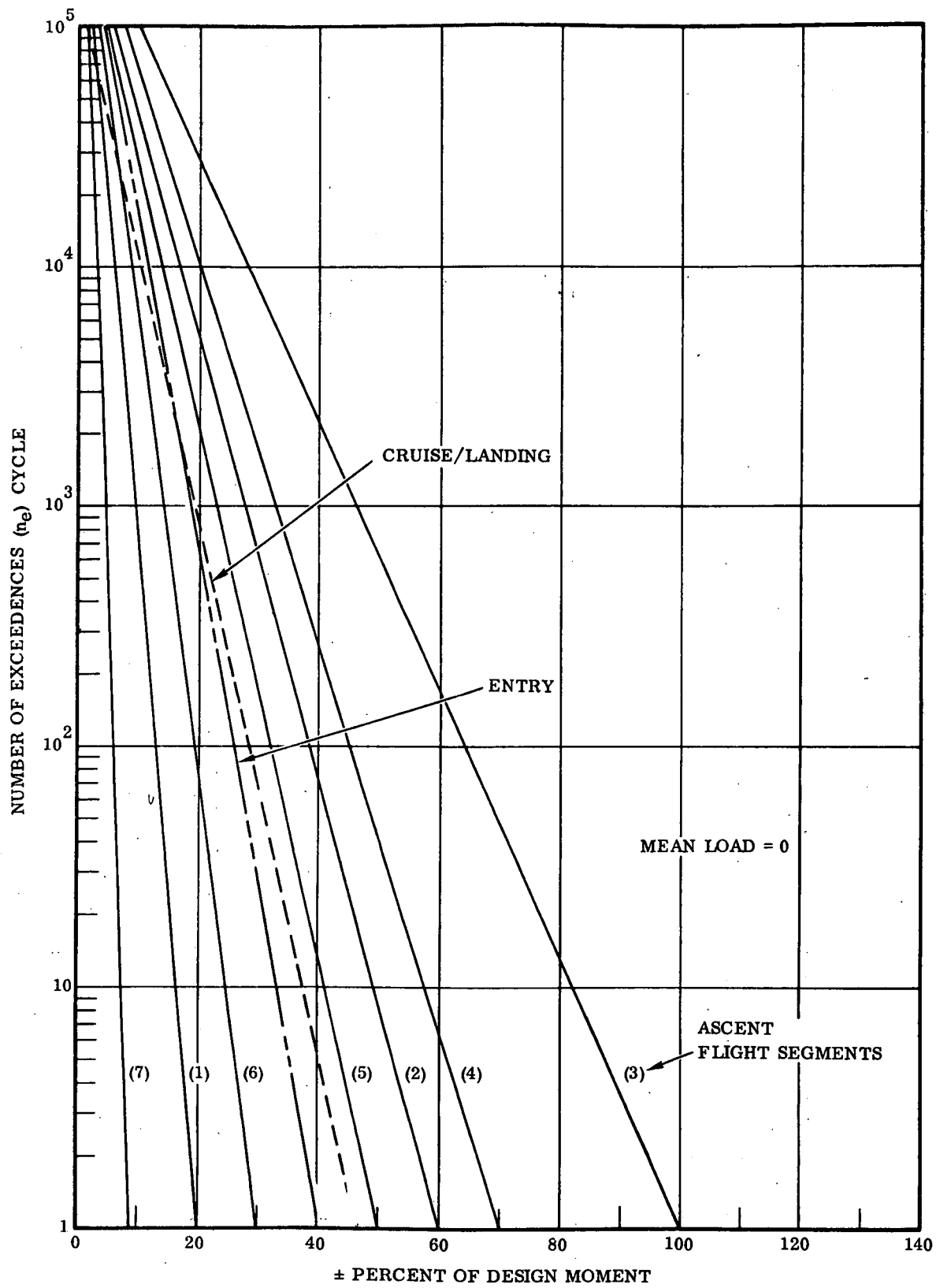


Figure 7-2. B-9U Vertical Tail Load Spectra

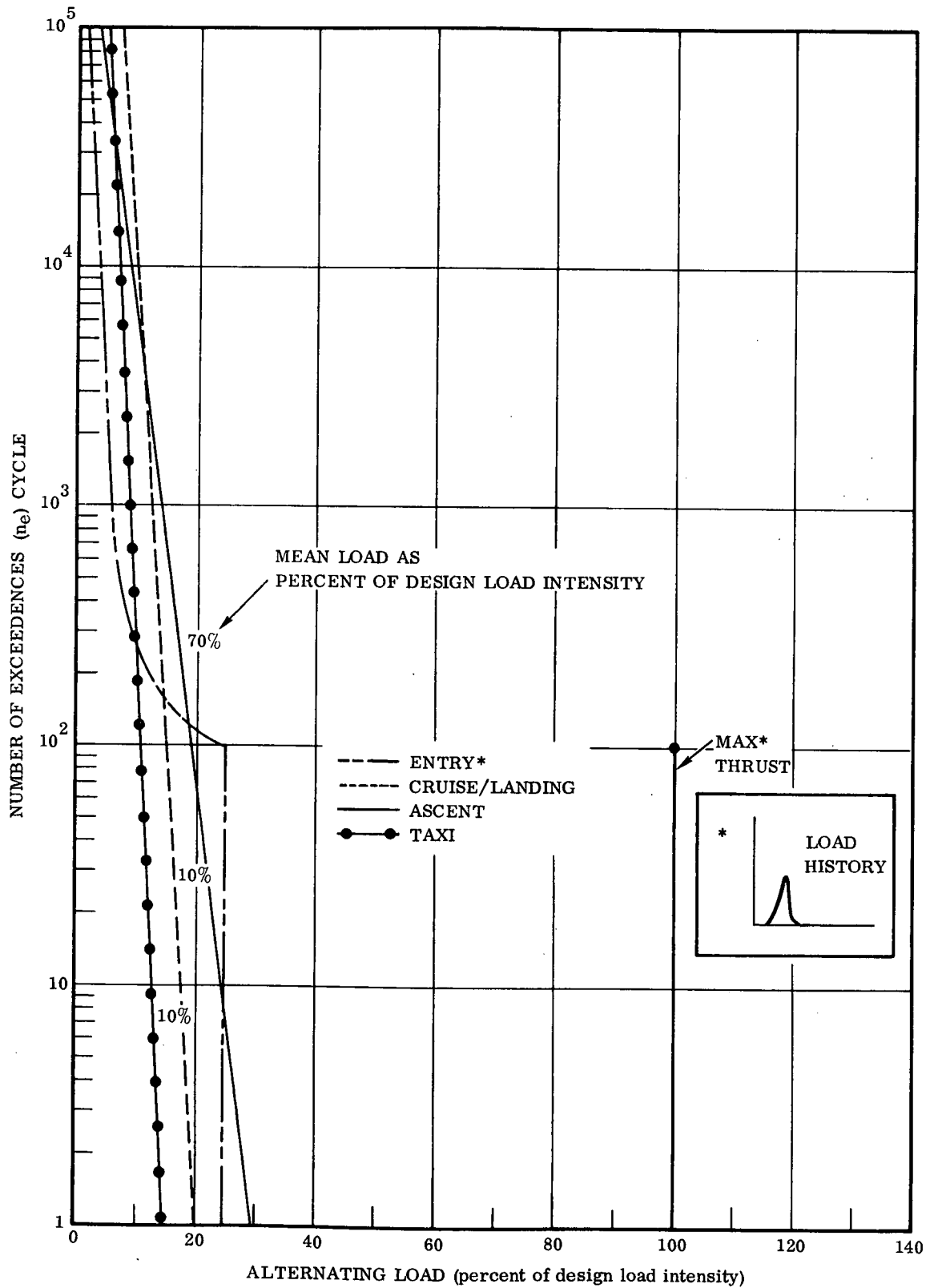


Figure 7-3. B-9U Fuselage Station 2600 Load Spectra

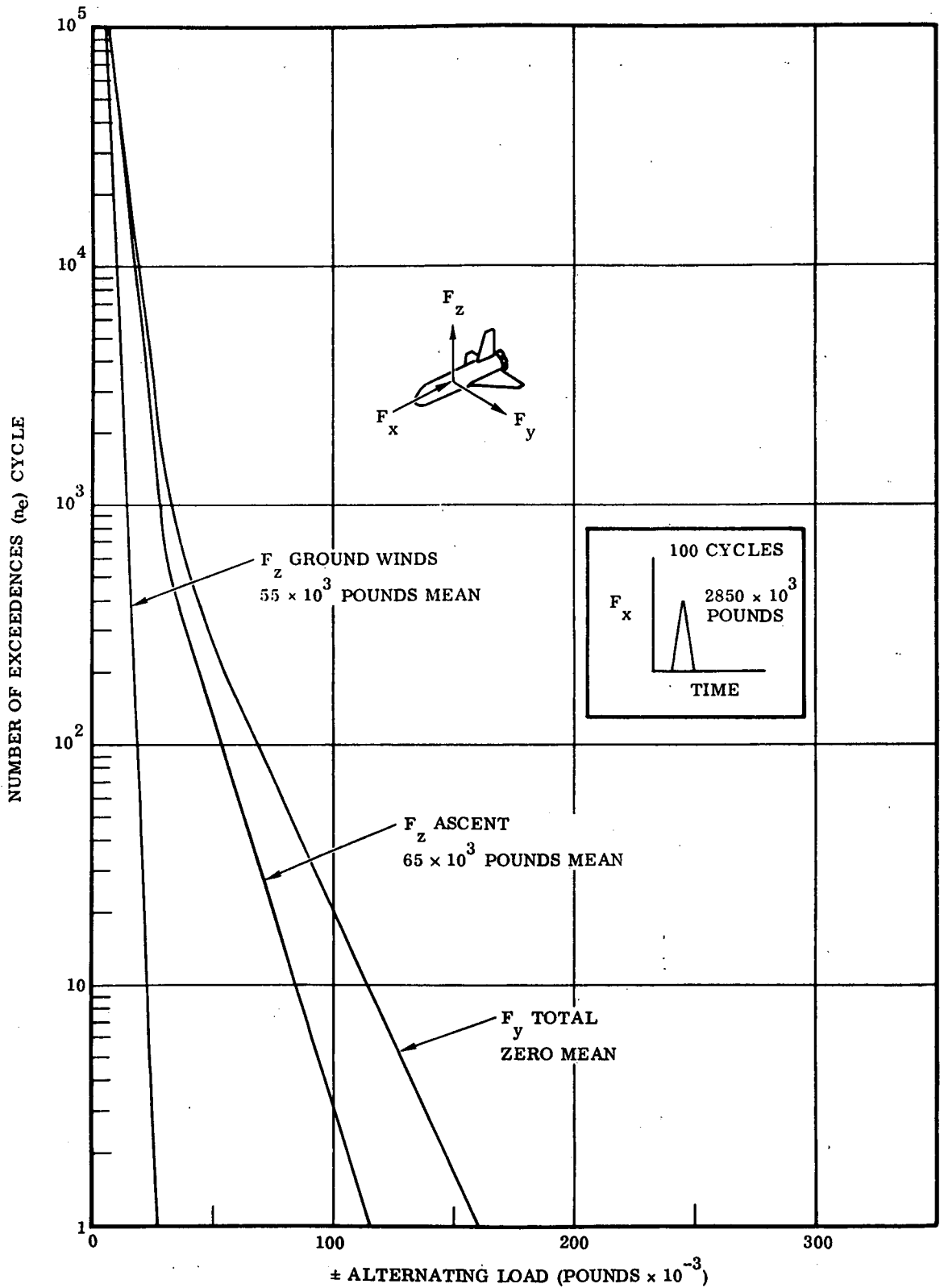


Figure 7-4. B-9U/Orbiter Forward Attach Load Spectra

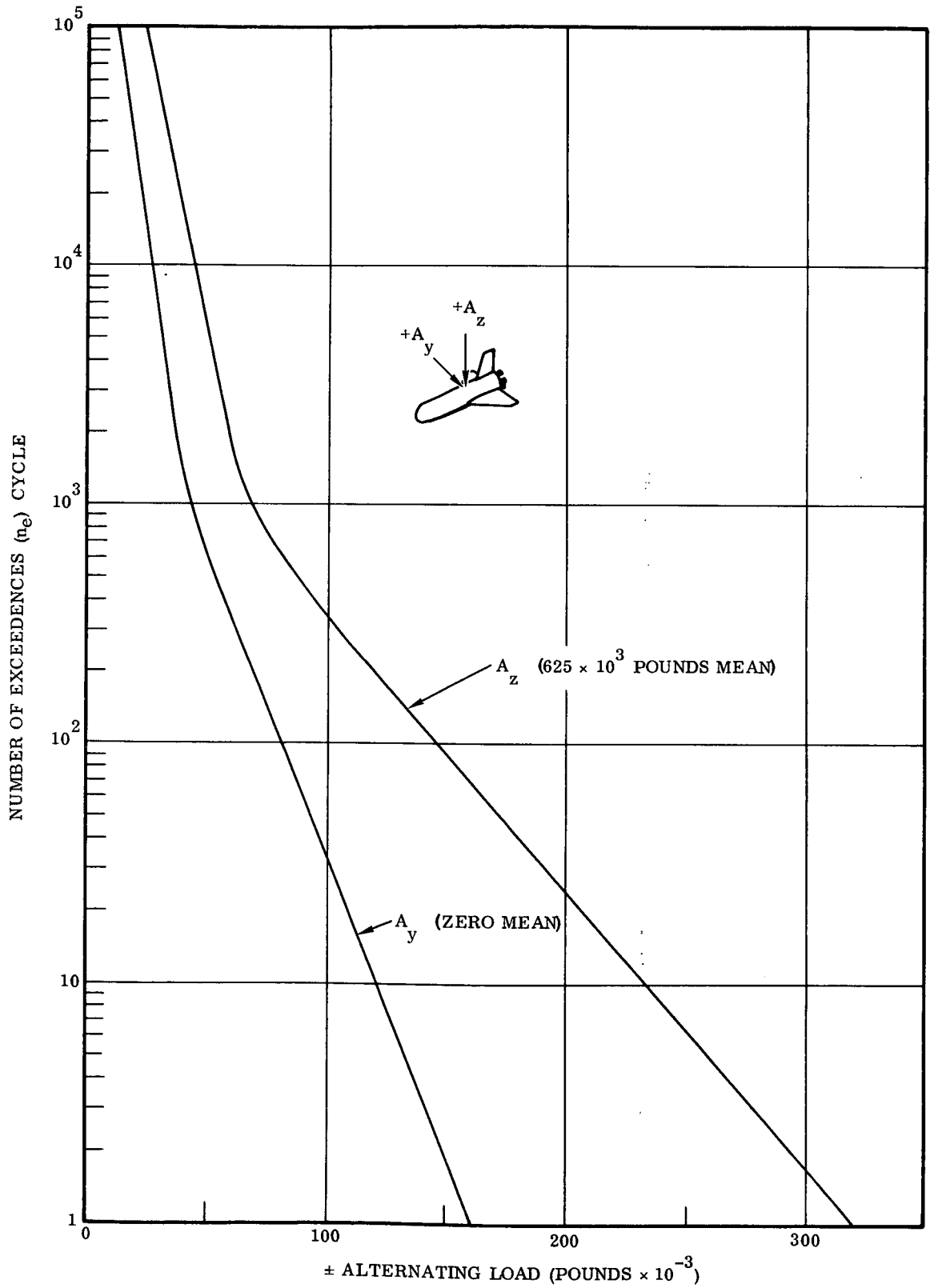


Figure 7-5. B-9U/Orbiter Aft Attachment Load Spectra

7.5 THRUST LOAD SPECTRA

Figure 7-6 is a plot of the total mean thrust versus time for the 12 booster main rocket engines. Superimposed on this is the transient thrust load spectra presented in Figure 7-7.

7.6 PROPELLANT TANKS PRESSURE LOAD SPECTRA

The main LH₂ and LO₂ propellant tank pressure schedules are presented in Figures 7-8 and 7-9, respectively. Nominal ullage and ullage plus fuel head pressure at the lower tank apex are shown. In addition, the maximum design pressure (i.e., maximum relief valve setting plus fuel head) assuming a pressure regulator malfunction is shown. For fatigue and flaw growth studies, it will be assumed that a pressure regulator malfunction occurs once every 20 flights.

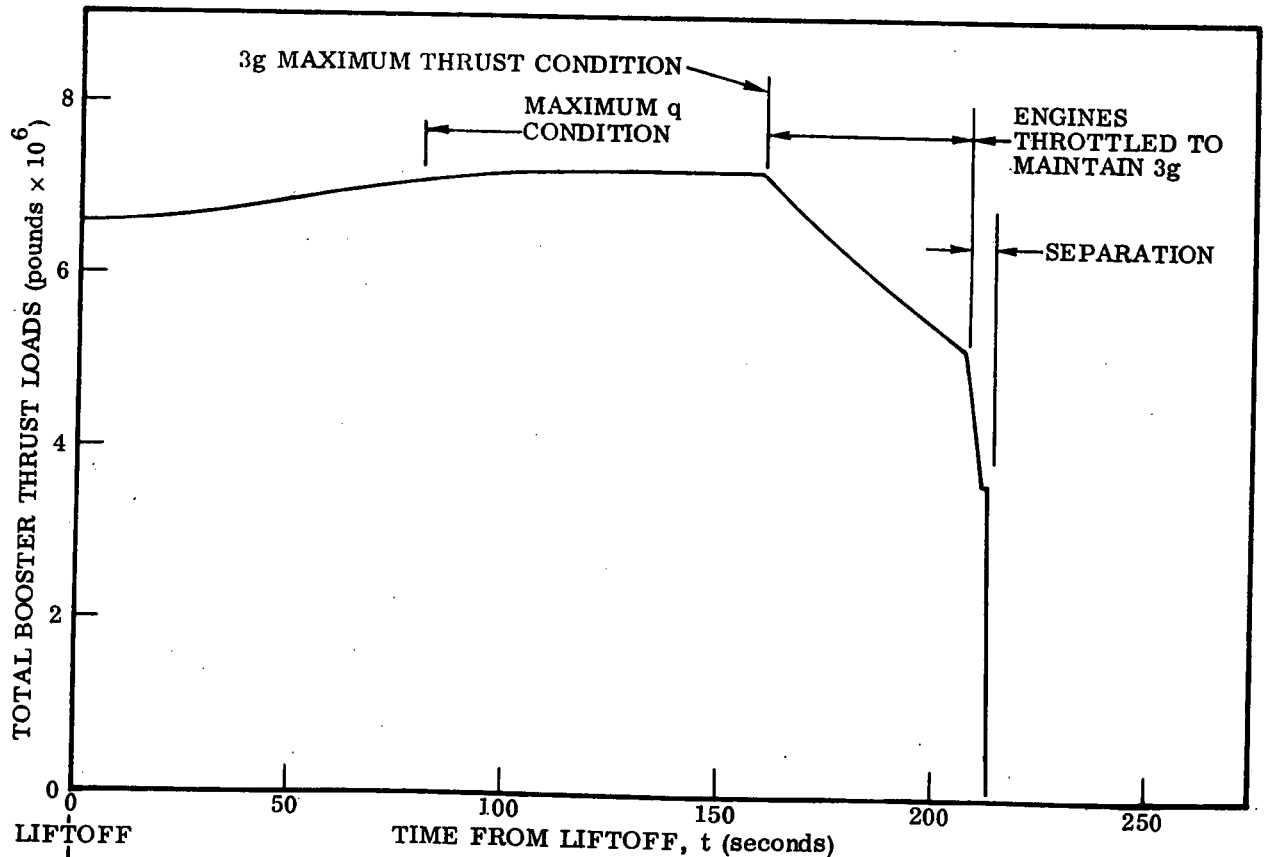


Figure 7-6. Total Mean Booster Main Engine Thrust

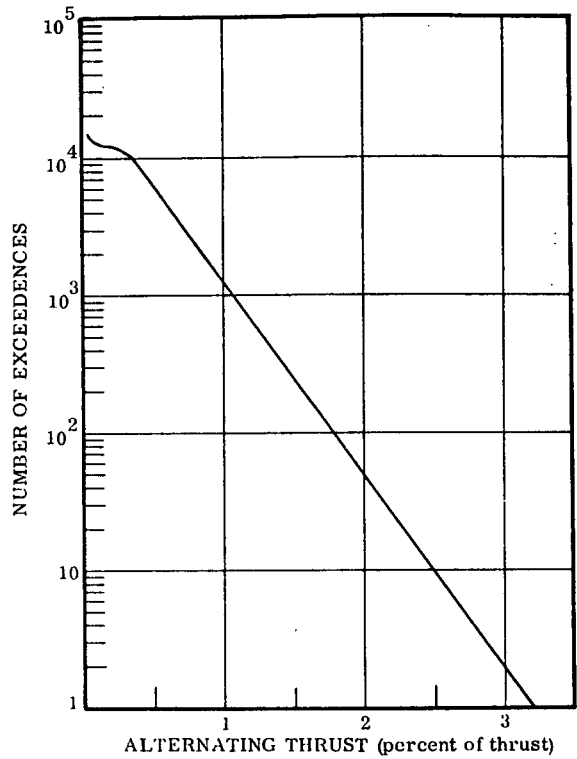


Figure 7-7. Thrust Spectra (One Flight)

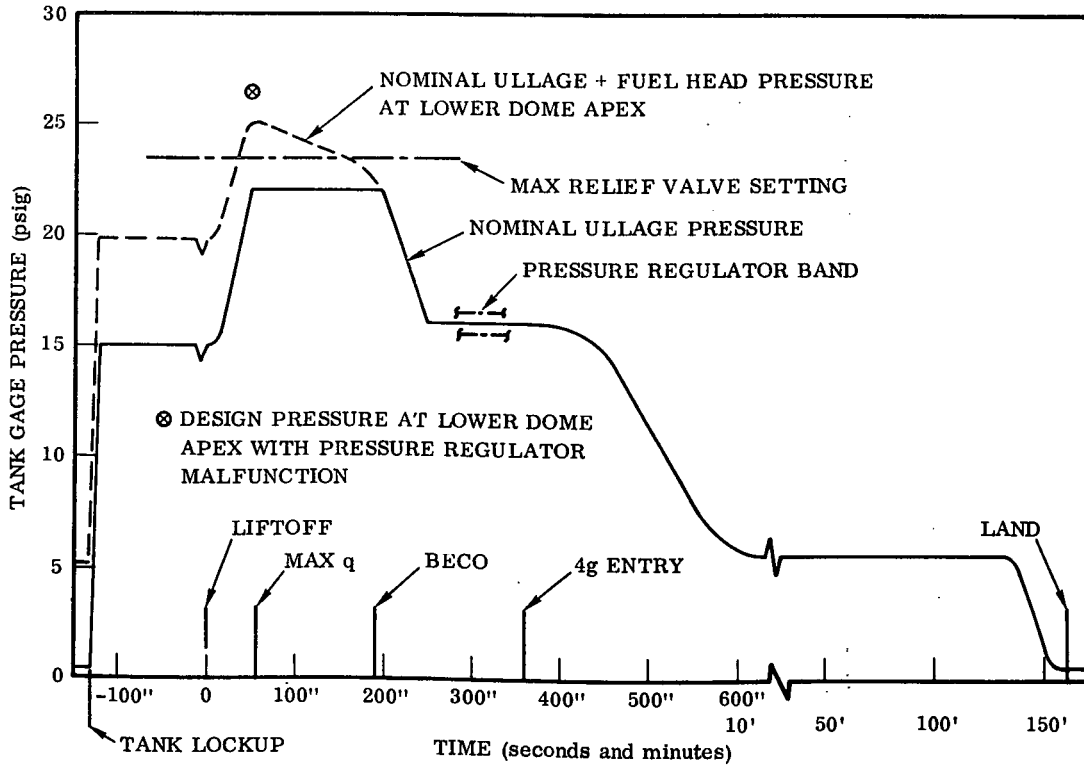


Figure 7-8. Booster Main LH₂ Tank Pressure Schedule

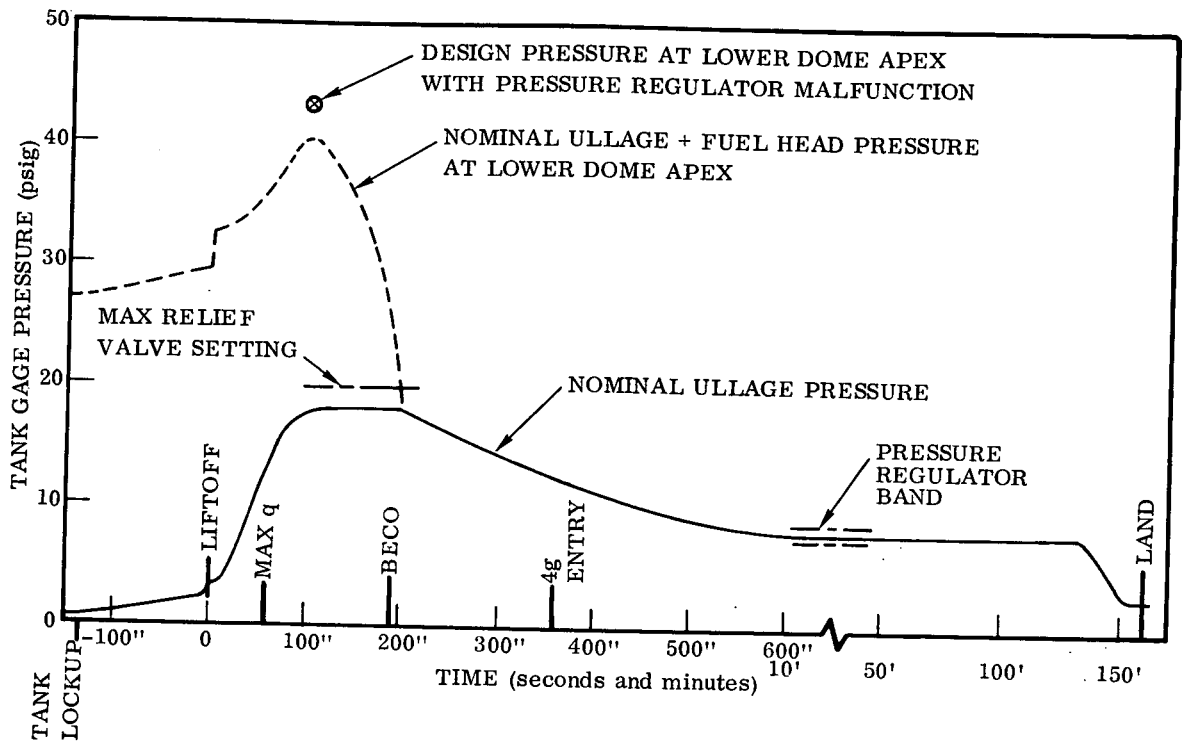


Figure 7-9. Booster Main LO₂ Tank Pressure Schedule

SECTION 8
FATIGUE ANALYSIS

A cumulative fatigue damage analysis has been performed for each baseline component to determine the safe-life number of missions. The service load spectra presented in Section 7 are used.

Material information used in classical fatigue analysis is usually in the form of S-N curves, constant life diagrams, or some such presentation of stress versus cycles to failure of test specimens. The fatigue curves of Figures 8-1 through 8-3 provide S-N data for 2219-T87 aluminum alloy at room temperature and for Ti-6Al-4V annealed titanium alloy at room temperature and 650° F, respectively.

The analysis is based on the following assumptions: 1) Miners hypothesis, 2) $K_t = 3.0$, 3) S-N data for 2219-T87 is assumed to be similar to that of 2024-T3, 4) Calculated

safe life = $\frac{100 \text{ missions}}{(\text{scatter factor})(\sum n/N)}$, and 5) Scatter factor = 4.0.

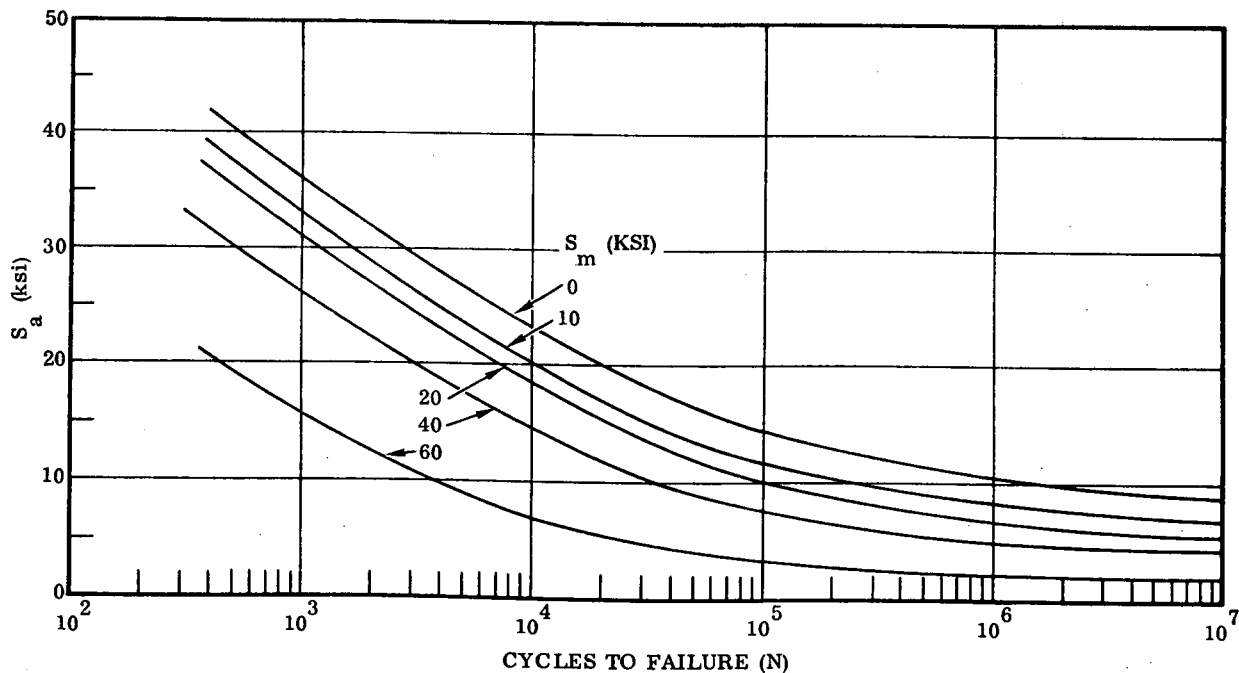


Figure 8-1. Estimated Fatigue Curves for 2219-T87 at Room Temperature with $K_t = 3.0$

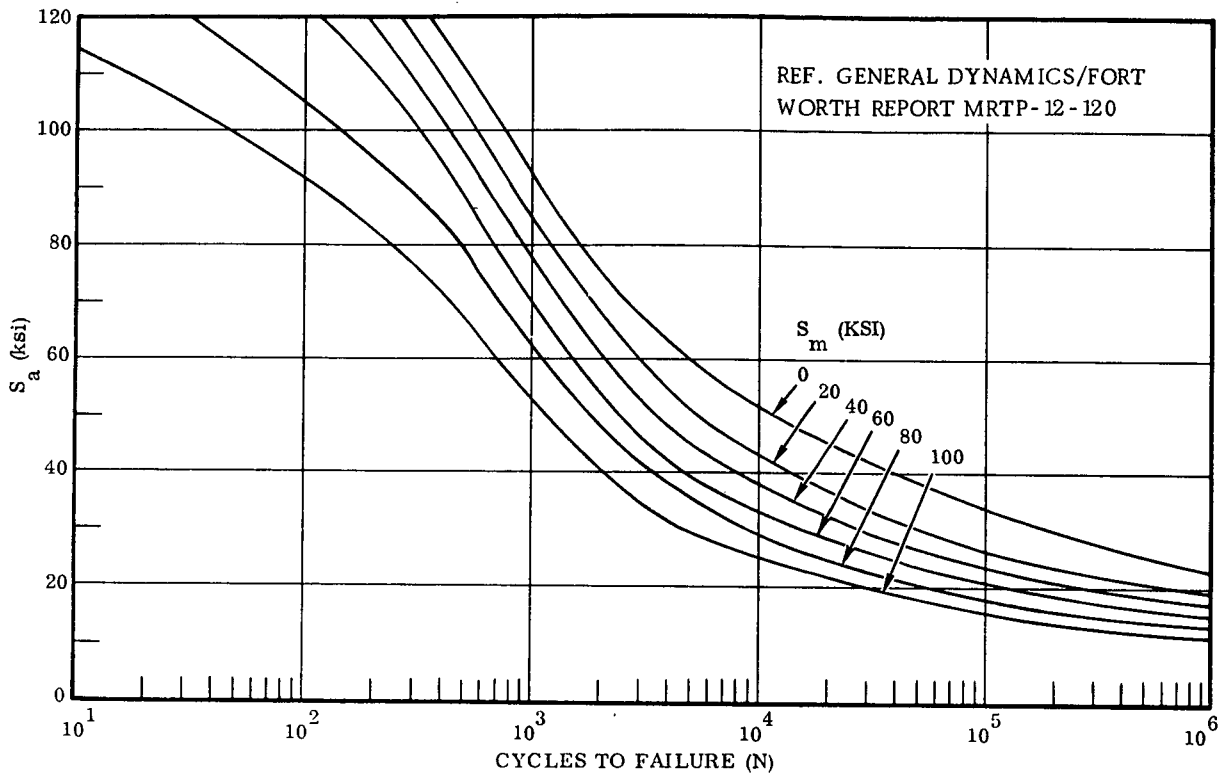


Figure 8-2. Fatigue Curves for Annealed 6Al-4V Ti at Room Temperature with $K_t = 3.0$

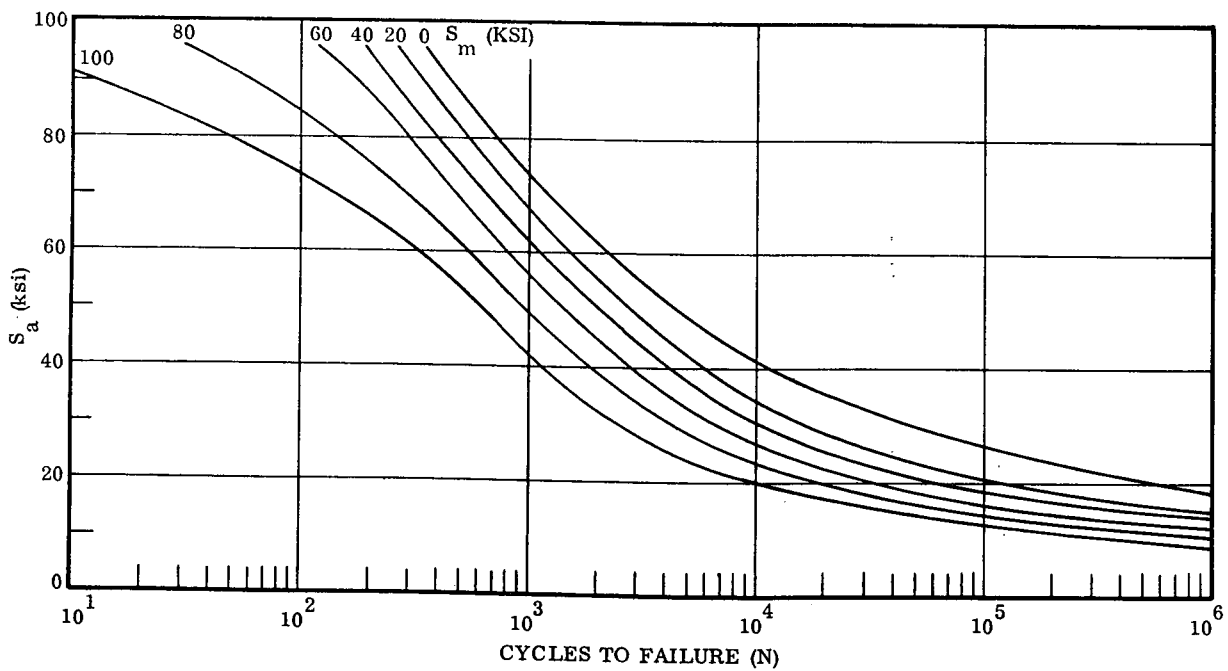


Figure 8-3. Fatigue Curves for Annealed 6Al-4V Ti at 650°F with $K_t = 3.0$

8.1 WING ANALYSIS

The analysis is based on a limit root bending moment of 189.1×10^6 in-lb; i. e., a limit stress of 91,200 psi at room temperature. To provide for one ferry flight per mission, the number of missions for the cruise/landing and taxi phases has been increased by a factor of two. Also, two G. A. G. cycles per mission are added (to the spectrum in Figure 7-1), using a minimum stress from the taxi phase and a maximum stress from the cruise/landing phase.

Damage from the various mission phases is:

<u>Mission Phase</u>	<u>n/N</u>
Ascent	0.0573
Entry	0.0561
Cruise/Landing	0.1009
Taxi	0
GAG	0.0100

$$\Sigma n/N = 0.2243$$

Most of the damage occurs in the ascent and entry portions of the mission.

8.2 VERTICAL TAIL ANALYSIS

Limit stress is set at 34,000 psi. To provide for one ferry flight per mission, the number of cycles for the cruise/landing phase has been increased by a factor of 2.0.

Summary of damage:

<u>Mission Phase</u>	<u>n/N</u>
Ascent	0.0002
Cruise/Landing	0

$$\Sigma n/N = 0.0002$$

8.3 FUSELAGE ANALYSIS

The fatigue damage control point is on the bottom of the shell at Fuselage Station 2600. Here the bending stresses and tank pressure stresses are combined for the various parts of the mission phase. Cruise/landing and taxi phases have the number of cycles doubled and two GAG cycles have been added for the same reasons given in the wing analysis. Room temperature S-N data is used because of the unavailability of -423° F data.

<u>Mission Phase</u>	<u>n/N</u>
Maximum Thrust	0.0038
Ascent	0.0001
Entry	0
Cruise/Landing	0
Taxi	0
GAG	0

$$\Sigma n/N = 0.0039$$

All the damage is caused by the maximum thrust condition.

8.4 AFT ORBITER SUPPORT FRAME ANALYSIS

The αq condition is non-damaging, and damage from the maximum βq is:

$$\Sigma n/N = 0.0054$$

8.5 THRUST STRUCTURE ANALYSIS

Design limit stress is set at:

$$\frac{F_{tu}}{ULF} = \frac{130.0}{1.4} = 92.9 \text{ ksi}$$

with the thrust alternating per Figure 7-7:

$$\Sigma n/N = 0.0285$$

8.6 PROPELLANT TANK ANALYSIS

The LO₂ and LH₂ tanks are both fatigue-critical adjacent to their upper domes. Each tank is scheduled through manufacture, preflight, and flight pressure cycles as shown in Table 8-1.

Table 8-1. B-9U Tankage Pressure Cycles

Phase	Condition	n (cycles)	Pressure (psi)	
			LO ₂	LH ₂
Manufacture	Proof Test	1	21.6	29.8
Preflight	Fueling	100	5.0	5.0
Flight	Nominal Ullage Pressure	95	18.0	22.0
Flight	Maximum Relief Valve Pressure	5	20.0	23.5

Each tank is cycled from zero pressure for each phase and a pressure regulator malfunction is assumed to occur in 5 percent of the flights. Then, the damage is:

Phase	$\Sigma n/N$	
	<u>LO₂</u>	<u>LH₂</u>
Manufacture	0.0003	0.0005
Preflight	0	0
Flight - nominal pressurization	0.0136	0.0095
Flight - relief pressurization	<u>0.0012</u>	<u>0.0007</u>
	$\Sigma n/N = 0.0151$	0.0107

Most of the damage is caused during flight; the proof test shows little damage and preflight fueling no damage at all.

Table 8-2 summarizes results of the fatigue analysis. The most critical components are the wing and thrust structure; the remaining items incur very little damage.

Table 8-2. Results of Safe Fatigue Life Analysis

Components	Type Load	$\Sigma n/N$ for One Service Life	Calculated Safe Fatigue Life (Missions)
LO ₂ Tank	Pressure	0.0151	1,687
LH ₂ Tank	Pressure	0.0107	2,450
	Flight	0.0039	6,410
Orbital Support Bulkhead	Flight	0.0054	4,630
Thrust Structure	Thrust	0.0285	887
Vertical Tail	Flight	0.0002	125,000
Wing	Flight	0.2243	111

PART II

PHASE II, SENSITIVITY TO LOADING PARAMETERS

// - /

TABLE OF CONTENTS

Section		Page
1	INTRODUCTION	II-7
2	STRUCTURAL WEIGHT/LOAD SENSITIVITY	II-9
2.1	WING STRUCTURE	II-9
2.1.1	Weight Sensitivity to Individual Design Loading Conditions	II-9
2.1.2	Wing Weight Sensitivity to Combined Design Loading Conditions	II-14
2.2	VERTICAL TAIL STRUCTURE	II-22
2.2.1	Vertical Stabilizer Weight Sensitivity With Individual Design Conditions	II-22
2.2.2	Vertical Stabilizer Weight Sensitivity With Combined Loads	II-24
2.3	FUSELAGE STRUCTURE	II-27
2.3.1	Structural Weight Sensitivity to αq Loads	II-27
2.3.2	Structural Weight Sensitivity to End Boost Acceleration	II-30
3	SENSITIVITIES OF LOADS TO VARIOUS CONFIGURATION AND FLIGHT PARAMETER CHANGES	II-49
4	REFERENCES	II-55

Preceding page blank

LIST OF FIGURES

Figure		Page
2-1	Booster Wing Structural Weight Variation with αq	II-11
2-2	Booster Wing Structural Weight Variation with η_z	II-12
2-3	Booster Wing Structural Weight Variation with Gust Velocity	II-12
2-4	Booster Wing Structural Weight Variation with Elevated Temperature	II-13
2-5	Booster Wing Structural Weight Variation about each Normalized Baseline Condition	II-13
2-6	B-9U Wing - Parametric Studies On Weight Sensitivities	II-21
2-7	B-9U Wing - Parametric Studies On Weight Sensitivities as a Percentage Increase or Decrease of the Baseline Design Total Structural Weight	II-22
2-8	Vertical Stabilizer Structural Weight Variation with βq	II-24
2-9	Vertical Stabilizer Structural Weight Variation with Lateral Gust Velocity	II-25
2-10	Vertical Stabilizer Structural Weight Variation for the Rudder Kick Condition	II-26
2-11	Vertical Stabilizer Weight Sensitivities to Various Load Parameters	II-28
2-12	Vertical Stabilizer Weight Sensitivity as a Percentage Change from the Baseline Total Structural Weight	II-28
2-13	Fuselage Weight Sensitivity to Maximum αq	II-29
2-14	Boost Axial Load Factor	II-30
2-15	Effect of End Boost g Limit on Orbiter Attachment Loads	II-41
2-16	Booster B-9U Axial Load Factor Versus Thrust	II-42
2-17	LO ₂ Tank Maximum Lower Dome Apex Pressure	II-43
2-18	LH ₂ Tank Maximum Lower Dome Apex Pressure	II-43
2-19	Effect of End Boost Acceleration on B-9U Booster Structure	II-44
2-20	Effect of End Boost on Fuselage Structure Weight	II-45
2-21	Comparison of ASOP Program Results on Effect of End Boost on Fuselage Structure Weight	II-47
3-1	Design αq Variations (Maximum Value) Isp Effects	II-49
3-2	Design αq Variations (Maximum Value) Fuel or Oxidizer Flow Rates	II-50
3-3	Design αq Variations (Maximum Value) Wind Effects (MSFC Synthetic Winds)	II-50
3-4	Design αq Variations (Maximum Value) Aerodynamic Effect (CN_{α} , CD , CP_{α})	II-50
3-5	Design αq Variations (Maximum Value) Booster Structural Weight and C. G. Variations	II-51
3-6	Design αq Variations (Maximum Value) Control System Gain Variations (K_{θ} , $K_{\dot{\theta}}$)	II-51
3-7	Design αq Variations (Maximum Value) Pitch Programmer Variations	II-51

LIST OF TABLES

Table	Page
2-1	II-9
2-2	II-10
2-3	II-11
2-4	II-14
2-5	II-15
2-6	II-16
2-7	II-17
2-8a	II-18
2-8b	II-19
2-8c	II-19
2-8d	II-20
2-9	II-23
2-10	II-23
2-11	II-23
2-12	II-27
2-13	II-29
2-14	II-31
2-15	II-32
2-16	II-33
2-17	II-34
2-18	II-35
2-19	II-36
2-20	II-37
2-21	II-38
2-22	II-39
2-23	II-40
2-24	II-47
3-1	II-53

SUMMARY

This part documents the work performed under Phase II of the study.

The summary table presents the load sensitivities for the various flight phases of the Convair Aerospace/North American Phase B B-9U delta wing booster. Included in the table are the effects on the wing, fuselage and vertical tail of weight change with respect to load variation.

For the wing, variation in Isp has the greatest influence on design with fuel flow rate and booster total structural weight effects being almost as important. Subsonic gust and entry normal acceleration (g) conditions are not as critical as the other conditions.

The fuselage is most sensitive to end boost acceleration indicating the importance of booster thrust limitation. Ascent dynamic pressure and subsonic gust velocities have the biggest influence on the vertical tail design.

Summary of Load Sensitivities

WING

$$\frac{\partial W^*}{\partial I_{sp}} = 1860 \text{ lb/\% variation}$$

$$\frac{\partial W}{\partial (\Delta \text{aero})} = 127 \text{ lb/\% variation}$$

$$\frac{\partial W}{\partial (\text{entry "g"})} = 7375 \text{ lb/g}$$

$$\frac{\partial W}{\partial W_{\text{fuel}}} = 1240 \text{ lb/\% variation}$$

flow rate

$$\frac{\partial W}{\partial (\text{control gains})} = 186 \text{ lb/\% variation}$$

$$\frac{\partial W}{\partial (\text{subsonic gust})} = 423 \text{ lb/fps gust}$$

$$\frac{\partial W}{\partial W_{\text{wind}}} = 744 \text{ lb/\% probability}$$

$$\frac{\partial W}{\partial (\text{pitch prog})} = 1240 \text{ lb/\% variation}$$

$$\frac{\partial W}{\partial (\text{str. weight})} = 1240 \text{ lb/\% variation}$$

*Wing Weight

FUSELAGE

$$\frac{\partial W^{**}}{\partial (\text{burnout "g's"})} = 7140 \text{ lb/g}$$

$$\frac{\partial W}{\partial (\alpha q)_{\text{tail}}} = 0.833 \text{ lb}/\alpha q$$

wind

$$\frac{\partial W}{\partial \beta q} = 0.5 \text{ lb}/\beta q$$

**Fuselage Weight

$$\frac{\partial W}{\partial (\alpha q)_{\text{head}}} = 1.1 \text{ lb}/\alpha q$$

wind

VERTICAL TAIL

$$\frac{\partial W^{***}}{\partial (\beta q)} = 1.75 \text{ lb/deg-psf}$$

$$\frac{\partial W}{\partial (V_{\text{gust}})} = 49 \text{ lb/fps gust}$$

$$\frac{\partial W}{\partial (\text{rudder kick})} = 22 \text{ lb/\% variation}$$

***Vertical Tail Weight

SECTION 1

INTRODUCTION

The primary objective of this phase of the study was to establish the importance of design loads variability in terms of their influence upon structural weight sensitivity. Establishing these sensitivities can lead to the proper in-depth analysis of those loads which most affect the structure. This study also isolates those areas where data inadequacies exist and points out the areas where the most cost effective loads analysis can be performed. The space shuttle is not unlike conventional aircraft in that it has a small number of flight conditions which produce design loads. Phase I of this study identified the following flight conditions as the significant load conditions: 1) ascent winds, 2) entry maximum load factor, 3) entry maximum temperature, 4) subsonic gust and, 5) subsonic maneuvers. This phase of the study uses those flight conditions to establish load sensitivity.

SECTION 2

STRUCTURAL WEIGHT/LOAD SENSITIVITY

To establish design criteria, a clear understanding of the importance of the loads in terms of structural weight must be gained. Relative sensitivities of structural weight to various loading parameters are found in this study using the finite element programs described in the Phase I report (Reference 1). Significant load parameters established in Reference 1 are varied to develop weight sensitivity coefficients for each parameter. The effects on wing and vertical tail boxes and fuselage shell components are considered in this Phase II study.

2.1 WING STRUCTURE

2.1.1 WEIGHT SENSITIVITY TO INDIVIDUAL DESIGN LOADING CONDITIONS. The effects of load change are established by varying the load levels of the four critical wing design conditions. Table 2-1 summarises the weights for these conditions with variations to maximum αq , maximum g, subsonic gust, and maximum temperature. Further details of the weight breakdown of major component parts are given for one condition, maximum αq , in Table 2-2. It is interesting to note that the skins are at a minimum gage throughout the range of the loads being investigated.

Table 2-1. Summary of B-9U Wing Structural Model Weights

Condition W1		Condition W2		Condition W3		Condition W4	
αq Max		Max g		Subsonic Gust		Max Temp	
αq deg-psf	Wt. (lb)	g	Wt. (lb)	Gust Velocity (fps)	Wt. (lb)	Temp. (°F)	Wt. (lb)
1750	10,103			35	8,842		
2000	10,831	3.0	10,267	40	9,344		
2250	11,591	3.5	11,155	45	9,847	410	10,572
2500	12,332	4.2	12,423	50	10,353	700	11,525
2750	13,085	4.5	12,961	55	10,865	900	12,359
3000	13,846	5.0	13,885	60	11,407		
3250	14,617			65	11,976		

Table 2-2. Breakdown of Structural Model Weight by Component Parts for Condition W1

Component Part		αq	1750	2000	2250	2500	2750	3000	3250
Ribs	Upper Caps		143	154	166	179	192	205	219
	Lower Caps		156	169	183	197	211	226	240
	Webs		1230	1263	1293	1323	1353	1383	1414
	Stiffeners		175	197	219	241	263	287	310
Spars	Upper Caps		2069	2369	2701	3018	3338	3654	3974
	Lower Caps		1883	2160	2438	2708	2990	3280	3564
	Webs		269	292	315	339	363	387	411
	Diagonals		343	392	441	492	541	589	639
Skins	Upper (Quadrilateral)		1779	1779	1779	1779	1779	1779	1779
	Lower (Quadrilateral)		1874	1874	1874	1874	1874	1874	1874
	Upper (Triangular)	1	91	91	91	91	91	91	91
	Lower (Triangular)		91	91	91	91	91	91	92

1 Skins are all at minimum gage (set at 0.04 inch)

To evaluate the rate of change of wing structural weight for the various changes in load parameters, some weight adjustments have to be made. The structural model does not include every detail of the wing and so the structural weights output, by the computer program, has to be increased to account for such items as the leading and trailing edges, engine bay formers, etc. This is achieved by assuming that the weight of the secondary structure changes at the same rate as that of the primary structure. Factors of increase and decrease in weight of the structure about the critical baseline condition (W2-entry at maximum g) are derived from Table 2-1 and shown in Table 2-3. These factors are then applied to the total structural wing weight. This weight given on page 4-3 of Reference 1, excludes the elevons and TPS system and is taken to be 50,800 pounds, for the complete wing.

Plots of these data are shown on Figures 2-1 through 2-4 and are generally straight line plots within the scope of the variables chosen.

From Figure 2-1:

$$\frac{\partial W}{\partial(\alpha q)} = 12.4 \text{ lb/deg - psf}$$

Figure Figure 2-2:

$$\frac{\partial W}{\partial g} = 7,375 \text{ lb/g}$$

From Figure 2-3:

$$\frac{\partial W}{\partial V_{\text{gust}}} = 423 \text{ lb/fps - gust}$$

From Figure 2-4:

$$\frac{\partial W}{\partial T} = 13.8 \text{ lb/}^\circ\text{F}$$

Table 2-3. Structural Model Weight Variation Factors

Condition W1		Condition W2		Condition W3		Condition W4	
Max αq		Max g		Subsonic Gust		Max Temp	
αq (deg-psf)	Wt. Factor	g	Wt. Factor	Gust Velocity (fps)	Wt. Factor	Temp. (°F)	Wt. Factor
1750	0.813			35	0.712		
2000	0.872	3.0	0.826	40	0.752		
2250	0.933	3.5	0.898	45	0.793	410	0.851
2500	0.993	4.2	1.000	50	0.833	700	0.928
2750	1.053	4.5	1.043	55	0.875	900	0.995
3000	1.115	5.0	1.118	60	0.918		
3250	1.177			65	0.964		

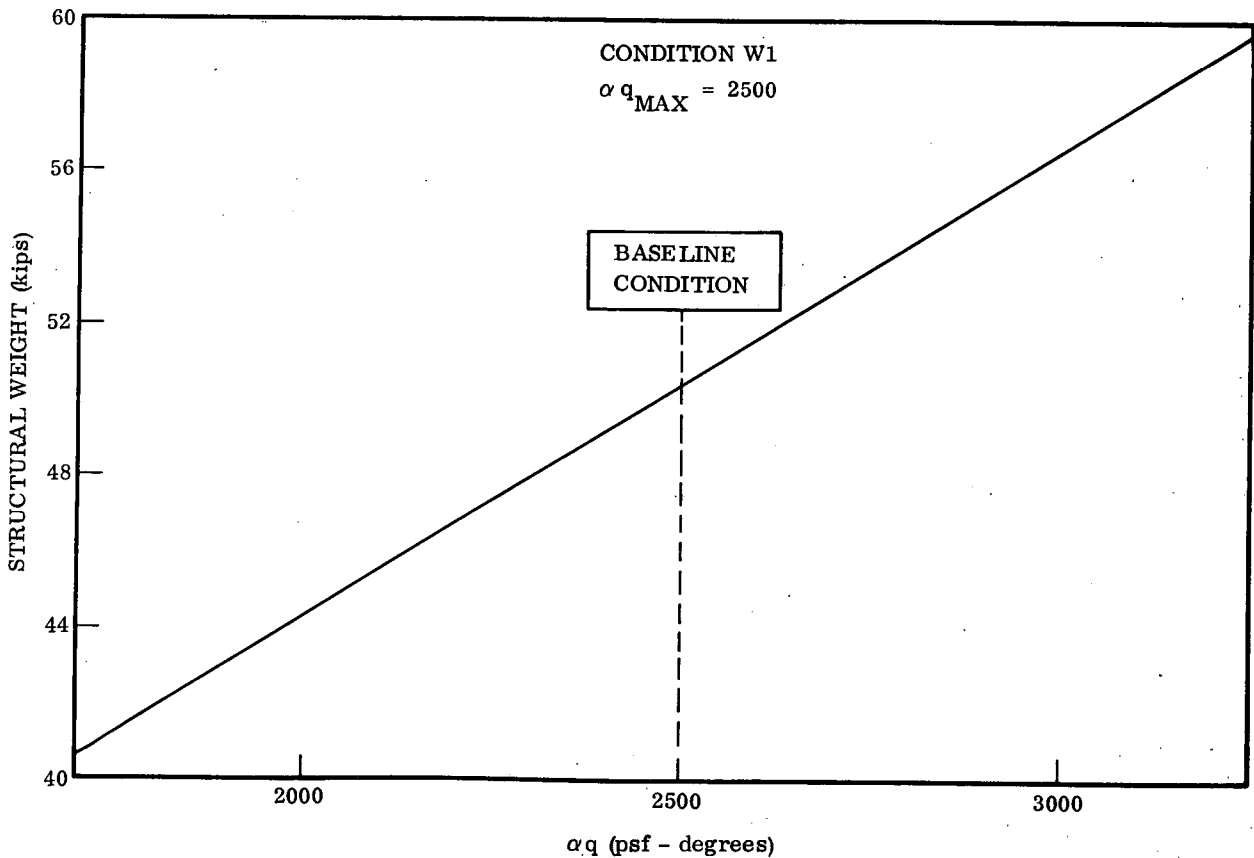


Figure 2-1. Booster Wing Structural Weight Variation with αq

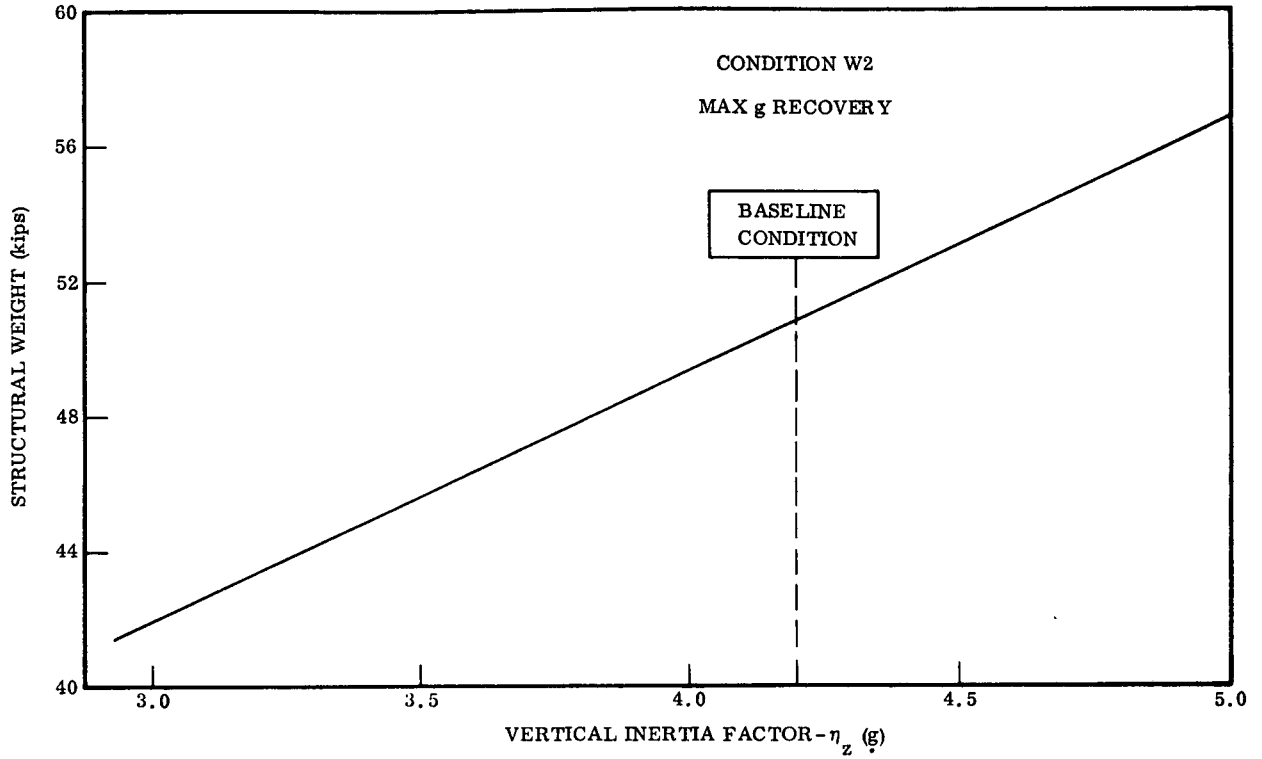


Figure 2-2. Booster Wing Structural Weight Variation with η_z

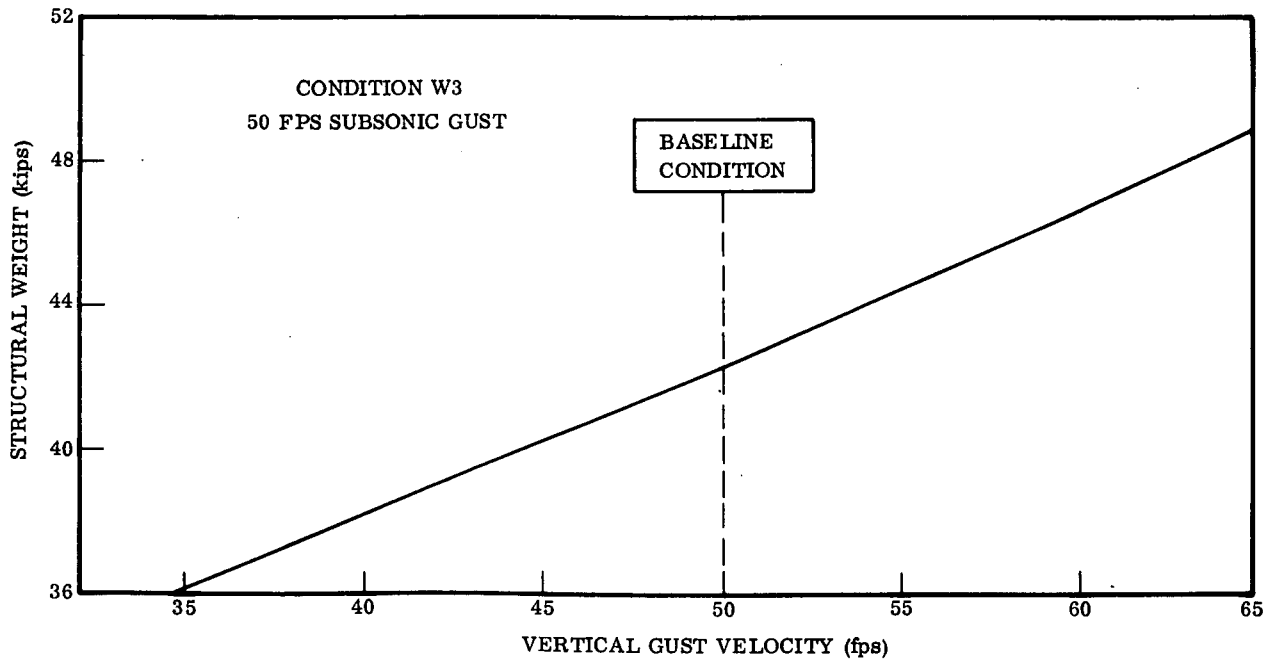


Figure 2-3. Booster Wing Structural Weight Variation with Gust Velocity

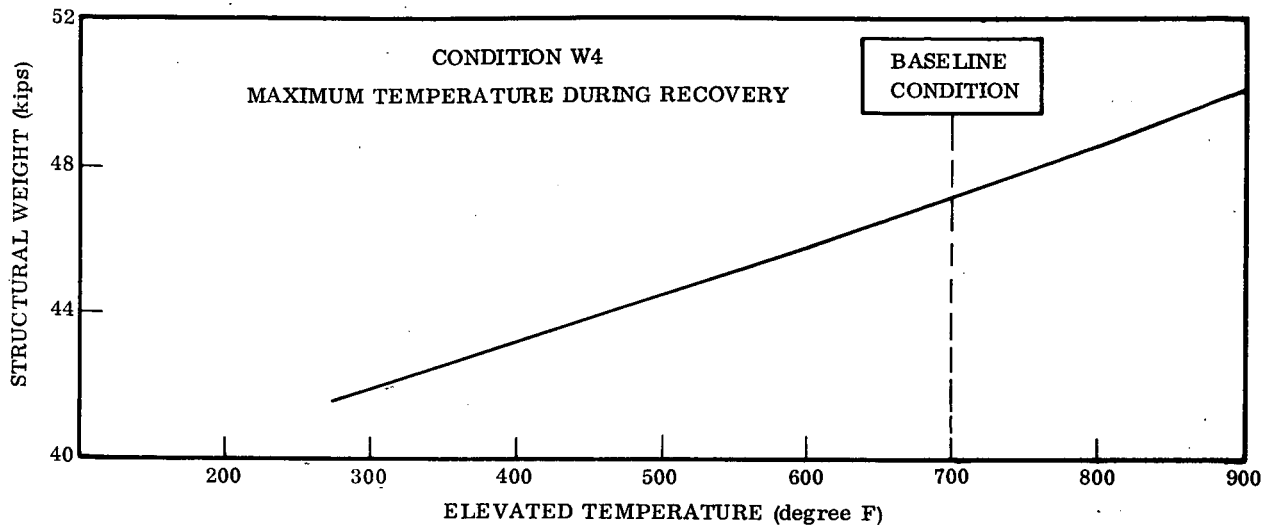


Figure 2-4. Booster Wing Structural Weight Variation with Elevated Temperature

By normalizing the data, Figure 2-5 shows condition W2 to be the most critical wing condition throughout the range of all the load levels considered.

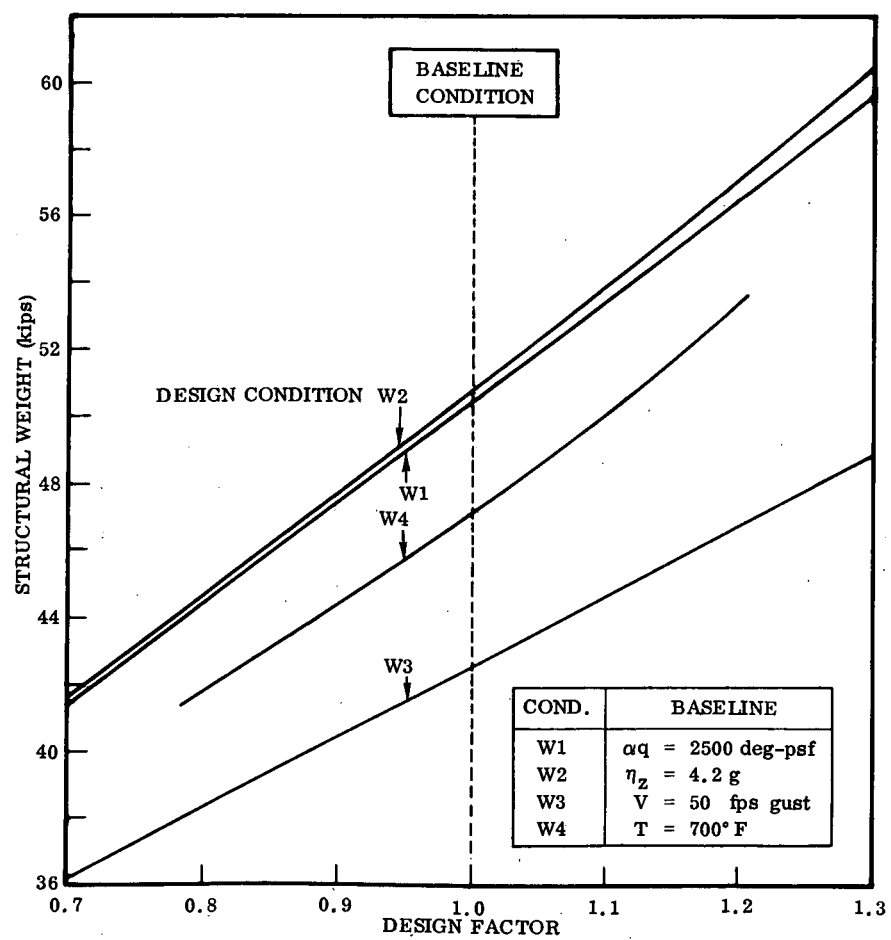
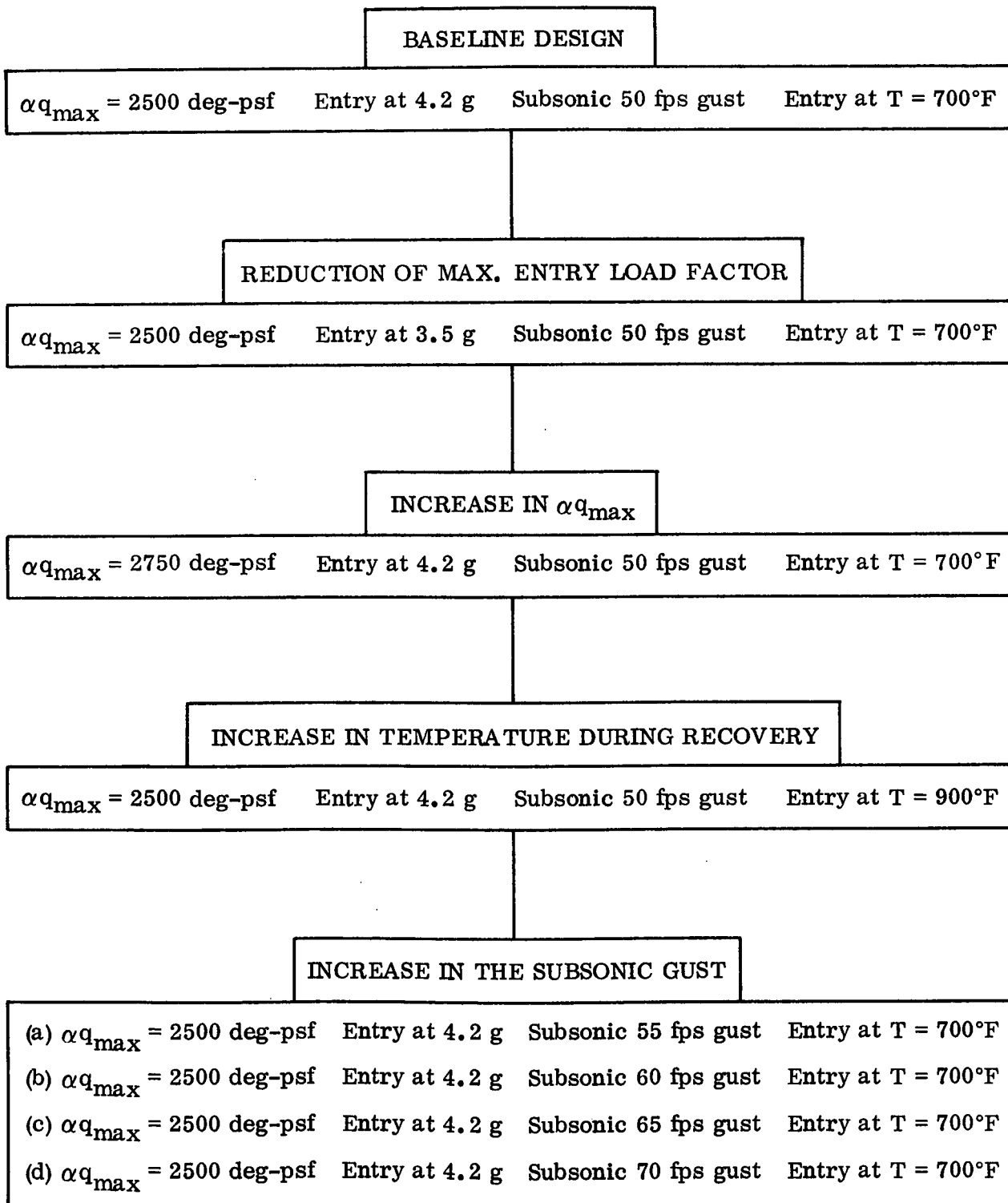


Figure 2-5. Booster Wing Structural Weight Variation about each Normalized Baseline Condition

2.1.2 WING WEIGHT SENSITIVITY TO COMBINED DESIGN LOADING CONDITIONS.
 The next approach taken was to combine all four design conditions into the synthesis program at once, varying one load at a time. Table 2-4 shows an outline of loads variation on the wing in the order used in the following investigation.

Table 2-4. Outline of Loads Variation on the Wing



The program first sizes the structure for each individual condition separately, then re-enters the maximum size for each element and reanalyzes and resizes for any selected number of times. Since the weight stabilizes early (Reference 1, Table 6-2), only one iteration is made for each of the parametric studies.

2.1.2.1 Reduction of Maximum Entry Load Factor. Reducing the maximum load factor during reentry from 4.2 g to 3.5 g, in combination with the other three baseline conditions, establishes αq_{max} as the most critical design condition (Reference Table 2-5). However, the weight saving is slight since the two conditions were very similar at the beginning. Using the input weight, after sizing, as the norm, the weight saving is only:

$$\Delta W = \left(\frac{12637 - 12471}{12637} \right) 100 = 1.3 \text{ percent}$$

Table 2-5. B-9U Wing - Weight Sensitivity to Loads

Reduction of Maximum Entry Load Factor:					
W1 - Ascent at αq_{max} with headwind (2500 deg-psf)					
W2 - Entry at maximum load factor (3.5 g)					
W3 - 50 fps gust in subsonic flight (50 fps)					
W4 - Entry at maximum temperature (700°F)					
Material Type	Structural Weight (pounds)				
	Input After Resize	Condition W3	Condition W4	Condition W1	Condition W2
Ribs					
Upper Caps	181	107	109	111	109
Lower Caps	202	105	121	128	129
Webs	1323	1172	1229	1270	1241
Stiffeners	265	185	233	239	210
Spars					
Upper Caps	3063	2256	2705	3048	2531
Lower Caps	2726	2074	2440	2761	2275
Webs	341	256	296	327	285
Diagonals	356	348	459	499	425
Skins					
Upper (Quadrilateral)	1779	1779	1779	1779	1779
Lower (Quadrilateral)	1874	1874	1874	1874	1874
Upper (Triangular)	91	91	91	91	91
Lower (Triangular)	91	91	91	91	91
Total Structural Model Weight	12471	10338	11427	12218	11040

1 Reference 1, Table 6-1.

Although the load factor was reduced to 3.5 g in Table 2-5, much the same weight saving could be achieved by a lesser reduction. It is reasonable to assume that there would be little change in the structural box weight for a reduction in load factor to 4.0 g, rather than to 3.5 g, as the αq_{\max} becomes the predominant condition with any small reduction in vertical load factor.

2.1.2.2 Increase in αq_{\max} . A slight increase in αq_{\max} raises the wing loads such that this becomes the critical design condition. Table 2-6 shows this to be true by a slight increase from 2500 deg-psf to 2750 deg-psf. It also shows that the total structural box weight is sensitive to slight changes in αq_{\max} . The increase in αq_{\max} from 2500 to 2750 deg-psf, a 10 percent increase, produces a weight increase of:

$$\Delta W = \left(\frac{13197 - 12637}{12637} \right) 100 = 4.4 \text{ percent}$$

Table 2-6. B-9U Wing - Weight Sensitivity to Loads

Increase in αq_{\max} :					
W1 - Ascent at αq_{\max} with headwind (2750 deg-psf)					
W2 - Entry at maximum load factor (4.2 g)					
W3 - 50 fps gust in subsonic flight (50 fps)					
W4 - Entry at maximum temperature (700°F)					
Material Type	Structural Weight (pounds)				
	Input After Resize	Condition W3	Condition W4	Condition W1	Condition W2
Ribs					
Upper Caps	197	108	110	115	114
Lower Caps	224	105	124	136	143
Webs	1353	1171	1229	1291	1278
Stiffeners	284	185	232	261	250
Spars					
Upper Caps	3368	2256	2256	3358	3062
Lower Caps	2999	2075	2421	3044	2770
Webs	364	258	298	352	325
Diagonals	573	347	456	549	515
Skins					
Upper (Quadrilateral)	1779	1779	1779	1779	1779
Lower (Quadrilateral)	1874	1874	1874	1874	1874
Upper (Triangular)	91	91	91	91	91
Lower (Triangular)	91	91	91	91	91
Total Structural Model Weight	13197	10340	11374	12941	12292

Where 12,637 pounds is the total structural weight of the baseline design and 13,197 pounds the increased αq_{max} design (Reference Table 2-6).

2.1.2.3 Increase In Temperature During Recovery. It takes an increase in maximum reentry temperature from 700°F to 900°F to make this the critical design condition — an increase of 29 percent, and this with negligible increase in total structural weight 12763-pounds. (See Table 2-7) compared with 12637-pounds (Reference 1, Table 6-2). The reason for this is that the load factor is much lower at maximum temperature than it is at maximum load factor.

Table 2-7. B-9U Wing - Weight Sensitivity to Loads

Increase in Temperature During Recovery:					
W1 - Ascent at αq_{max} with headwind (2500 deg-psf)					
W2 - Entry at maximum load factor (4.2 g)					
W3 - 50 fps gust in subsonic flight (50 fps)					
W4 - Entry at maximum temperature (900°F)					
Material Type	Structural Weight (pounds)				
	Input After Resize	Condition W3	Condition W4	Condition W1	Condition W2
Ribs					
Upper Caps	195	107	110	112	113
Lower Caps	222	105	128	131	142
Webs	1336	1173	1253	1270	1280
Stiffeners	284	185	261	238	250
Spars					
Upper Caps	3146	2256	3060	3045	3061
Lower Caps	2829	2072	2766	2761	2765
Webs	348	255	320	324	322
Diagonals	569	349	519	500	520
Skins					
Upper (Quadrilateral)	1779	1779	1779	1779	1779
Lower (Quadrilateral)	1874	1874	1874	1874	1874
Upper (Triangular)	91	91	91	91	91
Lower (Triangular)	91	91	91	91	91
Total Structural Model Weight	12763	10337	12251	12217	12288

2.1.2.4 Increase in the Subsonic Gust. The baseline value for a subsonic gust of 50 fps creates a design condition much below the other three design conditions. Giving a

structural weight of 10,353 pounds (Reference 1, Table 6-2). This is less than the design baseline weight of 12,637 pounds by:

$$\left(\frac{12637 - 10353}{12637} \right) 100 = 18 \text{ percent}$$

Table 2-8 shows increases in the subsonic gust in steps of 10 percent, and at 70 fps gust this condition becomes critical. It also shows that some elements are designed by the subsonic gust even at the 55 fps level since the total structural weight showed some increase (12,702 pounds over 12,637 pounds) when the total weight for the gust condition alone is still far below the critical design conditions (being only 10,852 pounds). This is because the pressure distribution for the subsonic flight has a center of pressure much further forward than the other three conditions. The other conditions all being supersonic and having a fairly uniform chordwise pressure distribution.

Table 2-8a. B-9U Wing - Weight Sensitivity to Loads (55 fps gust in subsonic flight)

Increase in the subsonic gust:					
W1 - Ascent at $\alpha_{q_{max}}$ with headwind (2500 deg-psf)					
W2 - Entry at maximum load factor (4.2 g)					
W3 - 55 fps gust in subsonic flight (55 fps)					
W4 - Entry at maximum temperature (700°F)					
Material Type	Structural Weight (pounds)				
	Input After Resize	Condition W3	Condition W4	Condition W1	Condition W2
Ribs					
Upper Caps	196	108	109	112	113
Lower Caps	222	105	123	130	142
Webs	1336	1180	1229	1269	1278
Stiffeners	280	203	234	238	251
Spars					
Upper Caps	3139	2483	2694	3048	3064
Lower Caps	2784	2284	2427	2763	2764
Webs	345	268	294	323	323
Diagonals	564	386	461	501	521
Skins					
Upper (Quadrilateral)	1779	1779	1779	1779	1779
Lower (Quadrilateral)	1874	1874	1874	1874	1874
Upper (Triangular)	91	91	91	91	91
Lower (Triangular)	91	91	91	91	91
Total Structural Model Weight	12702	10852	11405	12219	12291

C-2

Table 2-8b. B-9U Wing - Weight Sensitivity to Loads (60 fps gust in subsonic flight)

Material Type	Structural Weight (pounds)				
	Input After Resize	Condition W3	Condition W4	Condition W1	Condition W2
Ribs					
Upper Caps	197	108	109	111	113
Lower Caps	222	105	123	131	142
Webs	1336	1190	1230	1270	1279
Stiffeners	287	222	235	240	251
Spars					
Upper Caps	3202	2719	2688	3047	3062
Lower Caps	2854	2488	2423	2759	2759
Webs	346	280	292	321	318
Diagonals	578	426	464	504	524
Skins					
Upper (Quadrilateral)	1779	1779	1779	1779	1779
Lower (Quadrilateral)	1874	1874	1874	1874	1874
Upper (Triangular)	91	91	91	91	91
Lower (Triangular)	91	91	91	91	91
Total Structural Model Weight	12858	11373	11399	12217	12284

Table 2-8c. B-9U Wing - Weight Sensitivity to Loads (65 fps gust in subsonic flight)

Material Type	Structural Weight (pounds)				
	Input After Resize	Condition W3	Condition W4	Condition W1	Condition W2
Ribs					
Upper Caps	198	109	108	111	113
Lower Caps	222	105	123	131	142
Webs	1336	1204	1232	1272	1281
Stiffeners	296	241	236	241	253
Spars					
Upper Caps	3292	2951	2677	3043	3055
Lower Caps	2977	2690	2420	2754	2755
Webs	349	293	290	318	316
Diagonals	599	466	467	507	527

Table 2-8c. B-9U Wing - Weight Sensitivity to Loads (65 fps gust in subsonic flight)
(Continued)

Material Type	Structural Weight (pounds)				
	Input After Resize	Condition W3	Condition W4	Condition W1	Condition W2
Skins					
Upper (Quadrilateral)	1779	1779	1779	1779	1779
Lower (Quadrilateral)	1874	1874	1874	1874	1874
Upper (Triangular)	91	91	91	91	91
Lower (Triangular)	91	91	91	91	91
Total Structural Model Weight	13104	11893	11387	12212	12277

Table 2-8d. B-9U Wing - Weight Sensitivity to Loads (70 fps gust in subsonic flight)

Material Type	Structural Weight (pounds)				
	Input After Resize	Condition W3	Condition W4	Condition W1	Condition W2
Ribs					
Upper Caps	199	109	108	111	113
Lower Caps	223	105	123	131	142
Webs	1337	1218	1234	1274	1283
Stiffeners	305	260	237	241	254
Spars					
Upper Caps	3416	3179	2672	3037	3052
Lower Caps	3129	2906	2411	2750	2751
Webs	353	307	289	317	316
Diagonals	621	507	469	509	528
Skins					
Upper (Quadrilateral)	1779	1779	1779	1779	1779
Lower (Quadrilateral)	1874	1874	1874	1874	1874
Upper (Triangular)	91	91	91	91	91
Lower (Triangular)	91	91	91	91	91
Total Structural Model Weight	13418	12428	11378	12207	12274

In summary Table 6-2 of Reference 1 and Tables 2-3 through 2-8 of this report are plotted as bar graphs in Figures 2-6 and 2-7. Figure 2-6 presents the change in total structural weight for each parametric study. And, Figure 2-7 gives similar information based on percentage change in structural weight over the baseline design. From

these graphs it can be seen that lowering the maximum entry load factor has little effect on the total structural wing weight whereas the weight is very sensitive to peak dynamic pressure. The entry temperature is not very critical up to 900°F. The subsonic gust condition designs certain portions of the wing box structure such that the total structural weight is influenced by any change to the gust velocity. However, it takes something like a 20 percent increase in gust velocity (50 to 60 fps) before the weight increases by one percent. From this study, the space shuttle booster wing, with the design shown in Reference 1 (including a TPS and titanium primary structure), is most sensitive to peak dynamic pressure and relatively insensitive to the other parameters considered.

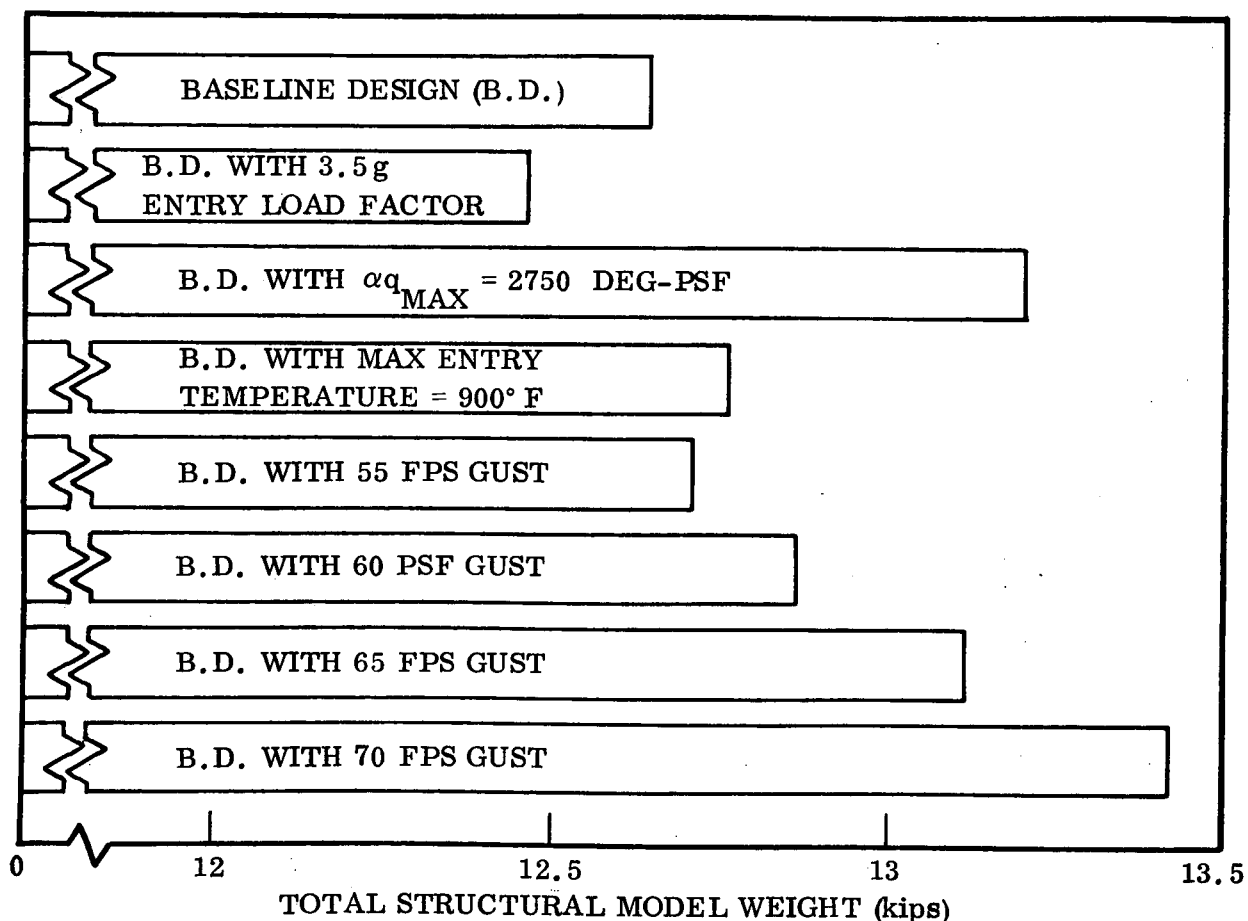


Figure 2-6. B-9U Wing - Parametric Studies On Weight Sensitivities

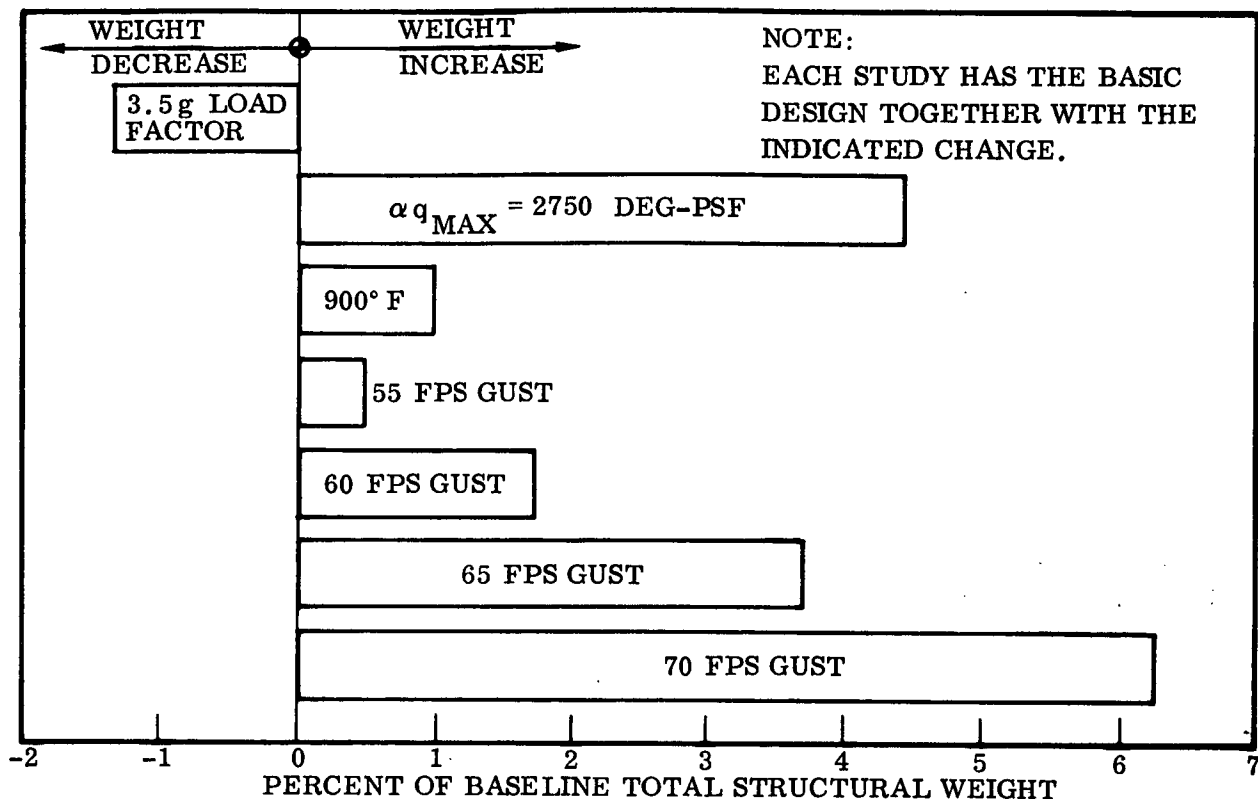


Figure 2-7. B-9U Wing - Parametric Studies On Weight Sensitivities as a Percentage Increase or Decrease of the Baseline Design Total Structural Weight

2.2 VERTICAL TAIL STRUCTURE

2.2.1 VERTICAL STABILIZER WEIGHT SENSITIVITY WITH INDIVIDUAL DESIGN CONDITIONS. The vertical tail is analyzed by the same process as that applied to the wing in Section 2.1. Table 2-9 summarizes the model structural weights derived from the computer program, for the three primary design conditions. To arrive at the total structural box weights, the variation factors of Table 2-10 are deduced by considering the design norm to be the maximum βq of 2400 deg-psf. Load variations for the three conditions are then given in Table 2-11 and plotted on Figures 2-8 through 2-10, based on a vertical stabilizer weight of 6660 pounds. This weight, given in Table 4-3 of Reference 1, excludes the vertical stabilizer tip and the rudder.

From Figure 2-8:

$$\frac{\partial W}{\partial(\beta q)} = 1.75 \text{ lb/deg-psf}$$

From Figure 2-9:

$$\frac{\partial W}{\partial V_{gust}} = 49 \text{ lb/fps-gust}$$

From Figure 2-10:

$$\frac{\partial W}{\partial R} = 21.8 \text{ lb/percent load change}$$

Where R is a percentage load change

Table 2-9. Summary of Vertical Tail Model Weights

Condition T1		Condition T2		Condition T3	
Maximum βq		Subsonic Gust		Rudder Kick	
βq (deg-psf)	Weight (pounds)	V (fps)	Weight (pounds)	Load Ratio	Weight (pounds)
1920	3187	40	2681	0.8	2678
2400	3632	50	2945	1.0	2895
2880	4104	60	3213	1.2	3152

Table 2-10. Structural Model Weight Variation Factors

Condition T1		Condition T2		Condition T3	
Maximum βq		Subsonic Gust		Rudder Kick	
βq (deg-psf)	Weight Factor	V (fps)	Weight Factor	Load Ratio	Weight Factor
1920	0.878	40	0.738	0.8	0.737
2400	1.000	50	0.811	1.0	0.797
2880	1.130	60	0.885	1.2	0.868

Table 2-11. Vertical Stabilizer Structural Weight Variation

Condition T1		Condition T2		Condition T3	
Maximum βq		Subsonic Gust		Rudder Kick	
βq (deg-psf)	Weight (pounds)	V (fps)	Weight (pounds)	Load Ratio	Weight (pounds)
1920	5850	40	4920	0.8	4910
2400	6660	50	5400	1.0	5310
2880	7530	60	5900	1.2	5780

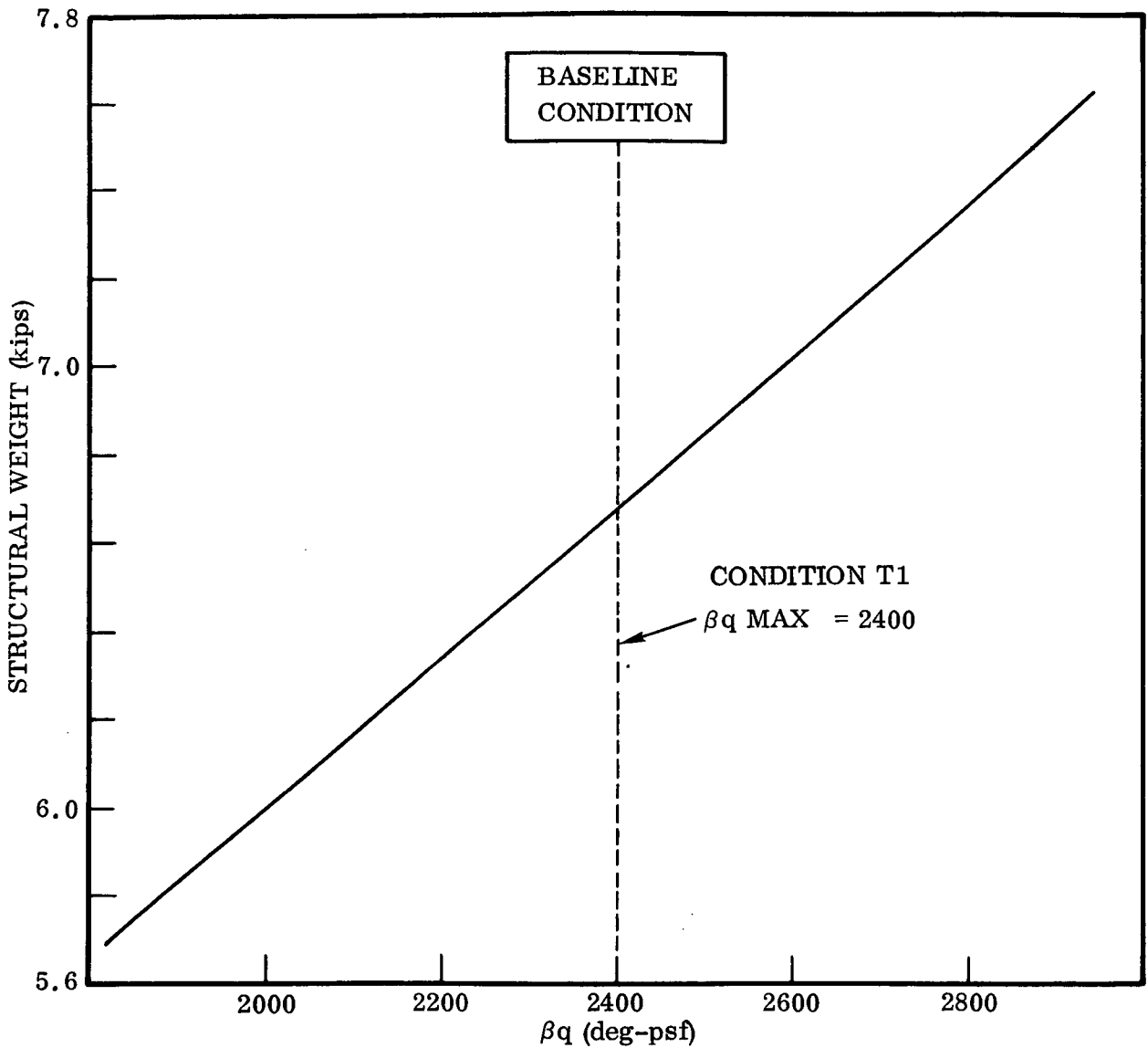


Figure 2-8. Vertical Stabilizer Structural Weight Variation with βq

2.2.2 VERTICAL STABILIZER WEIGHT SENSITIVITY WITH COMBINED LOADS. To define the sensitivity of the vertical stabilizer structural box to variable combined loads, all three load conditions are combined in the synthesis program. This baseline design loads criteria includes:

- a. Maximum βq of 2400 deg-psf
- b. 50 fps subsonic gust
- c. Rudder Kick (abrupt rudder movement from zero to maximum deflection).

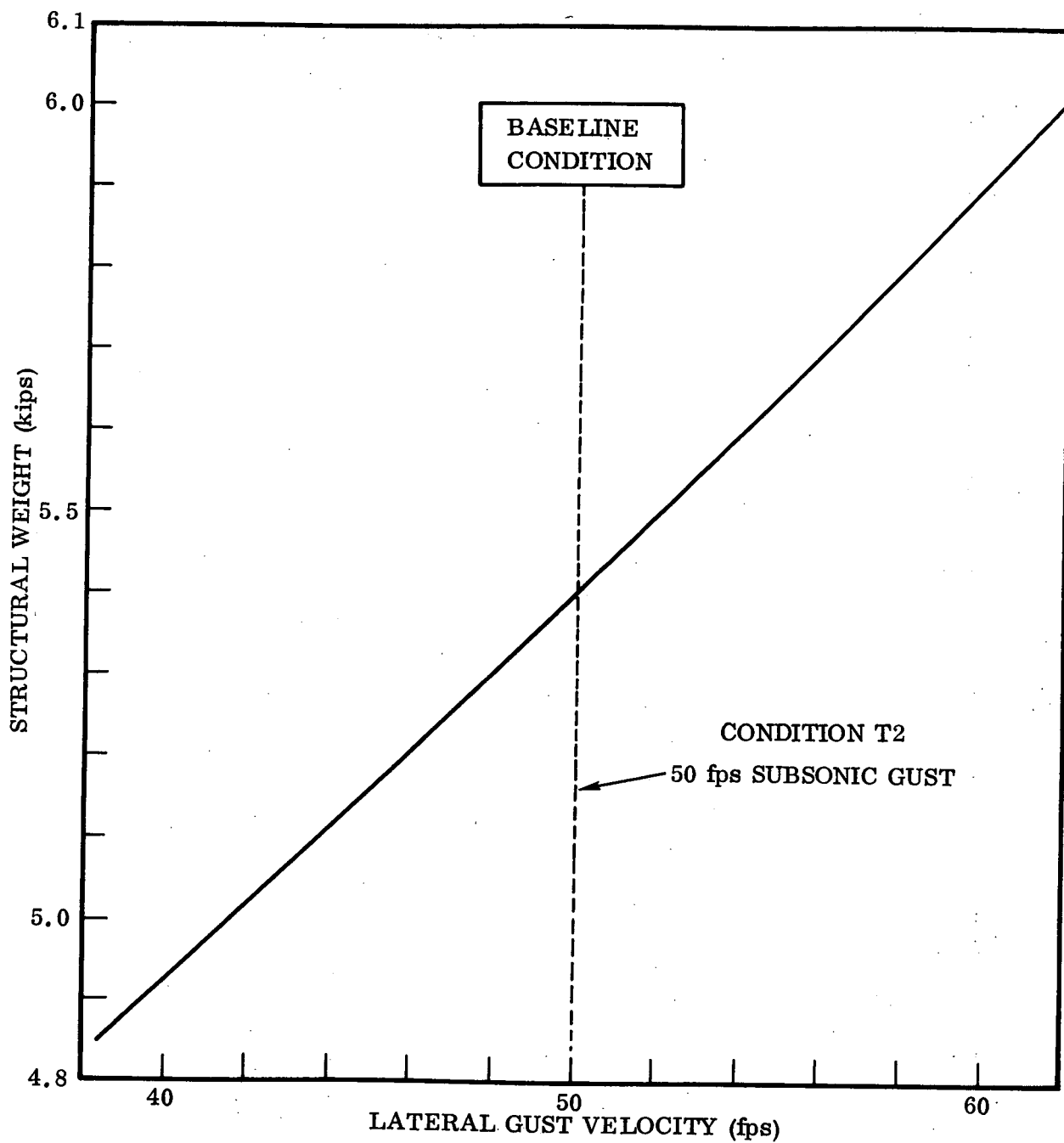


Figure 2-9. Vertical Stabilizer Structural Weight Variation with Lateral Gust Velocity

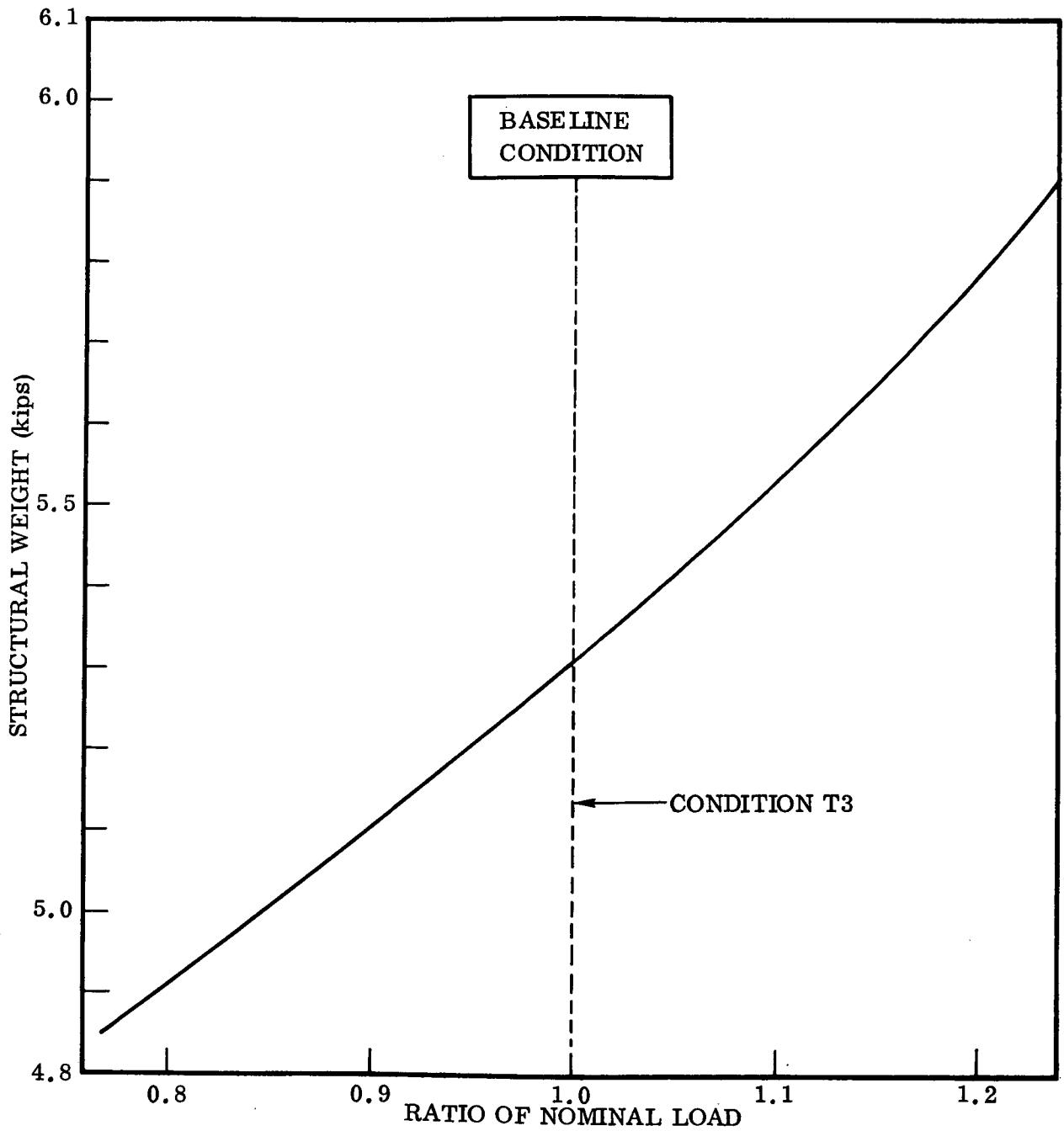


Figure 2-10. Vertical Stabilizer Structural Weight Variation for the Rudder Kick Condition

Table 2-12 summarizes the results of this analysis for a resized structure, and one iteration after resize, for various individual load changes. Figure 2-11 gives the relative effects of load variation on the model structural weight. Here it can be seen that varying the subsonic gust condition by as much as ± 20 percent does not affect the box design. And, changing the rudder kick condition by a similar amount only changes the weight slightly. This is because, as was shown in Reference 1, page 6-3, maximum dynamic pressure during ascent designs most of the vertical stabilizer. An increase in the surface load for the rudder kick condition of 20 percent causes a 2.4 percent weight increase (see Figure 2-12), and a 20 percent load decrease gives 0.8 percent weight decrease. Whereas raising the βq to 2880 causes a 12.3 percent weight penalty and lowering βq to 1920 promotes a weight saving of 10.5 percent of the structural box weight.

Table 2-12. Vertical Stabilizer Structural Model Sensitivity to Variable Combined Loads

Resized Structure						Input After Resize	First Iteration					
Ascent		Subsonic Gust		Rudder Kick			Ascent		Subsonic Gust		Rudder Kick	
βq_{max} (deg-psf)	Weight (pounds)	Velocity (fps)	Weight (pounds)	Load Ratio	Weight (pounds)	Weight (pounds)	βq_{max} (deg-psf)	Weight (pounds)	Velocity (fps)	Weight (pounds)	Load Ratio	Weight (pounds)
2400	3632	50	2945	1.0	2895	3684	2400	3674	50	2945	1.0	2910
1920	3187	50	2945	1.0	2895	3296	1920	3214	50	2939	1.0	2907
2880	4104	50	2945	1.0	2895	4138	2880	4153	50	2952	1.0	2904
2400	3632	40	2681	1.0	2895	3682	2400	3674	40	2706	1.0	2913
2400	3632	60	3213	1.0	2895	3690	2400	3674	60	3216	1.0	2910
2400	3632	50	2945	0.8	2678	3655	2400	3678	50	2950	0.8	2683
2400	3632	50	2945	1.2	3152	3771	2400	3665	50	2942	1.2	3166

2.3 FUSELAGE STRUCTURE

2.3.1 STRUCTURAL WEIGHT SENSITIVITY TO αq LOADS. In order to compute the booster fuselage structural weight sensitivity to αq loads, the structural weight is determined with no consideration of maximum αq as a design condition. Then the weight increases are determined from this baseline for maximum αq 's of ± 2800 , ± 3500 , and ± 4500 . The procedure for determining the weight increases includes the calculation of new internal loads and corresponding structural gages for each of the conditions listed.

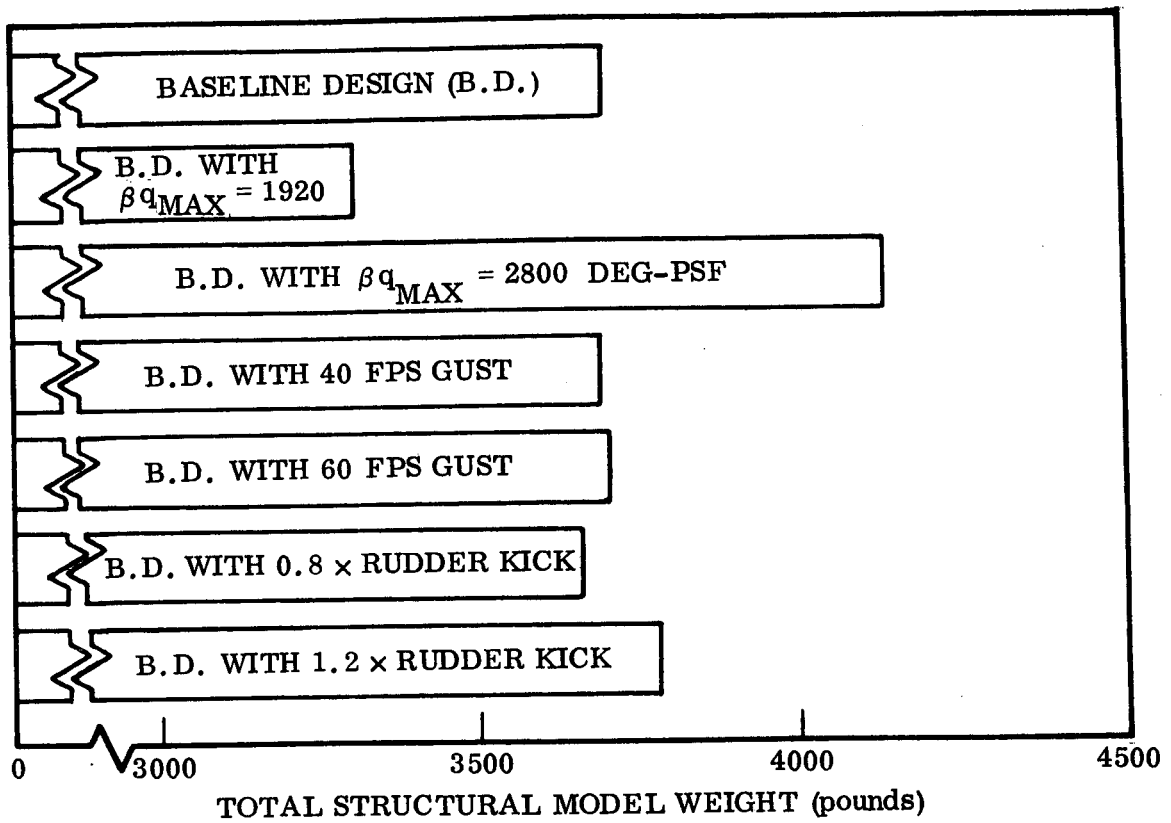


Figure 2-11. Vertical Stabilizer Weight Sensitivities to Various Load Parameters

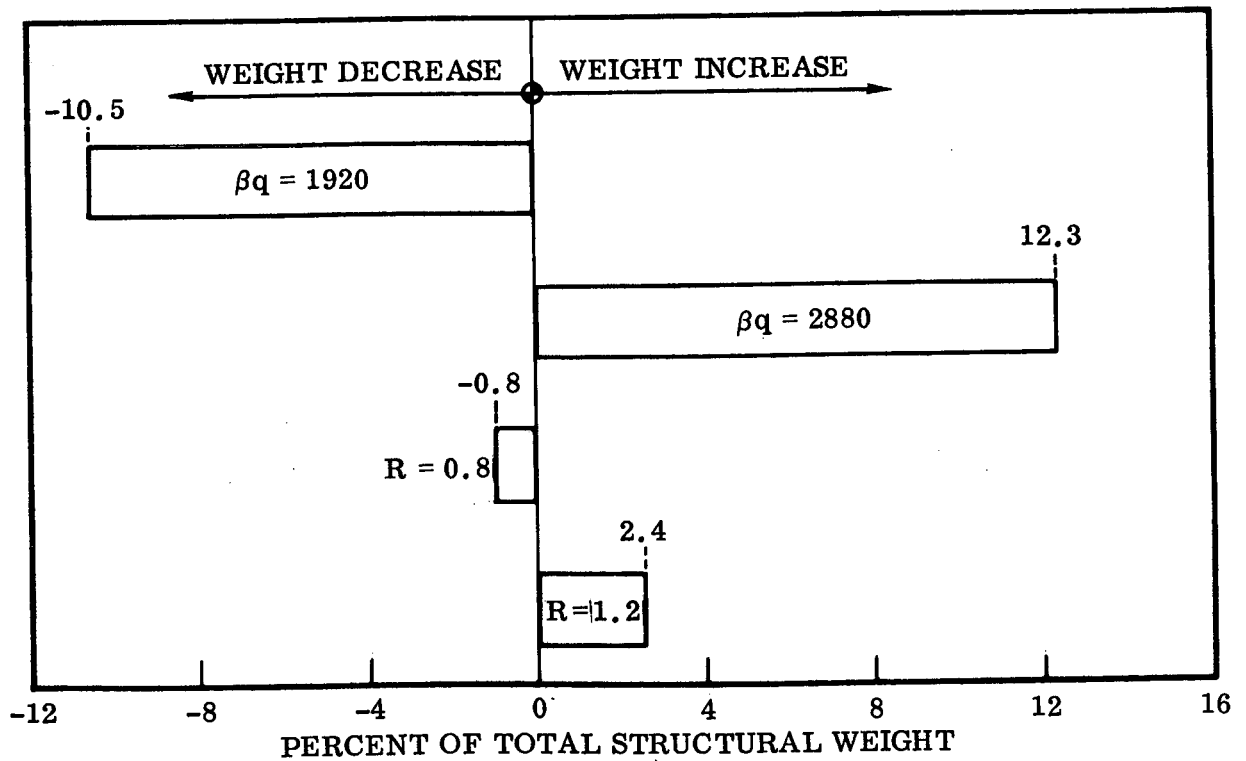


Figure 2-12. Vertical Stabilizer Weight Sensitivity as a Percentage Change from the Baseline Total Structural Weight

The results of this study are given in Table 2-13 and Figure 2-13. In Table 2-13, the actual calculated weight increases are presented. In Figure 2-13 these data are plotted as a function of maximum αq for the body and tanks. For maximum αq tailwinds, the weight plot consists almost entirely of the weight of the Station 2666 frame which provides aft support for the NR 161-C orbiter. The only other effect on the booster for maximum αq tailwinds is a 16-pound LH₂ tank weight increase for $\alpha q = -4500$. Therefore, larger body and tank increases of weight may be expected for maximum αq tailwind cases more severe than $q = -4500$. For maximum αq headwinds, the Station 2666 frame is unaffected and increases of weight plotted for the body and tanks are confined to the LH₂ tank. Beyond approximately $\alpha q = 3000$, engine gimbal angle limits are reached and internal body loads are relieved due to rotational acceleration giving no further weight increase.

Table 2-13. Fuselage Weight Increases Due to Maximum αq

Δ WEIGHT, POUNDS		
αq	BODY AND TANKS	
	Station 2666 Frame	LH ₂ Tanks
-4500	1958	16
-3500	1200	0
-2800	753	0
2800	0	755
3500	0	829
4500	0	746

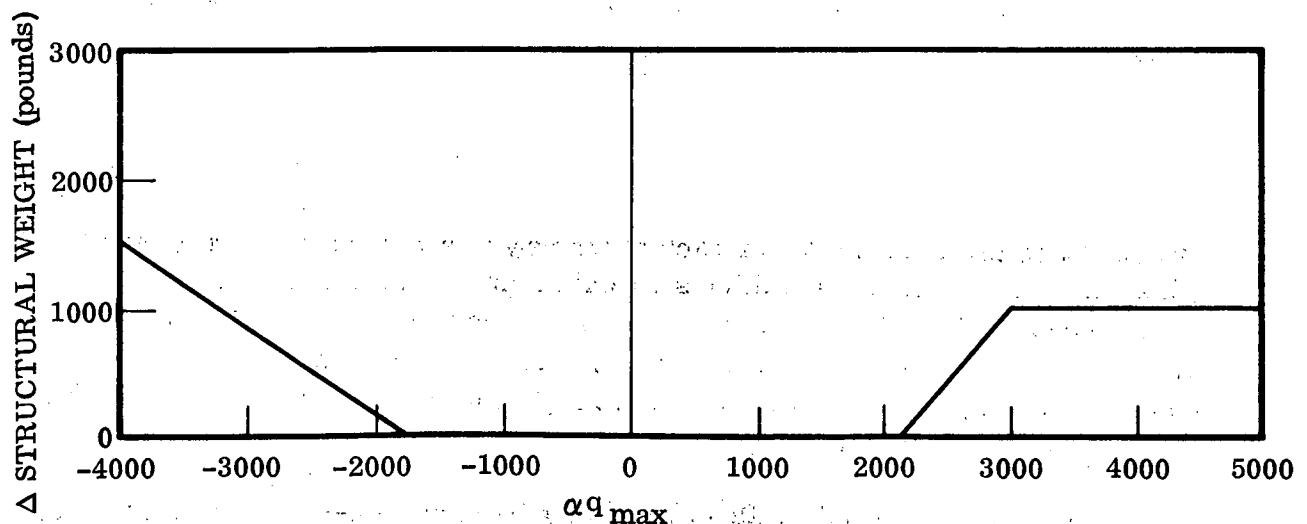


Figure 2-13. Fuselage Weight Sensitivity to Maximum αq

2.3.2 STRUCTURAL WEIGHT SENSITIVITY TO END BOOST ACCELERATION. An investigation is made to determine the effects of end boost acceleration on the booster fuselage structural weight, around the baseline limit of 3g. End boost accelerations of 2.5, 2.75, 3.25 and 3.50 g's are attained using the baseline trajectory and adjusting the time at which the main engines are throttled, then maintaining this g level until burnout (see Figure 2-14).

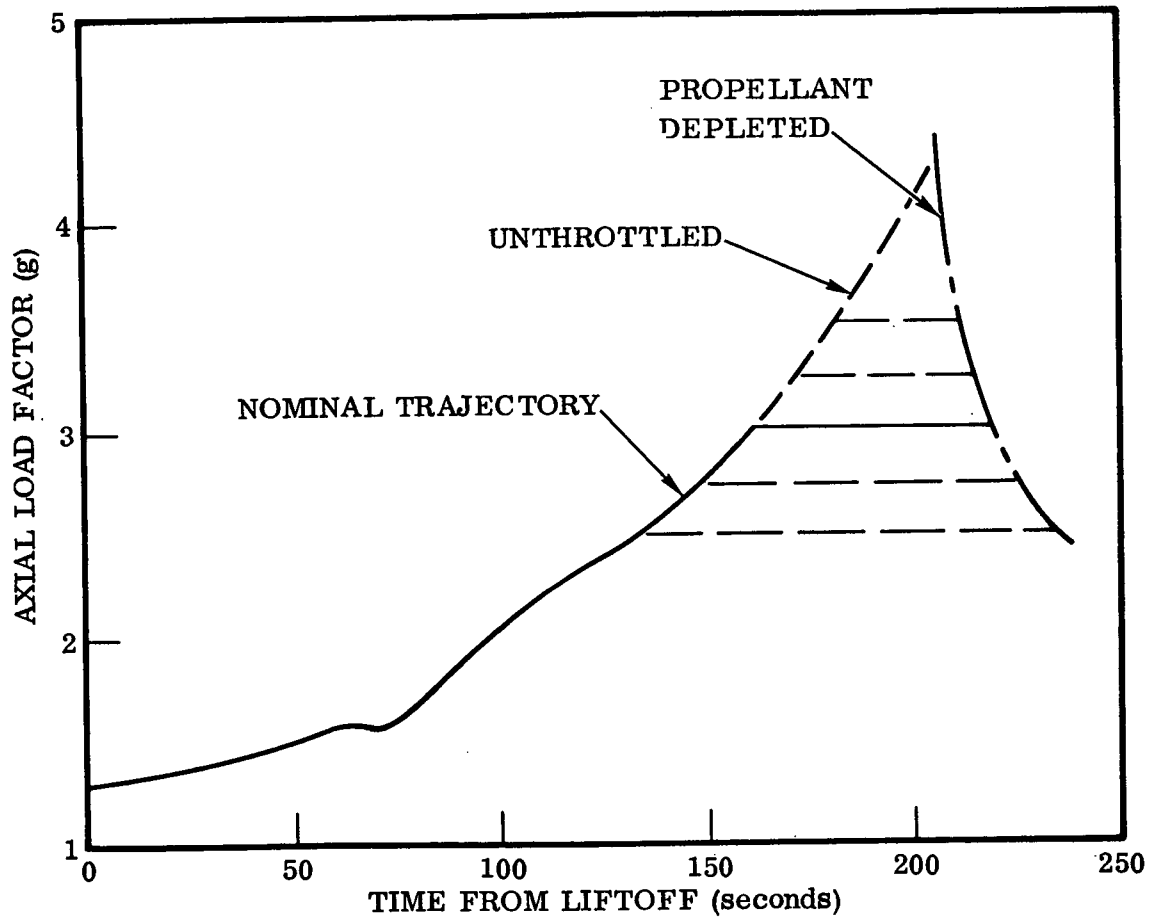


Figure 2-14. Boost Axial Load Factor

Internal loads are determined for each of the new g levels, at the point where throttling is started and at burnout. Conditions 10 and 11 (maximum thrust and booster burnout — Reference 1, Table 6-3) being modified with each run of the NETLD2 program. These conditions also account for a ten percent dynamic amplification of the axial g level. Weight sensitivity to these loads is resolved by resizing the fuselage for the two new conditions at each g level.

Peak ultimate axial load intensities are summarized in Tables 2-14 through 2-23. Tables 2-14 and 2-15 present the baseline design axial tension and compression load intensities at each of 48 stations at eight points around the fuselage, as explained in Reference 1,

Table 2-14. B-9U/161-C Ultimate Tension Internal Loads (Baseline)

PEAK ULTIMATE AXIAL TENSION LOAD INTENSITIES

STATION (IN)	NX1 (LB/IN)	NX2 (LB/IN)	NX3 (LB/IN)	NX4 (LB/IN)	NX5 (LB/IN)	NX6 (LB/IN)	NX7 (LB/IN)	NX8 (LB/IN)
1300	0(16)	0(16)	0(16)	0(16)	0(16)	0(16)	0(16)	0(16)
1036	5(12)	4(12)	0(15)	0(16)	1(11)	0(16)	0(15)	4(12)
1072	45(12)	32(12)	1(15)	3(11)	8(11)	3(11)	1(15)	32(12)
1131	73(12)	51(12)	3(15)	7(16)	13(8)	7(16)	3(15)	51(12)
1278	141(12)	98(12)	7(15)	28(16)	58(8)	28(16)	7(15)	98(12)
1337	173(12)	121(12)	9(15)	42(8)	89(8)	42(8)	9(15)	121(12)
1341	177(12)	124(12)	8(14)	121(15)	192(15)	121(15)	8(14)	124(12)
1477	288(12)	202(12)	14(14)	99(8)	191(8)	99(8)	14(14)	202(12)
1481	1411(12)	1322(12)	1229(10)	1280(8)	1374(8)	1280(8)	1229(10)	1322(12)
1600	1569(12)	1430(12)	1194(10)	1377(8)	1531(8)	1377(8)	1194(10)	1430(12)
1750	1820(12)	1601(12)	1149(10)	1539(8)	1791(8)	1539(8)	1153(9)	1601(12)
1854	2042(12)	1753(12)	1102(10)	1510(8)	1780(8)	1510(8)	1102(10)	1753(12)
1858	931(12)	640(12)	35(14)	86(13)	140(13)	85(13)	35(14)	640(12)
2006	1932(11)	853(11)	47(14)	155(13)	242(13)	153(13)	47(14)	853(11)
2022	2207(11)	996(11)	48(14)	166(13)	258(13)	164(13)	48(14)	996(11)
2026	2274(11)	1031(11)	45(14)	160(13)	251(13)	158(13)	45(14)	1031(11)
2042	2544(11)	1169(11)	47(14)	192(13)	242(13)	150(13)	47(14)	1169(11)
2094	3431(11)	1631(11)	52(14)	141(14)	219(13)	141(14)	52(14)	1631(11)
2098	3476(11)	1650(11)	52(14)	142(14)	217(13)	142(14)	52(14)	1650(11)
2180	3878(11)	1678(11)	60(14)	168(14)	213(14)	168(14)	60(14)	1678(11)
2184	5798(11)	3588(11)	1454(13)	1653(13)	1734(13)	1650(13)	1450(13)	3588(11)
2300	5803(11)	3577(11)	1444(13)	1656(13)	1743(13)	1653(13)	1439(13)	3577(11)
2400	5813(11)	3574(11)	1437(13)	1675(13)	1772(13)	1671(13)	1431(13)	3574(11)
2500	5820(11)	3568(11)	1433(13)	1709(13)	1821(13)	1704(13)	1426(13)	3568(11)
2500	5822(11)	3559(11)	1432(13)	1756(13)	1888(13)	1751(13)	1424(13)	3559(11)
2664	5822(11)	3552(11)	1431(13)	1793(13)	1940(13)	1787(13)	1422(13)	3552(11)
2668	5813(11)	3545(11)	1431(13)	1795(13)	1944(13)	1789(13)	1422(13)	3545(11)
2800	5193(11)	3092(11)	1429(13)	1886(13)	2072(13)	1879(13)	1419(13)	3092(11)
2864	4899(11)	2871(11)	1429(13)	1937(13)	2144(13)	1930(13)	1418(13)	2871(11)
2868	4870(11)	2856(11)	1429(13)	1940(13)	2149(13)	1933(13)	1418(13)	2856(11)
2950	4450(11)	2977(12)	1428(13)	2015(13)	2254(13)	2007(13)	1417(13)	2977(12)
3050	3796(12)	3103(12)	1428(12)	2172(13)	2477(13)	2164(13)	1428(12)	3102(12)
3161	3683(12)	3033(12)	1464(12)	2487(13)	2921(13)	2477(13)	1464(12)	3033(12)
3165	3615(12)	2980(12)	1448(12)	2497(13)	2938(13)	2487(13)	1448(12)	2980(12)
3293	2979(12)	2538(12)	1473(12)	2631(16)	3721(16)	2631(16)	1473(12)	2538(12)
3295	2968(12)	2530(12)	1473(12)	2643(16)	3737(16)	2643(16)	1473(12)	2530(12)
3373	2475(12)	2185(12)	1486(12)	2737(13)	3272(13)	2726(13)	1486(12)	2185(12)
3377	2394(12)	2123(12)	1469(12)	2742(13)	3281(13)	2730(13)	1469(12)	2123(12)
3538	1465(12)	1471(12)	1486(12)	2654(13)	3156(13)	2642(13)	1486(12)	1471(12)
3542	1391(12)	1414(12)	1469(12)	2651(13)	3155(13)	2639(13)	1469(12)	1414(12)
3679	943(12)	1105(12)	1559(13)	2228(13)	2506(13)	2229(13)	1561(13)	1105(12)
3693	-609(12)	-442(12)	25(13)	770(16)	1088(16)	770(16)	26(13)	-442(12)
3820	-447(16)	-316(16)	16(13)	516(12)	743(12)	516(12)	16(13)	-316(16)
3321	-119(16)	-84(16)	15(13)	132(12)	196(12)	132(12)	15(13)	-84(16)
3925	538(11)	478(11)	333(10)	290(10)	272(10)	290(10)	333(10)	478(11)
4065	0(7)	1(6)	2(6)	1(6)	0(7)	0(7)	0(7)	0(7)
4069	0(16)	1(6)	2(6)	1(6)	0(6)	0(16)	0(16)	0(16)
4300	0(16)	0(16)	0(16)	0(16)	0(16)	0(16)	0(16)	0(16)

Table 2-15. B-9U/161-C Ultimate Compression Internal Loads (Baseline)

PEAK ULTIMATE AXIAL COMPRESSION LOAD INTENSITIES

STATION (IN)	NX1 (LB/IN)	NX2 (LB/IN)	NX3 (LB/IN)	NX4 (LB/IN)	NX5 (LB/IN)	NX6 (LB/IN)	NX7 (LB/IN)	NX8 (LB/IN)
1000	0(16)	0(16)	0(16)	0(16)	0(16)	0(16)	0(16)	0(16)
1036	-5(11)	-4(11)	-4(9)	-4(12)	-5(12)	-4(12)	-3(9)	-4(11)
1072	-23(11)	-21(9)	-25(9)	-34(12)	-47(12)	-34(12)	-8(9)	-18(11)
1131	-57(11)	-50(9)	-59(9)	-55(9)	-75(12)	-53(12)	-24(10)	-48(11)
1278	-171(8)	-138(8)	-122(9)	-105(12)	-147(12)	-105(12)	-65(10)	-138(8)
1337	-231(8)	-184(8)	-142(9)	-132(12)	-185(12)	-132(12)	-77(10)	-184(8)
1341	-295(15)	-224(15)	-144(9)	-136(12)	-189(12)	-136(12)	-79(10)	-224(15)
1477	-435(8)	-343(8)	-205(9)	-225(12)	-313(12)	-225(12)	-131(7)	-343(8)
1481	-135(15)	-107(15)	-39(15)	-50(16)	-82(16)	-58(16)	-62(3)	-107(15)
1500	-232(6)	-167(6)	-50(2)	-111(16)	-158(16)	-111(16)	-90(3)	-176(6)
1750	-446(4)	-337(6)	-65(6)	-154(16)	-218(16)	-154(16)	-135(3)	-329(4)
1864	-665(4)	-503(6)	-117(6)	-166(16)	-234(16)	-166(16)	-178(3)	-490(4)
1868	-5396(4)	-5238(6)	-4868(6)	-4514(5)	-4388(5)	-4514(5)	-4819(4)	-5227(4)
2006	-4429(4)	-4742(4)	-5564(6)	-6397(5)	-7050(10)	-6397(5)	-5498(4)	-4742(4)
2022	-4315(4)	-4685(4)	-5648(6)	-6621(5)	-7670(10)	-6621(5)	-5579(4)	-4685(4)
2026	-4286(4)	-4671(4)	-5669(6)	-6678(5)	-7825(10)	-6678(5)	-5599(4)	-4671(4)
2042	-4171(4)	-4613(4)	-5753(6)	-7144(10)	-8447(10)	-7144(10)	-5681(4)	-4613(4)
2094	-3791(4)	-4421(4)	-6023(6)	-8733(10)	-10458(10)	-8733(10)	-5942(4)	-4421(4)
2098	-3773(4)	-4414(4)	-6043(6)	-8837(10)	-10507(10)	-8837(10)	-5962(4)	-4414(4)
2180	-3651(7)	-4437(4)	-6458(6)	-10594(10)	-12710(10)	-10594(10)	-6364(4)	-4437(4)
2184	-3166(4)	-3968(4)	-5999(6)	-8728(10)	-10852(10)	-8728(10)	-5905(4)	-3968(4)
2300	-3238(4)	-4026(4)	-6036(6)	-8773(10)	-10895(10)	-8773(10)	-5928(4)	-4026(4)
2400	-3343(7)	-4072(4)	-6052(6)	-8803(10)	-10923(10)	-8803(10)	-5944(4)	-4072(4)
2500	-4011(7)	-4118(4)	-6386(6)	-8830(10)	-10945(10)	-8830(10)	-5961(4)	-4118(4)
2500	-4675(7)	-4452(7)	-6107(6)	-8853(10)	-10963(10)	-8853(10)	-5978(4)	-4452(7)
2664	-5091(7)	-4751(7)	-6119(6)	-8866(10)	-10972(10)	-8866(10)	-5989(4)	-4751(7)
2668	-5111(7)	-4766(7)	-6120(6)	-8861(10)	-10964(10)	-8861(10)	-5990(4)	-4766(7)
2800	-5563(7)	-5096(7)	-6138(6)	-8485(10)	-10412(10)	-8485(10)	-6012(4)	-5096(7)
2864	-5773(7)	-5250(7)	-6146(6)	-8301(10)	-10141(10)	-8301(10)	-6023(4)	-5250(7)
2868	-5787(7)	-5260(7)	-6146(6)	-8289(10)	-10125(10)	-8289(10)	-6023(4)	-5260(7)
2950	-6060(7)	-5463(7)	-6162(6)	-8065(10)	-9788(10)	-8065(10)	-6045(4)	-5463(7)
3050	-6519(7)	-5828(7)	-6276(6)	-7956(10)	-9525(10)	-7956(10)	-6167(4)	-5828(7)
3161	-7061(7)	-6256(7)	-6401(6)	-7817(10)	-9206(10)	-7817(10)	-6301(4)	-6256(7)
3165	-7174(7)	-6346(7)	-6405(6)	-7812(10)	-9194(10)	-7812(10)	-6306(4)	-6346(7)
3293	-7480(7)	-6597(7)	-6491(6)	-7566(5)	-8701(10)	-7566(5)	-6404(4)	-6597(7)
3295	-7485(7)	-6601(7)	-6492(6)	-7564(5)	-8693(10)	-7564(5)	-6406(4)	-6601(7)
3373	-7671(7)	-6751(7)	-6536(6)	-7484(5)	-8368(10)	-7484(5)	-6458(4)	-6751(7)
3377	-7770(7)	-6831(7)	-6536(6)	-7479(5)	-8349(10)	-7479(5)	-6459(4)	-6831(7)
3538	-7646(7)	-6771(7)	-6593(6)	-7277(5)	-7584(5)	-7277(5)	-6536(4)	-6771(7)
3542	-7732(7)	-6841(7)	-6594(6)	-7271(5)	-7576(5)	-7271(5)	-6538(4)	-6841(7)
3679	-7196(7)	-6499(7)	-6681(6)	-7125(5)	-7325(5)	-7125(5)	-6743(3)	-6499(7)
3683	-9708(7)	-9017(7)	-8198(6)	-9195(10)	-9602(10)	-9195(10)	-8162(4)	-9017(7)
3920	-8869(7)	-8464(7)	-8263(6)	-8753(10)	-8991(10)	-8763(10)	-8251(4)	-8464(7)
3921	-8474(10)	-8457(10)	-8551(10)	-8605(10)	-8627(10)	-8605(10)	-8551(10)	-8497(10)
3925	-243(12)	-184(12)	-113(9)	-124(9)	-116(9)	-94(9)	-71(9)	-184(12)
4065	-0(15)	-0(15)	-0(15)	-0(15)	-0(15)	-1(6)	-2(6)	-1(6)
4069	0(16)	0(16)	0(16)	0(16)	0(16)	-1(6)	-2(6)	-1(6)
4300	0(16)	0(16)	0(16)	0(16)	0(16)	0(16)	0(16)	0(16)

Table 2-16. B-9U/161-C Ultimate Tension Internal Loads (2.50 End g Boost Limit)

PEAK ULTIMATE AXIAL TENSION LOAD INTENSITIES

STATION (IN)	NX1 (LB/IN)	NX2 (LB/IN)	NX3 (LB/IN)	NX4 (LB/IN)	NX5 (LB/IN)	NX6 (LB/IN)	NX7 (LB/IN)	NX8 (LB/IN)
1000	0(16)	0(16)	0(16)	0(16)	0(16)	0(16)	0(16)	0(16)
1036	5(12)	4(12)	0(15)	0(16)	1(11)	0(16)	0(15)	4(12)
1072	45(12)	32(12)	1(15)	3(16)	6(11)	3(16)	1(15)	32(12)
1131	73(12)	51(12)	3(15)	7(16)	13(8)	7(16)	3(15)	51(12)
1278	141(12)	98(12)	7(15)	28(16)	58(8)	28(16)	7(15)	98(12)
1337	173(12)	121(12)	9(15)	42(8)	89(8)	42(8)	9(15)	121(12)
1341	177(12)	124(12)	8(14)	121(15)	192(15)	121(15)	8(14)	124(12)
1477	288(12)	200(12)	14(14)	99(8)	191(8)	99(8)	14(14)	200(12)
1481	1411(12)	1322(12)	1249(10)	1291(10)	1374(8)	1291(10)	1249(10)	1322(12)
1600	1569(12)	1430(12)	1219(10)	1377(8)	1531(8)	1377(8)	1219(10)	1430(12)
1750	1820(12)	1601(12)	1181(10)	1539(8)	1791(8)	1539(8)	1181(10)	1601(12)
1964	2042(12)	1753(12)	1142(10)	1559(10)	1780(8)	1559(10)	1142(10)	1753(12)
1868	931(12)	640(12)	35(14)	66(13)	140(13)	85(13)	35(14)	640(12)
2006	1612(11)	829(12)	47(14)	155(13)	242(13)	153(13)	47(14)	829(12)
2022	1842(11)	850(12)	48(14)	166(13)	258(13)	164(13)	48(14)	850(12)
2026	1898(11)	891(12)	45(14)	160(13)	251(13)	158(13)	45(14)	891(12)
2042	2123(11)	976(11)	47(14)	152(13)	242(13)	150(13)	47(14)	976(11)
2094	2863(11)	1361(11)	52(14)	141(14)	219(13)	141(14)	52(14)	1361(11)
2098	2901(11)	1377(11)	52(14)	142(14)	217(13)	142(14)	52(14)	1377(11)
2180	3236(11)	1400(11)	60(14)	168(14)	213(14)	168(14)	60(14)	1400(11)
2184	5155(11)	3311(11)	1454(13)	1653(13)	1734(13)	1650(13)	1450(13)	3311(11)
2300	5159(11)	3301(11)	1444(13)	1656(13)	1743(13)	1653(13)	1439(13)	3301(11)
2400	5167(11)	3298(11)	1437(13)	1675(13)	1772(13)	1671(13)	1431(13)	3298(11)
2500	5173(11)	3293(11)	1433(13)	1709(13)	1821(13)	1704(13)	1426(13)	3293(11)
2600	5175(11)	3286(11)	1432(13)	1756(13)	1888(13)	1751(13)	1424(13)	3286(11)
2664	5175(11)	3280(11)	1431(13)	1793(13)	1940(13)	1787(13)	1422(13)	3280(11)
2668	5167(11)	3274(11)	1431(13)	1795(13)	1944(13)	1789(13)	1422(13)	3274(11)
2800	4650(11)	2897(11)	1429(13)	1886(13)	2072(13)	1879(13)	1419(13)	2897(11)
2864	4396(11)	2832(12)	1429(13)	1937(13)	2144(13)	1930(13)	1418(13)	2832(12)
2868	4380(11)	2838(12)	1429(13)	1940(13)	2149(13)	1933(13)	1418(13)	2838(12)
2950	4030(11)	2977(12)	1428(13)	2015(13)	2254(13)	2007(13)	1417(13)	2977(12)
3050	3796(12)	3103(12)	1428(12)	2172(13)	2477(13)	2164(13)	1428(12)	3102(12)
3161	3693(12)	3033(12)	1464(12)	2487(13)	2921(13)	2477(13)	1464(12)	3033(12)
3165	3615(12)	2980(12)	1448(12)	2497(13)	2938(13)	2487(13)	1448(12)	2980(12)
3293	2979(12)	2538(12)	1473(12)	2631(16)	3721(16)	2631(16)	1473(12)	2538(12)
3295	2968(12)	2530(12)	1473(12)	2643(16)	3737(16)	2643(16)	1473(12)	2530(12)
3373	2475(12)	2185(12)	1486(12)	2737(13)	3272(13)	2726(13)	1486(12)	2185(12)
3377	2394(12)	2123(12)	1469(12)	2742(13)	3281(13)	2730(13)	1469(12)	2123(12)
3538	1465(12)	1471(12)	1486(12)	2654(13)	3156(13)	2642(13)	1486(12)	1471(12)
3542	1391(12)	1414(12)	1469(12)	2651(13)	3155(13)	2639(13)	1469(12)	1414(12)
3679	943(12)	1105(12)	1559(13)	2228(13)	2506(13)	2229(13)	1561(13)	1105(12)
3683	-609(12)	-442(12)	25(13)	770(16)	1088(16)	770(16)	26(13)	-442(12)
3820	-447(16)	-316(16)	16(13)	516(12)	743(12)	516(12)	16(13)	-316(16)
3921	-119(16)	-84(16)	15(13)	132(12)	196(12)	132(12)	15(13)	-84(16)
3925	449(11)	399(11)	281(10)	191(10)	180(7)	191(10)	281(10)	399(11)
4065	0(7)	1(6)	2(6)	1(6)	0(7)	0(7)	0(7)	0(7)
4069	0(16)	1(6)	2(6)	1(6)	0(6)	0(16)	0(16)	0(16)
4300	0(16)	0(16)	0(16)	0(16)	0(16)	0(16)	0(16)	0(16)

Table 2-17. B-9U/161-C Ultimate Compression Internal Loads (2.50 End g Boost Limit)

PEAK ULTIMATE AXIAL COMPRESSION LOAD INTENSITIES

STATION (IN)	NX1 (LB/IN)	NX2 (LB/IN)	NX3 (LB/IN)	NX4 (LB/IN)	NX5 (LB/IN)	NX6 (LB/IN)	NX7 (LB/IN)	NX8 (LB/IN)
1000	0(16)	0(16)	0(16)	0(16)	0(16)	0(16)	0(16)	0(16)
1036	-4(11)	-4(9)	-4(9)	-4(12)	-5(12)	-4(12)	-3(9)	-4(11)
1072	-21(8)	-21(9)	-25(9)	-34(12)	-47(12)	-34(12)	-8(9)	-17(8)
1131	-55(8)	-50(9)	-59(9)	-55(9)	-75(12)	-53(12)	-22(7)	-45(8)
1278	-171(8)	-138(8)	-122(9)	-105(12)	-147(12)	-105(12)	-60(7)	-138(8)
1337	-231(8)	-184(8)	-142(9)	-132(12)	-185(12)	-132(12)	-76(7)	-184(8)
1341	-295(15)	-224(15)	-144(9)	-136(12)	-189(12)	-136(12)	-78(7)	-224(15)
1477	-435(8)	-343(8)	-205(9)	-225(12)	-313(12)	-225(12)	-131(7)	-343(8)
1481	-135(15)	-107(15)	-39(15)	-58(16)	-82(16)	-58(16)	-62(3)	-107(15)
1600	-232(6)	-167(6)	-50(2)	-111(16)	-158(16)	-111(16)	-90(3)	-176(6)
1750	-446(4)	-337(6)	-65(6)	-154(16)	-218(16)	-154(16)	-135(3)	-329(4)
1864	-665(4)	-503(6)	-117(6)	-156(16)	-234(16)	-156(16)	-178(3)	-490(4)
1868	-5396(4)	-5238(6)	-4868(6)	-4514(5)	-4388(5)	-4514(5)	-4819(4)	-5227(4)
2006	-4429(4)	-4742(4)	-5564(6)	-6397(5)	-6771(5)	-6397(5)	-5498(4)	-4742(4)
2022	-4315(4)	-4685(4)	-5648(6)	-6621(5)	-7054(5)	-6621(5)	-5579(4)	-4685(4)
2026	-4286(4)	-4671(4)	-5669(6)	-6678(5)	-7125(5)	-6678(5)	-5599(4)	-4671(4)
2042	-4171(4)	-4613(4)	-5753(6)	-6904(5)	-7426(10)	-6904(5)	-5681(4)	-4613(4)
2094	-3791(4)	-4421(4)	-6023(6)	-7973(10)	-9135(10)	-7973(10)	-5942(4)	-4421(4)
2098	-3773(4)	-4414(4)	-6043(6)	-8061(10)	-9245(10)	-8061(10)	-5962(4)	-4414(4)
2180	-3651(7)	-4437(4)	-6458(6)	-9562(10)	-11061(10)	-9562(10)	-6364(4)	-4437(4)
2184	-3166(4)	-3968(4)	-5999(6)	-8044(5)	-9196(10)	-8044(5)	-5905(4)	-3968(4)
2300	-3238(4)	-4026(4)	-6036(6)	-8067(5)	-9280(10)	-8067(5)	-5928(4)	-4026(4)
2400	-3343(7)	-4072(4)	-6062(6)	-8064(5)	-9348(10)	-8064(5)	-5944(4)	-4072(4)
2500	-4011(7)	-4118(4)	-6086(6)	-8100(5)	-9512(8)	-8100(5)	-5961(4)	-4118(4)
2600	-4675(7)	-4492(7)	-6107(6)	-8115(5)	-9826(8)	-8115(5)	-5978(4)	-4492(7)
2664	-5091(7)	-4751(7)	-6119(6)	-8256(8)	-10024(8)	-8256(8)	-5989(4)	-4751(7)
2668	-5111(7)	-4766(7)	-6120(6)	-8252(8)	-10017(8)	-8252(8)	-5990(4)	-4766(7)
2800	-5563(7)	-5096(7)	-6138(6)	-7949(5)	-9161(8)	-7949(5)	-6012(4)	-5096(7)
2864	-5773(7)	-5250(7)	-6146(6)	-7864(5)	-8984(10)	-7864(5)	-6023(4)	-5250(7)
2868	-5787(7)	-5260(7)	-6146(6)	-7859(5)	-8973(10)	-7859(5)	-6023(4)	-5260(7)
2950	-6060(7)	-5463(7)	-6162(6)	-7758(5)	-8758(10)	-7758(5)	-6045(4)	-5463(7)
3050	-6519(7)	-5828(7)	-6276(6)	-7722(5)	-8580(10)	-7722(5)	-6167(4)	-5828(7)
3161	-7061(7)	-6256(7)	-6401(6)	-7678(5)	-8369(10)	-7678(5)	-6301(4)	-6256(7)
3165	-7174(7)	-6346(7)	-6405(6)	-7677(5)	-8361(10)	-7677(5)	-6306(4)	-6346(7)
3293	-7480(7)	-6597(7)	-6491(6)	-7566(5)	-8048(5)	-7566(5)	-6404(4)	-6597(7)
3295	-7485(7)	-6601(7)	-6492(6)	-7564(5)	-8044(5)	-7564(5)	-6406(4)	-6601(7)
3373	-7671(7)	-6751(7)	-6536(6)	-7484(5)	-7911(5)	-7484(5)	-6458(4)	-6751(7)
3377	-7770(7)	-6831(7)	-6536(6)	-7479(5)	-7902(5)	-7479(5)	-6459(4)	-6831(7)
3538	-7646(7)	-6771(7)	-6593(6)	-7277(5)	-7584(5)	-7277(5)	-6536(4)	-6771(7)
3542	-7732(7)	-6841(7)	-6594(6)	-7271(5)	-7576(5)	-7271(5)	-6538(4)	-6841(7)
3679	-7196(7)	-6499(7)	-6681(6)	-7125(5)	-7325(5)	-7125(5)	-6743(3)	-6499(7)
3683	-9708(7)	-9017(7)	-8211(10)	-9122(10)	-9499(10)	-9122(10)	-8211(10)	-9017(7)
3820	-8869(7)	-8464(7)	-8375(10)	-8838(10)	-9030(10)	-8838(10)	-8375(10)	-8464(7)
3921	-8519(10)	-8560(10)	-8660(10)	-8759(10)	-8800(10)	-8759(10)	-8660(10)	-8560(10)
3925	-243(12)	-184(12)	-113(9)	-124(9)	-116(9)	-94(9)	-71(9)	-184(12)
4065	-0(15)	-0(15)	-0(15)	-0(15)	-0(15)	-1(6)	-2(6)	-1(6)
4069	0(16)	0(16)	0(16)	0(16)	0(16)	-1(6)	-2(6)	-1(6)
4300	0(16)	0(16)	0(16)	0(16)	0(16)	0(16)	0(16)	0(16)

Table 2-18. B-9U/161-C Ultimate Tension Internal Loads (2.75 End g Boost Limit)

PEAK ULTIMATE AXIAL TENSION LOAD INTENSITIES

STATION (IN)	NX1 (LB/IN)	NX2 (LB/IN)	NX3 (LB/IN)	NX4 (LB/IN)	NX5 (LB/IN)	NX6 (LB/IN)	NX7 (LB/IN)	NX8 (LB/IN)
1000	0(16)	0(16)	0(16)	0(16)	0(16)	0(16)	0(16)	0(16)
1036	5(12)	4(12)	0(15)	0(16)	1(11)	0(16)	0(15)	4(12)
1072	45(12)	32(12)	1(15)	3(11)	7(11)	3(11)	1(15)	32(12)
1131	73(12)	51(12)	3(15)	7(16)	13(8)	7(16)	3(15)	51(12)
1278	141(12)	98(12)	7(15)	28(16)	58(8)	28(16)	7(15)	98(12)
1337	173(12)	121(12)	9(15)	42(8)	89(8)	42(8)	9(15)	121(12)
1341	177(12)	124(12)	8(14)	121(15)	192(15)	121(15)	8(14)	124(12)
1477	288(12)	200(12)	14(14)	99(8)	191(8)	99(8)	14(14)	200(12)
1481	1411(12)	1322(12)	1238(10)	1290(10)	1374(8)	1290(10)	1238(10)	1322(12)
1600	1569(12)	1430(12)	1205(10)	1377(8)	1531(8)	1377(8)	1205(10)	1430(12)
1750	1820(12)	1601(12)	1164(10)	1539(8)	1791(8)	1539(8)	1164(10)	1601(12)
1854	2042(12)	1753(12)	1056(12)	1510(8)	1780(8)	1510(8)	1056(12)	1753(12)
1868	931(12)	640(12)	35(14)	86(13)	140(13)	85(13)	35(14)	640(12)
2006	1774(11)	829(12)	47(14)	155(13)	242(13)	153(13)	47(14)	829(12)
2022	2026(11)	914(11)	48(14)	156(13)	258(13)	154(13)	48(14)	914(11)
2026	2088(11)	946(11)	45(14)	160(13)	251(13)	158(13)	45(14)	946(11)
2042	2335(11)	1073(11)	47(14)	152(13)	242(13)	150(13)	47(14)	1073(11)
2094	3150(11)	1497(11)	52(14)	141(14)	219(13)	141(14)	52(14)	1497(11)
2098	3191(11)	1514(11)	52(14)	142(14)	217(13)	142(14)	52(14)	1514(11)
2180	3560(11)	1540(11)	60(14)	168(14)	213(14)	160(14)	60(14)	1540(11)
2184	5479(11)	3451(11)	1454(13)	1653(13)	1734(13)	1650(13)	1450(13)	3451(11)
2300	5483(11)	3440(11)	1444(13)	1656(13)	1743(13)	1653(13)	1439(13)	3440(11)
2400	5493(11)	3437(11)	1437(13)	1675(13)	1772(13)	1671(13)	1431(13)	3437(11)
2500	5499(11)	3432(11)	1433(13)	1709(13)	1821(13)	1704(13)	1426(13)	3432(11)
2600	5501(11)	3423(11)	1432(13)	1756(13)	1888(13)	1751(13)	1424(13)	3423(11)
2664	5501(11)	3417(11)	1431(13)	1793(13)	1940(13)	1787(13)	1422(13)	3417(11)
2668	5493(11)	3411(11)	1431(13)	1795(13)	1944(13)	1789(13)	1422(13)	3411(11)
2800	4924(11)	2995(11)	1429(13)	1986(13)	2072(13)	1879(13)	1419(13)	2995(11)
2864	4645(11)	2832(12)	1429(13)	1937(13)	2144(13)	1930(13)	1418(13)	2832(12)
2868	4627(11)	2839(12)	1429(13)	1940(13)	2149(13)	1933(13)	1418(13)	2838(12)
2950	4242(11)	2977(12)	1428(13)	2015(13)	2254(13)	2007(13)	1417(13)	2977(12)
3050	3796(12)	3103(12)	1428(12)	2172(13)	2477(13)	2164(13)	1428(12)	3102(12)
3161	3683(12)	3033(12)	1454(12)	2487(13)	2921(13)	2477(13)	1454(12)	3033(12)
3165	3615(12)	2980(12)	1448(12)	2497(13)	2938(13)	2497(13)	1448(12)	2980(12)
3293	2979(12)	2538(12)	1473(12)	2631(16)	3721(16)	2631(16)	1473(12)	2538(12)
3295	2968(12)	2530(12)	1473(12)	2643(16)	3737(16)	2643(16)	1473(12)	2530(12)
3373	2475(12)	2185(12)	1486(12)	2737(13)	3272(13)	2720(13)	1486(12)	2185(12)
3377	2394(12)	2123(12)	1469(12)	2742(13)	3281(13)	2730(13)	1469(12)	2123(12)
3538	1465(12)	1471(12)	1486(12)	2654(13)	3156(13)	2642(13)	1486(12)	1471(12)
3542	1391(12)	1414(12)	1469(12)	2651(13)	3155(13)	2639(13)	1469(12)	1414(12)
3679	943(12)	1105(12)	1559(13)	2228(13)	2506(13)	2229(13)	1561(13)	1105(12)
3683	-609(12)	-442(12)	25(13)	770(16)	1088(16)	770(16)	26(13)	-442(12)
3820	-447(16)	-316(16)	16(13)	516(12)	743(12)	516(12)	16(13)	-316(16)
3921	-119(16)	-84(15)	15(13)	132(12)	196(12)	132(12)	15(13)	-84(15)
3925	494(11)	439(11)	309(10)	201(10)	180(7)	201(10)	309(10)	439(11)
4065	0(7)	1(6)	2(6)	1(6)	0(7)	0(7)	0(7)	0(7)
4069	0(16)	1(6)	2(6)	1(6)	0(6)	0(16)	0(16)	0(16)
4300	0(16)	0(16)	0(16)	0(16)	0(16)	0(16)	0(16)	0(16)

Table 2-19. B-9U/161-C Ultimate Compression Internal Loads
(2.75 End g Boost Limit)

PEAK ULTIMATE AXIAL COMPRESSION LOAD INTENSITIES

STATION (IN)	NX1 (LB/IN)	NX2 (LB/IN)	NX3 (LB/IN)	NX4 (LB/IN)	NX5 (LB/IN)	NX6 (LB/IN)	NX7 (LB/IN)	NX8 (LB/IN)
1000	0(16)	0(16)	0(16)	0(16)	0(16)	0(16)	0(16)	0(16)
1036	-5(11)	-4(11)	-4(9)	-4(12)	-5(12)	-4(12)	-3(9)	-4(11)
1072	-21(11)	-21(9)	-25(9)	-34(12)	-47(12)	-34(12)	-8(9)	-17(11)
1131	-55(8)	-50(9)	-59(9)	-55(9)	-75(12)	-53(12)	-23(10)	-45(3)
1278	-171(8)	-138(9)	-122(9)	-105(12)	-147(12)	-105(12)	-60(16)	-139(9)
1337	-231(8)	-184(8)	-142(9)	-132(12)	-185(12)	-132(12)	-76(7)	-184(9)
1341	-295(15)	-224(15)	-144(9)	-135(12)	-189(12)	-136(12)	-78(7)	-224(15)
1477	-435(8)	-343(9)	-205(9)	-225(12)	-313(12)	-225(12)	-131(7)	-343(9)
1481	-135(15)	-107(15)	-39(15)	-58(16)	-82(16)	-58(16)	-62(3)	-107(15)
1600	-232(6)	-167(6)	-50(2)	-111(16)	-158(16)	-111(16)	-90(3)	-175(6)
1750	-446(6)	-337(6)	-65(6)	-154(15)	-218(16)	-154(16)	-135(3)	-329(4)
1864	-1567(10)	-1480(10)	-1270(10)	-1060(10)	-973(10)	-1060(10)	-1270(10)	-1480(10)
1868	-5396(4)	-5238(6)	-4868(6)	-4514(5)	-4388(5)	-4514(5)	-4819(4)	-5227(4)
2006	-4429(4)	-4742(4)	-5554(5)	-5397(5)	-6771(5)	-5397(5)	-5498(4)	-4742(4)
2022	-4315(4)	-4685(4)	-5648(6)	-5521(5)	-7054(5)	-6621(5)	-5579(4)	-4685(4)
2026	-4286(4)	-4671(4)	-5659(6)	-6670(5)	-7125(5)	-6678(5)	-5599(4)	-4671(4)
2042	-4171(4)	-4613(4)	-5753(6)	-6304(5)	-7660(10)	-6904(5)	-5681(4)	-4613(4)
2094	-3791(4)	-4421(4)	-6023(6)	-8184(18)	-9537(10)	-8184(10)	-5942(4)	-4421(4)
2098	-3773(4)	-4414(4)	-6043(6)	-8281(10)	-9658(10)	-8281(10)	-5962(4)	-4414(4)
2180	-3651(7)	-4437(4)	-6458(6)	-9931(10)	-11655(10)	-9931(10)	-6364(4)	-4437(4)
2184	-3166(4)	-3968(4)	-5999(6)	-8052(10)	-9794(10)	-8052(10)	-5905(4)	-3968(4)
2300	-3238(4)	-4026(4)	-6036(6)	-8139(10)	-9884(10)	-8139(10)	-5928(4)	-4026(4)
2400	-3343(7)	-4072(4)	-6062(6)	-8200(10)	-9956(10)	-8200(10)	-5944(4)	-4072(4)
2500	-4011(7)	-4118(4)	-6086(6)	-8260(10)	-10026(10)	-8260(10)	-5961(4)	-4118(4)
2600	-4675(7)	-4452(7)	-6197(6)	-8317(10)	-10093(10)	-8317(10)	-5978(4)	-4452(7)
2664	-5091(7)	-4751(7)	-6119(6)	-8353(10)	-10135(10)	-8353(10)	-5989(4)	-4751(7)
2668	-5111(7)	-4766(7)	-6120(6)	-8350(10)	-10130(10)	-8350(10)	-5990(4)	-4766(7)
2800	-5563(7)	-5095(7)	-6138(6)	-8076(10)	-9724(10)	-8076(10)	-6012(4)	-5095(7)
2864	-5773(7)	-5250(7)	-6146(6)	-7942(10)	-9526(10)	-7942(10)	-6023(4)	-5250(7)
2868	-5787(7)	-5250(7)	-6146(6)	-7934(10)	-9513(10)	-7934(10)	-6023(4)	-5260(7)
2950	-6050(7)	-5463(7)	-6152(6)	-7771(10)	-9266(10)	-7771(10)	-6045(4)	-5463(7)
3050	-6519(7)	-5828(7)	-6276(6)	-7722(5)	-9046(10)	-7722(5)	-6167(4)	-5828(7)
3161	-7061(7)	-6255(7)	-6401(6)	-7678(5)	-8785(10)	-7678(5)	-6301(4)	-6255(7)
3165	-7174(7)	-6346(7)	-6405(6)	-7677(5)	-8776(10)	-7677(5)	-6306(4)	-6346(7)
3293	-7480(7)	-6597(7)	-6491(6)	-7566(5)	-8397(10)	-7566(5)	-6404(4)	-6597(7)
3295	-7485(7)	-6601(7)	-6492(6)	-7564(5)	-8390(10)	-7564(5)	-6406(4)	-6601(7)
3373	-7671(7)	-6751(7)	-6536(6)	-7484(5)	-8114(10)	-7484(5)	-6458(4)	-6751(7)
3377	-7770(7)	-6831(7)	-6536(6)	-7479(5)	-8098(10)	-7479(5)	-6459(4)	-6831(7)
3538	-7646(7)	-6771(7)	-6593(6)	-7277(5)	-7584(5)	-7277(5)	-6536(4)	-6771(7)
3542	-7732(7)	-6841(7)	-6594(6)	-7271(5)	-7576(5)	-7271(5)	-6538(4)	-6841(7)
3679	-7195(7)	-6499(7)	-6681(6)	-7125(5)	-7325(5)	-7125(5)	-6743(3)	-6499(7)
3683	-9708(7)	-9017(7)	-8198(6)	-9283(10)	-9644(10)	-9283(10)	-8162(4)	-9017(7)
3820	-8869(7)	-8464(7)	-8317(10)	-8862(10)	-9087(10)	-8862(10)	-8317(10)	-8464(7)
3921	-8462(10)	-8511(10)	-8530(10)	-8753(10)	-8799(10)	-8750(10)	-8630(10)	-8511(10)
3925	-243(12)	-184(12)	-113(9)	-124(9)	-116(9)	-94(9)	-71(9)	-134(12)
4065	-0(15)	-0(15)	-0(15)	-0(15)	-0(15)	-1(6)	-2(6)	-1(6)
4069	0(16)	0(16)	0(16)	0(16)	0(16)	-1(6)	-2(6)	-1(6)
4300	0(16)	0(16)	0(16)	0(16)	0(16)	0(16)	0(16)	0(16)

Table 2-20. B-9U/161-C Ultimate Tension Internal Loads (3.25 End g Boost Limit)

PEAK ULTIMATE AXIAL TENSION LOAD INTENSITIES

STATION (IN)	NX1 (LB/IN)	NX2 (LB/IN)	NX3 (LB/IN)	NX4 (LB/IN)	NX5 (LB/IN)	NX6 (LB/IN)	NX7 (LB/IN)	NX8 (LB/IN)
1000	0(16)	0(16)	0(16)	0(16)	0(16)	0(16)	0(16)	0(16)
1036	5(12)	4(12)	0(15)	0(16)	1(11)	0(16)	0(15)	4(12)
1072	45(12)	32(12)	1(15)	3(11)	8(11)	3(11)	1(15)	32(12)
1131	73(12)	51(12)	3(15)	7(16)	13(8)	7(16)	3(15)	51(12)
1278	141(12)	98(12)	7(15)	28(16)	58(8)	28(16)	7(15)	98(12)
1337	173(12)	121(12)	9(15)	42(8)	89(8)	42(8)	9(15)	121(12)
1341	177(12)	124(12)	8(14)	121(15)	192(15)	121(15)	8(14)	124(12)
1477	268(12)	200(12)	14(14)	99(8)	191(8)	99(8)	14(14)	200(12)
1481	1411(12)	1322(12)	1217(10)	1298(10)	1374(8)	1298(10)	1217(10)	1322(12)
1600	1569(12)	1430(12)	1178(10)	1377(8)	1531(8)	1377(8)	1178(10)	1430(12)
1750	1820(12)	1601(12)	1129(10)	1539(8)	1791(8)	1539(8)	1153(9)	1601(12)
1964	2042(12)	1753(12)	1056(12)	1510(8)	1780(8)	1510(8)	1056(12)	1753(12)
1968	931(12)	640(12)	35(14)	86(13)	140(13)	85(13)	35(14)	640(12)
2106	2096(11)	925(11)	47(14)	155(13)	242(13)	153(13)	47(14)	925(11)
2022	2394(11)	1081(11)	48(14)	166(13)	258(13)	164(13)	48(14)	1081(11)
2026	2467(11)	1118(11)	45(14)	160(13)	251(13)	158(13)	45(14)	1118(11)
2042	2759(11)	1269(11)	47(14)	152(13)	242(13)	150(13)	47(14)	1269(11)
2094	3722(11)	1769(11)	52(14)	141(14)	219(13)	141(14)	52(14)	1769(11)
2098	3771(11)	1790(11)	52(14)	142(14)	217(13)	142(14)	52(14)	1790(11)
2180	4207(11)	1820(11)	60(14)	168(14)	213(14)	168(14)	60(14)	1820(11)
2184	6128(11)	3731(11)	1454(13)	1653(13)	1734(13)	1650(13)	1450(13)	3731(11)
2300	6133(11)	3718(11)	1444(13)	1656(13)	1743(13)	1653(13)	1439(13)	3718(11)
2400	6144(11)	3715(11)	1437(13)	1675(13)	1772(13)	1671(13)	1431(13)	3715(11)
2500	6151(11)	3708(11)	1433(13)	1709(13)	1821(13)	1704(13)	1426(13)	3708(11)
2500	6154(11)	3699(11)	1432(13)	1756(13)	1888(13)	1751(13)	1424(13)	3699(11)
2664	6154(11)	3691(11)	1431(13)	1792(13)	1940(13)	1787(13)	1422(13)	3691(11)
2668	6144(11)	3683(11)	1431(13)	1795(13)	1944(13)	1789(13)	1422(13)	3683(11)
2800	5472(11)	3193(11)	1429(13)	1886(13)	2072(13)	1879(13)	1419(13)	3193(11)
2864	5142(11)	2952(11)	1429(13)	1937(13)	2144(13)	1930(13)	1418(13)	2952(11)
2868	5121(11)	2936(11)	1429(13)	1940(13)	2149(13)	1933(13)	1418(13)	2936(11)
2950	4665(11)	2977(12)	1428(13)	2015(13)	2254(13)	2007(13)	1417(13)	2977(12)
3050	3796(12)	3103(12)	1428(12)	2172(13)	2477(13)	2164(13)	1428(12)	3102(12)
3161	3683(12)	3033(12)	1464(12)	2487(13)	2921(13)	2477(13)	1454(12)	3033(12)
3165	3615(12)	2980(12)	1448(12)	2497(13)	2938(13)	2487(13)	1448(12)	2980(12)
3293	2979(12)	2538(12)	1473(12)	2631(16)	3721(16)	2631(16)	1473(12)	2538(12)
3295	2968(12)	2530(12)	1473(12)	2643(16)	3737(16)	2643(16)	1473(12)	2530(12)
3373	2475(12)	2185(12)	1486(12)	2737(13)	3272(13)	2726(13)	1486(12)	2185(12)
3377	2394(12)	2123(12)	1469(12)	2742(13)	3281(13)	2730(13)	1469(12)	2123(12)
3538	1465(12)	1471(12)	1486(12)	2654(13)	3156(13)	2642(13)	1486(12)	1471(12)
3542	1391(12)	1414(12)	1469(12)	2651(13)	3155(13)	2639(13)	1469(12)	1414(12)
3679	943(12)	1105(12)	1559(13)	2228(13)	2506(13)	2229(13)	1561(13)	1105(12)
3583	-609(12)	-442(12)	25(13)	770(16)	1088(16)	770(16)	26(13)	-442(12)
3820	-447(16)	-316(16)	16(13)	516(12)	743(12)	516(12)	16(13)	-316(16)
3921	-119(16)	-84(16)	15(13)	132(12)	196(12)	132(12)	15(13)	-84(16)
3925	584(11)	518(11)	365(10)	218(10)	180(7)	218(10)	365(10)	518(11)
4065	0(7)	1(6)	2(6)	1(6)	0(7)	0(7)	0(7)	0(7)
4369	0(16)	1(6)	2(6)	1(6)	0(6)	0(16)	0(16)	0(16)
4300	0(16)	0(16)	0(16)	0(16)	0(16)	0(16)	0(16)	0(16)

Table 2-21. B-9U/161-C Ultimate Compression Internal Loads
(3.25 End g Boost Limit)

PEAK ULTIMATE AXIAL COMPRESSION LOAD INTENSITIES

STATION (IN)	NX1 (LB/IN)	NX2 (LB/IN)	NX3 (LB/IN)	NX4 (LB/IN)	NX5 (LB/IN)	NX6 (LB/IN)	NX7 (LB/IN)	NX8 (LB/IN)
1000	0(16)	0(16)	0(16)	0(16)	0(16)	0(16)	0(16)	0(16)
1936	-6(11)	-5(11)	-4(9)	-4(12)	-5(12)	-4(12)	-3(9)	-5(11)
1972	-25(11)	-21(9)	-25(9)	-34(12)	-47(12)	-34(12)	-8(10)	-20(11)
1131	-62(11)	-52(11)	-59(9)	-55(9)	-75(12)	-53(12)	-27(10)	-52(11)
1278	-171(8)	-138(8)	-122(9)	-105(12)	-147(12)	-105(12)	-71(10)	-138(8)
1337	-231(8)	-184(8)	-142(9)	-132(12)	-185(12)	-132(12)	-84(10)	-184(8)
1341	-295(15)	-224(15)	-144(9)	-136(12)	-189(12)	-136(12)	-86(10)	-224(15)
1477	-435(8)	-343(8)	-205(9)	-225(12)	-313(12)	-225(12)	-138(10)	-343(8)
1481	-135(15)	-107(15)	-39(15)	-58(16)	-82(16)	-58(16)	-62(3)	-107(15)
1500	-232(6)	-167(6)	-50(2)	-111(16)	-158(16)	-111(16)	-90(3)	-176(6)
1750	-446(4)	-337(6)	-65(6)	-154(16)	-218(16)	-154(16)	-135(3)	-329(4)
1964	-665(4)	-516(10)	-348(10)	-179(10)	-234(16)	-179(10)	-348(10)	-516(10)
1968	-5396(4)	-5238(6)	-4868(6)	-4514(5)	-4388(5)	-4514(5)	-4819(4)	-5227(4)
2106	-4429(4)	-4742(4)	-5564(6)	-6397(5)	-6771(5)	-6397(5)	-5498(4)	-4742(4)
2122	-4315(4)	-4685(4)	-5648(6)	-6621(5)	-7387(10)	-6621(5)	-5579(4)	-4685(4)
2126	-4286(4)	-4671(4)	-5669(6)	-6670(5)	-7558(10)	-6678(5)	-5599(4)	-4671(4)
2142	-4171(4)	-4613(4)	-5753(6)	-6938(10)	-8243(10)	-6938(10)	-5681(4)	-4613(4)
2194	-3791(4)	-4421(4)	-6023(6)	-8690(10)	-10462(10)	-8690(10)	-5942(4)	-4421(4)
2198	-3773(4)	-4414(4)	-6043(6)	-8804(10)	-10605(10)	-8804(10)	-5962(4)	-4414(4)
2180	-3651(7)	-4437(4)	-6458(6)	-10755(10)	-12964(10)	-10755(10)	-6364(4)	-4437(4)
2184	-3166(4)	-3968(4)	-5999(6)	-8004(10)	-11113(10)	-8894(10)	-5905(4)	-3968(4)
2300	-3238(4)	-4026(4)	-6036(6)	-8984(10)	-11218(10)	-8984(10)	-5928(4)	-4026(4)
2430	-3343(7)	-4072(4)	-6062(6)	-9056(10)	-11303(10)	-9056(10)	-5944(4)	-4072(4)
2500	-4011(7)	-4118(4)	-6086(6)	-9124(10)	-11383(10)	-9125(10)	-5961(4)	-4118(4)
2600	-4675(7)	-4452(7)	-6107(6)	-9190(10)	-11460(10)	-9190(10)	-5978(4)	-4452(7)
2664	-5091(7)	-4751(7)	-6119(6)	-9231(10)	-11506(10)	-9231(10)	-5989(4)	-4751(7)
2668	-5111(7)	-4766(7)	-6120(6)	-9227(10)	-11500(10)	-9227(10)	-5990(4)	-4766(7)
2900	-5563(7)	-5096(7)	-6138(6)	-8878(10)	-10985(10)	-8878(10)	-6012(4)	-5096(7)
2964	-5773(7)	-5250(7)	-6146(6)	-8707(10)	-10732(10)	-8707(10)	-6023(4)	-5250(7)
2968	-5787(7)	-5260(7)	-6146(6)	-8696(10)	-10716(10)	-8696(10)	-6023(4)	-5260(7)
2950	-6060(7)	-5463(7)	-6162(6)	-8486(10)	-10397(10)	-8486(10)	-6045(4)	-5463(7)
3050	-6519(7)	-5828(7)	-6276(6)	-8350(10)	-10085(10)	-8350(10)	-6167(4)	-5828(7)
3161	-7061(7)	-6256(7)	-6401(6)	-8181(10)	-9712(10)	-8181(10)	-6301(4)	-6256(7)
3165	-7174(7)	-6346(7)	-6405(6)	-8174(10)	-9698(10)	-8174(10)	-6306(4)	-6346(7)
3293	-7480(7)	-6597(7)	-6491(6)	-7876(10)	-9179(10)	-7876(10)	-6404(4)	-6597(7)
3295	-7485(7)	-6601(7)	-6492(6)	-7871(10)	-9170(10)	-7871(10)	-6406(4)	-6601(7)
3373	-7671(7)	-6751(7)	-6536(6)	-7670(10)	-8836(10)	-7670(10)	-6458(4)	-6751(7)
3377	-7770(7)	-6831(7)	-6536(6)	-7658(10)	-8817(10)	-7658(10)	-6459(4)	-6831(7)
3538	-7646(7)	-6771(7)	-6593(6)	-7277(5)	-8062(10)	-7277(5)	-6536(4)	-6771(7)
3542	-7732(7)	-6841(7)	-6594(6)	-7271(5)	-8040(10)	-7271(5)	-6538(4)	-6841(7)
3679	-7196(7)	-6499(7)	-6681(6)	-7125(5)	-7325(5)	-7125(5)	-6743(3)	-6499(7)
3583	-9708(7)	-9017(7)	-8198(6)	-9331(10)	-9973(10)	-9391(10)	-8162(4)	-9017(7)
3820	-8869(7)	-8464(7)	-8263(6)	-8923(10)	-9222(10)	-8923(10)	-8251(4)	-8464(7)
3921	-8395(5)	-8408(10)	-8570(10)	-8732(10)	-8799(10)	-8732(10)	-8570(10)	-8408(10)
3925	-243(12)	-184(12)	-113(9)	-124(9)	-116(9)	-94(9)	-71(9)	-184(12)
4165	-0(15)	-0(15)	-0(15)	-0(15)	-0(15)	-1(6)	-2(6)	-1(6)
4069	0(16)	0(16)	0(16)	0(16)	0(16)	-1(6)	-2(6)	-1(6)
4300	0(16)	0(16)	0(16)	0(16)	0(16)	0(16)	0(16)	0(16)

Table 2-22. B-9U/161-C Ultimate Tension Internal Loads (3.50 End g Boost Limit)

PEAK ULTIMATE AXIAL TENSION LOAD INTENSITIES

STATION (IN)	NX1 (LR/IN)	NX2 (LR/IN)	NX3 (LR/IN)	NX4 (LR/IN)	NX5 (LR/IN)	NX6 (LR/IN)	NX7 (LR/IN)	NX8 (LR/IN)
1000	0(16)	0(15)	0(16)	0(16)	0(16)	0(16)	0(16)	0(16)
1036	5(12)	4(12)	0(15)	0(16)	1(11)	0(16)	0(15)	4(12)
1072	45(12)	32(12)	1(15)	4(11)	9(11)	4(11)	1(15)	32(12)
1131	73(12)	51(12)	3(15)	7(16)	12(8)	7(16)	3(15)	51(12)
127A	141(12)	98(12)	7(15)	28(16)	58(8)	28(16)	7(15)	98(12)
1337	173(12)	121(12)	9(15)	42(8)	89(8)	42(8)	9(15)	121(12)
1341	177(12)	124(12)	8(14)	121(15)	192(15)	121(15)	8(14)	124(12)
1477	288(12)	200(12)	14(14)	99(8)	191(8)	99(8)	14(14)	200(12)
1481	1411(12)	1322(12)	1206(10)	1289(10)	1374(8)	1299(10)	1206(10)	1322(12)
1600	1569(12)	1430(12)	1164(10)	1377(8)	1531(8)	1377(8)	1177(9)	1430(12)
1750	1820(12)	1601(12)	1111(10)	1539(8)	1791(8)	1539(8)	1153(9)	1601(12)
1864	2042(12)	1753(12)	1056(12)	1510(8)	1780(8)	1510(8)	1056(12)	1753(12)
1868	931(12)	640(12)	35(14)	86(13)	140(13)	85(13)	35(14)	640(12)
2006	2257(11)	996(11)	47(14)	155(13)	242(13)	153(13)	47(14)	996(11)
2022	2578(11)	1164(11)	48(14)	166(13)	258(13)	164(13)	48(14)	1164(11)
2026	2657(11)	1204(11)	45(14)	160(13)	251(13)	158(13)	45(14)	1204(11)
2042	2972(11)	1366(11)	47(14)	152(13)	242(13)	150(13)	47(14)	1366(11)
2094	4009(11)	1905(11)	52(14)	141(14)	219(13)	141(14)	52(14)	1905(11)
2098	4061(11)	1927(11)	52(14)	142(14)	217(13)	142(14)	52(14)	1927(11)
2180	4531(11)	1960(11)	60(14)	168(14)	213(14)	168(14)	60(14)	1960(11)
2184	6452(11)	3871(11)	1454(13)	1653(13)	1734(13)	1690(13)	1450(13)	3871(11)
2300	6458(11)	3857(11)	1444(13)	1656(13)	1743(13)	1653(13)	1439(13)	3857(11)
2400	6470(11)	3954(11)	1437(13)	1675(13)	1772(13)	1671(13)	1431(13)	3854(11)
2500	6478(11)	3846(11)	1433(13)	1709(13)	1821(13)	1704(13)	1426(13)	3846(11)
2600	6481(11)	3836(11)	1432(13)	1756(13)	1888(13)	1751(13)	1424(13)	3836(11)
2664	6481(11)	3823(11)	1431(13)	1793(13)	1940(13)	1787(13)	1422(13)	3828(11)
2668	6470(11)	3820(11)	1431(13)	1795(13)	1944(13)	1799(13)	1422(13)	3829(11)
2800	5746(11)	3291(11)	1429(13)	1886(13)	2072(13)	1879(13)	1419(13)	3291(11)
2864	5391(11)	3032(11)	1429(13)	1937(13)	2144(13)	1930(13)	1418(13)	3032(11)
2868	5368(11)	3015(11)	1429(13)	1940(13)	2149(13)	1933(13)	1418(13)	3015(11)
2950	4877(11)	2977(12)	1428(13)	2015(13)	2254(13)	2007(13)	1417(13)	2977(12)
3050	3854(11)	3103(12)	1428(12)	2172(13)	2477(13)	2164(13)	1428(12)	3102(12)
3161	3683(12)	3033(12)	1464(12)	2487(13)	2921(13)	2477(13)	1464(12)	3033(12)
3165	3615(12)	2980(12)	1448(12)	2497(13)	2938(13)	2487(13)	1448(12)	2980(12)
3293	2979(12)	2538(12)	1473(12)	2631(16)	3721(16)	2631(16)	1473(12)	2538(12)
3295	2968(12)	2530(12)	1473(12)	2643(16)	3737(16)	2643(16)	1473(12)	2530(12)
3373	2475(12)	2185(12)	1486(12)	2737(13)	3272(13)	2726(13)	1486(12)	2185(12)
3377	2394(12)	2123(12)	1469(12)	2742(13)	3281(13)	2730(13)	1469(12)	2123(12)
3538	1465(12)	1471(12)	1486(12)	2654(13)	3156(13)	2642(13)	1486(12)	1471(12)
3542	1391(12)	1414(12)	1469(12)	2651(13)	3155(13)	2639(13)	1469(12)	1414(12)
3679	943(12)	1105(12)	1559(13)	2228(13)	2506(13)	2229(13)	1561(13)	1105(12)
3683	-609(12)	-442(12)	25(13)	770(16)	1088(16)	770(16)	26(13)	-442(12)
3820	-447(16)	-316(16)	16(13)	516(12)	743(12)	516(12)	16(13)	-316(16)
3921	-119(16)	-84(16)	15(13)	132(12)	196(12)	132(12)	15(13)	-84(16)
3925	629(11)	560(10)	393(10)	227(10)	180(7)	227(10)	393(10)	560(10)
4065	0(7)	1(6)	2(6)	1(6)	0(7)	0(7)	0(7)	0(7)
4069	0(16)	1(6)	2(6)	1(6)	0(6)	0(16)	0(16)	0(16)
4300	0(16)	0(16)	0(16)	0(16)	0(16)	0(16)	0(16)	0(16)

Table 2-23. B-9U/161-C Ultimate Compression Internal Loads
(3.50 End g Boost Limit)

PEAK ULTIMATE AXIAL COMPRESSION LOAD INTENSITIES

STATION (IN)	NX1 (LR/IN)	NX2 (LR/IN)	NX3 (LR/IN)	NX4 (LR/IN)	NX5 (LR/IN)	NX6 (LR/IN)	NX7 (LR/IN)	NX8 (LR/IN)
1000	9(16)	0(16)	0(16)	0(16)	0(16)	0(16)	0(16)	0(16)
1036	-6(11)	-5(11)	-4(9)	-4(12)	-5(12)	-4(12)	-3(9)	-5(11)
1072	-27(11)	-22(11)	-25(9)	-34(12)	-47(12)	-34(12)	-9(10)	-22(11)
1131	-67(11)	-56(11)	-59(9)	-55(9)	-75(12)	-53(12)	-29(10)	-56(11)
1278	-171(8)	-138(8)	-122(9)	-105(12)	-147(12)	-105(12)	-77(10)	-138(8)
1337	-231(8)	-184(8)	-142(9)	-132(12)	-185(12)	-132(12)	-91(10)	-184(8)
1341	-295(15)	-224(15)	-144(9)	-136(12)	-189(12)	-136(12)	-93(10)	-224(15)
1477	-435(8)	-343(8)	-205(9)	-225(12)	-313(12)	-225(12)	-149(10)	-343(8)
1481	-135(15)	-107(15)	-79(15)	-58(15)	-82(15)	-58(15)	-62(3)	-107(15)
1600	-232(6)	-167(6)	-50(2)	-111(15)	-158(15)	-111(15)	-90(3)	-175(6)
1750	-446(4)	-337(6)	-65(6)	-154(15)	-218(15)	-154(15)	-135(3)	-329(4)
1864	-665(4)	-503(6)	-117(6)	-156(15)	-234(15)	-156(15)	-178(3)	-490(4)
1868	-5396(4)	-5238(6)	-4868(6)	-4514(5)	-4388(5)	-4514(5)	-4819(4)	-5227(4)
2006	-4429(4)	-4742(4)	-5564(6)	-6397(5)	-6967(10)	-6397(5)	-5498(4)	-4742(4)
2022	-4315(4)	-4685(4)	-5648(6)	-6621(5)	-7656(10)	-6621(5)	-5579(4)	-4695(4)
2026	-4286(4)	-4671(4)	-5659(6)	-6678(5)	-7840(10)	-6678(5)	-5599(4)	-4671(4)
2042	-4171(4)	-4613(4)	-5753(6)	-7085(10)	-8578(10)	-7085(10)	-5681(4)	-4613(4)
2094	-3791(4)	-4421(4)	-6023(6)	-8973(10)	-10969(10)	-8973(10)	-5942(4)	-4421(4)
2098	-3773(4)	-4414(4)	-6043(6)	-9097(10)	-11123(10)	-9097(10)	-5962(4)	-4414(4)
2190	-3651(7)	-4437(4)	-5458(6)	-11199(10)	-13666(10)	-11199(10)	-6364(4)	-4437(4)
2184	-3166(4)	-3968(4)	-5999(6)	-9341(10)	-11819(10)	-9341(10)	-5905(4)	-3968(4)
2300	-3238(4)	-4025(4)	-5036(6)	-9441(10)	-11935(10)	-9441(10)	-5928(4)	-4026(4)
2400	-3343(7)	-4072(4)	-6062(6)	-9519(10)	-12028(10)	-9519(10)	-5944(4)	-4072(4)
2500	-4011(7)	-4118(4)	-6086(6)	-9594(10)	-12116(10)	-9594(10)	-5961(4)	-4118(4)
2600	-4675(7)	-4452(7)	-6107(6)	-9665(10)	-12199(10)	-9665(10)	-5978(4)	-4452(7)
2664	-5091(7)	-4751(7)	-6119(6)	-9706(10)	-12250(10)	-9709(10)	-5989(4)	-4751(7)
2668	-5111(7)	-4766(7)	-6120(6)	-9704(10)	-12242(10)	-9704(10)	-5990(4)	-4766(7)
2800	-5563(7)	-5095(7)	-6138(6)	-9316(10)	-11659(10)	-9316(10)	-6012(4)	-5096(7)
2864	-5773(7)	-5250(7)	-6146(6)	-9124(10)	-11387(10)	-9124(10)	-6023(4)	-5250(7)
2868	-5787(7)	-5260(7)	-6146(6)	-9112(10)	-11369(10)	-9112(10)	-6023(4)	-5260(7)
2950	-6060(7)	-5463(7)	-6162(6)	-8877(10)	-11013(10)	-8877(10)	-6045(4)	-5463(7)
3050	-6519(7)	-5928(7)	-6276(6)	-8712(10)	-10650(10)	-8712(10)	-6167(4)	-5929(7)
3161	-7061(7)	-6256(7)	-6401(6)	-8507(10)	-10216(10)	-8507(10)	-6301(4)	-6256(7)
3165	-7174(7)	-6346(7)	-6405(6)	-8499(10)	-10200(10)	-8499(10)	-6306(4)	-6346(7)
3293	-7480(7)	-6597(7)	-6491(6)	-8151(10)	-9603(10)	-8151(10)	-6404(4)	-6597(7)
3295	-7485(7)	-6601(7)	-6492(6)	-8145(10)	-9593(10)	-8145(10)	-6406(4)	-6601(7)
3373	-7671(7)	-6751(7)	-6536(6)	-7913(10)	-9209(10)	-7913(10)	-6458(4)	-6751(7)
3377	-7770(7)	-6831(7)	-6536(6)	-7899(10)	-9188(10)	-7899(10)	-6459(4)	-6831(7)
3538	-7646(7)	-6771(7)	-6593(6)	-7358(10)	-8342(10)	-7358(10)	-6576(4)	-6771(7)
3542	-7732(7)	-6841(7)	-6594(6)	-7344(10)	-8320(10)	-7344(10)	-6538(4)	-6841(7)
3679	-7196(7)	-6499(7)	-6681(6)	-7125(5)	-7539(10)	-7125(5)	-6743(3)	-6499(7)
3683	-9708(7)	-9017(7)	-8198(6)	-8493(10)	-10149(10)	-8493(10)	-8162(4)	-9017(7)
3820	-8869(7)	-8464(7)	-8253(6)	-8954(10)	-9293(10)	-8954(10)	-8251(4)	-8464(7)
3921	-8395(5)	-8397(5)	-8535(10)	-8716(10)	-8794(10)	-8718(10)	-8535(10)	-8397(5)
3925	-243(12)	-184(12)	-113(9)	-124(9)	-116(9)	-94(9)	-71(9)	-184(12)
4065	-0(15)	-0(15)	-0(15)	-0(15)	-0(15)	-1(6)	-2(6)	-1(6)
4069	0(16)	0(16)	0(16)	0(16)	0(16)	-1(6)	+2(6)	-1(6)
4300	0(16)	0(16)	0(16)	0(16)	0(16)	0(16)	0(16)	0(16)

page 6-4. Tables 2-16 through 2-23 are similar tables for other g levels investigated. These tables are used to determine delta weight change with end boost variation for the intertank and LH₂ tank. The LO₂ tank is designed to a minimum ultimate compression load intensity of 1000 lb/in. and this value is not exceeded by any condition investigated.

The interstage attach structure includes the separation linkage system, the longerons for orbiter axial load introduction and the forward and aft interstage bulkheads. Figure 2-15 presents plots of the interstage attach loads versus end boost g level. The aft attachment load is maximum for maximum α q tail winds and is not sensitive to end boost g level.

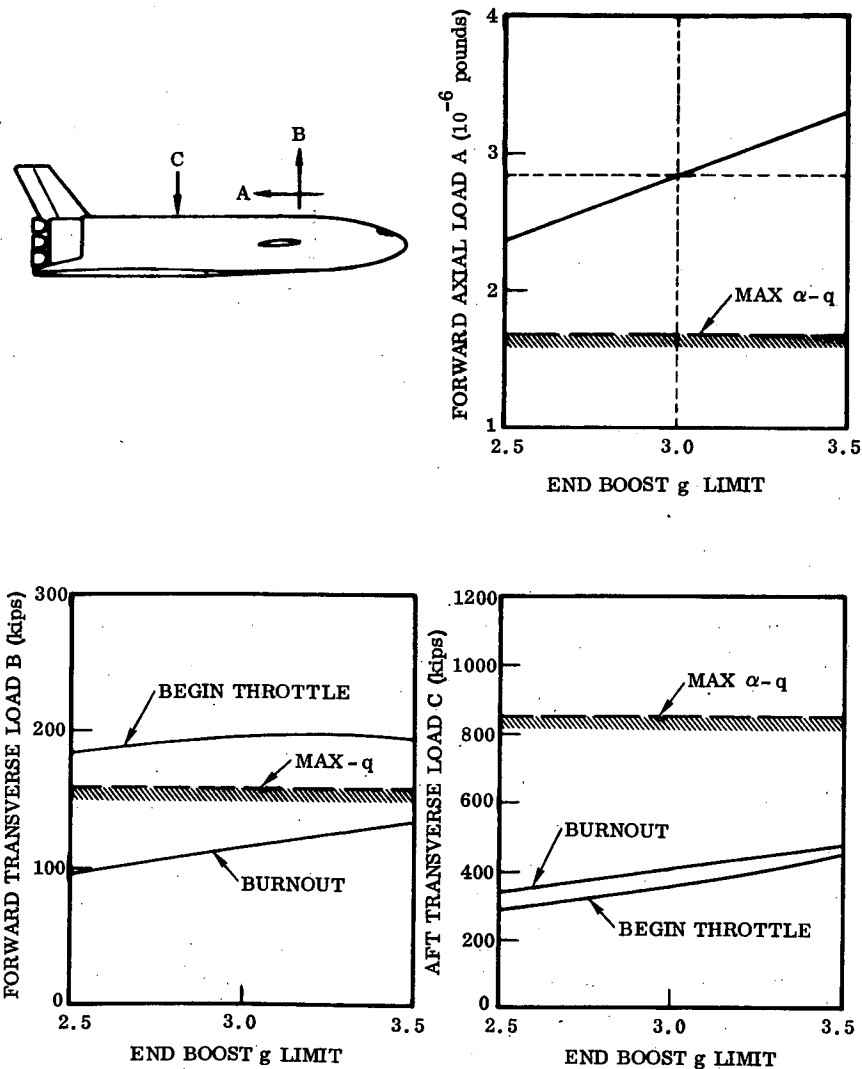


Figure 2-15. Effect of End Boost g Limit on Orbiter Attachment Loads

The booster thrust structure is designed to some degree by the maximum thrust load. Maximum thrust attained for all g levels investigated is that of maximum vacuum thrust, as shown in Figure 2-16.

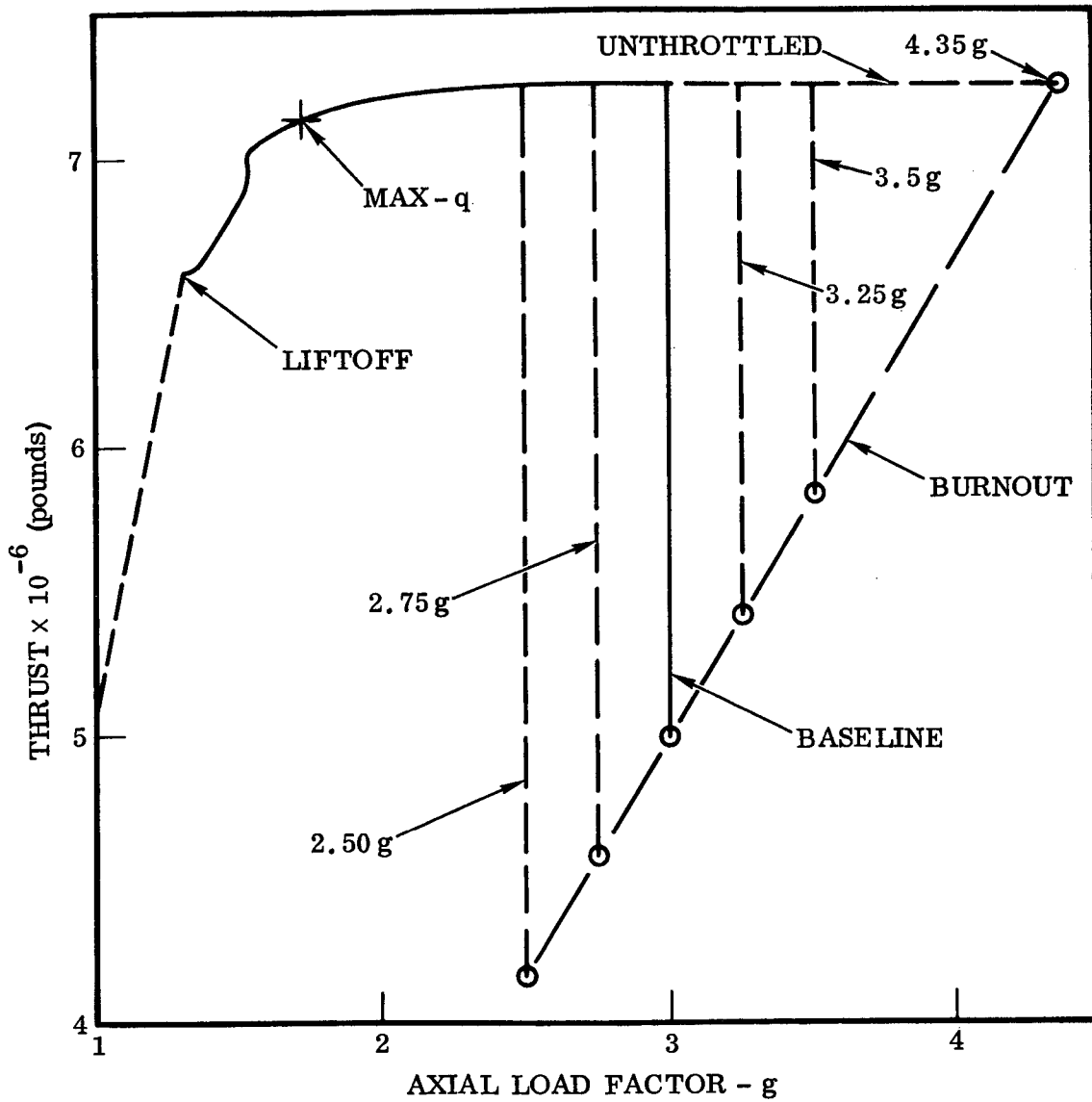


Figure 2-16. Booster B-9U Axial Load Factor Versus Thrust

The maximum lower dome apex pressures for the LO_2 tank and the LH_2 tank are shown in Figures 2-17 and 2-18, respectively. These plots show that the end boost g level variations within the range of this study have no effect on peak design pressures and do not produce weight variations.

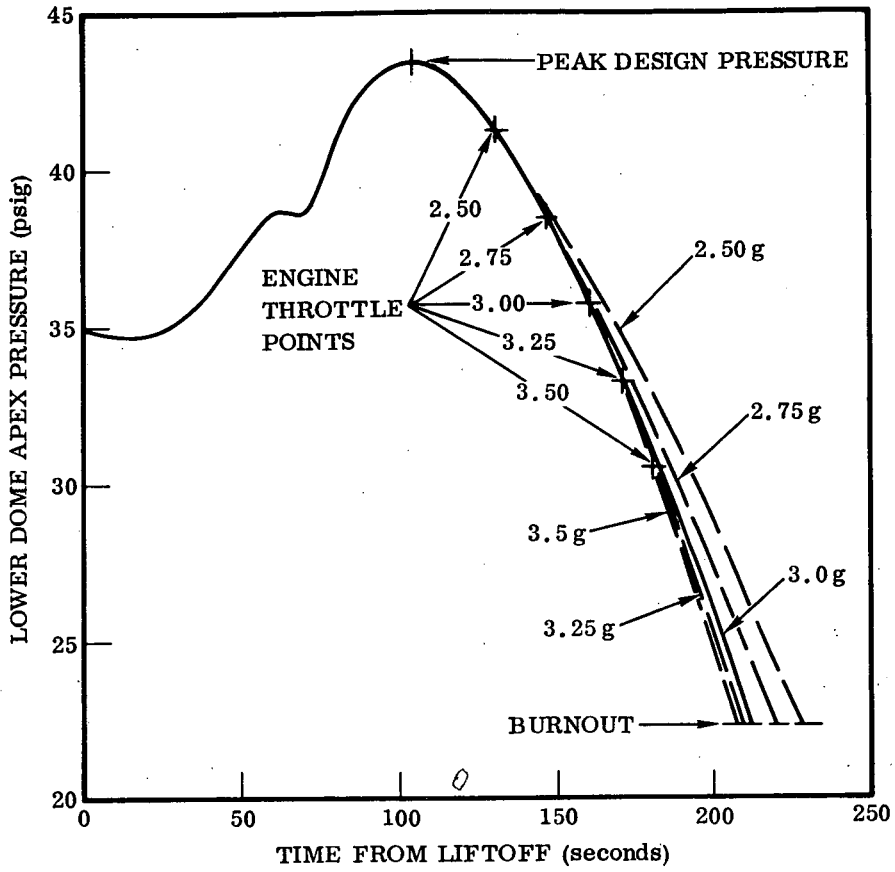


Figure 2-17. LO₂ Tank Maximum Lower Dome Apex Pressure

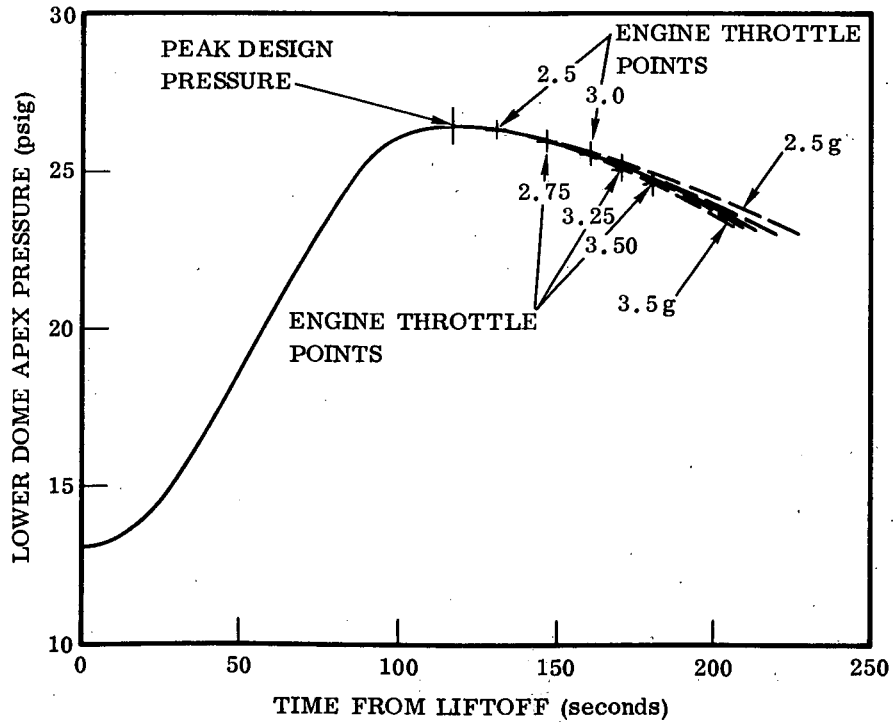


Figure 2-18. LH₂ Tank Maximum Lower Dome Apex Pressure

Effects of end boost acceleration on booster structural weight are shown in Figure 2-19 as plots of delta weight versus end boost g level for the interstage attach structure, the intertank structure and the thrust structure, and as delta unit weight versus g level for

NOTE: LO₂ TANK UNIT WEIGHT DOES NOT VARY FOR THE RANGE OF g LEVELS INVESTIGATED.

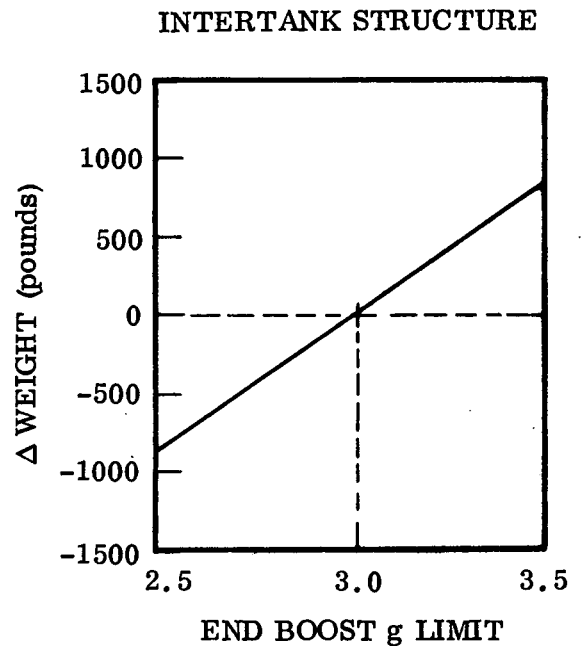
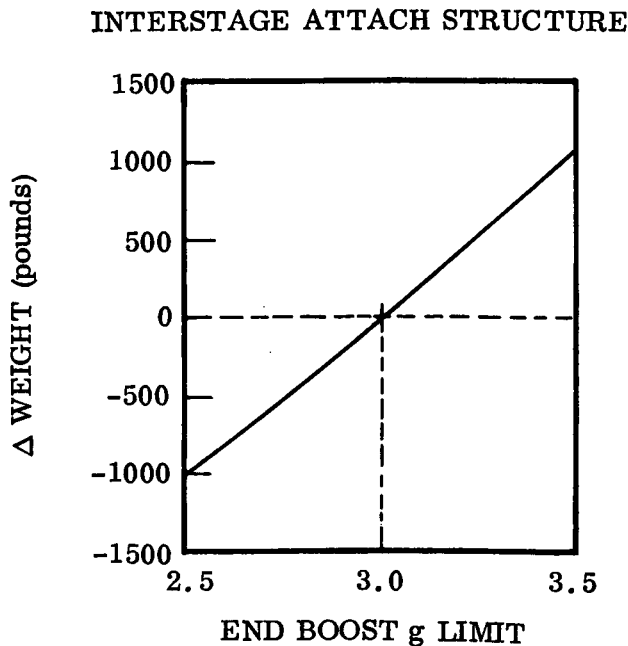
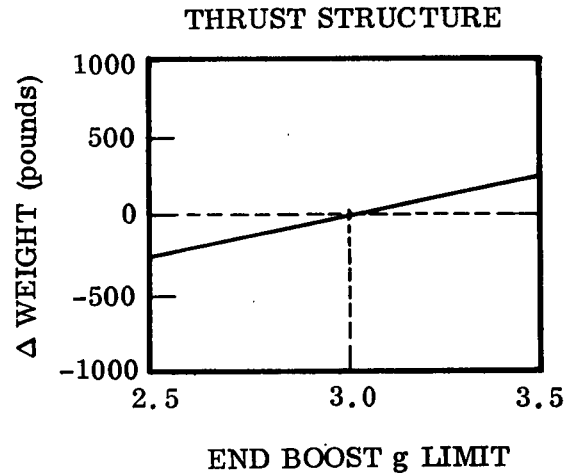
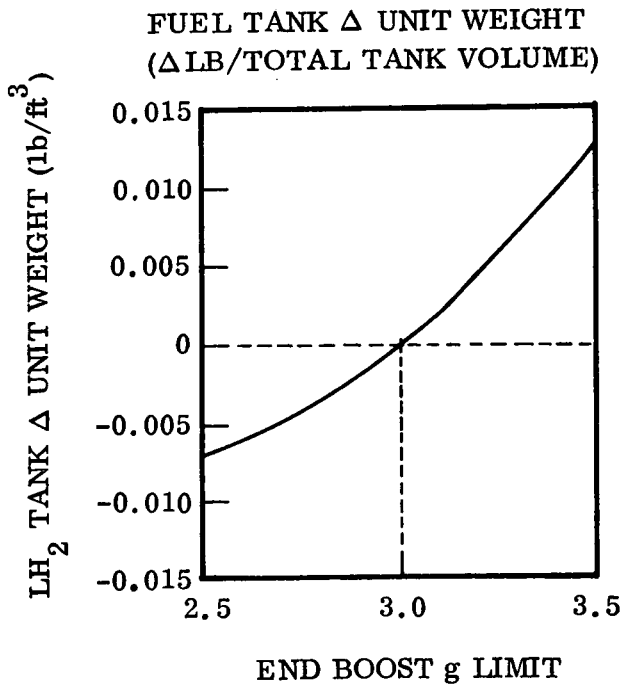


Figure 2-19. Effect of End Boost Acceleration on B-9U Booster Structure

the LH₂ tank. The propellant tanks are designed to maximum compressive load intensities coupled with maximum hoop tension load intensities, due to ullage pressure plus head pressure. The thrust structure delta weight variation is due to the dynamic amplification factor of ten percent of the g level. The intertank structure includes the shear material required for introduction of orbiter drag loads from the longeron into the shell, as well as stiffening required to carry compressive loads due to the weight of the LO₂.

Figure 2-20 gives the total effect of end boost acceleration on the fuselage structure weight. A LH₂ tank volume of 120,000 ft³ is used to calculate the tank weight.

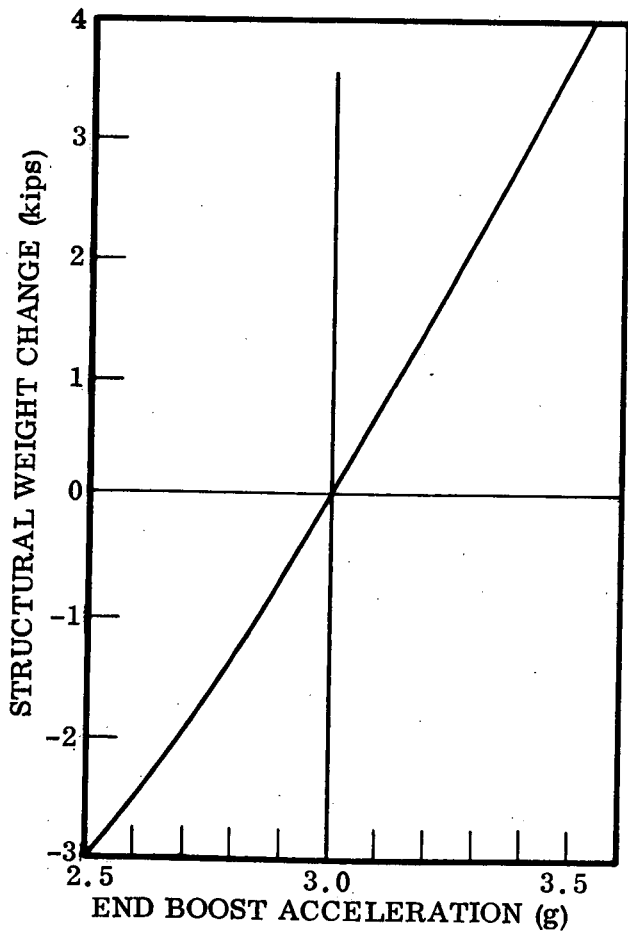


Figure 2-20. Effect of End Boost on Fuselage Structure Weight

An independent study of the fuselage weight sensitivity using ASOP (Reference 2) is compared with the more approximate method previously investigated. In order to make a valid comparison of the two methods, the percentage change in weight versus g must be examined since the structures used for the two methods are not identical. Weight breakdown for the preceding analysis includes:

	<u>Weight (pounds)</u>
Main LH ₂ Tank	
Barrel Section	57,290
Baffles	575
Orbiter Attach Structure	5,350
Main LO ₂ Tank	
Barrel Section	9,583
Baffles	1,200
Orbiter Attach Structure	3,315
Forward Adapter Section	3,652
Intertank Basic Structure	14,141
Orbiter Bulkheads — Intertank Section	5,482
Thrust Structure	30,000
Total Body Group Weight	130,588

These items are shown in Table 4-4 of Reference 1 and the list is complete except for the tank domes, nose section, and miscellaneous secondary structure.

For ASOP, the total weight after two optimization iterations is 87,871 pounds. This is for the baseline 3g condition and does not include the weight of the thrust structure. So the difference in total weight for the two methods is: $130,588 - (87,871 + 30,000) = 12,717$ pounds and shows a great weight saving from the more precise finite element approach. Varying the axial load factor to 2.7 g and 3.2 g gives structural weights of 86,904 pounds and 88,756 pounds, respectively. These data are summarized in Table 2-24, along with the percentage change in weight. These values are shown against the original plot (excluding the thrust structure effect) on Figure 2-21. Agreement is fairly good, however, the more exact analysis lowers the slope of the curve, giving less of a variation in structural weight for a change in end boost acceleration.

Table 2-24. Effect of End Boost on Fuselage Structure Weight From ASOP

Load Factor	Fuselage Weight W-pounds	ΔW (pounds)	Percentage Change in Weight
3.00	87,871	—	0
2.74	86,904	-967	-1.10
3.20	88,756	885	1.01

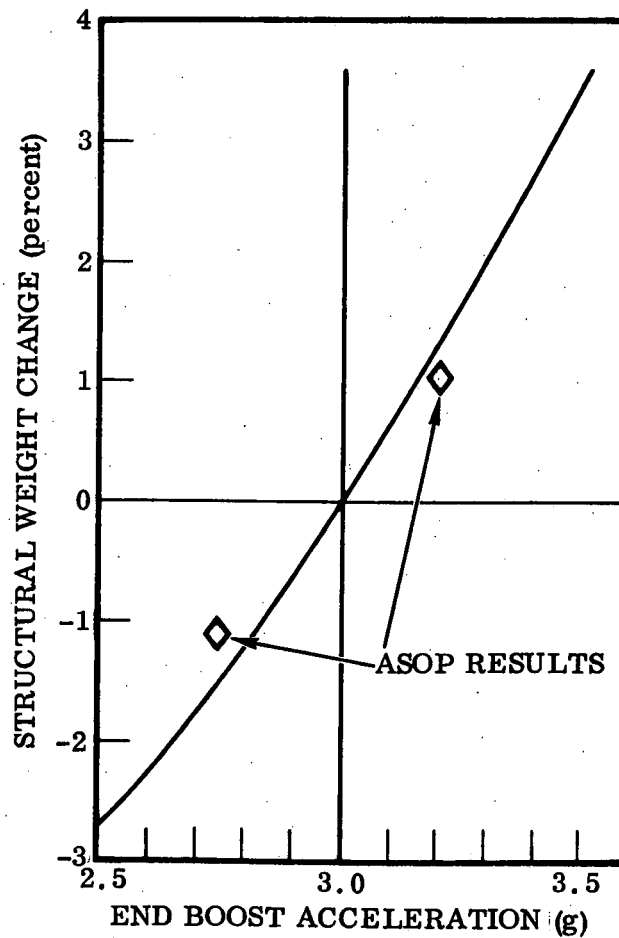


Figure 2-21. Comparison of ASOP Program Results on Effect of End Boost of Fuselage Structure Weight

SECTION 3

SENSITIVITIES OF LOADS TO VARIOUS CONFIGURATION AND FLIGHT PARAMETER CHANGES

To establish good design criteria for any vehicle, a clear understanding must be gained of the importance of the loads in terms of their influence upon structural weight. Once this understanding is reached, an assessment can be made of the sensitivity of structural weight to loading parameter variability and probability. The first phase of this study identified the significant loads and preceding sections of this report have presented the sensitivity of structure weight to load variations. This section relates the load variations to: 1) thrust variation, 2) aerodynamic parameter variations, 3) wind probability levels, 4) structural weight and center of gravity uncertainties, 5) control parameter uncertainties, and 6) changes in guidance laws.

Since one of the most significant loads occurs during ascent and is a direct function of the maximum (αq), the majority of the work performed was centered around variations in the maximum (αq) during ascent. These variations were obtained by running a six degree-of-freedom ascent simulation of the B-9U space shuttle configuration. The wind profiles used were the Marshall synthetic winds. Nominal conditions used the 95 percent wind profile and the 99 percent shear build-up and back-off tables. The results of these simulated flights are presented in Figures 3-1 through 3-7.

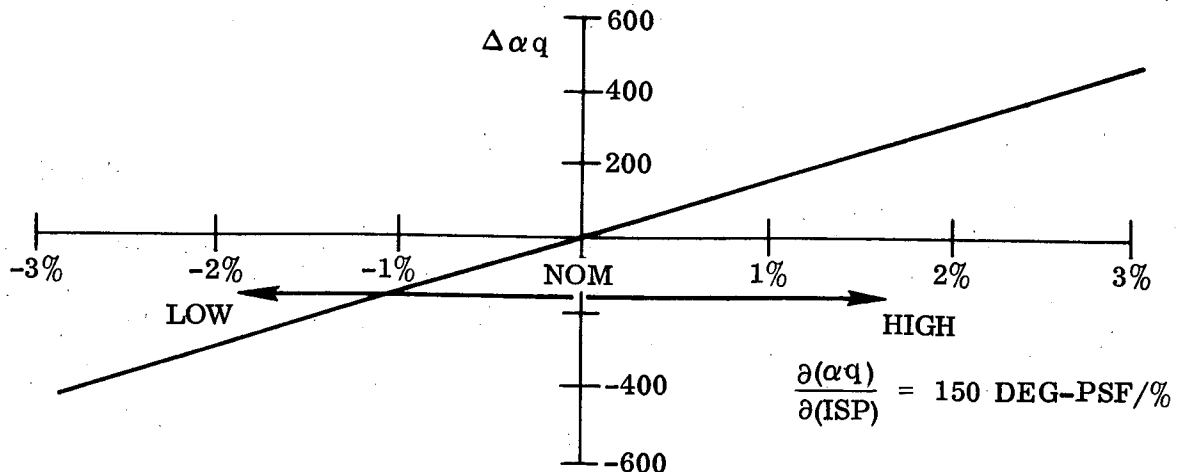


Figure 3-1. Design αq Variations (Maximum Value) Isp Effects

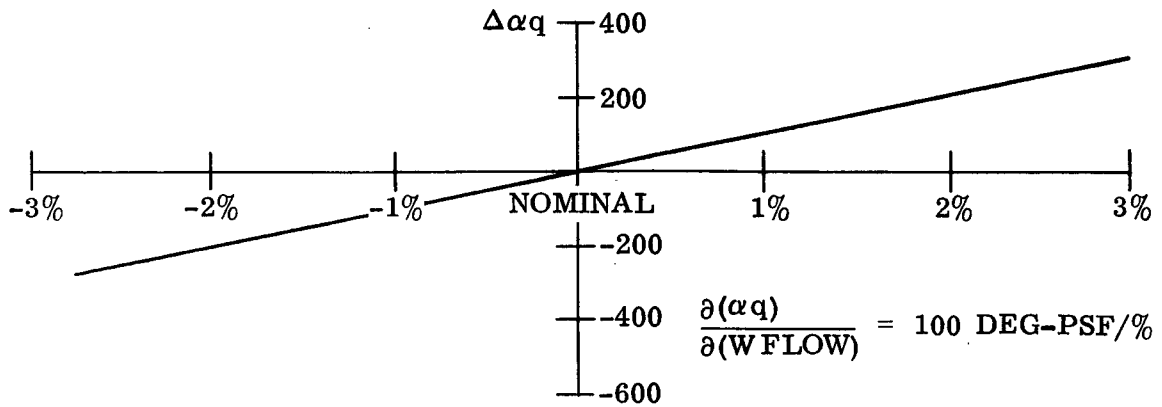


Figure 3-2. Design αq Variations (Maximum Value) Fuel or Oxidizer Flow Rates

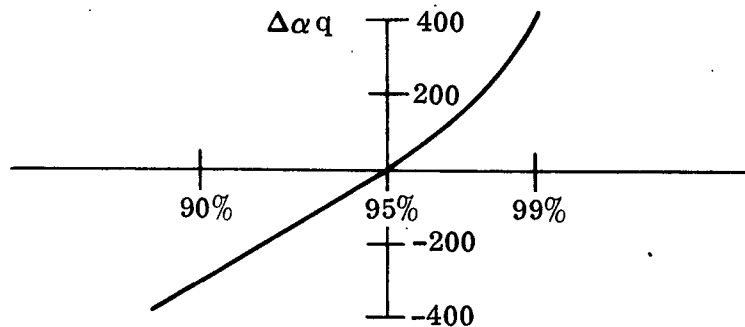


Figure 3-3. Design αq Variations (Maximum Value) Wind Effects (MSFC Synthetic Winds)

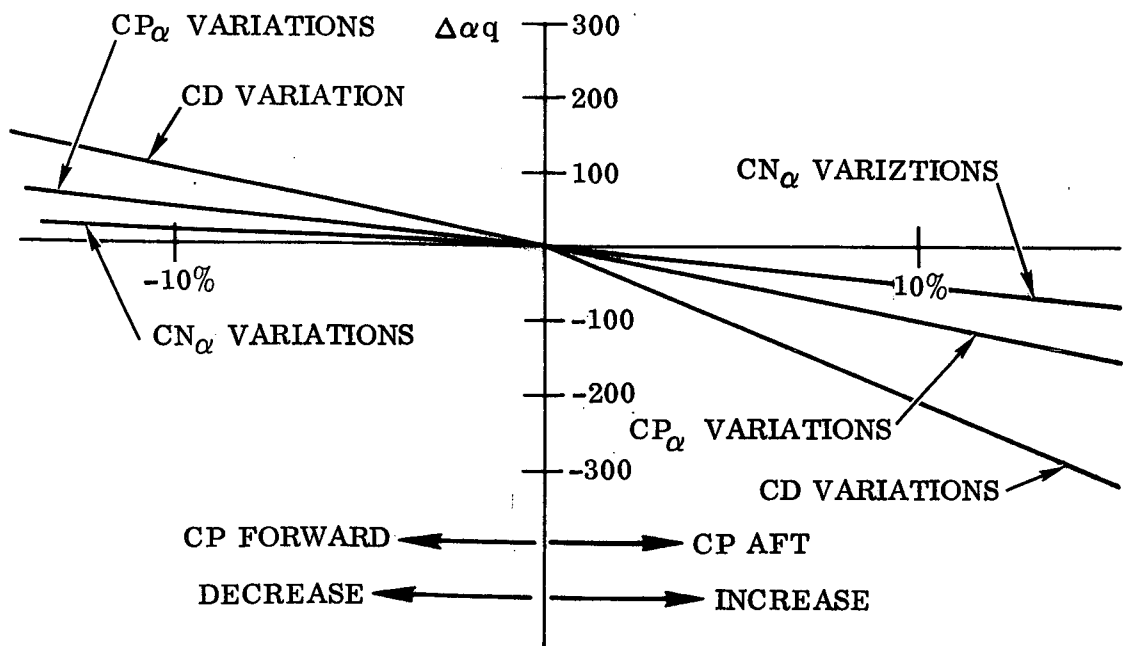


Figure 3-4. Design αq Variations (Maximum Value) Aerodynamic Effect (CN_α , CD , CP_α)

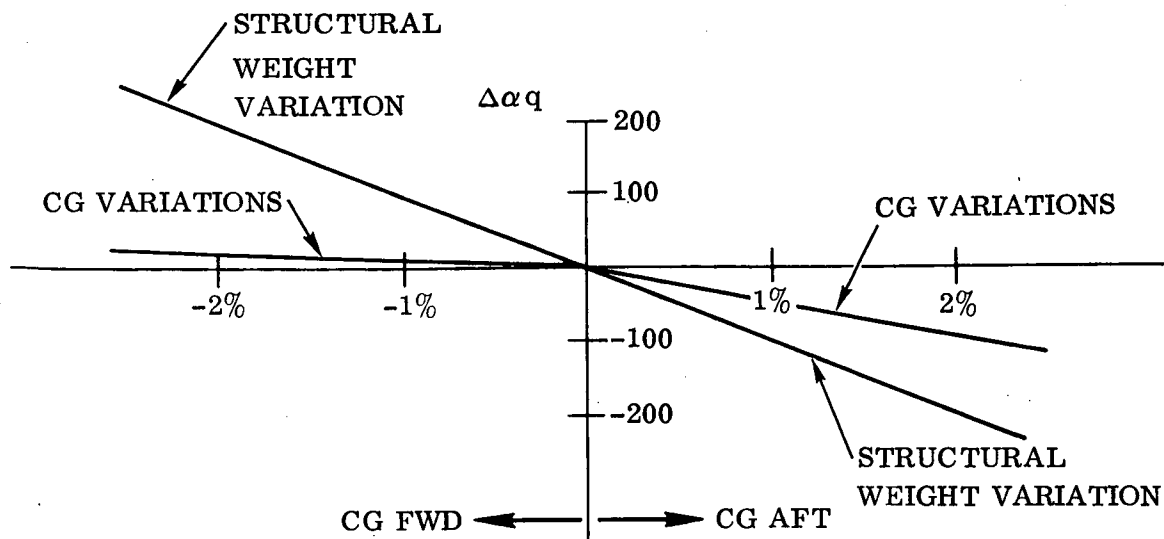


Figure 3-5. Design αq Variations (Maximum Value) Booster Structural Weight and C.G. Variations

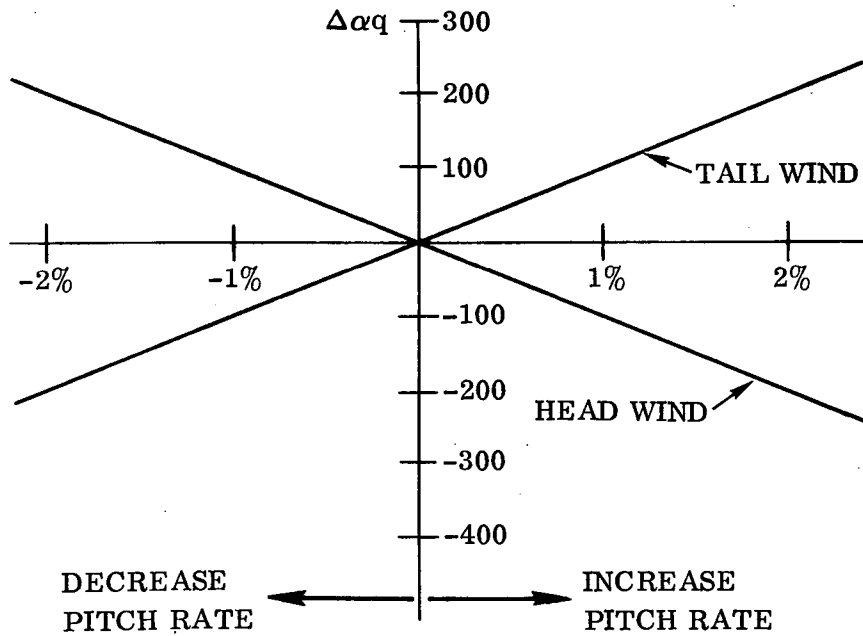


Figure 3-6. Design αq Variations (Maximum Value) Control System Gain Variations ($K_\theta, K_{\dot{\theta}}$)

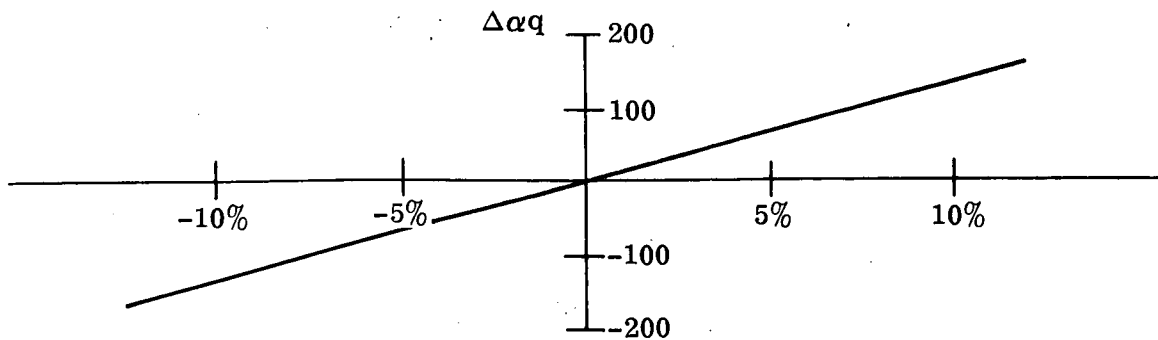


Figure 3-7. Design αq Variations (Maximum Value) Pitch Programmer Variations

Thrust variations can be divided between variation in engine efficiency which is measured as I_{SP} and fuel oxidizer flow rate. Engine specifications direct that the total thrust variation not exceed ± 2 percent. The specification does not distinguish between I_{SP} and fuel/oxidizer flow rate. Therefore, this analysis considered the independent events that either the I_{SP} is off nominal or the flow rate is off nominal. Figures 3-1 and 3-2 present the results.

Wind profile probability effects are presented in Figure 3-3. Considerations were given to the 90, 95, and 99 percent wind profiles. The effect of wind probability as nonlinear in that an increase in αq of 400 deg-psf occurs when going to the 99 percent wind from the 95 percent wind but only a 300 deg-psf reduction occurs when going down to 90 percent wind from the 95 percent wind. All winds had the same shear build-up and gust.

During the early design phase, aerodynamic data are usually not refined to the degree which structural analysis would prefer. Therefore, a sensitivity analysis was conducted on aerodynamic variables such as, drag, normal force, and center of pressure. Figure 3-4 presents the aerodynamic sensitivities effects. These effects were for a ten percent variation and the results indicate that they are not very significant.

Guidance and control sensitivities can be evaluated by variations in autopilot gains and pitch programmer. The pitch programmer for the nominal case has been established to minimize loads. Therefore, small variations in pitch programmer can produce significant load changes. Figure 3-6 presents the results of pitch programmer variations. The range of variations did not extend beyond two percent because of the extreme sensitivity of this parameter.

Control system parameter studies were pitch attitude (K_θ) and pitch rate ($K\dot{\theta}$) gains. Pitch attitude gain controls the response of the vehicle to winds by holding an aerodynamically-stable vehicle from pitching into the wind. The B-9U is aerodynamically stable and therefore increasing the gain increases the load. Pitch rate gain determines the vehicle damping and a vehicle with little damping will have high loads due to overshoot. However, the B-9U appears to be insensitive to small variations in pitch rate gain. Figure 3-7 presents the control system gain variation effects.

These sensitivities can be integrated with the sensitivities discussed in Section 2 to obtain structural weight sensitivities to the various parameters discussed above. For example, to obtain the structural weight (W_s) sensitivity to I_{SP} variations the partial of αq to I_{SP} $\left(\frac{\partial \alpha q}{\partial I_{SP}}\right)$ is computed at the nominal condition, then:

$$\frac{\partial(W_s)}{\partial(\alpha q)} \cdot \frac{\partial(\alpha q)}{\partial(I_{SP})} = \frac{\partial(W_s)}{\partial(I_{SP})}$$

or numerically for the wing

$$\frac{\partial(W_s)}{\partial(\alpha q)} = 310 \text{ lb/percent}$$

$$\frac{\partial(\alpha q)}{\partial(I_{SP})} = 150 \text{ deg-psf/percent}$$

$$\frac{\partial(W_s)}{\partial(I_{SP})} = 1860 \text{ lb/percent } I_{SP}$$

In a like manner, various structural weight partials can be computed. Table 3-1 summarizes these structural weight sensitivities.

Table 3-1. Structural Weight Sensitivities

<u>WING</u>		
$\frac{\partial(W_s)}{\partial()}$		
I_{SP}	1860	lb/percent Variation
WFLOWRATE	1240	lb/percent Variation
WIND	744	lb/percent Probability
AERODYNAMIC	127	lb/percent Variation
BOOSTER TOTAL STRUCTURAL WEIGHT	1240	lb/percent Variation
CONTROL SYSTEM	186	lb/percent Variation
GUIDANCE	1240	lb/percent Variation
ENTRY g's	215	lb/percent Variation
SUBSONIC GUST	423	lb/fps Gust
<u>FUSELAGE</u>		
$\frac{\partial W^{**}}{\partial(\text{BURNOUT "g's"})}$	215	lb/percent Variation

SECTION 4

REFERENCES

1. Sealey, D.M. and Kuchta, B.J., Combined Loading Criteria Influence on Structural Performance — Phase I, Relative Weight Sensitivity to Loading, Convair Aerospace Report GDC-DDE71-003, October 1971.
2. Dwyer, W.J., Emerton, R.K. and Ojalvo, I.R., An Automated Procedure for the Optimization of Practical Aerospace Structures, AFFDL-TR-70-118, March 1971.

PART III

**PHASE III, LOADING PARAMETER VARIABILITY, INADEQUACY,
AND PROBABILITY AS A FUNCTION OF SYSTEM DESIGN**

///-1

TABLE OF CONTENTS

<u>Section</u>		<u>Page</u>
1	INTRODUCTION	III-5
2	DISCIPLINE INVOLVEMENT IN DESIGN DEFINITION	III-7
	2.1 RESPONSIBILITIES OF VARIOUS DISCIPLINES	III-7
	2.2 RELATIVE INVOLVEMENT OF DISCIPLINES	III-8
	2.3 CONTRIBUTION OF EACH DISCIPLINE	III-8
3	CRITICALITY OF LOAD PARAMETERS AND LOADING PROBABILITY AND VARIABILITY	III-13
	3.1 MAXIMUM THRUST CONDITION	III-13
	3.2 ASCENT HEADWIND	III-15
	3.3 PRESSURIZATION	III-17
	3.4 MAXIMUM g ENTRY	III-19
	3.5 LAUNCH	III-19
	3.6 MAXIMUM TEMPERATURE	III-20
	3.7 OTHER CONDITIONS	III-20
4	VARIABILITY OF LOAD PARAMETERS WITH PROGRAM SCHEDULE	III-21
5	INADEQUATE LOAD DATA -- POSSIBLE IMPROVEMENTS	III-25
	5.1 DATA USUALLY LACKING FOR DETERMINATION OF LOADS	III-25
	5.2 WHAT CAN BE DONE TO GET BETTER DATA EARLY IN DESIGN	III-25
	5.3 THINGS THAT CAN INCREASE LOADS	III-25
	5.4 POSSIBLE IMPROVEMENTS TO BETTER DEFINE DESIGN LOADS	III-26

LIST OF FIGURES

<u>Figure</u>		<u>Page</u>
2-1	Discipline Involvement	III-9
3-1	Improved LH ₂ Tank Loading (N_x) with Constant Pressure	III-16
3-2	Effects of Combined Dynamic Pressure and Axial Load Factor	III-17
3-3	Optimum Weight of Tank Panels	III-18

LIST OF TABLES

<u>Table</u>		<u>Page</u>
2-1	Contribution of Each Discipline to Vehicle Net Design Loads	III-10
3-1	Related Load Parameters and Design Conditions	III-14
4-1	Variability of Load Parameters	III-22
4-2	Percentage Variation on Total System Weight	III-23
5-1	Possible Improvements to Better Define Design Loads	III-27

SUMMARY

This part documents the work performed under Phase III of the study. The objective of this phase was to establish loading parameter variability as a function of program schedule from concept definition to final design. This must be done to highlight those areas where additional testing or advanced analysis should be performed before embarking on configuration feasibility studies. The typical aerospace vehicle design involves many design disciplines and multiple interaction on decisions wherein one specialist is constrained by the requirements of others.

For the Convair Space Shuttle Phase B study, four different sets of booster design load changes were made. However, most of the structure remained critical for the same design conditions throughout this design period; consequently, there were no radical configuration changes. A high percentage of the total B-9U booster vehicle weight is in the fuselage; therefore, load variations that primarily affect the fuselage provide the most variation in system performance. The biggest impact on the total design structural weight of the booster is related with the thrust characteristics.

Vehicle configuration is chiefly dictated by mission requirements, along with engine choice, aerodynamic and performance requirements. The largest number of unknown quantities and general lack of data at this point lie within the aerodynamic field. For this concept of the space shuttle booster, wind criteria (probabilistic levels) and other probabilistic design criteria are sufficiently specified that further technology studies are not warranted. However, aerodynamic characteristics must be established early in the design because they will have a significant impact on structure design and weight.

Preliminary design of aerospace structures requires evaluation of a large number of design alternatives to arrive at the best configuration. It is less concerned with the definition of one specific configuration than the best of the design possibilities for a new system. Automation of as much as possible of the design process can shorten the design time and allow more comprehensive analysis to be made in the total design process.

SECTION 1
INTRODUCTION

Structural criteria for the space shuttle vehicle are beset by a number of important problems. This situation arises partly because of the many new environments and combinations of environments that the shuttle mission introduces and partly because of the extreme sensitivity of shuttle payload capability to inert weight. Mainly the problem centers around the question of adequate definition of design loads early in the design evolution. Without good design loads the feasibility evaluation of a space shuttle concept may lead to a conclusion that at a later day, when design loads are adequately defined, may be reversed. Whereas simple criteria concepts and arbitrary factors were sufficient for simple vehicles, it has become more and more necessary to consider the nature of most of the important design conditions for these complex, high-performance vehicles.

The objective of this phase of the study is to establish loading parameter variability and probability as a function of program schedule from concept definition to final design. This work is done to highlight those areas where additional testing or advanced analysis should be performed before embarking on configuration feasibility studies. Included in the tracing of design load conditions are such important parameters as trajectory definition, guidance and control subsystem definition, natural environment, thermal prediction, landing characteristics, establishment of aerodynamic characteristics, and establishment of structural dynamic characteristics and mission requirements and profiles.

SECTION 2

DISCIPLINE INVOLVEMENT IN DESIGN DEFINITION

2.1 RESPONSIBILITIES OF VARIOUS DISCIPLINES

The design of a new aerospace vehicle is presently a complex, long-term process. At the onset, a set of objectives is identified in such areas as weight, performance, payload, and range, which is specified with a fairly good knowledge of the available design technology and constraints. Vehicle configuration is chiefly dictated by mission requirements, engine choice, aerodynamic and performance requirements, and system packaging. The configuration designer integrates these and other design requirements into a three-view drawing of the vehicle, which is then analyzed by the various disciplines. Each of the disciplines has an influence on the design loads.

The extent and thoroughness of aerodynamic analysis in aerospace vehicle design depends on the stage of design. At the conceptual stage, the analysis is simple because of insufficient design definition, wind tunnel test, and usually tight schedules. Later, data such as geometry can be obtained, and a more extensive analysis is undertaken. As the design evolves, a compilation of empirical and statistical data can be analyzed and better aerodynamic data can be provided. When wind tunnel data becomes available, it is incorporated into the aerodynamics analysis, changing the analytical approach. Similar changes occur when flight test data becomes available.

The structural dynamic function in an aerospace vehicle design task consists of determining limit and fatigue loads due to maneuvers, gusts, landing, taxi, and other transient loading conditions, and of establishing stiffness requirements to preclude aeroelastic instabilities and to ensure control surface effectiveness. In the initial design analysis, the vehicle is assumed to be rigid. Maneuver, gust, and landing loads are computed for preliminary sizing of the structure. From the preliminary sizing of the structural members, stiffness and mass distributions are obtained for aeroelastic and structural dynamic analysis. Based on these results, stiffnesses are increased where required and the entire analysis is repeated to obtain a new set of loads. This model is also used to determine fatigue load spectra.

In the preliminary design stage of a new vehicle, the weights engineer concentrates his efforts on weight and mass properties estimation and weight control. Throughout the design development period property data is provided to other engineering groups — to the vibrations group for analysis of flutter and dynamic problems, to the basic loads and strength groups for calculation of structural loads and stress, and to the aerodynamics group for calculation of performance and control characteristics. In addition, component weights, material identification, and identification of dissimilar parts and pieces are furnished to the cost estimating department.

The structures group is primarily responsible for the structural integrity of a designed system or vehicle. Safety commensurate with light weight are the paramount structural design requirements. These requirements are also intended to ensure adequate strength, rigidity, and service life for the system in performing its mission. Before any part of the structure can be sized according to strength or rigidity, the true external loads on the vehicle must be determined. The environment in which the structure will operate (load, temperature, corrosion, sonic fatigue, etc.,) must be established and materials selected to satisfy weight, damage tolerance, and strength requirements. After the structure is defined, its rigidity can be used to investigate dynamic effects.

2.2 RELATIVE INVOLVEMENT OF DISCIPLINES

The typical aerospace vehicle design involves many design disciplines and multiple interactions on decisions wherein one specialist is constrained by others' requirements. Until such a time arrives when the total design process is fully automated, these constraints will remain with us.

Relative involvement of the various disciplines might be as shown in Figure 2-1. As indicated, some disciplines are heavily involved in the early stages of design and not at all in the later phases.

The first problem confronting the designer of the structural parts of a designed system or vehicle is that of determining just what loads are to be expected on his structure and how these loads are distributed. Critical loads come from many sources, from aerodynamic forces, propulsion, inertia, control systems, launching, gusts, thermal, recovery, landing, etc.

2.3 CONTRIBUTION OF EACH DISCIPLINE

During the Convair Space Shuttle Phase B study, four different sets of booster design load changes were made. However, most of the structures remained critical for the same design conditions throughout this design period; consequently, there were no radical configuration changes.

The wing remained equally critical for the αq maximum headwind and 4g maximum recovery conditions. Fuselage skins and domes continued to be designed by the proof tank pressures with the skin reinforcement remaining critical for the liftoff with ground winds and 3g maximum thrust conditions. There was a change in the canard design condition — it changed on the last load cycle. Originally the canard was designed by the 4g maximum recovery condition but this condition was replaced by the 2.5g subsonic maneuver; however, the loads stayed at much the same level. The vertical tail also saw some change in loads. It began with the βq maximum condition overriding all other conditions, then settled down with the subsonic gust condition having a side load equal to the βq maximum condition.

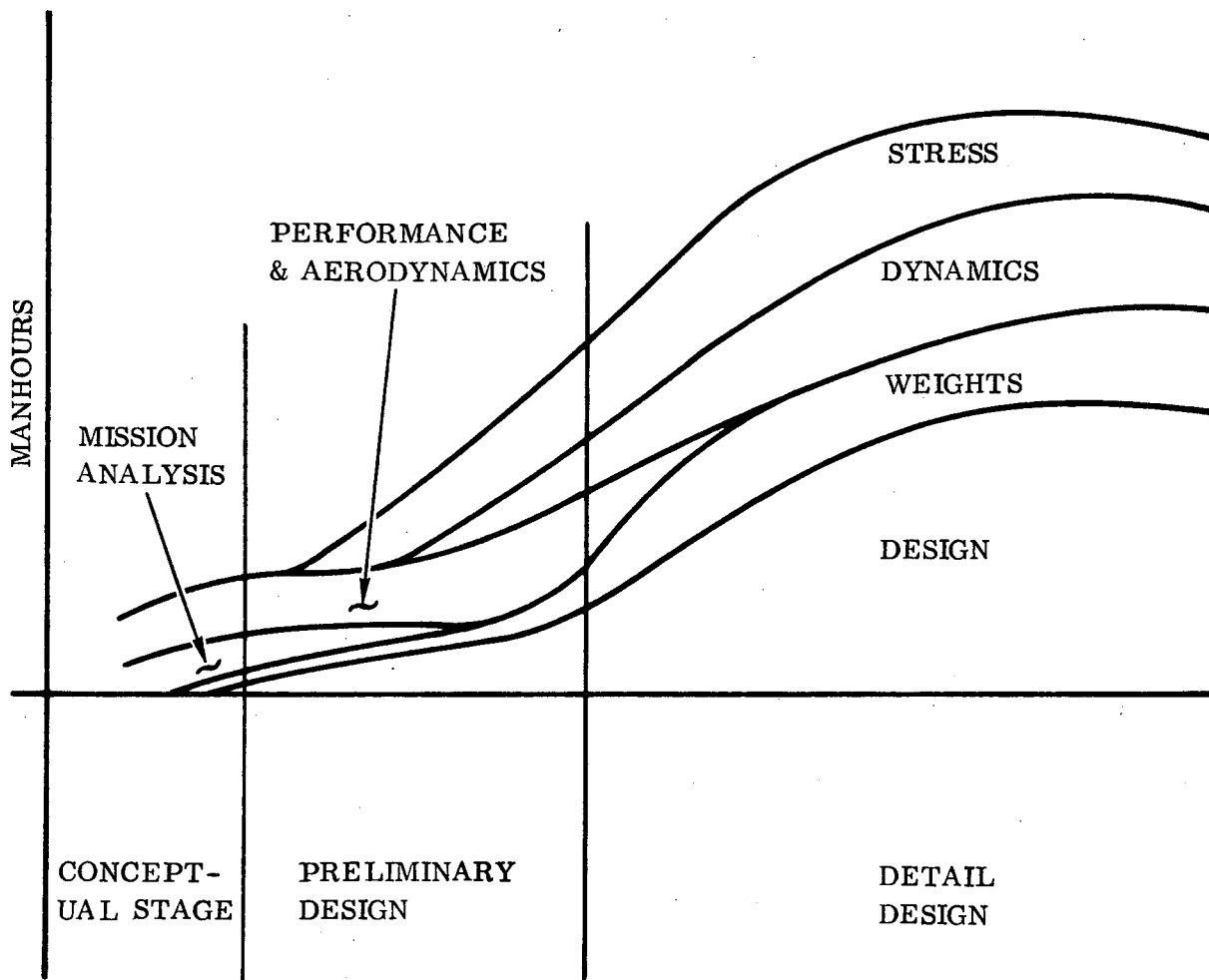


Figure 2-1. Discipline Involvement

These were the major load changes, and, of course, there were numerous minor changes within the Phase B study. Each time the loads changed the various disciplines were affected to some degree and with each other. Contributions of each discipline to the vehicle net loads are outlined in Table 2-1.

Table 2-1 points out that to keep within a rigid time schedule, unless the design process is fully automated the design group suffers by having to wait for all the interdependent disciplines to present them with loads. Very often one cycle is not fully completed before another is started, leading to a disjointed rather than a step-by-step thought process, and does not give a true picture of the direction each different idea suggests. Thus the baseline design should be frozen as early as possible to allow greater detail of the design to materialize and for more time to be spent on the accuracy of the design loads. With the advent of a fully automated design process such as IPAD (Integrated Program for Aerospace-Vehicle Design), the turnaround time for optimum design studies will be greatly improved and these problems will disappear.

Table 2-1. Contribution of Each Discipline to Vehicle Net Design Loads

Discipline	Input to Load Determination	Problems	Group Needs From Other Groups
Pre-design	Vehicle configuration, trajectory information, basic geometry	Baselines are never frozen	Previous vehicle data
Aerodynamics	Distributed load coefficients for each vehicle	Data base does not exist for new configurations; therefore, wind tunnel tests are required. Need long lead time	Mach numbers and other trajectory data from Dynamics
Dynamics	α , β , q at various critical conditions, wind distributions, aeroelastic loads and dynamic amplification factors	Detailed structural description is usually lacking	Overall aero coefficient data from Aerodynamics. Mass properties
Mass Properties	Distributed mass properties for each vehicle	Structural detail is lacking. New structural concepts are beyond empirical data	Vehicle geometric description from Pre-design. Preliminary tank sizes
Thermodynamics	Temperature histories for each mission profile	Require complex solutions that are extremely vehicle dependent. No data base guide. Need long lead time	Aero data. Trajectory from Dynamics. Geometry from Pre-design
Design Group	Definition of basic structure for determination of load paths	Need a frozen baseline	Loads

Of the design load conditions found to be critical for the B-9U vehicle, half were considered to be deterministic and half probabilistic. The wing is critical for maximum αq , which is probabilistic, and a limited 4g recovery, which is deterministic. Fuselage tank pressures, skin reinforcement, and 3g maximum thrust are deterministic, and liftoff and ground winds are probabilistic. The canard is designed by a subsonic maneuver condition, which is deterministic, and the vertical tail by maximum βq and subsonic gust conditions, which are probabilistic.

SECTION 3

CRITICALITY OF LOAD PARAMETERS AND LOADING PROBABILITY AND VARIABILITY

The summary table presented in the Phase I report (page xii) indicates the order of design load criticality for the Convair Aerospace/North American, Phase B, B-9U delta-wing space shuttle booster. This order is dependent to a large extent on the particular design configuration: whether the structure is "hot" or is protected from the thermal environment in some manner, how the orbiting vehicle is mated to the booster vehicle (tandem or piggyback), synchronous or nonsynchronous burns of the booster and orbiter engines, pressure fed or pump systems, etc. Any change in the baseline configuration can drastically change the critical loads order.

A high percentage of the total B-9U booster vehicle weight is in the fuselage; therefore, load variations that primarily affect the fuselage provide the most variation in system performance. Table 3-1 lists the critical load conditions in order of rank and indicates whether the loads are deterministic or probabilistic. Each of the critical conditions is made up from various load parameters; these effects are noted in the table.

3.1 MAXIMUM THRUST CONDITION

Mass distribution and relative cg locations of the booster and orbiter are very important for this condition. Placing the orbiter in tandem with the booster reduces offset bending moments on the booster fuselage. The B-9U has the LO₂ tank forward of the LH₂ tank, thus imposing heavy axial forces on the aft fuselage from the higher density LO₂ fuel. However, the gain in structural design by interchanging the tanks could cause an instability in the flight of the vehicle due to the shortening of the couple arm between the vehicle cg and the control mechanisms, be they elevons or engine gimbaling.

Aerodynamic forces have little effect on load sensitivity since at this point in the flight the vehicle is almost out of the atmosphere.

The B-9U vehicle is constrained to a maximum axial boost of 3g by throttling the engines, and for this particular configuration it is close to the optimum value when related to structural weight. Any change in configuration or mission constraints such as payload, boost, or trajectory could present a different optimum.

Engines are gimbaled, allowing the thrust to be vectored, so that the booster may be controlled during the ascent flight portion of the mission. If the gimbal angle is limited below that required to keep the vehicle on course, the vehicle will drift, loads will increase, performance is affected, and the system weight increases.

Table 3-1. Related Load Parameters and Design Conditions

Load Rank	Load Condition	Load Parameters												
		1	2	3	4	5	6	7	8	9				
	Maximum Thrust	X												
	Ascent: Head-Wind		X											
	Pressurization			X										
	Entry: Maximum g			X										
	Launch: Pad Winds					X								
	Ascent: Side Winds					X								
	Ascent: Tailwinds					X								
	Rudder Kick											X		
	Maximum Temperature												X	
	Mass Properties	X	X		X	X	X	X	X	X	X	X	X	X
	Aerodynamic Characteristics	X	X		X	X	X	X	X	X	X	X	X	X
	Guidance System Definition		X		X				X	X	X			X
	Control System Definition		X		X				X	X	X			X
	Thrust Characteristics	X	X		X		X		X	X	X			
	Abort Capabilities	X	X							X	X			
	Heating Constraints				X									X
	Mission Constraints	X	X		X	X				X	X			X
	Wind Statistics		X					X		X	X			
	Pilot Capability												X	
	Structural Dynamic Properties	X	X					X		X	X			
	Slosh		X							X	X			
	Acoustic							X						
	Tank Pressures at Given Condition	X	X		X					X	X			
	Probabilistic Loads		X					X		X	X			
	Deterministic Loads	X			X	X						X	X	

To allow for unknown dynamic loading a dynamic amplification factor of 1.1 has been applied to the thrust. This factor allows for transient effects caused by throttling and shutoff at maximum allowable thrust and at booster burnout. As the vehicle becomes better defined, the 10% factor will be replaced by true dynamic loads. With an automated design procedure this factor may be eliminated and the true dynamic effects found within the program iteration cycle.

Tank skin gages are designed by pressure, and the skin is stiffened by frames and stringers, to carry bending and axial loads. Loads on the stringers are the net of longitudinal tension from pressure and compression, in the main, from axial acceleration forces. Figure 3-1 shows that by controlling the tank pressure to the design value and holding it constant may reduce the tank weight by improving the compression stability. However, this weight saving has to be balanced against the weight of the pressure control mechanism.

3.2 ASCENT HEADWIND

Mass distribution and relative cg locations are almost as important for the ascent headwind condition as they are for the maximum thrust condition. Maximum αq occurs at approximately 90 seconds into the ascent, and at this point the axial load factor has built up to about 2g.

The most important load parameter for this condition rests with the aerodynamic characteristics. Any change in the aerodynamic data can vastly change the system weights. Hiding the wings (switchblade) on the ascent portion of the trajectory could relieve aerodynamic load effects and possibly save weight. Optimizing the guidance system to minimize αq loads will relieve loads on the system. The more control from aerodynamic surfaces means less thrust offset effect and generally a lighter structure. Abort is most dangerous when the vehicle is passing through the maximum dynamic pressure range. Separation of booster and orbiter is difficult; there should be no abrupt change in g-level, and fuel must be burnt off before recovery. Load effects will vary according to the type of failure, be it structural, pumps, engine, guidance, etc.

Mission constraints can vary the attitude of the vehicle relative to the winds and can be important in αq , βq type loads. Severe constraints may lead to large thrust gimbal angles and correspondingly large loads on the aft fuselage structure. Likewise, the wing could bear heavy loads should the control be by elevon or similar type aerodynamic control surface. Obviously for this condition, ascent headwind, it is all-important to obtain the best definition of wind statistics possible. These are probabilistic loads and, of the numerous methods existing for determining ascent loads, a good approach to the problem is given in NASA contract NAS 1-6024, Determination of Methods for Establishing Space Shuttle Load Spectra.

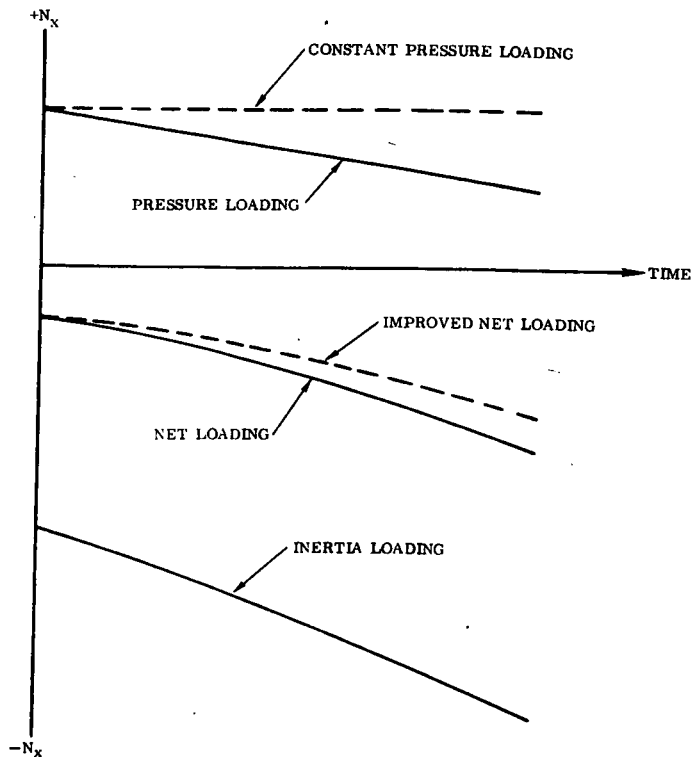


Figure 3-1. Improved LH₂ Tank Loading (N_x) with Constant Pressure

During the Phase B design study of the booster for the space shuttle, a dynamic load factor of 1.2 was applied to the wind loads to cover unknowns:

- a. Statistical variation in wind loads.
- b. Vehicle dynamic response.

Early information, lowering this factor, gives obvious benefits.

Reduction in lateral inertia loads will relieve slosh loads — this effect being most prominent in this condition. These effects are more severe in the LO₂ tank — the LH₂ having a much lower density.

Where portions of the body may be designed by a combination of loads from maximum αq , axial load factor, and tank pressure, some relief can be obtained by judicious scheduling of the thrust/weight profile. Figure 3-2 shows how this might be achieved. Points a and b are basic design parameters, and b' is an alternate axial load factor coincident with maximum dynamic pressure. This lowering of the axial load factor reduces the inertia loads and the tank pressures from dynamic head, thus saving weight.

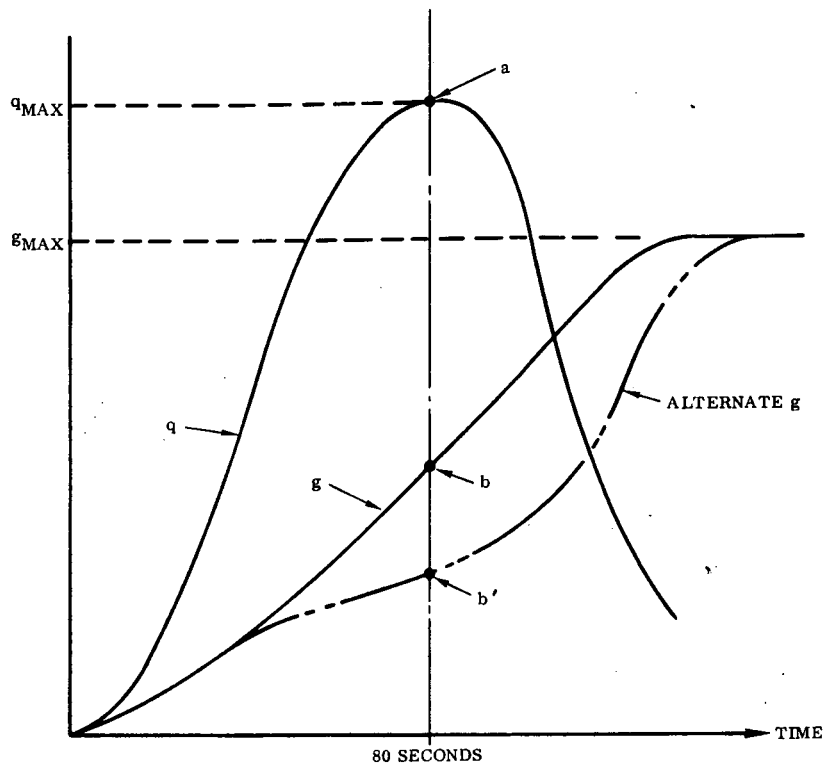


Figure 3-2. Effects of Combined Dynamic Pressure and Axial Load Factor

What has been said for the ascent headwind condition is also true for the similar conditions:

- a. Ascent side winds.
- b. Ascent tailwinds.

3.3 PRESSURIZATION

The B-9U booster fuselage is 67% of the prime structural weight, and the propellant tanks form a large portion of the fuselage weight. Skin gages are determined mainly by the propellant tank pressures, but in some instances they are more critical for panel stability. Figure 3-3 shows several curves of allowable load index for various combinations of effective thickness (t) and skin thickness (t_{skin}). Considering the curve for $N_x = 6000\text{-lb/in}$, it can be seen that where the panel is critical for stability, rather than hoop tension, at a skin gage less than that giving the minimum effective thickness some advantage can be gained by using a higher skin thickness.

As the tanks are mainly designed by pressure it seems reasonable to hold the ullage pressure to a workable minimum. On viewing Figures 7-8 and 7-9 in the Phase I report, first impressions are that the design pressure at the lower dome can be reduced by

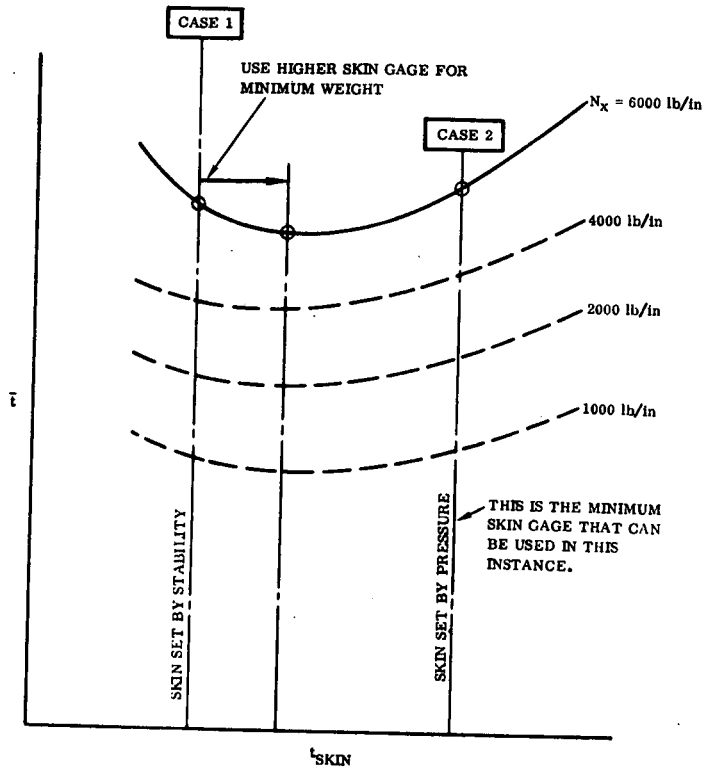


Figure 3-3. Optimum Weight of Tank Panels

adjusting the ullage pressure during the ascent portion of flight. However, the following reasoning shows how the minimum ullage pressure for the LO₂ tank has been set for the B-9U vehicle and proves that for this particular design the design pressures cannot be lowered.

Determination of an optimum LO₂ tank ullage pressure is dependent on both structural and thermodynamic considerations.

To satisfy the needs of the high-speed turbopumps used on high-performance rocket engines, the propellant at the pump inlet must be subcooled to avoid cavitation or liquid vaporization in the pump. The amount of subcooling required is specified by the net positive suction head (NPSH) requirement for the pump, which is a minimum differential that must exist between the local static pressure and the local liquid vapor pressure. An NPSH value of 8 psi is typical. The LO₂ tank is normally filled at slightly above atmospheric pressure (15 psia) and is mass boiling. Pressurization is required to suppress the boiling and provide some subcooling; a minimum is normally 2 psig. With tolerances on valve operation of ± 1 psi, the operating pressure set by the regulator valve becomes 17 ± 1 psia with a relief valve setting of 19 ± 1 psia. NPSH requirements are satisfied by the static head of LO₂, especially when the tank is located forward. A static head value for LO₂ is approximately 0.5 psi per foot per g of acceleration. When

this is not the case, the ullage pressure must be raised to satisfy the NPSH requirement. At high altitudes and in space, the atmospheric pressure approaches zero, which means the tank pressure becomes 20 psig. The ullage pressure cannot be dropped because it is as close as practical to the LO_2 vapor pressure. A 20 psia ullage pressure, therefore, represents a minimum value for pressurization.

3.4 MAXIMUM g ENTRY

Since loads are proportional to weight for a given g-level, it is important to know minimum and maximum weights and weight distributions for this condition. It is especially important for the wing, which is the main lifting surface of the vehicle, and it is the critical design condition for the B-9U booster wing. The optimum entry trajectory should produce temperatures and loads that combine to give the lightest structure. Lowering the normal acceleration will relieve the related balanced loads — thus saving vehicle structural weight, but these may be offset by increased temperature effects and increased flyback fuel.

Other than the optimum structural weight criteria or mission constraints, some thought has to be given to the human factor and to what is reasonable for the human frame to withstand.

3.5 LAUNCH

Like the maximum thrust condition, relative cg locations of the booster and orbiter are of great import during launch. These are extremely configuration oriented and can have a large effect on the vehicle bending moments. Much of what has been said of the maximum thrust condition is also true at the time of launch. In addition, transient loads caused by vortex shedding are highly configuration dependent and must be determined, under the present state-of-the-art, by extensive wind tunnel testing of accurate aeroelastic models. At this stage in the flight profile, it is best to have the aerodynamic surfaces as small as possible.

A 0.2g increase has been applied to the thrust/weight ratio of the complete system at liftoff to account for unknown dynamic forces. These are primarily axial effects coming from release at launch and from transient engine thrust (so-called POGO effect). Improved and faster modal response analysis will help reduce this weight penalty early in the design process. Yet another phase involving structural dynamics is the effect of space-shuttle-to-tower attachment. Tradeoff studies were made shifting the attachment location to minimize the dynamic response effects.

Acoustic damage is most prominent at launch and decreases with altitude as the air density decreases. Engine noise is the principal source of the problem — coupled with related effects from the ground support structure. On the B-9U booster the aft 600 inches of fuselage and part of the wing structure are critical for sonic fatigue. Judicious placement of the launch tower and ground support structure or ways of reflecting the noise away from the vehicle can relieve acoustic effects as can reduction in noise level and exposure time.

3.6 MAXIMUM TEMPERATURE

Maximum temperature occurs during reentry, and the booster reaches peak temperatures at approximately 420 seconds within the flight, some 100 seconds after passing through the maximum normal acceleration of the vehicle. This condition has similar load parameters to the maximum-g entry condition, as is shown in Table 3-1. The difference is in the intensity of load factor and temperature. Table 3-1 also shows the maximum temperature condition to have a low criticality ranking. This is dependent upon the B-9U design philosophy to minimize differential thermal expansions and thereby minimize thermal stresses. To achieve this a thermal protective system (TPS) is used where temperatures are excessive. Other devices include extensive segmentation of secondary structure, corrugated skins, compatibility of materials and gages of outside skins and substructures, etc. Although heating rates in the B-9U are substantial, the recovery flight path generates only a modest total heat load because the time at peak heating is relatively low.

3.7 OTHER CONDITIONS

Other conditions not mentioned in Table 3-1 had little effect on the B-9U design. These conditions include servicing, towing, staging, subsonic gust, maneuver, landing, and taxi.

SECTION 4

VARIABILITY OF LOAD PARAMETERS WITH PROGRAM SCHEDULE

Table 4-1 lists the percentage load variation within the design cycle and the percentage variation on the total system weight, for various load parameters. To arrive at the percentage of total weight, reference is made to earlier phase reports: to the partials given in Phase II and the structural weight breakdown in Phase I. These are used in the construction of Table 4-2 for independent components and then combined for the total vehicle in Table 4-1.

The biggest impact on the total design weight of the B-9U booster is related with the thrust characteristics. Both variation of the I_{sp} and the fuel/oxidizer flow rate cause relatively large changes to αq , which in turn create large weight changes. Variabilities of the gross liftoff weight (GLOW) due to changes in mission or payload will also affect the thrust characteristics.

Closely following the thrust criteria, in relative importance for advanced knowledge, are the structural dynamic properties. Until such time that the member sizes, stiffness, and mass distribution are determined, the initial design assumes the vehicle to be rigid, and to allow for dynamic loading dynamic load amplification factors are used. These factors can lead to extreme variation in structural weight; in the case of the B-9U booster they amount to six-tenths of one percent of the total system weight. With a system weighing five million pounds we are dealing with a fluctuation of 30,000 pounds, which is the equivalent of a 10% change in structural weight.

Good definitions of mass properties, guidance system, and acoustic damage are important in the early design phase. These parameters can amount to two-tenths of one percent of total system weight. They are dependent on the interrelation of booster and orbiter centroidal mass locations, relative position of LO_2 and LH_2 tanks, engine noise, etc. From the mass property standpoint, vehicle configuration is all-important. Lining up the system in a symmetrical fashion, in tandem or symmetrical cluster, will relieve offset bending moments on the vehicles. Limiting the mission to give the lowest GLOW will relieve the acoustic damage. Resolving a mission guidance system, so that the weight sensitivities to loads and probabilities for critical conditions are obtained early in the program schedule, will shorten the program schedule.

Other load parameters, affecting the design versus schedule time, of less significance are also shown in Table 4-1. These include:

- a. Heating constraints, which are extremely configuration oriented, depend largely on mission constraints and trajectory parameters.

Table 4-1. Variability of Load Parameters

Load Parameters	Percent Load Variation Within Design Cycle	Percent Variation on Total System Weight	Reasons for Variations
Mass Properties	3	0.228	Relative location of orbiter and booster cg's. Interchange of LO ₂ and LH ₂ tanks. Orbiter attach location
Aerodynamic Characteristics	20	0.065	No initial data base. Dependent on configuration.
Guidance System Definition	10	0.251	Pitch programmer variations
Control System Definition	10	0.042	Pitch rate variations
Thrust Characteristics	15	0.627	I _{sp} off nominal
		0.432	Flow rate off nominal
Abort Capabilities	—	—	Not design critical
Heating Constraints	20	0.100	Variation of entry trajectory
Mission Constraints	50	0.100	Human factors
Wind Statistics	10	0.181	Configuration oriented
Pilot Capability	2	Neg.	
Structural Dynamic Properties	10	0.595	Lack of member sizes, stiffness, and mass distributions
Slosh	30	Neg.	
Acoustic	30	0.210	Changes to engine noise and analysis of acoustic loads
Tank Pressures	5	0.045	Changes to maximum thrust limitation

Table 4-2. Percentage Variation on Total System Weight

1	2	3	4	5	6
Component	Load Parameter	Percent Variation Table 4-1	$\frac{\partial w}{\partial ()}$ lb/% Var'n. Phase II	$\frac{\partial w}{\partial ()}$ lb ③ × ④	Percent Variation on Total System Weight*
Wing	I _{sp}	15	1,860	27,900	0.5528
	Fuel Flow	15	1,240	18,600	0.3685
	Wind	10	744	7,440	0.1474
	Aero	20	127	2,540	0.0503
	Gains	10	186	1,860	0.0369
	Pitch Prog.	10	1,240	12,400	0.2457
	Entry g	3	295	885	0.0175
	Gust	20	212	4,240	0.0840
	Struct. Wt.	3	1,240	3,720	0.0737
	Heating	20	97	1,940	0.0384
Fuselage	Burnout	15	215	3,220	0.0638
	Tailwind	10	21	210	0.0042
	Headwind	10	28	280	0.0055
	Side Wind	10	12	120	0.0024
Vertical Stabilizer	Side Wind	10	42	420	0.0083
	Gust	10	25	250	0.0050
	Rudder Kick	2	22	220	0.0044

*Total System Weight = Booster + Orbiter
 = 4.188 + 0.859 = 5.047 M-lb

- b. Wind statistics are also greatly dependent on the configuration.
- c. Although pressures design the tank skins, they are not too important from a load variability standpoint.
- d. Control systems and aerodynamic characteristics are relatively important.

It is also interesting to see that pilot capability (flight maneuvers, landing), slosh, and abort parameters have negligible effect on the definition of design loads in the design evolution.

SECTION 5

INADEQUATE LOAD DATA — POSSIBLE IMPROVEMENTS

5.1 DATA USUALLY LACKING FOR DETERMINATION OF LOADS

At the onset, after a set of objectives is identified in the areas of weight, performance, payload, range, etc., mission analysis studies are performed. Vehicle configuration is chiefly dictated by mission requirements, along with engine choice, aerodynamic and performance requirements. A large number of unknown quantities and general lack of data at this point lie within the aerodynamic field.

Aerodynamic analysis can be broadly divided into three categories: 1) drag analysis, 2) lift analysis, and 3) stability and control analysis. To achieve good load data normally entails wind tunnel testing and this is especially true where the design is somewhat out of the ordinary. The piggyback configuration of the space shuttle vehicle, with the interaction of the two bodies, is a rather unconventional vehicle, and therefore leaves us lacking when it comes to the determination of loads.

Very often the structural description is not good enough to obtain accurate mass properties. Mass property distributions along with structural stiffnesses are normally not gained in sufficient time to avoid the use of dynamic load factors, which are sometimes an unnecessary weight penalty. In addition, lack of payload definition, determination of wind statistics, and thermal dynamic parameters can be the cause of inadequate load data.

5.2 WHAT CAN BE DONE TO GET BETTER DATA EARLY IN DESIGN

As indicated in Table 2-1 some of the things that can lead to better loads data early in design are:

- a. Freeze the baseline design early in the program.
- b. Obtain wind tunnel tests as soon as possible.
- c. Give an adequate detailed structural description.
- d. Fully automated design.

5.3 THINGS THAT CAN INCREASE LOADS

A few things that can increase loads are:

- a. Change in mission requirements (performance, payload, range, etc.).

- b. Increased thrust or thrust vector.
- c. Engines not constrained by throttling.
- d. Maximum entry load factor.
- e. Aerodynamic characteristics.
- f. Maximum αq .
- g. Center-of-gravity locations and mass properties.
- h. Rigidity of the vehicle.
- i. Control limitations.
- j. Launch site.

5.4 POSSIBLE IMPROVEMENTS TO BETTER DEFINE DESIGN LOADS

Table 5-1 outlines some of the improvements that may be made to better define design loads. The table is self explanatory. Also, Table 2-1 indicates that in a noncomputerized environment the detailed design variables are manipulated in groups involving several disciplines. Automation makes it possible to speed up this process, and it appears that the best way to better define design loads, or design as a whole, is to work towards a fully automated system.

Table 5-1. Possible Improvements to Better Define Design Loads

<p style="text-align: center;">AERODYNAMICS</p> <p>Wind tunnel tests. Analytical prediction improvements</p>	<p style="text-align: center;">PROPULSION</p> <p>Need best information on the mission. Well-defined interfaces with other disciplines. Engine performance</p>
<p style="text-align: center;">STRUCTURES</p> <p>Improved automated design procedures. Improved weight and inertia predictions</p>	<p style="text-align: center;">MASS PROPERTIES</p> <p>Improve weight prediction methods. Early property data to dynamics group</p>
<p style="text-align: center;">MISSION ANALYSIS</p> <p>Overall requirements. Pilot capabilities</p>	<p style="text-align: center;">TRAJECTORY ANALYSIS</p> <p>Improved methods for incorporating abort. Improved guidance definition</p>
<p style="text-align: center;">CONTROL DYNAMICS</p> <p>Reponse to winds analysis. Failure analysis. Design with both static and dynamic criteria in view, in first stages of design</p>	<p style="text-align: center;">STRUCTURAL DYNAMICS</p> <p>Faster modal analysis. Improved modal response analysis</p>
<p style="text-align: center;">ENVIRONMENT</p> <p>Acoustic. Wind criteria, Water impact loads. Corrosion. Temperature</p>	<p style="text-align: center;">THERMODYNAMICS</p> <p>Early radiation equilibrium temperatures for trajectory optimization and TPS</p>

PART IV

METHODS FOR DETERMINING STATISTICS OF
TOTAL LOAD EXCEEDANCES

IV-1

TABLE OF CONTENTS

Section		Page
1	INTRODUCTION	IV-5
2	DESIGN PHILOSOPHY	IV-7
3	PROBABILITY OF SURVIVAL	IV-9
	3.1 FIRST EXCURSION FAILURE	IV-9
	3.2 FATIGUE FAILURE	IV-10
	3.3 RELIABILITY TECHNIQUES	IV-13
4	LOAD LEVEL EXCEEDANCES FOR COMBINED LOADING	IV-19
5	APPLICATION TO SIGNIFICANT SPACE SHUTTLE LOADING SITUATIONS	IV-23
6	CONCLUSIONS AND RECOMMENDATIONS FOR FURTHER STUDY	IV-27
7	REFERENCES	IV-29
Appendix		
A	BASIC STATISTICAL CONCEPTS	IV-31

SUMMARY

This part documents the work performed under Phase IV of the study. Beginning with a discussion of design philosophy, methods for determining statistics of total load exceedances are presented. These methods are applicable to realistic combined load conditions anticipated for the space shuttle. The methods presented are based on conventional reliability concepts. Both first passage and fatigue modes of failure are considered in the failure definitions used in the analyses. It is shown that estimates of the probability of failure may be obtained through the use of ensemble averages of response threshold crossing rates. Means of determining threshold crossing rate averages for combined loading situations are presented.

SECTION 1

INTRODUCTION

This part presents the fourth and final phase of the Combined Loading Criteria Influence on Structural Performance study, and is devoted to the consideration of design criteria concepts, particularly those concepts related to the establishment of load exceedance statistics. The results of the first three phases of this study include the determination of significant loading parameters for the shuttle vehicles and the relative effects on structural performance (weight) of these individual significant parameters. Herein consideration will be given to how load parameters should be combined, in an analysis, to realistically represent the total loads anticipated for the shuttle vehicles. For these combined load situations, we further demonstrate methods of computing statistics of load level exceedance so that realistic factors of safety can be determined.

The final goal, that of establishing realistic design criteria with associated probabilities of exceedance or confidence levels, is inherently related to basic design philosophies. That is, prior to establishing space shuttle design criteria for combined loading situations a review of fundamental concepts concerning structural design is in order. Therefore, the first two sections present general design concepts and basic statistical concepts. The final sections show how available techniques may be applied to practical space shuttle load situations.

SECTION 2

DESIGN PHILOSOPHY

Associated with any structural design problem is a set of design objectives. These objectives may only indirectly influence the design process, but taken in their entirety they constitute the design constraints and establish the ground rules for the design criteria. For a flight vehicle system, structural safety and low structural weight are two of the more prominent design objectives -- these two objectives have been chosen for consideration in this study.

Other design objectives are also of concern for the space shuttle. Cost, manufacturability, and maintainability (for the reusable shuttle structure) are but three of the numerous important design objectives which are discussed in Reference 1. However, in general, structural reliability and weight are especially interrelated requiring their simultaneous investigation. Consider, for example, the simple axial-load carrying structural element. While a variation in overall geometry (i. e. change in length or cross sectional area) for such a member might have little effect on, say, its manufacturability, the same variation could easily produce significant changes in both the element's weight and its strength. While the simplicity of this example is perhaps exaggerated the described interrelation between weight and strength is commonly found in highly sophisticated structural systems. Thus, we are currently interested in determining estimates of space shuttle structural reliability considering a special set of load parameters, this set of parameters having been selected due to the pronounced affect on system weight caused by its constituents.

Aside from design objectives, the primary topic requiring discussion in this Design Philosophy section is the "mode of failure". We generally think of material fracture as being the only mode of failure; however, an excessively large deformation, a tank leakage, an excessive wear caused by severe environment or load, or any other mechanical situation or malfunction that prevents the system from performing its design requirements constitutes a failure.

The following considers the failure modes of primary load carrying structural members. Much of the discussion presented is based on the excellent survey on design philosophy and failure criteria given in Reference 2.

In initiating the design of a complex structural system, first considerations (preliminary design) are generally given to basic static strength requirements of the structure. The purchasing agency, if one is involved, often specifies that a certain load (limit) shall not cause appreciable permanent deformation and that the maximum anticipated load (or ultimate load) shall not cause static failure of the structure. Analytical techniques, some of which are semi-empirical, have been sufficiently well developed that

adequate static strength design can usually be accomplished with near-zero margins of safety. For highly redundant configurations made of the more ductile materials typically used for conventional aircraft structure, slight errors in static load analyses usually lead to no serious problems because in these cases the stresses tend to redistribute themselves. Furthermore, in addition to a sophisticated static analysis, some type of strength test is often performed to ensure adequate design. Unfortunately, for a structural system that is expected to see repeated usage, static analysis and static testing are not sufficient to guarantee structural safety, since flaw-growth and fatigue failure potential may not be detected. Indeed, it is generally agreed that adequate design for safety must include considerations of fracture due to either a single severe load (first excursion failure) or due to crack propagation induced by repeated loading.

For the space shuttle vehicles, consideration should be given to both first excursion failure and failure due to repeated loading. It is true that the number of load cycles anticipated for most of the reusable structure is quite low compared with the number of load cycles expected for, say, a military aircraft. However, the space shuttle environment will be significantly more severe than any other previously considered in relation to possible damage aggravation. In particular, the temperature and noise environments would be expected to accelerate flaw growth rates, at least for much of the exterior structure. To be prudent, as we must be in designing a manned flight vehicle, both types of failure are considered in this report.

SECTION 3

PROBABILITY OF SURVIVAL

3.1 FIRST EXCURSION FAILURE

If failure is likely to occur when some response quantity, stress for instance, exceeds a specified level then there is a great deal of practical interest in determining the probability that a given response level not be exceeded. This classic problem is known as the first passage problem and its general solution has been sought for many years. Unfortunately, even for the case of a simple structural system subjected to a stationary random excitation, no exact solution has been given. However, numerous approximate solutions have been suggested — an excellent review of these is given in Reference 3.

Since the determination of the first excursion failure will be essential to later discussions we present some basics concerning the subject at this time. Let us first consider a simple linear system whose motion is governed by the second order equation:

$$\ddot{X}(t) + 2\zeta \omega_0 \dot{X}(t) + \omega_0^2 X(t) = F(t)/m \quad (3-1)$$

where $X(t)$ is the system displacement, ζ is the damping ratio, ω_0 is the undamped natural frequency, m is the system mass, and $F(t)$ is the forcing function. Differentiation with respect to time is indicated by the dot. We wish to find the statistics which describe the event that the magnitude of the response process, $|X(t)|$, exceed the threshold level, X_0 . Let us consider first the probability, P_S , that the maximum value of $|X(t)|$ in a time interval $0 \leq t < T$ not exceed X_0 , that is:

$$P_S = P [|X(t)| < X_0, 0 \leq t < T] \quad (3-2)$$

The probability that $X(t)$ exceed X_0 for the first time during $T \leq t < T + dT$ is equal to $p_F dT$ where (Reference 3):

$$\frac{dP_S}{dT} = -p_F$$

We have already stated that the exact form for the first crossing density, p_F , is generally not available. Results of simulation studies indicate that for small values of T the initial conditions strongly influence p_F ; for large values of T , however, p_F is proportional to an exponential term:

$$p_F = C e^{-dT} \quad (3-3)$$

It has also been found (Reference 3) that for high threshold levels, C approaches unity.

It is clear from examining equation (3-3) that the term d is a crucial one. For the approximate expressions for p_F which have been given in the literature, d has been found to be in some cases very sensitive to the assumptions made. The simplest approximation is determined by assuming that the up crossings of the stationary response occur so rarely that these crossings can be assumed to be independent of one another. The instants, then, at which $|X(t)|$ crosses X_0 from below constitute a Poisson process with average rate $2E[N+(X_0)]$ where $E[N+(X_0)]$ is the average number of threshold crossings of the response above the level X_0 . It is easy to show (see Reference 4) that for this approximation p_F is given by:

$$p_F = d e^{-dT}, \quad d = 2 E [N+(X_0)] \quad (3-4)$$

and we have assumed that X_0 is large enough for C to be very nearly equal to unity. $E[N+(X_0)]$ is of course dependent upon the system parameters, ζ , ω_0 , m and the forcing function $F(t)$ given in equation (3-1).

The assumption of independent crossings has been attacked on the grounds that crossings are more likely to occur in clusters or clumps. Hence, other approximations based on; 1) the assumption of independent envelope crossings, 2) the assumption of independent peaks, and 3) the assumption of independent envelope peaks (to mention a few) have also been suggested. We will not go into further detail concerning this problem, but the reader should be aware that there are numerous approximations for p_F in addition to the simple one given in this report. Figure 6 of Reference 3 and Figure 2 of Reference 5 show that when compared with the other techniques and with simulation results, the approach given herein is conservative.

3.2 FATIGUE FAILURE

The service loads experienced by a structural element may never exceed the design values. From the standpoint of first excursion analyses, then, failure might never occur. Yet it is known that failure can occur in this case through a complex mechanism whose overall result is appropriately called fatigue.

Accurate methods for predicting fatigue life have been sought for some time. Unfortunately, the applications of available techniques to the prediction of fatigue life have not resulted in consistent accuracy. This fact is really not very surprising when one considers that almost unlimited number of significant parameters affecting the fatigue life. Hardrath (Reference 2) has categorized these parameters as follows:

- a. Material characteristics
- b. Effect of environment

- c. Structural configuration
- d. Service loading

For a typical flight vehicle structure, the difficulties that arise in estimating the parameters implied by the above categories are enormous. For instance material properties are, at best, only statistically describable. Further, not only is the environment difficult to predict but fatigue test data are not even available for numerous load-environment conditions that might be anticipated for the space shuttle vehicles. Also, the fastened joints and changes in shape of the structural members introduce an almost uncountable number of potential stress concentrations. Category 4, though, is perhaps the most

TRANSPORT LOAD SPECTRUM, 7075-T6 SHEET, $K_T = 4$

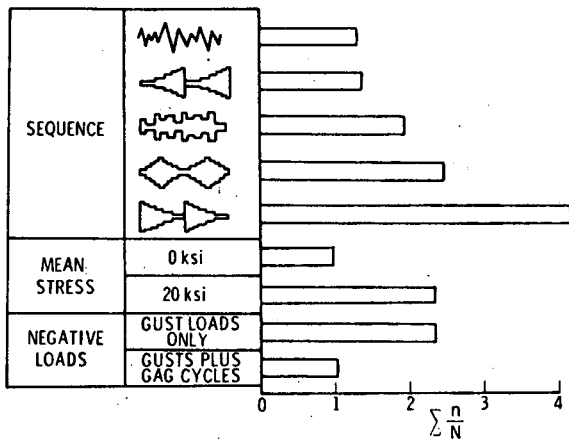


Figure 3-1. Loading Factors Influencing $\Sigma n/N$. (From Reference 2)

important one from the standpoint of estimation difficulty. The major effort in a fatigue study is the construction of service load spectra. (A recent investigation of methods available for establishing space shuttle load spectra is given in Reference 6.) For accurate estimations of fatigue life, the loading sequences as well as the load magnitudes must be determined, since it has been shown that the total damage ($\Sigma n_i/N_i$) is influenced by load sequence, mean load, and whether or not negative loads are included. These effects are demonstrated in Figure 3-1. It is easy to imagine the difficulties involved in trying to predict service loads with such accuracy.

On the more encouraging side, we note that the fatigue problem has been studied by many capable investigators (see the references and bibliography given in Reference 2). Furthermore, a wealth of practical experience has been accumulated over recent years. Thus, while we still employ a good deal of conservatism in fatigue analysis (i. e. scatter factors on the order of 4) we are continually gaining valuable design information.

Recently, the concepts of fracture mechanics have been applied to the prediction of failures induced by repeated loading. The fundamental concepts of fracture mechanics are based on an equivalence of the rate of release of energy due to local redistribution of stress and the energy required to produce new surfaces as the crack grows. The actual analyses are complicated by the plastic deformation that takes place during crack growth. Thus, often, the significant parameters used in fracture mechanics must be established empirically from test data. Nevertheless, the results of studies performed to date are quite encouraging. The concepts have recently been applied to the prediction of fatigue life by assuming the existence of a minute flaw (usually one assumes the flaw to be just barely undetectable by visual means). Then the length of time or number of load cycles until a critical combination of crack length and applied stress produces failure, is computed.

Yang and Heer (Reference 7) have shown how the concepts of fracture mechanics may be applied in a statistical approach for determining fatigue life. Some of the analysis given in Reference 7 are used later in this report. Therefore, a brief review of the section of that work related to fracture criteria is given.

Let "a" represent the size of a flaw at a structural location of interest. From the Griffith-Irwin fracture criteria, then,

$$a = Q (K_I/\sigma)^2 \quad (3-5)$$

and

$$a = Q (K_{IC}/R)^2 \quad (3-6)$$

where K_I is a stress intensity factor, σ is applied stress, K_{IC} is the critical stress intensity factor associated with the resisting stress R , and Q is a state parameter. (see Reference 8 for typical values and more explicit definitions). The rate of flaw extension with respect to the number of stress cycles, n , is given by:

$$\frac{da}{dn} = C(K_I)^b \quad (3-7)$$

where C is a suitable constant and b depends upon the material and environmental conditions. Generally, b ranges from 2 to 4. Substituting equation (3-5) into (3-7) gives:

$$\frac{da}{dn} = (\sigma\sqrt{a})^b D \quad (3-8)$$

where

$$D = C/Q^{b/2}$$

Assuming that $b = 2$ in what follows, we integrate equation (3-8) with respect to each load cycle and see that:

$$\ln a_n - \ln a_o = D \sum_{j=1}^n \sigma_j^2 \quad (3-9)$$

where σ_j is the j^{th} peak of the stress response. Thus, equation (3-9) gives the relationship between the initial flaw size a_o and the flaw size after n load cycles, a_n , in terms of material properties and the stress peaks σ_j . This basic development of fracture mechanics relationships will be used in the next section.

3.3 RELIABILITY TECHNIQUES

The difficulties associated with the determination of safety factors for structural design problems are briefly described by Freudenthal, Garrelts, and Shinozuka in Reference 9. This reference is the final report of the ASCE Task Committee on factors of safety. It was concluded (after 10 years of existence of the committee) that while a definition of the term "factor of safety" could be formulated, the recommending of forms and values of such factors for future structural design problems required a quantity of work that cannot reasonably be expected from a committee. Hence, although a general definition for the "factor of safety" was given in Reference 9, a suitable choice for this factor, for a given design problem, is not always easily determined.

Slightly differing interpretations and uses of the safety factor have created considerable confusion regarding its meaning. This problem is briefly mentioned in Reference 1 (page 4-3) and avoided by giving an explicit definition of the term "factor of safety" as it applies in Reference 1. To avoid ambiguities in this report, we shall give, in this section, a definition of the safety factor as it will be used herein. Our definition of the safety factor does not necessarily agree with that given in Reference 1. Any factor leading to the uncertainties in structural resistance and/or applied loading is included in our definition. This section also discusses the general analysis techniques used to estimate structural reliability.

We begin by considering the structural resistance, R , and the applied stress or load, σ , for a given structure. The ratio, ν , given by

$$\nu = R/\sigma \quad (3-10)$$

is a measure of the safety, and deterministic R and σ , ν is the factor of safety. If R and σ are random variables (see Appendix A for statistical definitions) then following the development given in Reference 9, the probability of failure, P_F , is given by:

$$P_F = \int_0^{\infty} \{1 - F_{\sigma}(x)\} p_R(x) dx = \text{PROB. } [\nu < 1] \quad (3-11)$$

where $F_{\sigma}(x)$ is the distribution function for the loading and $p_R(x)$ is the probability density of the resisting stress. Also, R and σ have been assumed to be statistically independent.

We assume now that the "minimum" resistance, R_p , has associated with it a finite probability of occurrence, p , given by:

$$p = \text{PROB. } [R_p > R] \quad (3-12)$$

For example, the probability that the ultimate tensile stress (for a particular structural member) is less than 120,000 psi might be 0.01. Thus $p = 0.01$, $R_p = 120,000$ psi, and we would expect only 1 out of 100 of these members to fail at a stress level below 120,000 psi. Similarly, we consider, q , the probability that the applied load (or stress) exceeds some value, σ_q . That is:

$$q = \text{PROB. } [\sigma_q < \sigma] \tag{3-13}$$

Let R_o and σ_o denote the central locations of the distributions of R and σ and define the parameters α and β by the equations:

$$R_p = \alpha R_o \tag{3-14}$$

$$\sigma_q = \beta \sigma_o \tag{3-15}$$

In accordance with Reference 9, we define the central factor of safety, ν_o , as:

$$\nu_o = R_o / \sigma_o \tag{3-16}$$

Also, we define the conventional factor of safety, $\bar{\nu}$, as:

$$\bar{\nu} = R_p / \sigma_q \tag{3-17}$$

The interpretation of these parameters may be facilitated by examining Figure 3-2 which shows the probability densities for the random variables R and σ , which are $p_R(x)$ and $p_\sigma(x)$, respectively. Notice that the shaded areas are equal in magnitudes to the probability values p and q .

The probability of failure P_F is:

$$P_F = \text{PROB. } [R/\sigma < 1]$$

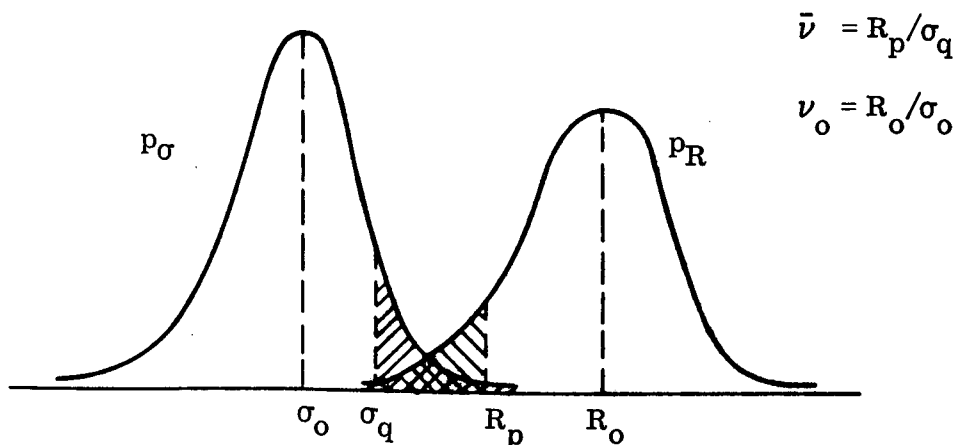


Figure 3-2. Strength and Load Probability Densities

For various values of p , q , ν_0 , and $\bar{\nu}$ the probability of failure is given in Reference 9 for the case of log-normal distributions for R and σ . It may be useful to recognize that for any type of distribution of R and S , the probability that R/σ is less than the conventional factor of safety is bounded by functions of p and q . In particular, Ang and Amin (Reference 10) show that:

$$pq < \text{PROB. } [R/\sigma < \bar{\nu}] < p + q - pq$$

Investigation of the reliability of multiple member structures can be made by extending the principles discussed previously (see, References 9 and 11). Specifically, the weakest-link concept is frequently used. This concept assumes collapse of the entire structure when any single member fails. This approach is conservative for fail-safe structure; furthermore, when this weakest-link concept is employed, it can be shown that the probability of failure for the entire structure P_{F_T} is approximately the sum of the individual component probabilities, i. e.

$$P_{F_T} \cong \sum_{i=1}^m P_{F_i} \quad m = \text{number of components} \quad (3-18)$$

Equation (3-18) can be shown to be an upper bound for the failure probability and its use may be uselessly conservative for structures consisting of a large number of components. We shall not go into further detail on this particular subject because our prime concern in this study involves individual components subjected to combined and repeated loading rather than overall system resistance.

We now consider the more realistic situation, in which the structural component is subjected to a sequence of loads. Actually, the applied loading would generally be a continuous process, but we shall assume that it is possible to replace this process with a sequence of N load cycles. These load cycles could, for instance, consist of the maximum load amplitudes and include dynamics effects. The probability that a component will fail in the $n+1^{\text{th}}$ load cycle, assuming it survived n load cycles, is called the failure rate or hazard function and is usually denoted by $h(n)$. This function is given by (Reference 7):

$$h(n) = \text{PROB. } \left[R_n \leq \sigma_{n+1} \mid \bigcap_{j=1}^n (R_{j-1} > \sigma_j) \right] \quad (3-19)$$

$$n = 1, 2, 3, \dots,$$

$$\text{and } h(0) = \text{PROB. } [R_0 \leq \sigma_1]$$

Equation (3-19) simply states that $h(n)$ is the conditional probability that $R_n \leq \sigma_{n+1}$ (recall that R denotes resistance and σ denotes applied stress or load) and is conditional on $\left\{ \bigcap_{j=1}^n (R_{j-1} > \sigma_j) \right\}$ where \bigcap denotes the intersection of the events.

In equation (3-9) we showed how the growth of a material flaw may be related to the stress peaks (or cycles of stress). If we substitute equation (3-5) into equation (3-9) we see that:

$$R_n = R_0 \exp \{-Z_n\} \quad (3-20)$$

if $\left\{ \bigcap_{j=1}^n (R_{j-1} > \sigma_j) \right\}$ occurs and where Z_n is given by:

$$Z_n = \frac{D}{2} \sum \sigma_j^2$$

Substituting equation (3-20) into (3-19) we obtain the result given in Reference 7 as:

$$h(n) = \text{PROB.} \left[R_n \leq \sigma_{n+1} \mid \bigcap_{j=1}^n (R_{j-1} > \sigma_j) \right] \quad (3-21)$$

where R_n is a random variable given by:

$$R_n = R_0 \exp \{-Z_n\}$$

Using the above equations Yang and Heer (Reference 7) treated a first passage problem in which the barrier level decreased monotonically. That is, they used the hazard function given by equation (3-21) where R_n , the resisting strength, decreases as the material flaw propagates. This approach is quite realistic and accounts for the interaction effects of the first passage and fatigue failures. In fact, it was determined in Reference 7 that neglecting this interaction of failure modes, or neglecting the dispersions in the strength properties, leads to unconservative estimates of structural reliability.

An alternate approach for determining probabilities of fatigue failure and associated factors of safety is given by Bieniek and Joanides in Reference 12. Their analysis accounts for variable amplitude loading as does that given in Reference 7; however, we feel that the simultaneous consideration of first passage and fatigue failure is essential to the accurate estimation of structural reliability.

We conclude Section 3 by briefly summarizing the material which has been presented. In Sections 3.1 and 3.2 first passage failure and fatigue failure concepts were treated individually. In Section 3.3 these modes of failure were considered simultaneously and their effects on structural reliability were assessed. Also considered was the statistical variation of material properties (i. e. , resisting strength). In addition, we have presented a widely accepted definition for the factor of safety that depends upon both material strength and applied load uncertainties. Each of these items of discussion is essential to this study of techniques for determining probabilities of load exceedance and associated factors of safety for space shuttle combined loading conditions.

SECTION 4

LOAD LEVEL EXCEEDANCES FOR COMBINED LOADING

Having established the link between applied loading and probability of failure and having shown how the factors of safety are defined, we turn our attention now to the consideration of the statistics associated with the applied loads. In particular, we shall try to establish methods for determining the statistics of load level exceedances when the total load is comprised of individual load sources which may be either deterministic or probabilistic.

We consider first the case of combining a single deterministic load with a single random load when both are acting in the same direction. If the deterministic load is constant in time, then the statistics of the combined load are quite simply obtained by adjusting the mean value to account for the deterministic load. For example, consider the force, $F(t)$, consisting of the components $R(t)$ and D where

$$F(t) = R(t) + D \quad (4-1)$$

and $R(t)$ is a random process while D is a deterministic constant. Then the mean value of $F(t)$, $\mu_F(t)$, is given by:

$$\mu_F(t) = E [F(t)] = \mu_R(t) + D$$

where $E \{ \}$ denotes the expectation operator and ensemble average (not time averages) are implied. All of the other statistics for $F(t)$ are unaffected by D and are simply the same as the corresponding statistics for $R(t)$, where $R(t)$ may be a stationary or non-stationary random process. A simple extension of this case is generated by allowing D to be a slowly varying time function. By slowly varying, we mean that with respect to the time variation of a typical realization of the process $R(t)$, $D(t)$ changes slowly with time. We now have the combined process given by:

$$F(t) = R(t) + D(t) \quad (4-2)$$

Again, only the first order statistics of $F(t)$ are affected by $D(t)$; however, due to the slow time trend of $D(t)$, $F(t)$ must be considered a nonstationary random process even if $R(t)$ is stationary. The type of process described by equation (4-2) with $D(t)$ "slowly" varying in time is representative of actual loading conditions anticipated for the space shuttle. For instance, this type of loading situation is likely to occur when the orbiter encounters atmospheric turbulence while performing a slow maneuver. In this example, $R(t)$ would represent the stationary random loading caused by the turbulence. The loading described by equation (4-2) also represents the excitation processes typically encountered during ascent. It has been shown (Reference 13) that the zonal ascent wind

velocity may be modeled by equation (4-2) with $R(t)$ a nonstationary random process and $D(t)$ a slowly varying mean wind. The use of this modeling technique leads to reasonably accurate estimations for response threshold crossing rates.

Since the load combination given by equation (4-2) is representative of numerous loading situations, it may be useful to present specific statistics for the total process, $F(t)$. For simplicity, we assume that the random process is Gaussian distributed with zero mean value, but we do not restrict the process to be stationary. The zero mean, Gaussian assumption simplifies our discussion since in that case the variance completely describes the process. We also note that for the physically realistic load situations mentioned (i. e. combined turbulence and maneuver, and launch vehicle ascent wind) the distributions of the wind velocity fluctuations have been found to be approximately Gaussian distributed. One can easily show that if $R(t)$ is Gaussian distributed and $D(t)$ is deterministic, then $F(t)$ as given by equation (4-2) is also Gaussian distributed. Knowledge of the ensemble average of the random rate at which $F(t)$ crosses the threshold level ξ at positive slope, denoted by $E [N+(\xi, t)]$, is valuable in estimating the reliability of the structure. It can be shown (Reference 4) that

$$E [N+(\xi, t)] = \int_0^{\infty} \dot{f} p_{12}(\xi, \dot{f}, t) d\dot{f} \quad (4-3)$$

where $p_{12}(f, \dot{f}, t)$ is the joint probability density of $\dot{F}(t)$ and $\frac{dF(t)}{dt}$ (or $\dot{F}(t)$). For $F(t)$ given by equation (4-2), the joint density is

$$p_{12}(f, \dot{f}, t) = (2\pi\sigma_1\sigma_2)^{-1} (1-\rho_{12}^2)^{-1/2} \exp \left\{ \left[-\left(\frac{r}{\sigma_1}\right)^2 + 2\rho_{12} \left(\frac{r}{\sigma_1}\right) \left(\frac{\dot{r}}{\sigma_2}\right) - \left(\frac{\dot{r}}{\sigma_2}\right)^2 \right] / 2(1-\rho_{12}^2) \right\} \quad (4-4)$$

where:

$$r = f - D(t)$$

$$\dot{r} = \dot{f} - \dot{D}(t)$$

$$\sigma_1 = E [(f - D(t))^2]$$

$$\sigma_2 = E [(\dot{f} - \dot{D}(t))^2]$$

$$\rho_{12} = E [(f - D(t)) (\dot{f} - \dot{D}(t))] / \sigma_1 \sigma_2$$

Replacing r by ξ , substituting equation (4-4) into equation (4-3), and integrating, one obtains:

$$E [N+(\xi, t)] = \sigma_2 (2\pi\sigma_1)^{-1} (1-\rho_{12}^2)^{1/2} \exp(-\eta^2/2) \{ \exp(-\mu^2) + \sqrt{\pi} \mu (1 + \text{ERF}(\mu)) \} \quad (4-5)$$

where ERF is the error function and

$$\eta = (\xi - D(t))/\sigma_1$$

$$\mu = \{ \dot{D}(t)/\sigma_2 + \rho_{12} \cdot \eta \} / \sqrt{2(1-\rho_{12}^2)}$$

For the case $D(t) = 0$, $E [N+(\xi, t)]$ given by equation (4-5) reduces to the corresponding expression given in Reference 14. It is quite simple to show that when $D(t) = 0$ and $R(t)$ is stationary (so that $\rho_{12} = 0$), equation (4-5) reduces to the well-known expression:

$$E [N+(\xi, t)] = \frac{\sigma_2 \exp(-\xi^2/2\sigma_1^2)}{2\pi\sigma_1}$$

The direct application of equation (4-5) to space shuttle loading conditions is discussed in Section 5 of this report.

A more complicated combined loading situation exists when multiple random loads are involved. Perhaps the single most difficult aspect associated with this problem is that total load statistics cannot be determined unless the joint statistics, such as the cross correlation functions are available in addition to the statistics associated with each individual process. Thus, the amount of statistical knowledge required can be hopelessly large, if a large number of random processes are involved.

Assuming that the necessary statistical information is available (this may be a tremendously optimistic assumption), we are still faced with the problems of designing for the combined random loading and of predicting structural reliability. These problems have been investigated by Fuller (Reference 15) and by Houbolt (Reference 16). Actually, in these two references, internal loads (as produced by combined bending and shear) were considered. The techniques discussed are applicable to other situations.

Following Fuller's analysis, we consider a nondimensional combined load vector, $F(t)$:

$$F(t) = f_1(t) i + f_2(t) j + f_3(t) k + \dots$$

where i, j, k , etc are unit vectors. The random functions, $f_1(t), f_2(t), f_3(t), \dots$, are assumed to have been normalized by their root-mean-square values. We now

consider a unit vector P which is fixed in direction, P is given by:

$$P = a_1 i + a_2 j + a_3 k + \dots$$

In Reference 15, the scalar product of F and P is then squared and averaged over time. This procedure leads to the matrix representation of $(F \cdot P)^2$ which is:

$$\begin{bmatrix} a_1 & a_2 & \dots & a_n \end{bmatrix} \begin{bmatrix} 1 & \rho_{12} & \dots & \rho_{1n} \\ \rho_{12} & 1 & \dots & \\ \cdot & \cdot & \dots & \\ \cdot & \cdot & \dots & \\ \cdot & \cdot & \dots & \\ \rho_{1n} & & & \rho_{nn} \end{bmatrix} \begin{Bmatrix} a_1 \\ a_2 \\ \cdot \\ \cdot \\ \cdot \\ a_n \end{Bmatrix}$$

for an n dimensional random vector, with ρ_{ij} the correlation coefficient for the components f_i and f_j . The maxima and minima may then be determined by computing the eigenvalues for the correlation coefficient matrix. By using this procedure one can establish the maximum combined loading condition. We note that difficulties are anticipated in extending the technique for use when the random loads are nonstationary, since one is then faced with the problem of determining the maximum as a function of time — the required computation may be excessive.

Houbolt (Reference 16) has considered the same type of problem, but has computed the statistics of combined load exceedances. Thus, while the methods of Reference 15 are applicable to the determination of limit and ultimate design loads, Reference 16 may be useful in assessing fatigue damage due to combined random loading. Without repeating the details presented in Reference 15, we simply state that the reference contains expressions for computing $E [N + (\xi, t)]$ when more than a single random load is considered and ξ is still interpreted as the threshold level.

SECTION 5

APPLICATION TO SIGNIFICANT SPACE SHUTTLE LOADING SITUATIONS

Recalling now those load conditions which were found to be significant (Phase I) we shall consider the application of the techniques discussed in Sections 3 and 4. The weight sensitivities for the significant load conditions have already been assessed (Phase II); therefore, when statistics of load exceedance are determined these statistics can be directly related to their influence on structural weight.

To discuss all conceivable combinations of loading conditions would be a tremendous task, and even if it could be done, most of the results would be configuration dependent. For this reason, the objective of this phase of the study is to define and document methods for combining significant loads so that determinable statistics of structural success might be computed. Thus, in this section we shall simply demonstrate how the previously discussed methods might be applied to typical load combinations. No doubt the reader will think of other important load combinations that could have been discussed.

It was found that major loads for the space shuttle vehicles include the loads attributable to: maximum thrust, ascent winds, tank pressurization, maximum acceleration during entry, ground winds and related effects, subsonic gust, maneuvers, separation and staging, rudder kick, and landing and taxi. Obviously, this list does not exhaust the load conditions which must be considered, but these loads design most of the major load-carrying structure of the space shuttle vehicles. Thus the following discussion will be concentrated on some of these load conditions.

Prior to launch, the space shuttle vehicles will be exposed to ground winds and related effects such as vortex shedding. It is assumed that the total wind velocity consists of a steady mean wind plus an oscillating turbulence component. Thus, the total wind velocity consists of a random process described approximately by an equation such as equation (4-1). The input statistics could be computed as discussed in Section 4. The determination of the total forces, due to ground wind effects, is much more complicated. Indeed, depending upon numerous parameters such as vehicle configuration parameters and Reynolds number, unsteady lift forces caused by vortex shedding may be present, in addition to the drag forces. Thus the total load acting on an element of the shuttle cross-section might be composed of two mutually perpendicular unsteady forces, say,

$$F(t) = F_D i + F_L j \quad (5-1)$$

where F_D represents the drag force and F_L represents the lift force. F_D would generally be composed of a steady plus random turbulence force as previously discussed. F_L could be a periodic oscillatory force or a random process depending upon the

Reynolds number (i. e. very different effects result for the subcritical, transcritical, and supercritical Reynolds number regimes). Thus, we have a situation for which the maximum load might be determined using the technique of Reference 15. Unfortunately, the ground wind analysis is even more complicated than has been implied. For instance, very little is known about the correlation between the drag forces and the lift forces so that application of our techniques to equation (5-1) would probably involve some drastic simplifying assumptions. Also, the drag and lift forces are known to vary along the length of the vertically erected launch vehicle, further complicating the problem. Other effects are also likely to be present, for instance the bending might be coupled with torsion, particularly for the space shuttle configuration which is far from being a circular cylinder. Analytical techniques alone are not sufficient to assess the probability of load exceedance due to ground winds, therefore, the analyses must be substantiated by test. Then, conservative empirical analyses based on the methods discussed in Section 3 and 4 may be used to predict bounds for structural reliability.

Just after liftoff, the primary fuselage axial loads are caused by the large thrust forces. Once the initial transients have subsided the fuselage loads induced by thrust can be considered as time varying deterministic loads. (We hesitate to call these forces deterministic since unpredictable variations in thrust magnitude are anticipated. However, these variations must be quite small if the trajectory requirements and other mission requirements are to be met.) In addition to thrust loads, and occurring at the same time, are the ground wind loads and, later, the ascent winds. The wind loads are especially significant in their effects on the aerodynamic surfaces, and are likely to produce significant fuselage bending. Thus, the total axial load in a longitudinal fuselage stiffener could be composed (at various flight times) of a time varying compression load due to thrust and an oscillatory random load due to wind effects. For this condition, one might approximately represent the axial force by equation (4-2). The average threshold crossing rate of axial stress could then be computed by equation (4-5), if the process is assumed to be Gaussian distributed.

Returning to the discussion of ascent winds, we consider now the statistics of load exceedance for a response quantity affected by the wind velocity. A response quantity of interest might be the vertical shear or bending moment at a wing root main spar location. (It is known that the ascent winds design significant portions of both the booster and the orbiter (Reference 6); therefore, an analysis technique for estimating ascent load exceedance probabilities is mandatory if structural weight is to be minimized.) We may assume that the wind velocity is represented by equation (4-2) where $D(t)$ is the ensemble mean, time varying wind velocity and $R(t)$ is a nonstationary random process. The validity of this assumption has been verified (Reference 13) by comparing nonstationary analytical results with simulation results using FPS-16 Radar/Jimsphere March wind data. Equation (4-5) can be used to estimate the average number of response exceedances.

Once $E [N+(\xi, t)]$ has been determined for the ascent wind condition (whether it be determined by nonstationary analysis or simulation) more information than simple crossing rate statistics can be obtained. Beer and Lennox (Reference 17) have shown that the probability of survival for a structural component is given by

$$P_{S\alpha} = 1 - \int_0^{Z_M} P_{\alpha}(Z) dZ \quad (5-2)$$

where α is the barrier or failure level for the component in question, Z is the altitude of the launch vehicle, and

$$P_{\alpha}(Z) \cong U_{\alpha}(Z) \exp \left\{ - \int_0^Z U_{\alpha}(l) dl \right\} \quad (5-3)$$

where

$$U_{\alpha}(Z) = E [N+(\alpha, Z)]$$

Notice that $U_{\alpha}(Z)$ could be written as a function of time into launch instead of altitude, thus the determination of the average threshold crossing rate is useful in the prediction of survival probability (see Section 3.1).

As a final example, consider the subsonic flight of the orbiter. The combined loading condition caused by turbulence encounter during a slow maneuver may be described by equation (4-2). Maneuver and turbulence have been treated individually for flight vehicles for some time. Yet, the combined condition has been given little consideration in the past. The use of equation (4-5) is directly applicable to this problem with the correlation coefficient, ρ_{12} , equal to zero if the turbulence is assumed to be stationary.

Before concluding this section we should mention another technique for computing the statistics of combined load exceedances. This method is the well known Monte Carlo approach. Recent work by Shinozuka (Reference 18) has led to an attractive means of digitally simulating both stationary and nonstationary random processes. The simulation technique leads to a direct means of determining ensemble response statistics. The method is particularly attractive when nonlinear systems are involved (such as for taxi roughness studies).

As a final note, we remind the reader of the versatility of the Tchebycheff inequality. Frequently, the random processes in question are not Gaussian distributed. In these situations crossing rate and other higher order statistics may be difficult to estimate. Even then, however, use of only the mean and variance enables one to construct an upper bound estimate of the event $|F(t) - \mu_F(t)| \geq \epsilon$ for any t (see Reference 4, page 39) where $F(t)$ is the non-Gaussian process and ϵ is some constant.

SECTION 6

CONCLUSIONS AND RECOMMENDATIONS FOR FURTHER STUDY

The application of the techniques in Section 5 to the space shuttle vehicle is not a trivial matter. Indeed, the estimation of the probability of success for any practical structural system exposed to a complex loading sequence is an extremely difficult task. Prior success along these lines has often been due to excessive conservatism. With greater emphasis on weight savings, however, we are finding that our techniques are perhaps not so accurate as we had originally assumed, and in some cases we find that the required techniques are simply not available. We also have found that failure may occur even through the margins of safety in our analysis were positive — this possible outcome has been recognized for some years as may be seen by examining Reference 19.

For the space shuttle we must be concerned with both fatigue and first passage modes of failure; therefore, although we admit that much improvement is still possible, we feel that the techniques outlined in this report will provide a realistic means of determining probabilities of load exceedance. It is specifically concluded that the technique of considering a first passage problem with decreasing barrier is the most realistic available means of estimating space shuttle reliability. Also, the fracture mechanics methods discussed in Section 3.2 are expected to be valuable in the reliability studies. It is also concluded that the techniques discussed for combining time dependent and probabilistic loads are applicable to typical space shuttle loading conditions.

A great deal of work remains to be done in this area, however. Recently, it has been shown that the maximum vibration for the Titan launch vehicle occurs as a result of booster engine ignition (Reference 20). At that time, severe transient responses are incurred and these responses are nonstationary random processes. Prediction of the maximum response (essential to the estimation of reliability) is generally quite difficult by conventional means. The distribution of maximum stress response is approximately given by a Gumbel distribution of extremes. Utilization of this information, however, requires some experimental data. Thus, for the space shuttle, additional effort is required before we can make realistic estimates of load exceedance statistics for such nonstationary transient load conditions.

Furthermore, although a means of estimating the probability of survival considering first passage failure was established for vehicle ascent loading, more effort is required before we can rationally include the consideration of fatigue failure. That is, the first passage problem with decreasing barriers and nonstationary random excitation should be investigated in application to the ascent wind loading.

SECTION 7
REFERENCES

1. ANON. ; "Structural Design Criteria Applicable to a Space Shuttle", NASA SP-8057, January 1971.
2. Hardrath, H. F. ; "Fatigue and Fracture Mechanics", J. of Aircraft, Vol. 8, No. 3, March 1971, pp. 129-142.
3. Crandall, S. H. ; "First-Crossing Probabilities of the Linear Oscillator," J. Sound and Vibration, Vol. 12, No. 3, 1970, pp. 285-299.
4. Lin, Y. K. ; Probabilistic Theory of Structural Dynamics, McGraw-Hill, New York, 1967.
5. Yang, J.-N. ; "Nonstationary Envelope Process and First Excursion Probability," JPL Quarterly Technical Review, Vol. 1, No. 4, January 1972, pp. 1-12.
6. Kuchta, B. J., Howell, L. J., and Sealey, D. M. ; "Determination of Methods for Establishing Space Shuttle Load Spectra", General Dynamics Report GDC-DDE71-007, also NASA CR-112033, November 1971.
7. Yang, J.-N., and Heer, E. ; "Reliability of Randomly Excited Structures," AIAA Journal, Vol. 9, No. 7 July 1971, pp. 1262-1268.
8. Wilhem, D. P. ; "Fracture Mechanics Guidelines for Aircraft Structural Applications," Technical Report AFFDL-TR-69-111, February 1970.
9. Freudenthal, A. M., Garrelts, J. M., and Shinozuka, M. ; "The Analysis of Structural Safety", Journal of the Structural Division, ASCE, Vol. 92, No. ST1, February 1966, pp. 267-325.
10. Ang. A. H. S., and Amin, M. ; "Safety Factors and Probability in Structural Design," Journal of the Structural Division, ASCE, Vol. 95, No. ST7, July 1969, pp. 1389-1405.
11. Ang. A. H. S., and Amin, M. ; "Reliability of Structures and Structural Systems," Journal of the Engineering Mechanics Division, ASCE, Vol. 94, No. EM2, April 1968, pp. 671-691.
12. Bieniek, M. P., and Joanides, J. C. ; "Safety Factors and the Probability of Failure in Fatigue," AIAA Journal, Vol. 9, No. 4, April 1971, pp. 753-754.
13. Howell, L. J., Kuchta, B. J., and Barnes, R. E. ; "Nonstationary Ascent Wind Analysis," General Dynamics Report GDCA-DDE72-002, NASA Contract number NAS1-6024, February 1972.

14. Howell, L. J., and Lin, Y. K.; "Response of Flight Vehicles to Nonstationary Atmospheric Turbulence", AIAA Journal, Vol. 9, No. 11, November 1971, pp. 2201-2207.
15. Fuller, J. R.; "Designing for Combined Random Loads," Journal of Spacecraft and Rockets, Vol. 8, No. 4, April 1971, pp. 396-398.
16. Houbolt, J. D.; "Exceedances of Structural Interaction Boundaries for Random Excitation," AIAA Journal, Vol. 6, No. 11, November 1968, pp. 2175-2183.
17. Beer, F. P., and Lennox, W. C.; "Determination of the Survival Probability of a Launch Vehicle Rising Through a Random Wind Field," Journal of Spacecraft and Rockets, Vol. 3, No. 4, April 1966, pp. 472-476.
18. Shinozuka, J., and Wen, Y. K.; "Monte Carlo Solution of Nonlinear Vibrations", AIAA Journal, Vol. 10, No. 1, January 1972, pp 37-40.
19. Hilton, H. H., and Feigen, M.; "Minimum Weight Analysis Based on Structural Reliability", Journal of the Aerospace Sciences, Vol. 27, No. 9, September 1960, pp. 641-652.
20. Yang, J.-N.; "Statistical Distribution of Spacecraft Maximum Structural Response", Journal of Spacecraft and Rockets, Vol. 9, No. 1, January 1972, pp. 57-59.

APPENDIX A
BASIC STATISTICAL CONCEPTS

A very cursory review of some relevant statistical concepts is presented in this appendix. For a complete presentation of the probabilistic theory utilized in this report the reader may consult Reference 4, from which the material presented herein was taken.

We begin by considering the characteristics of a random variable. The probabilistic nature of a random variable may be described by the distribution function. For the random variable, \bar{x} , the distribution function $F_{\bar{x}}(x)$ is the probability of the event $\bar{x} \leq x$, that is:

$$F_{\bar{x}}(x) = \text{PROB. } [\bar{x} \leq x]$$

The distribution function is a nondecreasing function and must satisfy the relations:

$$F_{\bar{x}}(-\infty) = 0; \quad F_{\bar{x}}(+\infty) = 1$$

The probability density function, $p_{\bar{x}}(x)$, is defined as the derivative of the distribution function (when it exists):

$$p_{\bar{x}}(x) = \frac{d F_{\bar{x}}(x)}{dx}$$

By inversion we see that:

$$F_{\bar{x}}(x) = \int_{-\infty}^x p_{\bar{x}}(y) dy$$

and that:

$$\int_{-\infty}^{+\infty} p_{\bar{x}}(y) dy = F_{\bar{x}}(+\infty) = 1$$

Therefore, the probability density is non-negative and the area under the probability density curve is always equal to unity.

The first moment or expected value of the random variable \bar{x} is defined as

$$E[\bar{x}] = \int_{-\infty}^{\infty} x p_{\bar{x}}(x) dx = \mu_{\bar{x}}$$

The expected value is also known as the mean or ensemble average. The n^{th} order moment is defined as

$$E[\bar{x}^n] = \int_{-\infty}^{\infty} x^n p_{\bar{x}}(x) dx$$

Let $\mu_{\bar{x}}$ be the first moment of x ; then $E[(\bar{x} - \mu_{\bar{x}})^n]$ is the n^{th} central moment of \bar{x} . Of special importance are the second central moments:

$$E[(\bar{x} - \mu_{\bar{x}})^2] = E[\bar{x}^2] - \mu_{\bar{x}}^2 = \sigma_{\bar{x}}^2$$

$\sigma_{\bar{x}}^2$ is known as the variance of \bar{x} and $\sigma_{\bar{x}}$ is the standard deviation. In the case of two random variables:

$$E[(\bar{x}_1 - \mu_{\bar{x}_1})(\bar{x}_2 - \mu_{\bar{x}_2})] = K_{\bar{x}_1 \bar{x}_2}$$

$K_{\bar{x}_1 \bar{x}_2}$ is called the covariance of \bar{x}_1 and \bar{x}_2 .

A random variable \bar{x} is Gaussian distributed, or normal, if its probability density may be written

$$p_{\bar{x}}(x) = \frac{1}{\sqrt{2\pi} \sigma_{\bar{x}}} \exp\left\{-\frac{(x - \mu_{\bar{x}})^2}{2 \sigma_{\bar{x}}^2}\right\}, \quad -\infty < x < \infty$$

The most important feature of a Gaussian distributed random variable is that it is completely characterized by its mean and its variance.

Jointly distributed random variables, $\bar{x}_1, \bar{x}_2, \dots, \bar{x}_m$, may be represented by the probability density

$$p_{\bar{x}_1 \bar{x}_2 \dots \bar{x}_n}(x_1, x_2, \dots, x_n) =$$

$$\frac{1}{(2\pi)^{n/2} |S|^{1/2}} \exp \left\{ -\frac{1}{2|S|} \sum_{j=1}^n \sum_{k=1}^n |S|_{jk} (x_j - \mu_{\bar{x}_j})(x_k - \mu_{\bar{x}_k}) \right\}$$

where $|S|$ is the determinant of the matrix of variances and covariances

$$[S] = \begin{bmatrix} \sigma_{\bar{x}_1}^2 & K_{\bar{x}_1 \bar{x}_2} & \dots & K_{\bar{x}_1 \bar{x}_n} \\ K_{\bar{x}_2 \bar{x}_1} & \sigma_{\bar{x}_2}^2 & \dots & K_{\bar{x}_2 \bar{x}_n} \\ \vdots & \vdots & \ddots & \vdots \\ K_{\bar{x}_n \bar{x}_1} & K_{\bar{x}_n \bar{x}_2} & \dots & \sigma_{\bar{x}_n}^2 \end{bmatrix}$$

and $|S|_{jk}$ is the cofactor of the element in the j^{th} row and the k^{th} column.

As described in Reference 4, "A random process is a parametered family of random variables with the parameter (or parameters) belonging to an indexing set (or sets)." In our discussion, time, t , is the parameter with which we shall deal.

The statistical characteristics of a random process are described by its probability structure

$$p_{\bar{x}}(x_1, t_1)$$

$$p_{\bar{x}}(x_1, t_1; x_2, t_2)$$

$$p_{\bar{x}}(x_1, t_1; x_2, t_2; \dots; x_n, t_n)$$

where the lower order probability densities can be obtained from the higher-order ones from a compatibility condition. The moment functions of a random process are defined by

$$E[\bar{x}(t_1)] = \int x p_{\bar{x}}(x, t_1) dx$$

$$E[\bar{x}(t_1) \bar{x}(t_2)] = \iint x_1 x_2 p_{\bar{x}}(x_1, t_1; x_2, t_2) dx_1 dx_2 \quad \text{etc.}$$

The first and second moment functions are quite important in practice and are given special symbols:

$$E [\bar{x}(t_1)] = \mu_{\bar{x}}(t_1), \text{ the mean}$$

$$E [\bar{x}(t_1) \bar{x}(t_2)] = \phi_{\bar{x}\bar{x}}(t_1, t_2), \text{ the autocorrelation function}$$

$$E [\bar{x}(t_1) \bar{y}(t_2)] = \phi_{\bar{x}\bar{y}}(t_1, t_2), \text{ the cross-correlation function where } \bar{y}(t)$$

is another random process that may or may not be related to $\bar{x}(t)$.

A random process $\bar{x}(t)$ is stationary (strongly homogeneous) if its complete probability structure is independent of a shift of the parametric origin. If the first and second probability density functions (only) are independent of such a translation, the process is said to be weakly stationary.

Two important properties of weakly stationary random processes are: 1) that the mean value of the process is constant with respect to the parameter time:

$$E [\bar{x}(t)] = \mu_{\bar{x}}$$

and 2) that the autocorrelation function is an even function of time difference only

$$E [\bar{x}(t_1) \bar{x}(t_2)] = R_{\bar{x}\bar{x}}(\tau), \quad \tau = t_2 - t_1$$

The Fourier transform of the autocorrelation function of a weakly stationary random process is the spectral density function:

$$\Phi_{\bar{x}\bar{x}}(\omega) = \frac{1}{2\pi} \int_{-\infty}^{\infty} R_{\bar{x}\bar{x}}(\tau) e^{-i\omega\tau} d\tau \geq 0$$

The spectral density plays an important role in the probabilistic analysis of structural dynamics and its use in frequency domain analyses is well known.